Detection of factors that determine the quality of industrial minerals

An infrared sensor-based approach for mining and process control

Guatame-Garcia, Adriana

DOI
10.4233/uuid:30966f68-cea2-4669-93da-23a477d0978b

Publication date
2019

Document Version
Final published version

Citation (APA)
Guatame-Garcia, A. (2019). *Detection of factors that determine the quality of industrial minerals: An infrared sensor-based approach for mining and process control*. [Dissertation (TU Delft), Delft University of Technology]. https://doi.org/10.4233/uuid:30966f68-cea2-4669-93da-23a477d0978b

DETECTION OF FACTORS THAT DETERMINE THE QUALITY OF INDUSTRIAL MINERALS

an infrared sensor-based approach for mining and process control

Adriana Guatame-García

DETECTION OF FACTORS THAT DETERMINE THE QUALITY OF INDUSTRIAL MINERALS

AN INFRARED SENSOR-BASED APPROACH FOR MINING AND PROCESS CONTROL

DETECTION OF FACTORS THAT DETERMINE THE QUALITY OF INDUSTRIAL MINERALS

AN INFRARED SENSOR-BASED APPROACH FOR MINING AND PROCESS CONTROL

Proefschrift

ter verkrijging van de graad van doctor
aan de Technische Universiteit Delft,
op gezag van de Rector Magnificus prof.dr. ir. T.H.J.J. van der Hagen
voorzitter van het College voor Promoties,
in het openbaar te verdedigen op
dinsdag 15 oktober om 10:00 uur

door

Adriana GUATAME-GARCÍA

Master of Science in Geo-information Science and Earth Observation,
Universiteit Twente, Enschede, Nederland
geboren te Chía, Colombia.

This dissertation has been approved by the promotors.

Composition of the doctoral committee:

Rector Magnificus,	chairperson
Dr. M.W.N. Buxton	Delft University of Technology, promotor
Prof. dr. ir. J.D. Jansen	Delft University of Technology, promotor
Independent members:	
Prof. dr. F.D. van der Meer	University of Twente
Dr. N. Zajzon	University of Miskolc, Hungary
Prof. dr. S.E. Marsh	University of Nottingham, United Kingdom
Dr. ir. D.L. Schott	Delft University of Technology
Prof. dr. G. Bertotti	Delft University of Technology
Prof. dr. M. Menenti	Delft University of Technology, reserve member

This research was financially supported by the European FP7 project "Sustainable technologies for calcined industrial minerals in Europe" (STOICISM), grant NMP2-LA-2012-310645 and the EIT Raw Materials KAVA funding "Integrated system for monitoring and control of product quality and flexible energy delivery in calcination" (MONICALC), grant 15045.

Cover design by Carlos Guatame García

Printed by ProefschriftMaken, the Netherlands
ISBN 978-94-6366-198-0

An electronic version of this dissertation is available at
http://repository.tudelft.nl/.

I don't know anything,
but I do know that everything is interesting
if you go into it deeply enough.

Richard Feynman

CONTENTS

SUMMARY

Industrial minerals are essential to human activity. The products derived from them make an integral part of a wide range of materials that are ubiquitously present in our daily lives. The performance and attributes of these materials depend significantly on the properties and quality of the industrial minerals and the products generated from them. These characteristics are ensured by the selection and mining of adequate ores, and by using various beneficiation and processing strategies to modify or enhance the original properties of the minerals.

One example of these strategies is calcination, in which the minerals are subject to thermal treatment. The success of the generation of high-quality products by using this technique partly depends on the capability of the plant to detect the factors that can degrade the quality of the raw ore, feed for calcination and final product. It also depends on its ability to inform and adapt the operations according to the presence of such factors. A possible approach for doing this is to characterise the minerals and materials with sensor technologies that can generate information on-site and in real-time, focusing on the identification of the degrading factors. Their timely detection can give operational feedback to the process and aid in the generation of high-quality products.

This Thesis aims to develop methods for the detection of factors that determine the quality of industrial mineral products by using data derived from infrared sensors, which have the potential to be implemented in mining and process control. For doing this, three commodities that are relevant to the market and that represent different applications have been selected. First, kaolin is presented as an example of minerals used in the generation of performance and speciality products (additives that improve the characteristics of a particular material). Then, perlite and diatomite are used as examples of minerals to produce process aids (materials used for filtration and absorption). The characterisation of these three commodities in the raw ore stage enables the development of methods for the early identification of impurities and the generation of data that can impact the extraction efficiency of the ore. The characterisation of the feeds for calcination aids to develop infrared-based tools to monitor the quality and consistency of the material, and to produce data that promotes a proactive control of the calcination process. The characterisation of the calcined products enables the development of measurements that serve as a proxy to some of the parameters that define the quality of the final product, in order to provide operational feedback for the calciner.

The kaolin case study focuses on mineral impurities and the properties of kaolinite, as the primary mineral in the ore and the feed. In the infrared spectra, by using a combination of existing methods, it is possible to pinpoint the iron-bearing minerals and the clay minerals that are detrimental to the process. This applies only for the cases where the mineral concentration is not too low, and the spectral features are not overwhelmed by those of kaolinite. This is possible in the raw ore, but not in the feed for calcination that has been highly refined. In contrast, the use of a spectral index to determine the

properties of kaolinite is more reliable to characterise the feed, since the spectra of the material are nearly pure. The quality of the calcined product, on the other hand, depends on the soluble Al_2O_3 content, a parameter that cannot be directly detected in the infrared spectra. Therefore it is necessary to use complementary datasets and observations and to use chemometric methods for data analysis. The implementation of this approach enables the development of an infrared-based measurement that can predict the soluble Al_2O_3 content in the calcined product. This measurement can be integrated into other systems to influence the operation of the calciner retroactively.

Even though perlite and diatomite serve the same applications and are composed mainly by opal, their ores differ significantly regarding their origin and composition. This implies that the factors that affect the quality of the product are also different. In the perlite case, the detrimental factors are related to chemical impurities and to the potential of the ore to produce fine particles during processing. These two factors can be related to the infrared spectra by correlating them to the mineralogy of the ore. The development of a spectral index permits the distinction between the mineral phases and the establishment of correlations with the detrimental factors by applying chemometrics. For the diatomite case, the presence of carbonates hinders the purity and performance of the products. Opal and carbonates can be differentiated in the infrared spectra, and by implementing chemometric methods, it is possible to classify the ore according to quality grades. In both cases, perlite and diatomite, the results can be implemented to support decision-making at the mining stage, and to further advice the beneficiation process.

This research shows the capacity of infrared sensor-based technologies to retrieve information, directly or indirectly, about the factors that affect the quality of industrial minerals at a lower cost and with comparable efficiency to other analytical methods. This information –generated on-site and in real-time– is highly relevant for performing optimisation at different stages of mining and processing. The implementation of the proposed methods would have a direct impact on the efficient use of the mineral resources by increasing the possibility of using low-grade or sub-economic deposits, therefore expanding the resource and limiting the generation of waste material. The implementation of the results of this research would also impact the generation of high-quality products, not only by ensuring the compliance of standards but also by enabling more efficient use of the energy during mining and calcination, with immediate consequences on, for example, the CO_2 footprint of the processes. Overall, the use of the results presented in this work would contribute to the development of practices that support sustainable development in the industrial minerals sector.

SAMENVATTING

Industriële mineralen zijn essentieel voor menselijke activiteiten. De producten die hiervan gemaakt worden zijn onderdeel van een breed scala aan materialen die alom aanwezig zijn in ons dagelijks leven. De kwaliteit en kenmerken van deze materialen zijn sterk afhankelijk van de eigenschappen van de industriële mineralen en de producten die hieruit gewonnen worden. Deze eigenschappen worden gewaarborgd door de selectie en mijnbouw van geschikte ertsen, en door toepassing van verschillende verwerking strategieën die de oorspronkelijke materiaaleigenschappen van de mineralen veranderen of verbeteren.

Een voorbeeld van een verwerkingsstrategie is het calcinatie proces, waarbij de mineralen worden onderworpen aan thermische behandeling. De effectiviteit om met deze techniek producten van hoge kwaliteit te maken hangt af van het vermogen van de fabriek om de factoren te detecteren die van invloed zijn op de kwaliteit van het erts, de fabrieksinvoer en het uiteindelijke product. Het is ook afhankelijk van de mogelijkheden om deze factoren te gebruiken om deelprocessen in de fabriek hierop aan te passen. Een mogelijke aanpak hiervoor is de karakterisering van de mineralen en materialen met sensor technieken die op locatie real-time informatie kunnen leveren voor de identificatie van kwaliteitsfactoren. De snelle detectie kan operationele feedback leveren over het proces en kan bijdragen aan het maken van producten van hoge kwaliteit.

Dit promotieonderzoek heeft als doel methodes te ontwikkelen voor de detectie van factoren die de kwaliteit van industriële mineralen beschrijven door data van infrarood sensoren te gebruiken die mogelijk geïmplementeerd kunnen worden in de mijnbouw en procesbeheersing. Om dit te doen zijn er drie grondstoffen geselecteerd die relevant zijn voor de afzetmarkt en die verschillende toepassingen hebben. Allereerst wordt kaolien gepresenteerd als voorbeeld van mineralen die gebruikt worden voor het maken van prestatiegerichte en speciale producten (additieven die de eigenschappen van een bepaald materiaal verbeteren). Daarna worden perliet en diatomiet als voorbeeld gebruikt van mineralen waarmee proceshulpmiddelen geproduceerd worden (materialen gebruikt voor filtratie en absorptie). De karakterisering van deze drie grondstoffen vlak nadat ze zijn gemijnd maakt het mogelijk methodes te ontwikkelen voor de snelle indicatie van verontreinigingen en het verkrijgen van data die gebruikt kan worden om de efficiëntie van ertsextractie te bevorderen. De karakterisering van de invoer voor calcinatie draagt bij aan de ontwikkeling van op infrarood gebaseerde instrumenten voor het monitoren van de kwaliteit en consistentie van het materiaal, en aan de productie van data die de proactieve controle van het calcinatieproces bevorderen. De karakterisering van gecalcineerde producten maakt het mogelijk meetmethodes te ontwikkelen voor de detectie van parameters die de kwaliteit van het eindproduct beschrijven, zodat directe operationele feedback geleverd kan worden.

De kaolien casus is gericht op mineraalverontreinigingen en de eigenschappen van kaoliniet, wat het voornaamste mineraal in het erts en de fabrieksinvoer is. Door een

combinatie van bestaande methodes toe te passen op infrarood spectra kunnen ijzerhoudende mineralen en kleimineralen gedetecteerd worden die schadelijk zijn voor het verwerkingsproces. Dit is alleen van toepassing op gevallen waar de mineraalconcentratie niet te laag is, en de spectrale eigenschappen niet overschaduwd worden door die van kaoliniet. Dit is mogelijk voor het gemijnde erts, maar niet voor de invoer voor het calcinatieproces wat sterk geraffineerd is. Anderzijds is het gebruik van een spectrale index voor de bepaling van de eigenschappen van kaoliniet betrouwbaarder voor de calcinatie invoer omdat de spectra van dit materiaal zuiverder zijn. De kwaliteit van het gecalcineerde product is echter afhankelijk van het oplosbare Al_2O_3 gehalte, wat niet direct bepaald kan worden uit de infrarood spectra. Hiervoor is het nodig om aanvullende datasets en observaties te gebruiken en chemometrische methodes toe te passen voor data analyse. De implementatie van deze aanpak maakt het mogelijk om een op infrarood gebaseerde meetmethode te ontwikkelen waarmee het oplosbare Al_2O_3 gehalte in het gecalcineerde product voorspeld kan worden. Deze meetmethode kan geïntegreerd worden in andere systemen om op retroactieve wijze de aansturing van het calcinatieproces te bevorderen.

Ondanks dat perliet en diatomiet dezelfde toepassingen hebben en voornamelijk bestaan uit opaal, zijn de ertsen hiervan significant verschillend op basis van oorsprong en samenstelling. Dit houdt in dat de factoren die de kwaliteit van het product bepalen ook verschillend zijn. In het geval van perliet zijn de schadelijke factoren gerelateerd aan chemische verontreinigingen en de kans dat fijne stofdeeltjes geproduceerd worden tijdens de ertsverwerking. Deze twee factoren kunnen gerelateerd worden aan de infraroodspectra door ze te correleren aan de mineralogie van het erts. De ontwikkeling van een spectrale index maakt het mogelijk om onderscheid te maken tussen mineraalfases en om correlaties te vinden met schadelijke factoren door chemometrie toe te passen. Voor diatomiet wordt de zuiverheid en kwaliteit van de producten negatief beïnvloed door de aanwezigheid van carbonaten. Opaal en carbonaten kunnen worden onderscheiden in infrarood spectra, en door chemometrische methodes te implementeren is het mogelijk om ertsen te classificeren op basis van kwaliteit. Voor zowel perliet en diatomiet kunnen de resultaten geïmplementeerd worden om de besluitvorming tijdens de mijnbouw te ondersteunen, en advies uit te brengen voor het ertsverwerkingsproces.

Dit onderzoek beschrijft de mogelijkheden om technologieën gebaseerd op infrarood sensoren te gebruiken om zowel direct als indirect informatie te verzamelen over de factoren die van invloed zijn op de kwaliteit van industriële mineralen tegen lagere kosten en vergelijkbare effectiviteit als andere analytische methodes. Deze informatie –op locatie in real-time verzameld– is zeer relevant voor de optimalisatie van de verschillende onderdelen van mijnbouw en ertsverwerking. De implementatie van de voorgestelde methodes zullen direct van invloed zijn op het efficiënt gebruik van mineraal grondstoffen door meer mogelijkheden te creëren om lage kwaliteit of slecht rendabele ertsvoorkomens te ontginnen, en daardoor de voorziening in grondstoffen te verbeteren en de productie van afvalmateriaal te beperken. Implementatie van de resultaten van dit onderzoek zullen ook van invloed zijn op het maken van hoge kwaliteit producten, niet alleen door de naleving van standaarden te waarborgen, maar ook door efficiënter gebruik te maken van energie tijdens mijnbouw en calcinatie, met directe consequenties voor bijvoorbeeld de CO_2 uitstoot van de processen. Het gebruik van de resultaten die in dit proefschrift gepresenteerd worden zal bijdragen aan de ontwikkeling van richtlijnen die de duurzame

ontwikkeling in de industriële mineralen sector bevorderen.

I

PREAMBLE

1

INTRODUCTION

The first chapter of this Thesis gives an introduction to the main concepts related to industrial minerals and the industrial minerals sector. It also presents the commodities that are subject of study as well as the research scope and approach. The last part of the chapter gives a general overview of the structure and the content of the subsequent chapters.

1

We are surrounded by industrial minerals. Even though their presence often passes unnoticed to our eyes, many of the products that we use in our daily life contain products derived from industrial minerals. They support essential aspects of human activity, from infrastructure to food and pharmaceutical products. For example, the smoothness of paper is imparted by clay minerals, and the filters that clean the water supply systems of our cities contain porous silicate minerals. These subtle applications make industrial mineral commodities of great economic importance to society and therefore to the mining sector. The ubiquity of industrial mineral applications and the needs of the society increase the demand for the generation of products. At the same time, increasing environmental awareness promotes the implementation of sustainable practices in the mining industry. This scenario opens up opportunities to investigate and to develop techniques that contribute to the optimisation of the mining and processing of industrial minerals and the generation of high-quality products, and that support sustainable development in the industrial minerals sector.

1.1. INDUSTRIAL MINERALS

1.1.1. THE INDUSTRIAL MINERALS SECTOR

The term "industrial mineral" is not restricted to a single mineral specimen, but also includes mineral mixtures and rocks. Industrial minerals are defined as “Earth materials that are utilised because of their characteristic physical and /or chemical properties and not because their metal content and which are not energy sources” (Christidis, 2011). In addition to this, industrial minerals are a source of non-metals or metals utilised in the industry because of their properties. Others are used as natural construction materials or to develop synthetic materials. Industrial minerals are versatile, and therefore it is common for a single type of mineral to serve several applications. It is also usual for different minerals to compete for the same application. An example of a commodity used in various applications is limestone, which can be used as filler and whiting material, in acid-water treatment and as a dimension stone. Examples of commodity competition for a particular application are the use of kaolin, calcite or talc as fillers in the paper industry, and the substitution of bentonite by palygorskite as drilling additives (Chang, 2002*a*,*b*; Christidis, 2011; Scott, 2011). Because of this, the mining industry is continuously seeking opportunities to substitute materials to ensure supply in case of shortage, to reduce costs or to develop new applications for emerging markets (Jeffrey, 2006).

Unlike the metal ores, in which the mineral concentrate determines the grade, the value of industrial minerals depends on the existence of a market for a particular mineral and on the facility to add value by tailoring the mineral properties to suit specific market needs (Christidis, 2011). The specifications can be set by the end-users, by national or international institutions, or by legislation. Highly specialised markets give more value to the commodities, although strict specifications often result in a decreased proportion of the ore that is suitable for such applications. In the mining value chain, that is to say, at the different stages and processes that a mining project undergoes to generate mineral products (Figure 1.1), the opportunities to add value to a commodity occur at the mineral deposit (prior to the resource extraction), during processing and at commercialisation (Harris, 2006). From these stages, practices that enable process optimisation and efficiency in the utilisation of the mineral resource can be implemented at mining and

mineral processing.

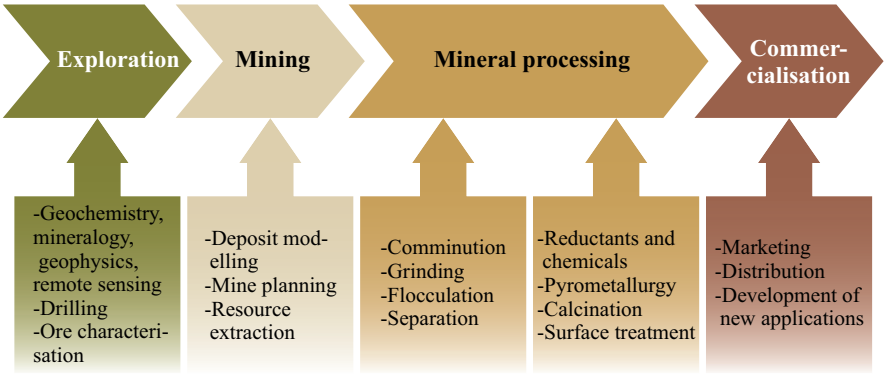

Figure 1.1: Stages of the mining value chain and activities followed at each stage.

The attributes of the resource determine the physical and chemical characteristics of the industrial minerals, and it dictates the extent of the processing and beneficiation. The processing strategies tailor the physical and chemical properties of the mineral by means of, for example, crushing, milling, flocculation, calcination or surface treatment. More complex processes add more value to the industrial mineral products, as illustrated in Figure 1.2. Processes that result in an actual transformation of the raw material and generation of sophisticated products, as is the case in calcination or surface treatment, add value considerably. However, the use of these methods is also very demanding since they involve a high consumption of other resources such as water or energy (Harris, 2006).

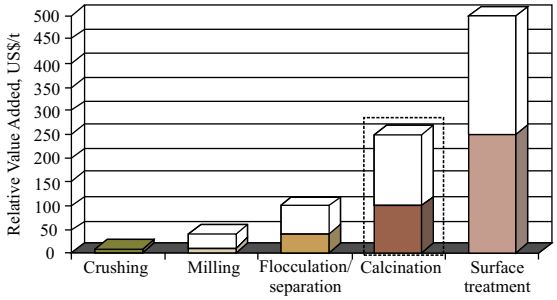

Figure 1.2: Relative value-added contribution from the processing of industrial minerals by stage. Unshaded portions of bars represent potential ranges of value that can be obtained from each process (Reproduced after Harris (2006), with permission). Calcination is highlighted as is the focus of this study.

There is a vast amount of industrial minerals and even a more substantial amount of products derived from them. Industrial minerals can range from single mineral specimens such as diamond and gypsum, to rocks such as bauxite and kaolin. The products derived from them include, but are certainly not limited to, filters, fillers, coatings, abrasives, refractories, pigments and construction materials. As a consequence, there are also multiple classification schemes based on the type of stakeholders, from academics to

industry and investors. Nevertheless, since the driving force in the industrial minerals sector is the market, the most used classifications are based on the end-used applications. However, for the study of industrial minerals, the fundamental aspects regarding the geology and mineralogy of the deposits and the commodities should always be taken into account (Scott, 2011).

Following the end-use applications, Harris (2006) classified the industrial minerals into chemical and physical. The chemical industrial minerals are those that are a source of specific chemical elements or compounds. In contrast, physical industrial minerals are those that have particular properties that enhance the performance of the end-product. This group is further classified into structural, performance, process aids, and speciality minerals (Table 1.1). The last three generally require advanced processing strategies to meet the market specifications. The performance and speciality minerals are those used as additives to improve the characteristics of certain compounds. They are commonly used as, but not limited to, fillers, coatings and extenders. Speciality minerals, although small in volume have the highest added value since they are the most specialised. Process aids support processes such as filtration and absorption.

Table 1.1: Types of physical industrial minerals (Modified after Harris (2006)). The minerals in bold are the subject of this Thesis

Market segment	**Function**	**Major industrial minerals**
Structural minerals	Aggregates	Sand and gravel, crushed stone
Performance minerals	Additives that improve the characteristics of a compound	**Kaolin**, calcium carbonate, talc, mica
Speciality minerals	Additives that improve the characteristics of a compound. Highly specialised	Speciality clays (smectite, palygorskite, **kaolin**), calcium carbonate
Process aids	Materials that facilitate the achievement of the desired results in a process (e.g. filtration, absorption)	**Diatomite**, **perlite**, palygorskite, bentonite, barite

One of the processing strategies used to tailor the properties of minerals used in speciality and performance minerals and process aids is calcination. In this process, also known as thermal treatment, the mineral is heated to high temperatures to modify the structure of the mineral, altering its inherent properties (Pruett and Pickering, 2006). In speciality and performance minerals, the thermal treatment seeks to modify properties such as chemical reactivity, cation exchange capacity, colour or hardness of industrial minerals such as clays or limestone (Almenares et al., 2017; Chandrasekhar and Ramaswamy, 2002; Krishnan et al., 2019; Teklay et al., 2014). In process aids for filtration and absorption, the aim is to modify the pore structure and the particle size of minerals as in the case of diatomite and perlite (Barker and Santini, 2006; Ediz et al., 2010; Martinovic et al., 2006). In industrial processing plants, calcination is carried out in industrial furnaces or reactors of various designs. The process consumes large amounts of energy making it one of the highest operational expenses. Therefore, it is important that the systems have the capability to optimise the energy efficiency (Glass, 2016).

1.1.2. SUSTAINABILITY IN THE MINING AND PROCESSING OF INDUSTRIAL MINERALS

The focus of the industrial minerals sector in the last decade has been on the sustainable extraction and processing of the commodities . This trend is a response to the high energy costs (especially in sophisticated processes as calcination), diminishing water resources, and increased sensitivity towards environmental stewardship (Kogel et al., 2014). Many mineral companies have embraced the concept of sustainable development, defined by the Bruntland Comission (United Nations, 1987) as "development that meets the needs of the present without compromising the ability of future generations to meet their own needs". Furthermore, the international minerals community (ICMM, 2003) proposed a series of sustainable development principles which encourage the development of practices that aim to reduce the energy consumption, use of water, CO_2 emissions and generation of mineral waste, at the time that they improve mine safety and comply with health and environmental regulations. The sustainable development in mining aims not only to minimise the environmental impact but also to promote long-term economic prosperity and maximise the use of mineral resources.

Kogel (2015) presented resource efficiency as one of the pillars of sustainable development in mining. For achieving resource efficiency, it is necessary to implement improved mining and processing methods. Buxton and Benndorf (2013) stated that on-site material characterisation using sensor-derived data enables the optimisation of the processes that take place along the mining value chain. It does so by, among others, discriminating ore from waste, ensuring the quality and homogeneity of the material that is fed at different stages of the mining and processing and by ensuring adherence of the product to quality specifications. One of the sensor technologies that has proven to be successful in the on-site characterisation of material at different stages of the mining value chain is infrared (IR) spectroscopy (Dalm et al., 2017; Haavisto and Hyötyniemi, 2011; Kirsch et al., 2018).

Since the end-use properties drive the mining and processing of industrial minerals, one of the biggest challenges to improve resource efficiency and foster sustainable development relies on the assurance of the accomplishment of such properties. For doing so, it is necessary to have the capability of detecting the factors that affect the end-use properties by using data derived from, for example, infrared sensors. This information is needed for increasing the ability at the mine or processing plant of timely performing any operational changes required to generate industrial mineral products according to the desired properties.

1.2. RESEARCH SCOPE AND APPROACH

This Thesis originated from the necessity of the mining industry for generating products derived from industrial minerals that meet the ever-demanding needs of the market and that comply with the challenges imposed by sustainable development. Among the plethora of industrial minerals, this work focuses on those that utilise calcination as an essential part of the process to generate performance and speciality minerals as well as process aids. This Thesis seeks to develop methods for the detection of factors that determine the quality parameters of industrial minerals by using data derived from infrared sensors that can be implemented in mining and process control.

1

For industrial minerals that undergo calcination as part of the processing, value-added as well as resource efficiency can be improved either at the deposit or at the calciner. To this end, this study focuses on the stages prior to the resource extraction, and pre- and post-calcination Figure 1.3.

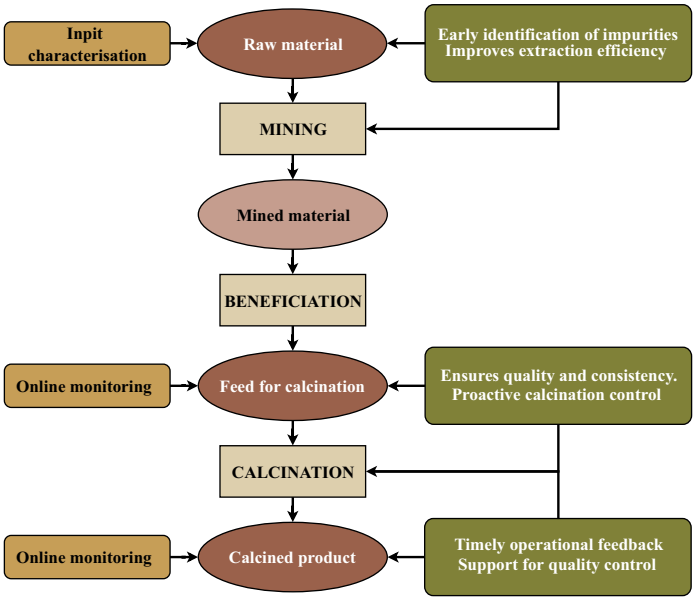

Figure 1.3: Schematic representation of the research approach.

The in-pit material characterisation will address the study of raw materials based on drill-cores, mince face and run-of-mine (ROM) samples aiming to identify the properties of the ore before mining. This study will create methods to detect the factors that reduce the quality of industrial mineral ores directly at the pit, enabling the early identification of the primary source impurities or other detrimental factors.

The study of the calcination stage will address the characterisation of the feed for calcination, that is to say, material that has been already refined through other beneficiation techniques, and the characterisation of the calcined product, namely material that has been subject to thermal treatment. For the feed for calcination, this study will generate infrared-based tools to monitor the quality and consistency of the feed for calcination, which are meant to facilitate proactive control of the calcination process. For the calcined product, this study will develop measurements that serve as a proxy for quality parameters of the final product, which will enable timely operational feedback, at the time that support quality control routines.

This work serves as a pilot study to explore the potential of using infrared-based characterisation in the mining and processing of calcined industrial minerals, opening the possibilities of extrapolating the generated outcomes to other commodities.

The present study is based on three industrial mineral commodities that are repre-

sentative of performance and speciality minerals as well as process aids and adsorbents. The case study for performance and speciality minerals is the kaolin that is extracted and processed in Cornwall and Devon (south-west England). The analyses for the kaolin case cover the mining and calcination stages. For the process aids for filtration and absorption, the perlite deposits in Zeytindağ (Turkey) and the diatomite deposits in Elche de la Sierra (Spain) were selected as case studies, covering only the mining stage. As a common factor, kaolin, perlite and diatomite have quality parameters related, but not restricted, to chemical inertness. Consequently, the factors that determine the quality of these minerals will focus on this particular aspect. Table 1.2 presents a general description of the kaolin, perlite and diatomite commodities[1].

Table 1.2: Mineral composition and trade-name of the industrial minerals that are subject of this study. The mineral names in bold are those that are essential to the commodity; trade-names in bold are the ones used in this work.

Industrial mineral	**Material and mineral composition**	**Trade name**
Kaolin	**Kaolinite**, muscovite, illite, biotite, quartz, feldspars	**Kaolin** **Calcined kaolin** Metakaolin China clay
Perlite	**Volcanic glass (opal)**, clay minerals, zeolites	**Perlite** Expanded perlite
Diatomite	**Opaline silica**, clay minerals, carbonates, evaporites	**Diatomite** Diatomaceous Earth (DE) Calcined DE

1.3. THESIS AT A GLANCE

To achieve the aims of this research, this Thesis is divided into four parts. Part I, the preamble, introduces the concepts and technologies that are the core of this work; Part II is based on a kaolin case study, as the example for the performance and speciality minerals; Part III is based on perlite and diatomite case studies, as examples of the process aids for filtration and absorption; Part IV, the epilogue, presents the general discussion, conclusions and recommendations from this research. A more detailed description of the structure of the Thesis and the contents of the individual chapters is given in Table 1.3, which presents an overview of their objectives, methods, main findings and conclusions.

Table 1.3: Overview of the thesis structure, presenting the objectives, methods, main findings and conclusions of every chapter. IR: infrared, PLS-R: partial least squares regression, SVR: support vector regression, PCA: principal component analysis. (Next page).

[1] In this Thesis, the mineral names follow the terminology of the Handbook of Clay Science (Bergaya and Lagaly, 2006), in which mineral names are in low case and the term metakaolinite is preferred over metakaolin

Part	Chapter	Objective	Methods	Main findings and conclusions
PART I PREAMBLE	Chapter 1 Introduction	To present the context of the research, its relevance and definition of terms. To state the research the scope and approach		
	Chapter 2 Sensor-based material characterisation	To review the importance of sensor technologies, with particular emphasis on infrared spectroscopy, in the mining industry for the real-time analysis of industrial minerals.	Literature review	
PART II PERFORMANCE AND SPECIALITY MINERALS	Chapter 3 Kaolin	To present kaolin as an important industrial mineral for performance and speciality applications and to review its properties, the mining and processing techniques that it undergoes, as well as its uses.	Literature review	
	Chapter 4 Infrared characterisation of the kaolin deposits in SW England	To present the kaolin deposit that serves as a case study, and to provide the infrared mineralogical characterisation of the ore with a focus on the detection of factors that are detrimental for the quality of the ore.	Literature review Infrared spectroscopy (point data and hyperspectral images) Samples: rocks and drill cores	Despite its exceptional quality, the kaolin ore has iron impurities that are detected in the IR spectra. Kaolinite mineral has a high crystallinity that can be measured using the IR spectrum. The IR data provides information about the content, quality and distribution of the ore. This information has implications for mine planning and beneficiation.
	Chapter 5 Characterisation of the kaolin calcination process using infrared spectroscopy	To assess the suitability of IR spectroscopy as a potential technique for the online characterisation of the calcination of kaolin	Infrared spectroscopy X-ray diffraction Thermogravimetry analysis Samples: kaolin powders calcined in the laboratory at different temperatures	The calcination reaction can be entirely characterised using IR spectroscopy by using the kaolinite and water features. There is a correlation between the standard for quality control, the mineral composition of the material and the presence of water; the later can be detected in the IR spectra. There is potential for the use of IR technology for the online measurement of the kaolin calcination reaction.
	Chapter 6 Infrared-based prediction of soluble Al_2O_3 for product quality control	To use multivariate calibration methods to predict the soluble Al_2O_3 content in calcined kaolin.	Infrared spectroscopy Multivariate calibration methods (PLS-R and SVR) Samples: final products obtained from a processing plant	Soluble Al_2O_3 can be inferred from the IR spectrum given its correlation with γ-alumina and water. Multivariate calibration using SVR methods can predict the soluble Al_2O_3 content with an error that is acceptable for monitoring purposes. The SVR model can detect changes in the quality of the production.
	Chapter 7 Framework for monitoring and control of the production of calcined kaolin	To propose an infrared-based framework for online monitoring and quality control of the kaolin feed and the calcination products.	Infrared spectroscopy Spectral indices and SVR multivariate calibration Samples: Feed and products obtained from the production stream at a processing plant	The characterisation of the feed for calcination ensures consistency of the throughput and enables proactive control of the calciner. A combination of two SVR models can be used as a proxy for the quality standard. The results of the prediction models can be integrated into the control strategy of the calciner and influence the settings for feed rate and temperature.

Part	Chapter	Objective	Methods	Main findings and conclusions
PART III PROCESS AIDS: FILTERS AND ABSORBENTS	Chapter 8 Perlite and diatomite	To present perlite and diatomite as the major industrial minerals used as process aids, particularly as filters and absorbents, and to review their properties, the mining and processing techniques that they undergo, as well as their uses.	Literature review	
	Chapter 9 Infrared detection of the variability in perlite ore that influences the quality of its calcined products	To identify the variability in the perlite ore that is related to the generation of fine particles and to the presence and concentration of heavy metals with a tool that can be used routinely in the pit.	Infrared spectroscopy Particle size analysis X-ray fluorescence Multivariate statistics (PCA) and spectral indices Samples: Run-of-mine samples and rocks	The variations in the perlite ore are related to geological processes. They allow the prediction of the generation of fine particles during processing, as well as the concentration of chemical impurities. These variations are linked to the dominant mineralogy in the ore, which can be determined from the IR spectra. The method for the determination of the dominant mineralogy can be used in the pit.
	Chapter 10 Infrared determination of the quality of carbonate-rich diatomite ores	To identify the types of carbonate impurities present in diatomite ore and their associations with the silica phase.	Infrared spectroscopy Environmental scanning electron microscopy X-ray fluorescence Multivariate statistics (PCA) Samples: Run-of-mine samples (rocks, rock chips and powders)	The use of IR spectroscopy enables the identification of the type of carbonates present in the diatomite ore. It also enables the classification of the quality grade of the ore based on the carbonate content. The amount of carbonate is related to the way it is associated with the silica phase. The results are useful to optimise the beneficiation strategies of the diatomite ore.
PART IV EPILOGUE	Chapter 11 Discussion	To provide a general discussion about the key findings in the thesis, indicating the links between the research objectives and the achieved results.		
	Chapter 12 Conclusions and recommendations	To present the general conclusions of the Thesis, as well as the recommendations derived from it.		

1

REFERENCES

Almenares, R. S., Vizcaíno, L. M. , Damas, S. , Mathieu, A. , Alujas, A. and Martirena, F. (2017), 'Industrial calcination of kaolinitic clays to make reactive pozzolans', *Case Studies in Construction Materials* **6**, pp. 225–232. DOI: 10.1016/j.cscm.2017.03.005

Barker, J. M. and Santini, K. (2006), Perlite, *in* J. E. Kogel, N. C. Trivedi, J. M. Barker and S. T. Krukowski, eds, 'Industrial Minerals and Rocks', 7th edn, Society for Mining, Metallurgy, and Exploration, pp. 685–702.

Bergaya, F. and Lagaly, G. (2006), General introduction: Clays, clay minerals, and clay science, *in* F. Bergaya, B. K. Theng and G. Lagaly, eds, 'Handbook of Clay Science', Vol. 1 of *Developments in Clay Science*, Elsevier, Chapter 1, pp. 1–18. DOI: 10.1016/S1572-4352(05)01001-9

Buxton, M. and Benndorf, J. (2013), The use of sensor derived data in optimization along the mine-value-chain: An overview and assessment of techno-economic significance, *in* 'Proceedings of the 15th International ISM Congress, Aachen, Germany', pp. 324–336.

Chandrasekhar, S. and Ramaswamy, S. (2002), 'Influence of mineral impurities on the properties of kaolin and its thermally treated products', *Applied Clay Science* **21**(3-4), pp. 133–142. DOI: 10.1016/s0169-1317(01)00083-7

Chang, L. (2002*a*), Diatomite, *in* S. L. Snavely, ed., 'Industrial mineralogy: materials, processes and uses', Prentice Hall, Chapter 10.

Chang, L. (2002*b*), Perlite and pumice, *in* S. L. Snavely, ed., 'Industrial mineralogy: materials, processes and uses', Prentice Hall, Chapter 28.

Christidis, G. E. (2011), Industrial Minerals, *in* G. E. Christidis, ed., 'Advances in the characterization of industrial minerals', Vol. 9 of *European Mineralogical Union notes in mineralogy*, Mineralogical Society of Great Britain and Ireland, Chapter 1, pp. 1–12. DOI: 10.1180/emu-notes.9.1

Dalm, M., Buxton, M. W. N. and van Ruitenbeek, F. J. A. (2017), 'Discriminating ore and waste in a porphyry copper deposit using short-wavelength infrared (SWIR) hyperspectral imagery', *Minerals Engineering* **105**, pp. 10–18. DOI: 10.1016/j.mineng.2016.12.013

Ediz, N., Bentli, İ. and Tatar, İ. (2010), 'Improvement in filtration characteristics of diatomite by calcination', *International Journal of Mineral Processing* **94**(3-4), pp. 129–134. DOI: 10.1016/j.minpro.2010.02.004

Glass, H. J. (2016), Geometallurgy – Driving innovation in the mining value chain, *in* 'The Third AusIMM International Geometallurgy Conference (GeoMet) 2016', Vol. 3, The Australasian Institute of Mining and Metallurgy: Melbourne, pp. 21–28.
URL: *https://www.ausimm.com.au/publications/epublication.aspx?ID=16947 [Accessed June 2018]*

Haavisto, O. and Hyötyniemi, H. (2011), 'Reflectance spectroscopy in the analysis of mineral flotation slurries', *Journal of Process Control* **21**, pp. 246–253. DOI: 10.1016/j.jprocont.2010.10.015

Harris, T. (2006), Applying industrial marketing concepts to industrial minerals, *in* J. E. Kogel, N. C. Trivedi, J. M. Barker and S. T. Krukowski, eds, 'Industrial Minerals and Rocks', 7th edn, Society for Mining, Metallurgy, and Exploration, pp. 61–65.

ICMM (2003), ICMM Sustainable development framework, Technical Report C 020/290503, International Council on Mining and Metals.
URL: *https://www.iucn.org/sites/dev/files/import/downloads/minicmmstat.pdf [Accessed March, 2019]*

Jeffrey, K. (2006), Characteristics of the industrial minerals sector, *in* J. E. Kogel, N. C. Trivedi, J. M. Barker and S. T. Krukowski, eds, 'Industrial Minerals and Rocks', 7th edn, Society for Mining, Metallurgy, and Exploration, pp. 3–6.

Kirsch, M., Lorenz, S. , Zimmermann, R. , Tusa, L. , Möckel, R. , Hödl, P. , Booysen, R. , Khodadadzadeh, M. and Gloaguen, R. (2018), 'Integration of terrestrial and drone-borne hyperspectral and photogrammetric sensing methods for exploration mapping and mining monitoring', *Remote Sensing* **10**(9), pp. 1366.1–1366.31. DOI: 10.3390/rs10091366

Kogel, J. E. (2015), Sustainable development and the minerals industry, *in* J. W. Fergus, B. Mishra, D. Anderson, E. A. Sarver and N. R. Neelameggham, eds, 'Materials and Resources II', Vol. II of *Engineering solutions for sustainability*, The minerals, metals & materials society (TMS) – Springer, Cham, pp. 25–34.

Kogel, J. E., Trivedi, N. and Herpfer, M. A. (2014), 'Measuring sustainable development in industrial minerals mining', *International Journal of Mining and Mineral Engineering* **5**(1), pp. 4–18. DOI: 10.1504/ijmme.2014.058921

Krishnan, S., Emmanuel, A. C. , Shah, V. , Parashar, A. , Mishra, G. , Maity, S. and Bishnoi, S. (2019), 'Industrial production of limestone calcined clay cement: experience and insights', *Green Materials* **7**(1), pp. 15–27. DOI: 10.1680/jgrma.18.00003

Martinovic, S., Vlahovic, M. , Boljanac, T. and Pavlovic, L. (2006), 'Preparation of filter aids based on diatomites', *International Journal of Mineral Processing* **80**(2-4), pp. 255–260. DOI: 10.1016/j.minpro.2006.05.006

Pruett, R. J. and Pickering, S. M. (2006), Kaolin, *in* J. E. Kogel, N. C. Trivedi, J. M. Barker and S. T. Krukowski, eds, 'Industrial Minerals and Rocks', 7th edn, Society for Mining, Metallurgy, and Exploration, pp. 383–400.

Scott, P. W. (2011), The geological setting for industrial mineral resources, *in* G. E. Christidis, ed., 'Advances in the characterization of industrial minerals', Vol. 9 of *European Mineralogical Union notes in mineralogy*, Mineralogical Society of Great Britain and Ireland, Chapter 2, pp. 13–34. DOI: 10.1180/emu-notes.9.2

Teklay, A., Yin, C. , Rosendahl, L. and Bøjer, M. (2014), 'Calcination of kaolinite clay particles for cement production: A modeling study', *Cement and Concrete Research* **61-62**, pp. 11–19. DOI: 10.1016/j.cemconres.2014.04.002

United Nations (1987), Our common future, General Assembly Resolution 42/187, The World Commission on Environment and Development.
URL: *http://www.un-documents.net/our-common-future.pdf [Accessed March, 2019]*

2

SENSOR-BASED MATERIAL CHARACTERISATION

This chapter reviews the importance of sensor technologies, with particular emphasis on infrared spectroscopy, in the mining industry for the real-time analysis of industrial minerals.

Sensor-based characterisation of minerals is increasingly becoming more widespread in the minerals industry. The implementation of sensor technologies that permit the generation of real-time data can significantly support mining and processing activities. Among the different technologies developed with this purpose, infrared spectroscopy is one of the most used ones. The scientific and technological developments have made it possible to use infrared technologies for the proximal and remote detection and characterisation of minerals. The benefits of its analytical capabilities include the use of different spectral ranges allow the identification of a large variety of minerals and the determination of characteristics such as crystal structure and composition. Many instruments have been designed with features that allow them to be operational in different environments.

2.1. SENSOR APPLICATIONS IN REAL-TIME CHARACTERISATION

In the minerals industry, the need for optimisation of the processes and the assurance of safety has promoted the implementation of (semi-)automated systems for material characterisation, sorting and process control, among others. In this scenario, the utilisation of sensors that detect the mineral content of ore and waste products directly at the mine site or the processing plant, in a non-invasive manner and that deliver information in real-time has become a matter of growing interest.

The requirements for such sensors, as estated by Buxton and Benndorf (2013) and Dalm et al. (2019) (*in* Dalm (2018)), include the capacity of detecting the properties of the material that are relevant for the process or that hold a relationship with the targeted properties. In addition, the retrieved information must aid in the development of prediction models, supported by historical data, which have potential use for feedforward control and optimisation of the processes. Furthermore, the data acquisition should occur in "real-time ", that is to say, in a way that the information gathered and its interpretation can be used in a timely manner for decision making. Overall, the use of sensor technologies must lead to the improvement of the economics of the mining value chain.

There are some critical points along the mining value chain where the utilisation of sensors could bring the maximum benefit to the process (Buxton and Benndorf, 2013). These are resource definition, mine planning and grade control, sorting, pre-processing and quality control. The specific type of information and the time-scale that defines the real-time concept vary at each of these points. For example, for resource definition and mine planning, only general mineralogy of the ore might be required and real-time could be defined in the scale of hours. In contrast, sorting, pre-processing and quality control would entail the detection of more specific chemical or physical properties, and the real-time requirement could be in the scale of minutes or even seconds. In the industrial minerals sector, the definition of the properties of interest and the economic aspects depend directly on the targeted markets.

In general, the primary objective of the use of sensors along the value chain is:

- Discriminate the ore (e.g. based on grade, chemistry, mineralogy) from sub-economic waste
- Reduce the variability of the feed

- Enable the generation of a homogeneous product and ensure the adherence to quality specifications
- Provide reconciliation data for real-time monitoring and control
- Reduce the need for off-line analyses

Sensors used for material characterisation are mostly based on the interaction between the analysed material with the electromagnetic radiation. The differences in energy along the electromagnetic spectrum and the type of interaction enable the detection of different material properties. Dalm et al. (2019) (*in* Dalm (2018)) reviewed the opportunities for sensor technologies in (potential) applications in the mining industry. Among them, infrared reflectance (IR) spectroscopy was identified as the technique with the broadest scope for utilisation in the minerals industry, not only for its capabilities on mineral identification but also due to its technological maturity. Based on these considerations, IR spectroscopy was selected as the main analytical technique used in this work. Consequently, this discussion will continue on the characteristics of IR spectroscopy and its use on the study of industrial minerals.

2.2. INFRARED SPECTROSCOPY IN THE CHARACTERISATION OF INDUSTRIAL MINERALS

Infrared reflectance spectroscopy has become a popular technique among geochemists and mineralogists since it is relatively rapid, inexpensive, and requires little or no sample preparation. As a consequence, IR is becoming increasingly established in the mining industry in applications such as mining monitoring (Kirsch et al., 2018), ore sorting (Dalm et al., 2017) and characterisation of slurries (Haavisto and Hyötyniemi, 2011). Infrared is used to determine the mineral composition and bonding of the molecules that constitute them. This makes possible the identification of minerals based on their functional groups, as is the case of, for example, clay minerals (OH), carbonate minerals (CO_3) and silicates (SiO_4) (Farmer, 1974*a*) . Infrared spectroscopy is also used in the determination of the crystal structure and reactivity of the minerals. With this information, it is possible to define algorithms for different applications. The enhanced sensitivity of modern spectrometers and the versatility of the sampling capabilities have not only facilitated the development of laboratory and field instruments but also has opened the possibility of making direct links between these environments (Madejová et al., 2011).

Depending on the application and instrumentation, the IR spectrum is recorded in frequency or wavelength units. For laboratory applications, frequencies are typically expressed in wavenumbers (cm^{-1}); whereas for remote sensing, hand-held and online applications, it is common to use wavelength expressed in micrometres (μm). For convenience in instrumentation and sampling, the IR spectrum is split into ranges depending upon the application field, likewise the usage of the units. Since the scope of this work is towards mining and processing on-site applications, the remote sensing, hand-held and online convention is used. In this sense, the units appear in wavelengths, and the spectral ranges are defined as Visible – Near Infrared (VNIR), Short-Wave Infrared (SWIR), Mid-Wave Infrared (MWIR) and Long-Wave Infrared (LWIR). Table 2.1 presents the wavelength and wavenumber equivalent for these spectral ranges.

Table 2.1: Equivalent wavelengths and wavenumbers of the main spectral ranges used in this work (Based on Gupta (2003) and Hackwell et al. (1996))

Spectral absorption band or range	**Wavelength** (μm)	**Wavenumber** (cm^{-1})
VNIR range	0.35–1.00	28 571–10 000
SWIR range	1.00–2.50	10 000–4000
MWIR range	2.50–7.00	4000–1429
LWIR range	7.00–16.00	1429–625

2.2.1. PRINCIPLES OF INFRARED SPECTROSCOPY

Spectroscopy is the study of the interaction between matter and electromagnetic radiation as a function of the wavelength. Such interaction can occur as reflectance, absorption or emission. Reflectance covers the portion of the energy that bounces back to the medium, absorption applies to the energy that the sample retains, and emission refers to the energy emitted by a material that is in thermal equilibrium with a heat source. Since the frequency, intensity and width of the signals are responsive to the atomic structure and to the composition of the material, the information derived from these energy interactions is, in general terms, of the same nature (Balan and Kloprogge, 2017). However, the amount of energy available, as well as the geometry of the reflectance mode, favours its use in the development of IR instrumentation, particularly in the analysis of powders and in remote sensing applications.

The different signals generated in the electromagnetic spectrum are a response of the so-called electronic and vibrational processes. In the electronic processes, as explained by Hunt (1977) and Clark (1999), the reponse signals are produced by changes in the position of the electrons either inside an ion among orbital levels, or by inter-element transitions in transition metals. Depending on the nature of the response signal, the electronic processes can be described as crystal field effects, charge transfer, conduction bands or colour centres. The response signals have characteristical high energy, low wavelength and broad features in the VNIR range.

The vibrational processes are the product of the spring-like behaviour of the molecular bonds, which can contract and stretch making the entire system vibrate. The frequency and intensity of the vibration is a function of the strength of the molecular bond and the mass of the elements in the molecule (Clark, 1999). The main vibration modes are called fundamentals, which can be classified as lattice modes if they refer to entire molecular groups in respect to the crystal lattice, or internal modes if they are related to isolated molecules. These can be internal stretching modes when related to the bond length, or internal bending modes when related to the bond angle (Madejová et al., 2011). Weaker secondary excitations occur as multiples of the fundamental vibrations. If the new vibration involves multiples of a single fundamental mode, it is known as an overtone; if it involves different fundamental modes, it is called combination tone.

The fundamental vibrations produced by minerals occur in the LWIR and MWIR ranges. Most of them are a consequence of the metal–oxygen (M–O) stretching modes and the metal–hydroxyl (M–OH) bending and lattice modes. The overtones and combination tones are strongly present in the SWIR range, mainly when they involve OH groups. All these vibrations make possible the identification of a significant portion of the mineral

species (Hunt, 1977; Madejová et al., 2011). Because of their nature, the vibrational modes are useful in the investigation of structural modifications in the crystal lattice of minerals, such as phase transformations or variations in their composition (Balan and Kloprogge, 2017).

2.2.2. INFRARED SPECTROSCOPY AND INDUSTRIAL MINERALS

In the study of industrial minerals, infrared spectroscopy provides information about the structure and reactivity of silicates, carbonates, sulphates, oxides and clay minerals (Farmer, 1974*b*; Hunt, 1977; Madejová et al., 2017; Schroeder, 2002). Most of the work has used laboratory data, which focuses in the MWIR and LWIR ranges. However, given the success in the use of field data and SWIR spectra in the study of alteration minerals for metallic ores, there is an increasing interest in using a similar approach for industrial minerals (Thompson et al., 1999). Figure 2.1 summarises the position of the main spectral bands used for the identification of the industrial minerals that appear in this thesis along with some other minerals commonly associated with them. Some of the spectral features in the LWIR range are not clear due to the reststrahlen effect (see Section 2.2.3).

Clay minerals are by far the biggest group of industrial minerals. In Figure 2.1 examples of kaolinite, muscovite, illite and montmorillonite are presented. In these phyllosilicates, the fundamental vibrations in the MWIR and LWIR ranges correspond to the Al–O and Si–O stretching modes around 10.0 µm, the Al–OH bending modes near 11.0 µm and the OH stretching modes around 2.7 µm. In the SWIR range, the Al–OH and OH vibrations generate combination tones at 2.2 µm and OH overtones at 1.4 µm. The exact location of these bands depends on the type of clay as well as its structure and composition (e.g. presence of Fe–OH or Mg–OH bonds). Water-bearing minerals, such as montmorillonite, have more pronounced OH stretching bands and a distinctive 1.9 µm feature typical of molecular water.

In tectosilicates, such as opal, quartz or plagioclase, the main features are due to the T–O and TOT vibrations around 9.0 µm to 10.0 µm and 12.0 µm to 14.0 µm, respectively, where T is the tetrahedrally coordinated ion (Al or Si). These features do not have overtones and, therefore, are not detectable in the SWIR range. In the case of opal, the presence of water leads to the occurrence of silanol groups (Si–OH), with a fundamental Si–OH bending vibration around 10.2 µm, and its respective overtone in the SWIR at 2.2 µm. Additionally, opal presents characteristic water features at 6.1 µm and from 2.6 µm to 3.0 µm, with the respective overtones and combinations in the SWIR range.

In carbonates such as calcite, the CO in-plane and out-of-plane bending modes generate vibrations near 14.0 µm and 11.0 µm. The respective overtones and combinations in the SWIR occur from 2.3 µm to 2.5 µm. The exact location of these bands depends on the presence of Ca or Mg, which allows the distinction between types of carbonate.

2.2.3. INFRARED INSTRUMENTATION FOR REAL-TIME APPLICATIONS

The recent technological advances and the growing demand in the application of IR spectroscopy have increased the affordability of IR instruments. The technological improvements are especially moving towards analysing the sample “as is”, minimising or avoiding any sample preparation and shortening the time required for recording of the spectra (Chryssikos and Gates, 2017).

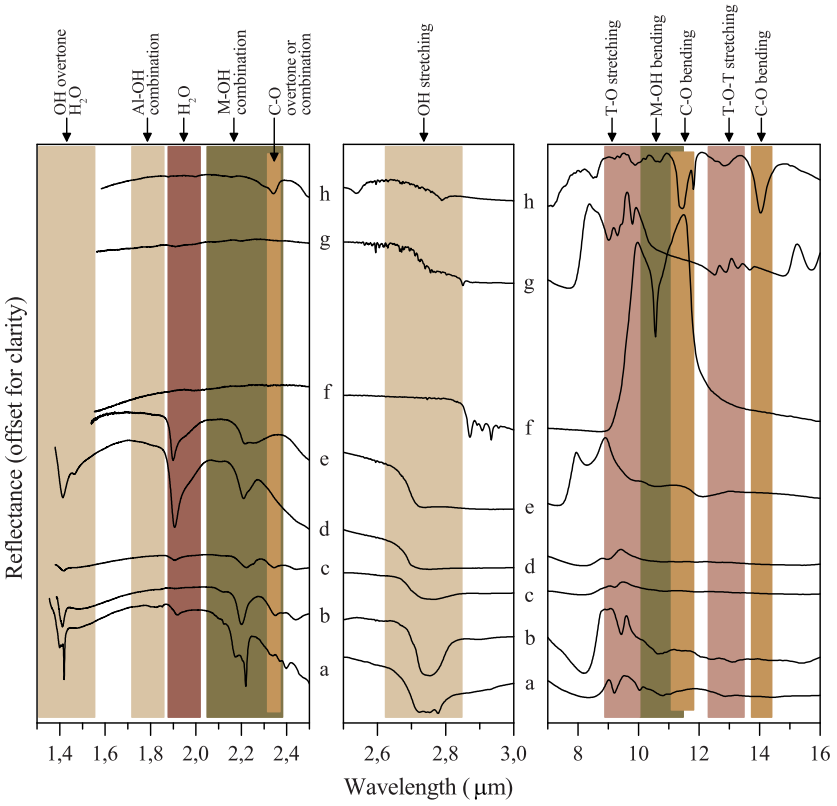

Figure 2.1: Major spectral absorption bands of some industrial minerals (**a**) kaolinite, (**b**) muscovite, (**c**) illite, (**d**) montmorillonite, (**e**) opal, (**f**) quartz, (**g**) Na-plagioclase, (**h**) calcite. Colour code: OH vibrations, M–OH vibrations, C–O vibrations, T–O vibrations (T = Al or Si), H–O–H vibrations. Spectra taken from Kokaly et al. (2017).

The reflectance instruments, depending on the mode of spectral collection, can be either dispersive IR or Fourier Transform IR (FTIR) (Madejová et al., 2011; Saptari, 2004). The dispersive IR instruments produce spectra by optically dispersing the detected energy into spectral components using a prism or grating. They typically record the spectra in wavelength units (nm or μm). In contrast, FTIR instruments use an interferometer between the source of energy and the detector. Such interferometer modulates the reflected energy and increases the speed of the scanning process, improving the quality of the spectrum, which is recorded in frequency units (cm^{-1}). Historically, dispersive IR has been used to develop remote sensing instruments, whereas FTIR has been preferred for laboratory instruments.

Different modes of analyses are possible depending on the recording geometry of the instruments. According to King et al. (2004), the most frequently used geometries for geological applications are Attenuated Total Reflectance (ATR), Directional-Hemispherical Reflectance (DHR), specular reflectance and diffuse reflectance.

- Attenuated Total Reflectance is perhaps the most used method for laboratory characterisation. The ATR makes use of a special prism to produce internal reflections from the surface of a given material. By making full contact with the sample surface, it measures a wave which amplitude decreases with distance, generally recorded in the MWIR and LWIR ranges.

- Directional-Hemispherical Reflectance is mostly used to collect scattered energy integrating all reflection directions over a complete hemisphere. For acquiring this spectrum, an integrating sphere coated with a surface that is diffusely reflective to IR radiation is commonly used. The spectrum is typically recorded in the MWIR and LWIR ranges. However, its quality depends on the particle size of the samples (Salisbury and Wald, 1992). Notably, the DHR spectrum is affected by the transparency features in the long wavelength region, as a consequence of the high volume scattering due to the small particle size (Cooper et al., 2002).

- Specular reflectance, also known as bidirectional or external reflectance, uses an incident IR beam at an air/sample interface; the intensity of the reflected beam depends on the direction of the incident energy and the surface characteristics of the sample. The bidirectional reflectance mode is preferred in remote sensing, hand-held and on-site applications the VNIR and SWIR ranges.

- Diffuse reflectance measures the scattered and reflected light in a diffuse manner, especially from loose powders, requiring minimum or no sample preparation. It differs from DHR in that it does not make use of an integrating sphere, but a diffuse reflectance accessory. The instrument can also integrate an interferometer, in which case FTIR spectra are recorded, and it is known as DRIFT spectroscopy. The reflection and refraction of the particles in different directions enhance the intensity of weak spectral bands, particularly in the SWIR and MWIR ranges. However, this enhancement overwhelms the response signal of already strong bands in the LWIR range due to specular distortions and high volume scattering, in the same fashion as in the DHR geometry. This phenomenon is known as the reststrahlen effect, which generates the so-called reststrahlen bands at wavelengths around 10 μm (Cooper

et al., 2002). Examples of this effect are the reststrahlen bands of quartz visible in Figure 2.1. The effect can be corrected by using, for example, KBr pellets, but it would be detrimental for real-time applications.

The potential applications of IR instruments also depend on the type of sampling needed to analyse a certain material, that is to say, the position of the sample regarding the spectrometer. The instruments that require internal sampling are only suitable for laboratory applications, whereas instruments that use external sampling can serve either laboratory or field applications. The accessories that allow external sampling are exclusive for specular and diffuse reflectance instruments; these include integrating spheres, optical fibre and external illumination heads (Chryssikos and Gates, 2017). The design of these instruments is driven by the need of having robust systems with a minimum amount of moving parts. For this reason, dispersive instruments (without interferometers) are preferred for the developing of field applications. The reduced quality of the spectra generated by the lack of an interferometer is compensated by targeting specific ranges of the spectrum, making possible to tune the resolution and the signal to noise ratio. Most of these instruments work in the VNIR and SWIR ranges.

Regarding the type of sample required for the spectral analyses, some of the instruments that use internal sampling also require the preparation of KBr pellets or the use of thin films to enhance the signal, particularly in the MWIR and LWIR ranges. Other instruments with internal sampling allow instead the use of pressed powders. The instruments that work with external sampling enable not only the analysis of powders but also of solids, which in the case of mineral and geological permits the study of whole rocks. Powder samples have the advantage of maximising the amount of reflected energy and the used of homogenised material that is representative of a larger volume of samples. Instruments designed to be used in field applications allow the use of samples with little or no need of sample preparation, that is to say, powders and solids. In these cases, the spectral response can vary according to samples characteristics such as grain size, surface roughness and porosity (Rost et al., 2018; Salisbury and Wald, 1992).

Spectrometers such as the pioneer Portable Infrared Mineral Analyser –PIMA– (Integrated Spectronics Pty. Ltd) or the Analytical Spectral Devices –ASD– FieldSpec (Malvern Panalytical) have been used since the 1990's and are nowadays well known as an important mineral characterisation tool for geologists and mineralogists (Thompson et al., 1999). These are dispersive instruments that record point data using specular reflectance in the VNIR and SWIR ranges; their use focuses on the detection of alteration minerals, particularly clays. Following the same principle, there has been significant development of hyperspectral imaging systems for the analysis of drill cores and hand samples. Examples of this technology are the SisuROCK hyperspectral core logger (SPECIM) (SPECIM, 2015) and the Hylogger system (CSIRO) (Schodlok et al., 2016). Recent technological developments have made possible the use of FTIR spectrometers in portable devices, extending the measurement capabilities to the MWIR and LWIR ranges, which enable the detection of a bigger suite of minerals.

In this work, different spectrometers were used with different purposes; a list of them and their main characteristics are summarised in Table 2.2 (point data) and Table 2.3 (imager).The preliminary mineral characterisation was generally carried out with laboratory spectrometers utilising different geometries and different parts of the infrared

spectrum. The assessment and development of methods for on-site and real-time application was done with portable and field instruments. The analysis of textures and mineral associations in whole rocks was done utilising hyperspectral imagers. Table 2.4 presents a comparison between the benefits and limitations on the use of these instruments. As stated previously, to facilitate the comparison and extrapolation of observations among instruments, in the following chapters of this Thesis, all the units were converted to wavelengths and expressed in micrometres (µm).

Table 2.2: Instrument specifications of the infrared spectrometers used in this work

Spectrometer	Manufacturer	Use	Recording units	Spectral range	Resolution	Set-up
Spectrum 100 FTIR	PerkinElmer	Laboratory	Wavenumbers	4000 to 600 cm^{-1} (2.50 to 16.67 µm)	2 cm^{-1}	ATR using a diamond crystal
Bruker Vertex 70 FTIR	Bruker	Laboratory	Wavenumbers	4000 to 625 cm^{-1} (2.50 to 16.00 µm)	4 cm^{-1}	Adapted for Directonal Hemispherical Reflectance (DHR) with an external integrating sphere(Hecker et al., 2011)
ASD FieldSpec	Malvern Panalytical	Field (Portable)	Wavelength (nanometers)	350 to 2500 nm (0.35 to 2.50 µm)	3 nm at 700 nm, 10 nm at 1400 nm and 2100 nm	Contact probe and internal light source for bidirectional reflectance
FTIR 4300	Agilent	Field (Handheld)	Wavenumbers	5200 to 600 cm^{-1} (1.90 to 16.67 µm)	4 cm^{-1}	Diffuse reflectance interface, coarse silver calibration

Table 2.3: Instrument specifications of the hyperspectral imager used in this work

Spectrometer	Manufacturer	Recording units	Range	Spectral resolution	Bands	Spatial resolution
SisuROCK spectral core logger	Specim	Wavelength (nm)	SWIR camera 900 to 2500 nm (0.9 to 2.5 µm)	10 nm	256	0.2 mm
			VNIR camera 400 to 1000 nm (0.4 to 1.0 µm	2.5 nm	96	0.09 mm
			RGB camera		3	0.16 mm

Table 2.4: Benefits and limitations of using the instrument listed in Tables 2.2 and 2.3

Spectrometer	Benefits	Limitations
Spectrum 100 FTIR	Spectral identification of fundamental vibrations. High spectral resolution, strong response in the LWIR range.	Weak response in the MWIR and SWIR ranges. Limited for the analysis of powder samples or pellets.
Bruker Vertex 70 FTIR	Spectral identification of fundamental vibrations. Useful for assessing the extrapolation of observations to field spectrometers (emulates the measuring conditions present in remote sensing applications.) It can be used for powder and solid samples. Good spectral resolution, strong response along the entire spectral range.	Presents excessive volume scattering in the LWIR range when dealing with powder samples. Requires a long measuring time for acquiring good quality spectra (40 minutes for 4096 scans).
ASD FieldSpec	Spectra of good quality acquired in a short period (approx. 1 minute for 50 scans). The spectral range is adequate for clay minerals, carbonates, oxides.	MWIR and LWIR ranges are not covered. Therefore, it is not possible to identify rock-forming minerals.
FTIR 4300	Spectra of good quality acquired in a short period (approx. 1 minute for 128 scans). Broader spectral range, especially with good quality spectra in the MWIR and LWIR. Allows the identification of fundamental and secondary absorptions that enable the identification of clay minerals, carbonates and rock-forming minerals. The instrument can be adapted to use also specular reflectance and ATR.	VNIR and part of the SWIR ranges are not available. Therefore, it is not suitable for the identification of oxides. The spectrum is noisy at the shortest wavelengths. In the diffuse mode, there is excessive volume scattering in the LWIR range when dealing with powder samples.
SisuROCK spectral core logger	Hyperspectral imaging of rocks samples (hand specimens and drill cores) with excellent spatial and spectral resolution. Spectral range suitable for the identification of alteration minerals.	Quality of the measurements affected by the characteristics of the sample (e.g. roughness, porosity)

REFERENCES

Balan, E. and Kloprogge, J. T. (2017), Theoretical aspects of infrared and raman spectroscopies, *in* W. P. Gates, J. T. Kloprogge, J. Madejová and F. Bergaya, eds, 'Infrared and Raman Spectroscopies of Clay Minerals', Vol. 8 of *Developments in Clay Science*, Elsevier, Chapter 2, pp. 6–33. DOI: 10.1016/B978-0-08-100355-8.00002-3

Buxton, M. and Benndorf, J. (2013), The use of sensor derived data in optimization along the mine-value-chain: An overview and assessment of techno-economic significance, *in* 'Proceedings of the 15th International ISM Congress, Aachen, Germany', pp. 324–336.

Chryssikos, G. D. and Gates, W. P. (2017), Spectral manipulation and introduction to multivariate analysis, *in* W. P. Gates, J. T. Kloprogge, J. Madejová and F. Bergaya, eds, 'Infrared and Raman Spectroscopies of Clay Minerals', Vol. 8 of *Developments in Clay Science*, Elsevier, pp. 64–106. DOI: 10.1016/b978-0-08-100355-8.00004-7

Clark, R. N. (1999), Spectroscopy of rocks and minerls, and principles of spectroscopy, *in* A. N. Rencz, ed., 'Remote Sensing for the Earth Sciences', 3rd edn, Vol. 3 of *Manual of Remote Sensing*, John Wiley and Sons, Chapter 1, pp. 3–58.

Cooper, B. L., Salisbury, J. W. , Killen, R. M. and Potter, A. E. (2002), 'Mid infrared spectral features of rocks and their powders', *Journal of Geophysical Research E: Planets* **107**(E4), pp. 1.1–1.17. DOI: 10.1029/2000JE001462

Dalm, M. (2018), Raw material beneficiation in mining – sensor-based sorting opportunities for hydrothermal ore deposits, PhD thesis, Delft University of Technology.
URL: *https://repository.tudelft.nl/islandora/object/uuid[Accessed November 2018]*

Dalm, M., Buxton, M. W. N. , Guatame-Garcia, L. A. , Desta, F. S. and van Ruitenbeek, F. J. A. (2019), *A review of sensors applicable to real-time raw material characterisation in mining.* Manuscript in preparation.

Dalm, M., Buxton, M. W. N. and van Ruitenbeek, F. J. A. (2017), 'Discriminating ore and waste in a porphyry copper deposit using short-wavelength infrared (SWIR) hyperspectral imagery', *Minerals Engineering* **105**, pp. 10–18. DOI: 10.1016/j.mineng.2016.12.013

Farmer, V. C. (1974*a*), *The infrared spectra of minerals*, Vol. 4 of *Mineralogical Society Monograph*, Mineralogical Society of Great Britain and Ireland. DOI: 10.1180/mono-4

Farmer, V. C. (1974*b*), The layer silicates, *in* V. C. Farmer, ed., 'The Infrared Spectra of Minerals', Vol. Monograph 4, Mineralogical Society, book section 15, pp. 331–364.

Gupta, R. P. (2003), Spectra of minerals and rocks, *in* R. P. Gupta, ed., 'Remote Sensing Geology', 2nd edn, Springer-Verlag Berlin Heidelberg, New York, pp. 33–52. DOI: 10.1007/978-3-662-05283-9

Haavisto, O. and Hyötyniemi, H. (2011), 'Reflectance spectroscopy in the analysis of mineral flotation slurries', *Journal of Process Control* **21**, pp. 246–253. DOI: 10.1016/j.jprocont.2010.10.015

Hackwell, J. A., Warren, D. W. , Bongiovi, R. P. , Hansel, S. J. , Hayhurst, T. L. , Mabry, D. J. , Sivjee, M. G. and Skinner, J. W. (1996), LWIR/MWIR imaging hyperspectral sensor for airborne and ground-based remote sensing, *in* 'SPIE 2819', Vol. 2819 of *Imaging Spectrometry II*, pp. 102–107. DOI: 10.1117/12.258057

Hecker, C., Hook, S. , van der Meijde, M. , Bakker, W. , van Werff, H. , Wilbrink, H. , van Ruitenbeek, F. , de Smeth, B. and van der Meer, F. (2011), 'Thermal infrared spectrometer for earth science remote sensing applications-instrument modifications and measurement procedures', *Sensors* **11**, pp. 10981–10999. DOI: 10.3390/s111110981

Hunt, G. R. (1977), 'Spectral signatures of particulate minerals in the visible and near infrared', *Geophysics* **42**, pp. 501–513. DOI: 10.1190/1.1440721

King, P. L., Ramsey, M. S. , McMillan, P. F. and Swayze, G. A. (2004), Laboratory Fourier Transform Infrared Spectroscopy methods for geologic samples, *in* P. L. King, M. S. Ramsey and G. A. Swayze, eds, 'Infrared spectroscopy in Geochemistry, Exploration

Geochemistry and Remote Sensing', Vol. 33 of *Short Course Series*, Mineralogical Association of Canada, Chapter 3, pp. 57–92.

Kirsch, M., Lorenz, S. , Zimmermann, R. , Tusa, L. , Möckel, R. , Hödl, P. , Booysen, R. , Khodadadzadeh, M. and Gloaguen, R. (2018), 'Integration of terrestrial and drone-borne hyperspectral and photogrammetric sensing methods for exploration mapping and mining monitoring', *Remote Sensing* **10**(9), pp. 1366.1–1366.31. DOI: 10.3390/rs10091366

Kokaly, Raymond F., Clark, Roger N. , Swayze, Gregg A. , Livo, K. Eric , Hoefen, Todd M. , Pearson, Neil C. , Wise, Richard A. , Benzel, William M. , Lowers, Heather A. , Driscoll, Rhonda L. and Klein, Anna J. (2017), 'USGS Spectral Library Version 7'.
URL: *https://speclab.cr.usgs.gov/spectral-lib.html [Accessed March 2018]*

Madejová, J., Balan, E. and Petit, S. (2011), Application of vibrational spectroscopy to the characterization of phyllosilicates and other industrial minerals, *in* G. E. Christidis, ed., 'Advances in the characterization of industrial minerals', Vol. 9 of *European Mineralogical Union notes in mineralogy*, Mineralogical Society of Great Britain and Ireland, Chapter 6, pp. 171–226. DOI: 10.1180/emu-notes.9.6

Madejová, J., Gates, W. P. and Petit, S. (2017), IR spectra of clay minerals, *in* W. P. Gates, J. T. Kloprogge, J. Madejová and F. Bergaya, eds, 'Infrared and Raman Spectroscopies of Clay Minerals', Vol. 8 of *Developments in Clay Science*, Elsevier, Chapter 5, pp. 107–149. DOI: 10.1016/b978-0-08-100355-8.00005-9

Rost, E., Hecker, C. , Schodlok, M. and van der Meer, F. (2018), 'Rock sample surface preparation influences thermal infrared spectra', *Minerals* **8**(11), pp. 475.1–475.21. DOI: 10.3390/min8110475

Salisbury, J. W. and Wald, A. (1992), 'The role of volume scattering in reducing spectral contrast of Reststrahlen bands in spectra of powdered minerals', *Icarus* **96**, pp. 121–128. DOI: 10.1016/0019-1035(92)90009-V

Saptari, V. (2004), Spectroscopy instrumentation, *in* J. A. R. Weeks, ed., 'Fourier Transform Spectroscopy instrumentation engineering', Vol. TT61 of *SPIE tutorial texts in optical engineering*, SPIE Publications, Chapter 1, pp. 1–9.

Schodlok, M. C., Whitbourn, L. , Huntington, J. , Mason, P. , Green, A. , Berman, M. , Coward, D. , Connor, P. , Wright, W. , Jolivet, M. and Martinez, R. (2016), 'HyLogger-3, a visible to shortwave and thermal infrared reflectance spectrometer system for drill core logging: functional description', *Australian Journal of Earth Sciences* **63**(8), pp. 929–940. DOI: 10.1080/08120099.2016.1231133

Schroeder, P. A. (2002), Infrared spectroscopy in clay science, *in* A. Rule and S. Guggenheim, eds, 'CMS workshop lectures', Vol. 11 of *Teaching clay science*, The Clay Mineral Society, Aurora, CO, pp. 181–206.

SPECIM (2015), 'Hyperspectral imaging in geology', Online.
URL: *http://www.specim.fi/hyperspectral-imaging-in-geology/ [Accessed July 2016]*

Thompson, A. J. B., Hauff, P. L. and Robitaille, A. J. (1999), 'Alteration mapping in exploration: Application of short-wave infrared (SWIR)spectroscopy', *SEG Newsletter* **1**(39), pp. 15–27.

II

PERFORMANCE AND SPECIALITY MINERALS

3

KAOLIN

This chapter presents kaolin as an important industrial mineral for performance and speciality applications, and reviews its properties, the mining and processing techniques that it undergoes, as well as its uses.

Parts of this chapter have been published in:
Guatame-Garcia, A., Buxton, M., Deon, F., Lievens, C. and Hecker, C. (2018). Toward an on-line Characterization of Kaolin Calcination Process Using Short-Wave Infrared Spectroscopy. *Mineral Processing and Extractive Metallurgy Review 39(6)*, 1-12. doi: 10.1080/08827508.2018.1459617.

Performance and speciality minerals are defined as industrial minerals that are engineered to provide a compound with the desired properties and performance, at the time that they reduce the costs for the compounds manufacture. Such compounds include but are not limited to rubber, paper, plastics, paints and coatings. Kaolin is one of the most commonly used minerals for performance and speciality applications. As performance mineral, kaolin is primarily used as a filler in paper and paints to improve their appearance and functionality, and in rubber and plastics to reduce surface reactivity and impart abrasion resistance. Speciality uses include applications in the pharmaceutical and cosmetic industries. Kaolin, as industrial mineral, is defined as a white or nearly white clay that comprises minerals from the kaolin group, being kaolinite the most abundant (Mortimer, 2001; Murray, 2006; Pruett and Pickering, 2006) . In the industry, the term "china clay" is often used to make reference to kaolin that contains well-ordered kaolinite (Christidis, 2011). The majority of the end-use applications require a refined kaolin product, which is produced by means of controlled mining and processing with strategies such as calcination (Kogel, 2014).

3.1. MINERALOGY AND GEOLOGICAL OCCURRENCE

The kaolin mineral group consists of kaolinite, dickite, halloysite and nacrite. These are dioctahedral 1:1 phyllosilicates composed of alternating silica tetrahedral sheets and alumina octahedral sheets (Figure 3.1); they have the general structural formula $Al_2Si_2O_5(OH)_4$ and chemical composition SiO_2 46.54%, Al_2O_3 39.50%, and H_2O 13.96%. The difference among the kaolin minerals lies in the stacking order of the unit layer. Kaolinite, which is the most common kaolin mineral and the one with the most significant industrial importance, is characterised by well-formed pseudohexagonal crystals and layer stacking that follows a 1M sequence (Figure 3.1) (Christidis, 2011; Pruett and Pickering, 2006).

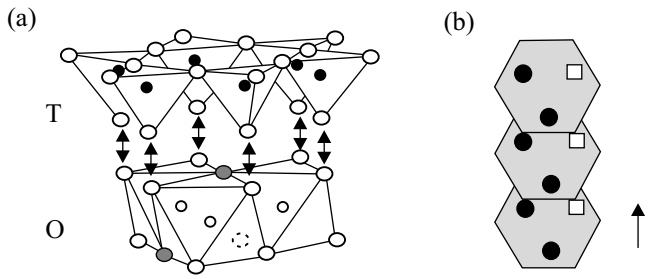

Figure 3.1: (**a**) Schematic 3D representation of the structure of kaolin minerals, showing the tetrahedral (T) and octahedral (O) sheets that form the unit cell. Large white circles are oxygens, large grey circles are hydroxyls, small white circles are octahedral aluminium ions, and small black circles are tetrahedral silicon ions. (**b**) Stacking sequence in minerals of the kaolin group. Black circles and white squares indicate occupied and vacant octahedral sites, respectively. (Reproduced after Christidis (2011), with permission)

The crystal lattice of kaolinite presents structural defects and occasional isomorphous substitution of Fe^{+3} for Al^{+3} in the octahedral layer. The terminology to describe the degree of the defects in kaolinite varies depending on the users (academics or industry), but it is generally regarded as well- or poorly crystallised, well- poorly ordered or high- or low defect. The relative level of defect is relevant for the different industrial applications

and is commonly determined by the Hinckley Index (HI) (Plançon et al., 1988).

Kaolin minerals are formed by the alteration of aluminosilicates, such as feldspars and some micas, in a process called kaolinisation. The interaction of these minerals with alteration fluids leaches out silica and alkali, giving place to the formation of, mainly, kaolinite (Equations (3.1) and (3.2)) (Psyrillos et al., 1998). Kaolin deposits are classified as primary or secondary, depending on the process that triggered the kaolinisation. Primary deposits are formed *in-situ* due to hydrothermal activity, circulation of groundwater or surface weathering, whereas secondary deposits are formed by the weathering, erosion and transport from the rock source to the kaolinite-rich sediment, as Figure 3.2 shows. The rock source is commonly granite or rhyolite; however, there are as well kaolin deposits formed from gneiss, arkose and other alkaline rocks (Bristow, 1987; Galán and Ferrell, 2013; Kogel, 2014; Murray and Keller, 1993).

$$\underset{\text{K-feldspar}}{2\,KAlSi_3O_8} + \underset{\text{water}}{3\,H_2O} \longrightarrow \underset{\text{kaolinite}}{Al_2Si_2O_5(OH)_4} + \underset{\text{silica}}{4\,SiO_2} + \underset{\text{alkali hydroxide}}{2\,K(OH)} \tag{3.1}$$

$$\underset{\text{Na-plagioclase}}{2\,NaAlSi_3O_8} + \underset{\text{water}}{3\,H_2O} \longrightarrow \underset{\text{kaolinite}}{Al_2Si_2O_5(OH)_4} + \underset{\text{silica}}{4\,SiO_2} + \underset{\text{alkali hydroxide}}{2\,Na(OH)} \tag{3.2}$$

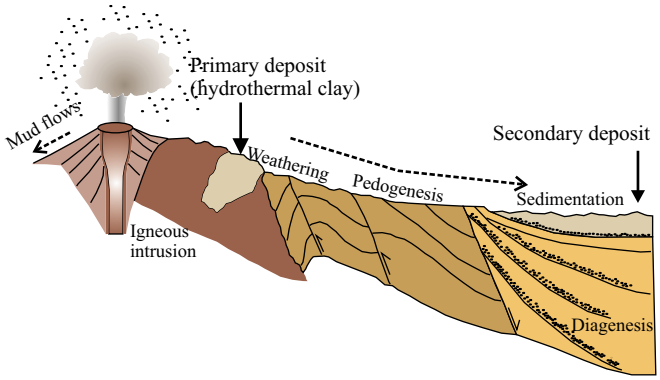

Figure 3.2: Geological setting for the formation of primary and secondary kaolin deposits (Modified after Galán and Ferrell (2013), with permission)

The mineral composition of a kaolin deposit depends on the composition of the parental rock, the mechanism of alteration, and the nature of the alteration fluid (in the cases related to hydrothermal activity). The most common accessory minerals are those resistant to alteration, such as quartz, tourmaline and zircon; in primary deposits, micas and biotite are often present, whereas clay minerals, iron oxides and hydroxides, and organic matter usually occur in secondary deposits (Christidis, 2011).

Compositionally, secondary deposits tend to be homogeneous. In contrast, the mineral assemblages in primary deposits are associated with the intensity of the kaolinisation. In turn, the kaolinisation degree inside a deposit can be variable depending on factors such as the distance to fractures and veins, or the source and temperature of the alteration fluid.

3.2. MINING AND PROCESSING

The selection of a given kaolin deposit for mining is based initially on the colour and grade of the ore. An important indicator to determine the presence of mineral impurities that can stain the kaolin products (e.g. iron oxides) is the characteristic (off) white colour of the kaolin clay. The abundance of kaolinite – detected using X-ray diffraction (XRD) or thermogravimetry analysis (TGA) – and the degree of crystal disorder in kaolinite – measured using the Hinckley Index – define the grade of the ore.

The aim of processing kaolin ore is to remove impurities, engineer particle size and shape, and enhance physical and chemical properties (e.g. colour and reactivity) through thermal and chemical treatment, depending on the end-user demands (Kogel, 2014). The simplified beneficiation process of kaolin is portrayed in Figure 3.3.

Kaolin deposits are mined using open pit methods. The differences in the design of the mine reflect the differences in the geometry of the ore body, which are in turn related to the type of deposit (Pruett and Pickering, 2006). When wet mining is employed, the kaolinised body is blasted and subsequently washed using high-pressure water hoses. In this way, the rock is disaggregated separating the kaolin clay from the matrix. The resulting suspension of kaolin, sand and mica forms a slurry that flows to the bottom of the pit. Mechanical classification systems remove the excess of sand and mica before the slurry is pumped out to the processing plant (Kogel, 2014; Prasad et al., 1991). Dry mining uses hydraulic backhoes and shovels. The mined ore is transported to stockpiles made up of similar quality. The clay is later fed into blungers to form a slurry, with the subsequent removal of the coarse fraction of sand and mica (Murray, 2006; Prasad et al., 1991).

All the beneficiation methods, except calcination, require kaolin to be in a slurry form. The fists step is the removal of material coarser than 250 µm, which consist mostly of quartz and feldspars, using gravity separation methods such as spiral or bucket wheel classifiers. Then, kaolin particles that are smaller than 53 µm are separated using hydrocyclones. Later, at the Dorr Oliver refiners, hydro separation is used to set apart light and heavy particles. Centrifuge in horizontal tubes is used to remove the kaolin from the remnant coarse fraction. The next step is the removal of excess water before conducting magnetic separation. Electromagnets remove iron- and titanium-bearing minerals, mainly micas and tourmaline, which can stain the calcined kaolin products. A filter press is later used to remove the excess of water by compacting the kaolin and forming a "cake". The kaolin cake passes through a drying unit and is later milled to generate a product in a powder form (Murray, 1980, 2006; Polito et al., 2013; Prasad et al., 1991). Up to this point, the product consists of around 90% of kaolinite and is known as *natural kaolin* or *crude kaolin*. In order to generate specific products, the highly refined kaolin undergoes further thermal treatment, which is explained in detail in the following section.

3.2.1. INDUSTRIAL CALCINATION OF KAOLIN

The industrial calcination of kaolin typically occurs in a Multiple Hearth Furnace (MHF), presented in Figure 3.4. The MHF is composed of eight hearths and eight burners that combust natural gas to provide the necessary heat to trigger the calcination reactions (Eskelinen et al., 2015; Gomez-Fuentes and Jämsä-Jounela, 2018; Thomas et al., 2009).

After passing through the drying unit, the kaolin is collected in a feed silo and then transferred to the calciner using an upper weigh feeder bin at the top of the furnace,

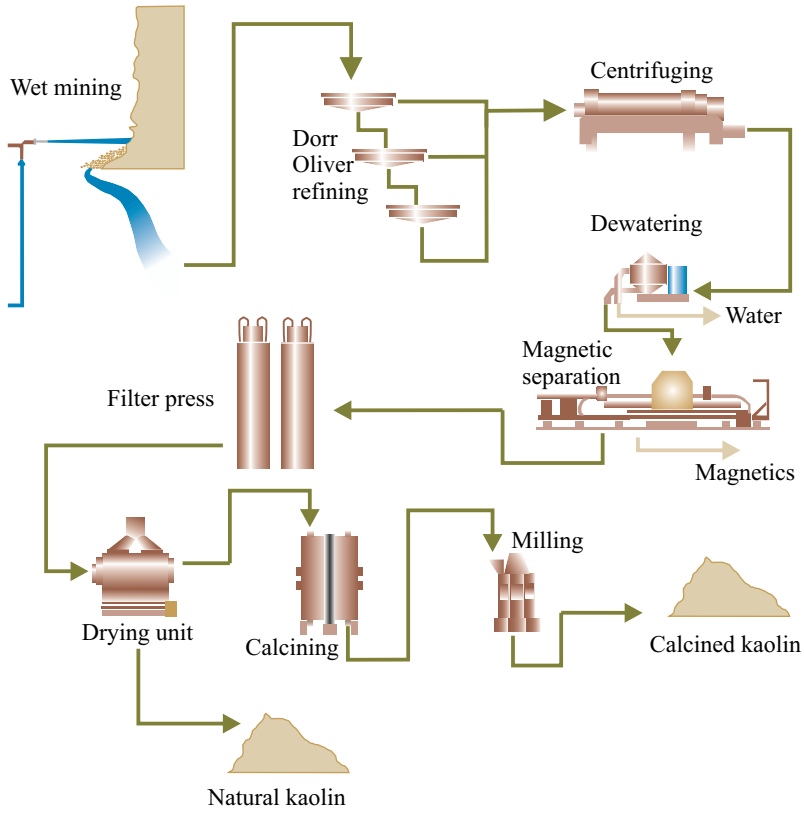

Figure 3.3: Simplified flowsheet for the processing of calcined kaolin (Reproduced with permission from Imerys Minerals, Ltd.)

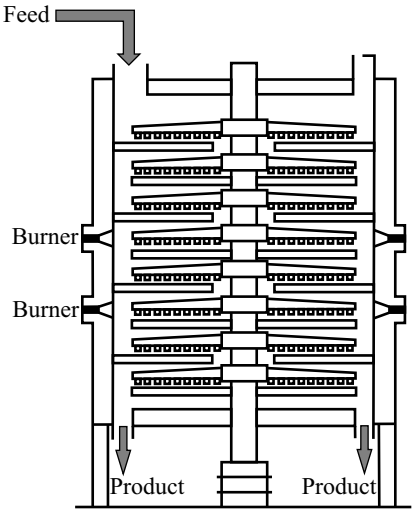

Figure 3.4: Schematic cross-section of a Multiple Hearth Furnace depicting the location of the feed inlet and product outlet, as well as the burners that control the temperature profile (Reproduced after Eskelinen et al. (2015), with permission).

followed by a weighed hopper via a rotary valve. The feed rate is expressed in kg/minute of zero moisture feed. Once inside the MHF, the kaolin flows downstream through the hearths of the furnace, stirred spirally by rotating rabble blades. Adjustment of the gas flow in the burners located at the fourth and sixth hearths controls the temperature inside the calciner. Following the changes in the temperature profile, the calcination reactions described in Section 3.2.2 occur. At the bottom of the eighth hearth, the calcined kaolin is discharged through two drop holes on either side of the furnace base. The calcined kaolin, which leaves the furnace with an approximate temperature of 750 °C, is first cooled down to 100 °C using a high flow stream of ambient air (blast cooling) and then taken to cooler-bag filters to reach ambient temperature. Thomas et al. (2009) calculated a residence time for the kaolin within the furnace of 42 minutes under standard operating conditions. According to the plant operators (Imerys Minerals, Ltd., personal communication May 24, 2017), the time comprised between discharge and blast cooling is about 30 minutes.

Due to the high temperature, the calcined powder tends to agglomerate, making necessary the use of millers to generate the required particle size. After milling, the calcined kaolin is sent to the bulk product silo or the packer.

3.2.2. THE CALCINATION REACTION

Calcination, or thermal treatment, is the process of heating a determined substance under its melting point. The thermal decomposition aims to modify the properties of the treated substance. In kaolin, the resulting *calcined kaolin* has, among others, reduced chemical reactivity and abrasiveness, and improved optical properties, expressed in terms of whiteness and brightness (Bundy, 1993; Chandrasekhar and Ramaswamy, 2002).

The thermal treatment of kaolin involves dehydration, dehydroxylation and recrystalli-

sation (Heller-Kallai, 2013). Structural changes in the kaolinite crystal lattice occur during the dehydroxylation and recrystallisation stages, presented here as the low- and high-temperature calcination domains. In the low-temperature domain, kaolinite transforms into metakaolinite (Brindley and Nakahira, 1959*a*); in the high-temperature domain, metakaolinite recrystallises to mullite (Brindley and Nakahira, 1959*b*). The transformations occurred during the calcination process can be depicted from the differential scanning calorimetry (DSC) and the thermogravimetric analysis (TGA) plots presented in Figure 3.5. The calcination reactions can be summarised as follows:

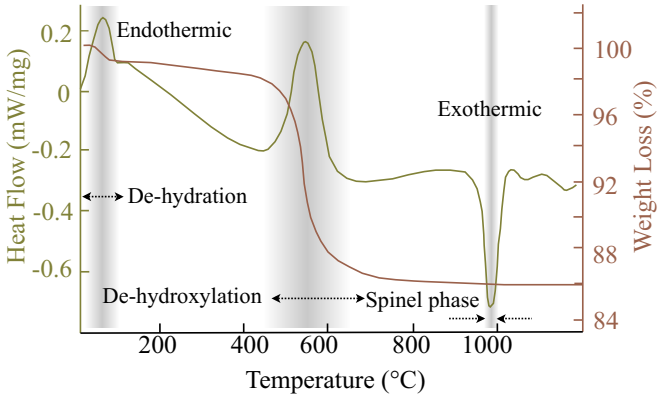

Figure 3.5: Differential scanning calorimetry (DSC) and thermogravimetric analysis (TGA) curves of the kaolin calcination process (reproduced with permission from Imerys Minerals, Ltd.)

KAOLINITE – METAKAOLINITE TRANSITION

In the low-temperature domain of the calcination reaction (500 to 800 °C), the transformation of kaolinite into metakaolinite is characterised by the removal of the chemically-bonded water and the breakdown of the hydroxyl bonds; metakaolinite contains a small proportion of residual hydroxyl groups, and after prolonged heating it releases water (Drits and Derkowski, 2015). Consequently, the kaolinite – metakaolinite transformation occurs according to the reaction:

$$Al_2Si_2O_5(OH)_4 \xrightarrow{450\text{-}700\,^\circ C} (Al_2O_3 \cdot 2\,SiO_2) + 2\,(H_2O)\uparrow \tag{3.3}$$

METAKAOLINITE – MULLITE TRANSITION

In the high-temperature domain (900 to 1200 °C), metakaolinite re-crystallises into a spinel phase. The reaction and the processes that undergo these transformations have been object of extensive research, and they are still subject of debate. According to Percival et al. (1974) and Gualtieri and Bellotto (1998), metakaolinite decomposes first into γ-alumina and Si-spinel, and later to mullite. The underwent chemical reactions are summarised by Ptáček et al. (2011) as follows:

$$2\,(Al_2O_3 \cdot 2\,SiO_2) \xrightarrow{980\,^{\circ}C} 2\,Al_2O_3 \cdot 3\,SiO_2 + SiO_2\,(\text{amorphous}) \tag{3.4}$$

$$3\,(2\,Al_2O_3 \cdot 3\,SiO_2) \xrightarrow{>1100\,^{\circ}C} 3\,(Al_2O_3 \cdot 2\,SiO_2) + 5\,SiO_2\,(\text{amorphous}) \tag{3.5}$$

The calcination reactions alter the surface properties of the clay mineral, as demonstrated by Drzal et al. (1983) and Bundy (1993), affecting the reactivity of the material. In particular, amorphous γ-alumina is highly reactive, and crystalline γ-alumina has a high water adsorption capacity, as MacIver et al. (1963) and Peri (1965) verified.

According to Murray and Lyons (1959), the exact temperature at which the processes start or end depends on the crystallinity degree, impurities and particle size of the raw kaolin. Besides, the residence time of the kaolin inside the furnace also influences the rate at which the reactions occur (Thomas et al., 2009).

Other reactions that involve the kaolin ancillary minerals include:

- 500 °C < 800 °C: Mica/illite dehydroxylation
- 800 °C < 950 °C: Mica/illite depletion
- 875 °C < 950 °C: Maximum amount of K feldspar (formed from the depleted mica)
- T < 1200 °C: Quartz dissolved in liquid face leading to cristobalite crystallisation

3.3. INDUSTRIAL PROPERTIES OF CALCINED KAOLIN

The desired properties calcined kaolin applications that determine its commercial value are brightness, particle size and chemical inertness. Other properties such as whiteness, viscosity, abrasiveness, and permeability are intimately related or consequence of the first three (Mortimer, 2001; Murray, 2000).

- Brightness
  Brightness is the most critical property that determines the commercial value of kaolin. It refers to the reflectance of a given wavelength under standard conditions. It is affected by the scattering of light, which is related to particle size, and by light absorption, which is related to coloured impurities. For industrial purposes, the standard ISO brightness is the quality control parameter for pulps and paper. It is defined by the norm ISO 2470 (International Organization for Standardization, 2009) as a mathematical function having an effective wavelength of 457 nm and a bandwidth of 44 nm. ISO brightness must be measured with a specific instrument and specific calibration routines determined in the ISO 2469 standard (International Organization for Standardization, 2007).

- Particle size
  Particle size and particle size distribution determine other kaolin properties such as colour, viscosity and abrasiveness. For applications in paper, paint and rubber, the desired particle size is smaller than 2 µm, as measured by sedimentation techniques.Fine particle size increases the surface area leading to higher kaolin

reactivity, higher reflectance (hence increased brightness) and low viscosity at high solid concentrations.

- Chemical inertness
  For specific applications, it is essential to avoid any chemical reactions between the calcined kaolin and the compound that uses it as filler (Wilson, 2006). The calcined kaolin product should not be reactive in a defined pH range. For this, insolubility, especially of alumina should be guaranteed (Taylor, 2005).

3.4. USES

The most significant markets of calcined kaolin – in terms of volume – are the paper, paint, rubber and plastics industries. New highly technical applications, such as speciality packaging and lightweight paper coatings, or specialised markets that demand strict parameters under the highest quality (e.g. pharmaceutical applications), are smaller in volume but their value is significantly higher (Kogel, 2014; Murray, 2000).

- Paper
  In paper manufacturing, kaolin is used as filler and coating. The whiteness and fine particle size give desired brightness, opacity, smoothness and gloss, at the same time that improves the paper printing characteristics and reduces the consumption of TiO_2. The quality of the calcined kaolin increases as brightness increases and particle size decreases.The content of calcined kaolin used as a filler in paper applications varies from 10 to 35 % (Wilson, 2006).

- Paint, rubber and plastics
  Kaolin is used as functional filler and extender, where the particle size and surface properties are the main control parameters. In paints, kaolin improves opacity and hiding power, replacing the more costly TiO_2 pigment (Ciullo, 2006). For rubber manufacturing, it is the most common non-black filling. The particle size distribution, particle shape and surface properties are used for improving the strengthand the resistance to tension and abrasion, mainly in cable insulation compounds (Harben and Dickson, 2006). In plastics, kaolin is used as filler in PVC compounds for sheathing and insulation purposes. The kaolin properties for these applications are comparable to those for paper filling, especially regarding high brightness and particle size. When these compounds are used in the pharmaceutical and food industries, the chemical inertness is of critical relevance.

REFERENCES

Brindley, G. W. and Nakahira, M. (1959*a*), 'The kaolinite-mullite reaction series: II, Metakaolin', *Journal of the American Ceramic Society* **42**, pp. 314–318. DOI: 10.1111/j.1151-2916.1959.tb14315.x

Brindley, G. W. and Nakahira, M. (1959*b*), 'The kaolinite-mullite reaction series: III, The high-temperature phases', *Journal of the American Ceramic Society* **42**, pp. 319–324. DOI: 10.1111/j.1151-2916.1959.tb14316.x

Bristow, C. M. (1987), 'World kaolins. Genesis, exploitation and application', *Industrial Minerals* **258**, pp. 45–59.

Bundy, W. M. (1993), The diverse industrial applications of kaolin, *in* H. H. Murray, H. Haydn, W. M. Bundy and C. C. Harvey, eds, 'Kaolin genesis and utilisation: Keller '90 Kaolin Symposium', The Clay Minerals Society special publication, The Clay Minerals Society, pp. 43–73.

Chandrasekhar, S. and Ramaswamy, S. (2002), 'Influence of mineral impurities on the properties of kaolin and its thermally treated products', *Applied Clay Science* **21**(3-4), pp. 133–142. DOI: 10.1016/s0169-1317(01)00083-7

Christidis, G. E. (2011), Industrial Clays, *in* G. E. Christidis, ed., 'Advances in the characterization of industrial minerals', Vol. 9 of *European Mineralogical Union notes in mineralogy*, Mineralogical Society of Great Britain and Ireland, Chapter 9, pp. 341–414. DOI: 10.1180/emu-notes.9.1

Ciullo, P. A. (2006), Paint and coatings, *in* J. E. Kogel, N. C. Trivedi, J. M. Barker and S. T. Krukowski, eds, 'Industrial Minerals and Rocks', 7th edn, Society for Mining, Metallurgy, and Exploration, pp. 1301–1310.

Drits, V. A. and Derkowski, A. (2015), 'Kinetic behavior of partially dehydroxylated kaolinite', *American Mineralogist* **100**, pp. 883–896. DOI: 10.2138/am-2015-5083

Drzal, L. T., Rynd, J. P. and Fort Jr, T. (1983), 'Effects of calcination on the surface properties of kaolinite', *Journal of Colloid and Interface Science* **93**, pp. 126–139. DOI: 10.1016/0021-9797(83)90392-2

Eskelinen, A., Zakharov, A. , Jämsä-Jounela, S. L. and Hearle, J. (2015), 'Dynamic modeling of a multiple hearth furnace for kaolin calcination', *AIChE Journal* **61**(11), pp. 3683–3698. DOI: 10.1002/aic.14903

Galán, E. and Ferrell, R. E. (2013), Genesis of clay minerals, *in* F. Bergaya and G. Lagaly, eds, 'Handbook of Clay Science', Vol. 5 of *Developments in Clay Science*, Elsevier, Chapter 3, pp. 83–126. DOI: 10.1016/b978-0-08-098258-8.00003-1

Gomez-Fuentes, J. and Jämsä-Jounela, S. L. (2018), 'Simplified mechanistic model of the Multiple Hearth Furnace for control development', *Simulation Notes Europe* **28**(3), pp. 97–100. DOI: 10.11128/sne.28.sn.10426

Gualtieri, A. and Bellotto, M. (1998), 'Modelling the structure of the metastable phases in the reaction sequence kaolinite-mullite by X-ray scattering experiments', *Physics and Chemistry of Minerals* **25**, pp. 442–452. DOI: 10.1007/s002690050134

Harben, P. W. and Dickson, E. M. (2006), Rubber, *in* J. E. Kogel, N. C. Trivedi, J. M. Barker and S. T. Krukowski, eds, 'Industrial Minerals and Rocks', 7th edn, Society for Mining, Metallurgy, and Exploration, pp. 1327–1335.

Heller-Kallai, L. (2013), Thermally modified clay minerals, *in* F. Bergaya and G. Lagaly, eds, 'Handbook of Clay Science', Vol. 5 of *Developments in Clay Science*, Elsevier, Chapter 10.2, pp. 411–433. DOI: 10.1016/B978-0-08-098258-8.00014-6

International Organization for Standardization (2007), 'Paper, board and pulps - measurement of diffuse radiance factor'. ISO Standard No. 2469:2007.
URL: *https://www.nen.nl/NEN-Shop/Norm/NENISO-24692007-en.htm [Retrieved September 2013]*

International Organization for Standardization (2009), 'Paper, board and pulps - measurement of diffuse blue reflectance factor. Part 1: Indoor daylight conditions (ISO brightness)'. ISO Standard No. 2471-1:2009.
URL: *https://www.nen.nl/NEN-Shop/Norm/NENISO-247012009-en.htm [Retrieved September 2013]*

Kogel, J. E. (2014), 'Mining and processing kaolin', *Elements* **10**(3), pp. 189–193. DOI: 10.2113/gselements.10.3.189

MacIver, D. S., Tobin, H. H. and Barth, R. T. (1963), 'Catalytic aluminas I. Surface chemistry of eta and gamma alumina', *Journal of Catalysis* **2**, pp. 485–497. DOI: 10.1016/0021-9517(63)90004-6

Mortimer, M. D. (2001), 'Process control developments in the United Kingdom china clay industry', *Transactions of the Institutions of Mining and Metallurgy, Section C: Mineral Processing and Extractive Metallurgy* **110**(JAN./APR.), pp. C50–C54.

Murray, H. H. (1980), 'Major kaolin processing developments', *International Journal of Mineral Processing* **7**(3), pp. 263–274. DOI: 10.1016/0301-7516(80)90022-8

Murray, H. H. (2000), 'Traditional and new applications for kaolin, smectite, and palygorskite: a general overview', *Applied Clay Science* **17**(5-6), pp. 207–221. DOI: 10.1016/s0169-1317(00)00016-8

Murray, H. H. (2006), Kaolin Applications, *in* H. H. Murray, ed., 'Applied Clay Mineralogy - Occurrences, Processing and Application of Kaolins, Bentonites, Palygorskite-Sepiolite, and Common Clays', Vol. 2 of *Developments in Clay Science*, Elsevier, Chapter 5, pp. 85–109. DOI: 10.1016/s1572-4352(06)02005-8

Murray, H. H. and Keller, W. D. (1993), Kaolins, kaolins, and kaolins, *in* H. H. Murray, W. M. Bundy and C. C. Harvey, eds, 'Kaolin Genesis and Utilization', The Clay Minerals Society, Boulder, Colorado, Chapter 1, pp. 1–24.

Murray, H. H. and Lyons, S. C. (1959), Further correlations of kaolinite crystallinity with chemical and physical properties, *in* A. Swineford, ed., 'Eighth National Conference on Clays and Clay Minerals', Clays and Clay Minerals, Elsevier Science, pp. 31–40. DOI: 10.1346/CCMN.1959.0080104

Percival, H. J., Duncan, J. F. and Foster, P. K. (1974), 'Interpretation of the kaolinite-mullite reaction sequence from infrared absorption spectra', *Journal of the American Ceramic Society* **57**, pp. 57–61. DOI: 10.1111/j.1151-2916.1974.tb10813.x

Peri, J. B. (1965), 'Infrared and gravimetric study of the surface hydration of gamma-alumina', *Journal of Physical Chemistry* **69**, pp. 211–219. DOI: 10.1021/j100885a032

Plançon, A., Giese, R. F. and Snyder, R. (1988), 'The Hinckley Index for kaolinites', *Clay Minerals* **23**, pp. 249–260. DOI: 10.1180/claymin.1988.023.3.02

Polito, S., Hoehn, T. May, J. and Sharp, G. (2013), 'Imerys Minerals Limited and Goonvean Limited - A report on the completed acquisition by Imerys Minerals Limited of the kaolin business of Goonvean Limited - Appendix C'.
URL: *https://assets.publishing.service.gov.uk/media/[Accessed February 2019]*

Prasad, M. S., Reid, K. J. and Murray, H. H. (1991), 'Kaolin: processing, properties and applications', *Applied Clay Science* **6**(2), pp. 87–119. DOI: 10.1016/0169-1317(91)90001-p

Pruett, R. J. and Pickering, S. M. (2006), Kaolin, *in* J. E. Kogel, N. C. Trivedi, J. M. Barker and S. T. Krukowski, eds, 'Industrial Minerals and Rocks', 7th edn, Society for Mining, Metallurgy, and Exploration, pp. 383–400.

Psyrillos, A., Manning, D. A. C. and Burley, S. D. (1998), 'Geochemical constraints on kaolinization in the St Austell Granite, Cornwall, England', *Journal of the Geological Society* **155**(5), pp. 829–840. DOI: 10.1144/gsjgs.155.5.0829

Ptáček, P., Šoukal, F. , Opravil, T. , Nosková, M. , Havlica, J. and Brandštetr, J. (2011), 'Mid-infrared spectroscopic study of crystallization of cubic spinel phase from metakaolin', *Journal of Solid State Chemistry* **184**(10), pp. 2661–2667. DOI: 10.1016/j.jssc.2011.07.038

Taylor, R. J. (2005), 'Treatment of metakaolin - patent number WO2005108295 A1'.
URL: *https://patents.google.com/patent/WO2005108295A1/en [Accessed February 2017]*

Thomas, R., Grose, D. , Obaje, G. , Taylor, R. , Rowson, N. and Blackburn, S. (2009), 'Residence time investigation of a multiple hearth kiln using mineral tracers', *Chemical Engineering and Processing: Process Intensification* **48**(4), pp. 950–954. DOI: 10.1016/j.cep.2009.01.003

Wilson, I. (2006), Filler and coating pigments for papermakers, *in* J. E. Kogel, N. C. Trivedi, J. M. Barker and S. T. Krukowski, eds, 'Industrial Minerals and Rocks', 7th edn, Society for Mining, Metallurgy, and Exploration, pp. 1287–1300.

4

INFRARED CHARACTERISATION OF THE KAOLIN DEPOSITS IN SW ENGLAND

This chapter presents the kaolin deposit that serves as a case study, and provides the infrared mineralogical characterisation of the ore with a focus on the detection of factors that are detrimental for the quality of the ore.

Some of the results presented in this chapter were obtained from the master thesis project:
Groenheide, S. (2016). Mapping the kaolin mineralization of the St. Austell granite (SW England) using VNIR and SWIR hyperspectral imaging. MSc. thesis, Delft University of Technology

In 2008, 1.36 million dry tonnes of kaolin were produced in England, from which 88 % were extracted from the St Austell Granite (Cornwall). In the same year, 1.19 million dry tonnes were exported, with Europe as the largest single market (BGS, 2009). Even though there has been a decline in sales in the last decade (1.01 million dry tonnes estimated for 2015), kaolin remains as Britain's second most important mineral export (Idoine et al., 2016). The kaolin mineralisation in the St Austell Granite is classified as a world-class deposit given its size and quality. The interest on the St Austell kaolin relies on its characteristic low iron content and kaolinite with a high level of structural order, which make this unique type of kaolin ideal as a raw material in the manufacturing of paper, paint and speciality applications, such as pharmaceutical and cosmetic industries. For these applications, the extraction of the ore has focused in those areas that exhibit the highest quality. However, future reserves might depend on other parts of the deposit with lesser ore quality. Aiming to understand the properties of the kaolin ore and the opportunities for the exploitation of different parts of the deposit, this study presents a review on the origin of the kaolin mineralisation in the St Austell Granite and a mineralogical characterisation of the ore. Samples from production and non-production pits were analysed using infrared (IR) spectroscopy to identify the characteristics of the ore that can influence the generation of high-quality kaolin products, namely the mineral associations in the ore and the kaolinite crystallinity. The observations are further discussed in view of their implications in the mining and processing of the kaolin ore.

4.1. GEOLOGICAL SETTING

4.1.1. GENESIS OF THE KAOLIN DEPOSITS IN SW ENGLAND

Kaolin mineralisation in south-west England occurs in some exposed areas of the Cornubian batholith. This magmatic body extends from the Scilly Islands, in the southwestern tip of Cornwall, to the eastern edge of Dartmoor, in southern Devon (Figure 4.1). The emplacement of the batholith took place by the intrusion of acidic magma in sedimentary Cambrian units during the latest stages of the Variscan Orogeny (290 to 280 Ma) (Brown, 1953; Exley et al., 1993). The igneous units are overlain by Tertiary beds followed by Quaternary deposits around the coasts. This long period of no sedimentation promoted the aerial denudation, letting the exposition of the batholith in seven major plutons, from east to west: Haig Frass, Isles of Scilly, Land's End, Tregoning-Godolphon, Carnmenellis, St. Austell, Bodmin Moor and Dartmoor (Exley et al., 1993; Murray, 2006).

There has been some controversy about the origin of the kaolin deposits in south-west England. Contrasting hypotheses supporting hydrothermal or weathering origin have been largely debated (Bray and Spooner, 1983; Konta, 1969; Murray and Keller, 1993). However, the most accepted explanation is the one proposed by Bristow (1993) and Bristow and Exley (1994). These researchers suggested that kaolinisation is the last stage of hydrothermal mineralisation followed by supergene alteration. The genesis of the English kaolin deposits, as explained by the multistage theory, occurred in six different stages:

Stage I: *Intrusion of the main batholith of biotite granite* (285 Ma), as a consequence of the Variscan orogeny. In addition to the heat generated by the magmatic intrusion, the abnormally high content of U and Th in the granite, along with their subsequent radioactive decay, provided a long-lasting source of heat for the alteration fluids during

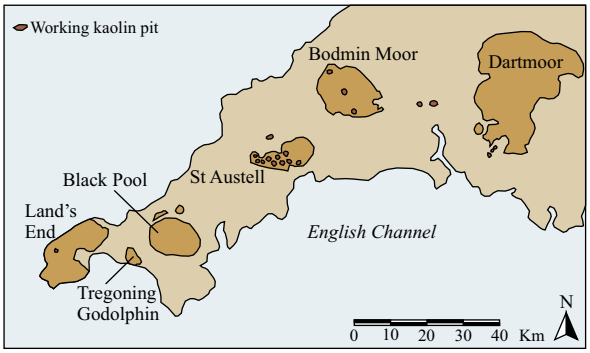

Figure 4.1: Map of south-west England showing the distribution of the areas of kaolinised granite in the Cornubian batholith (Haig Frass and Isles of Scilly plutons not shown). Reproduced after Murray (2006), with permission.

the Mesozoic and Cenozoic.

Stage II: *Early Sn/W mineralisation and associated alteration* (285 to 275 Ma)

Stage III: *(A) Intrusion of evolved lithium mica and topaz granites, (B) Main Sn/Cu mineralisation and associated tourmalisation and greisenisation, (C) Intrusion of felsitic dykes* (275 to 270 Ma). The strong metasomatism let to iron depletion and lithium enrichment in the old biotite granite; the residual iron was allocated in tourmaline veins. The alteration of the Na-plagioclase in the granite produced extremely white kaolinite. The meteoric waters that entered in the system boiled up due to the radiogenic heat, favouring fluids rich in metals. This resulted in tin, copper and other metalliferous mineral deposits.

Stage IV: *Cross-course faulting and mineralisation with the first episode of argillic alteration* (240 Ma). Permeability created by fractures along the granite allowed the intrusion of hydrothermal fluids with temperatures from 250 to 350 °C, easing argillisation (mainly illite and smectite).

Stage V: *Radiogenically-driven convective circulation of meteoric water with main kaolinisation* (200 to 60 Ma). A dominantly continental environment let the intrusion of fresh water to the system, which was heated up by the radiogenic elements. The former illite-smectite and some feldspars altered to kaolinite, and the freed silica formed quartz veins along the fractures. The strongest kaolinisation occurred along the quartz and hematite veins.

Stage VI: *Mesozoic – Palaeogene weathering* (180 to 25 Ma), the granite was exposed to sub-aerial conditions that made it prompt to weathering, accelerating the kaolinisation process. The erosion was not sufficiently active to remove the altered granite.

4.1.2. KAOLINISATION IN THE ST AUSTELL GRANITE

The most intensive alteration occurs in the St. Austell pluton. The uniqueness of the deposits at this location is a consequence of the low iron content in the parent granite, the combination of hydrothermal and mesogene/supergene alteration, and the relative stability of the terrain after the process took place. The deposits are typically funnel-like shaped, narrowing downwards as much as 200 m below the surface, as shown in

Figure 4.2. The most intense alteration occurs nearby fractures where the occurrence and temperature of hydrothermal fluids were higher (Bristow and Exley, 1994; Bristow et al., 2002; Murray, 2006).

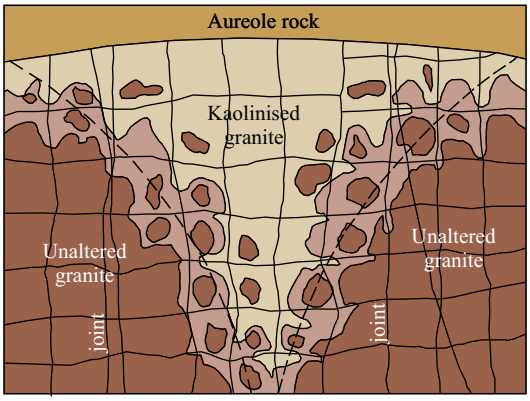

Figure 4.2: Characteristic funnel-like geometry of the kaolin deposits in SW England. Reproduced after Murray (2006), with permission.

Manning et al. (1996) classified the St Austell Granite into six different textural types: biotite granite, lithium-mica granite, three types of tourmaline granites, and topaz granite. Figure 4.3 displays the distribution of these granite types in the westernmost side of the pluton, where most of the commercial exploitation takes place. The biotite granite has a coarse texture, with megacrysts of K-feldspar, prismatic tourmaline and restite phases that include cordierite. As the name indicates, biotite is abundant in this type of granite. The Li-mica granite also has a coarse texture, with aggregates of topaz and tourmaline, and megacrysts of K-feldspars and Na-plagioclase. Li-mica of zinnwaldite composition is highly abundant in this type of granite. In the tourmaline granites, the globular quartz facies has a significant textural variation that includes large quartz grains, microperthite and Li-mica phenocrysts embedded in a fine-grained groundmass of quartz, K-feldspar, plagioclase, zinnwaldite and tourmaline. The medium-coarse-grained equigranular facies consist of medium grain size Li-mica, muscovite, microperthtic albite, tourmaline needles and topaz aggregates. The fine-grained equigranular facies differs from the medium-coarse facies not only by its finer texture but also by a smaller concentration of iron compared to the other tourmaline-bearing granites. Finally, the topaz granite has fine to medium grain size, contains less tourmaline than the other granites, but is abundant in topaz and fluorite.

In the St Austell Granite, intense kaolinisation occurs widely in the form of veins or large volumes of kaolinised granite. The kaolin veins are of hydrothermal origin and have an aplitic texture with quartz, plagioclase, K-feldspar, Li-mica and prismatic topaz. These veins have a thickness from 1 to 50 cm and present a clear transition from the fresh granite to the altered zone (Psyrillos et al., 1998). The kaolinised granite is related to areas with numerous fractures or hydrothermal veins, and it occurs over a length scale of tens or hundreds of meters. Despite the size of the kaolinised areas, the intensity of the alteration is rather uniform, and the kaolinised granite has similar characteristics

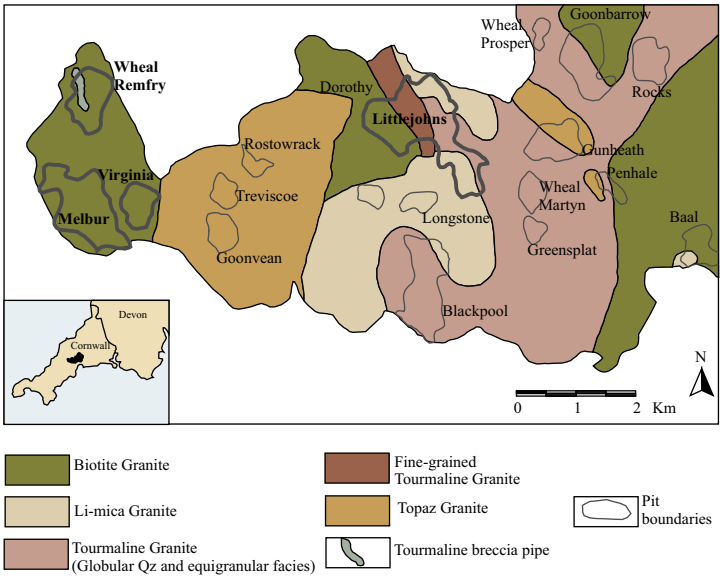

Figure 4.3: Distribution of the granite varieties in the St Austell Granite and the location of some of the kaolin pits. The samples used in this chapter come from the Melbur, Virginia, Wheal Remfry and Littejones pits (highlighted). Map reproduced after Manning et al. (1996), with permission

regardless of the variability of the parental granite. The kaolinite in these areas has characteristically vermiform morphology. Other minerals present in the kaolinised granite include hydrothermal muscovite, illite, montmorillonite, quartz and feldspar. Quartz-hematite and tourmaline veins frequently occur in the kaolinised areas (Manning et al., 1996; Psyrillos et al., 1998).

The kaolinised areas that are suitable for commercial exploitation, targeted for paper and performance minerals, are related to the granites where tourmaline or Li-mica are the dominant Fe-bearing minerals, rather than biotite. Tourmaline and Li-micas are more resistant to kaolinisation. Therefore they do not liberate the iron that they host, limiting the incorporation of impurities in the kaolin (Manning et al., 1996). Most of the production comes from the Littlejohns and Wheal Martyn pits, and formerly from the Blackpool pit (Figure 4.3). The kaolin extracted from the biotite granite is normally used for the ceramics market where the quality is not defined by the puritiy or crystallinity of the kaolinite. However, based on the markets prospects, there is a growing interest for using these deposits for the paper and specialties applications.

4.2. MATERIALS AND METHODOLOGY

4.2.1. SAMPLES

Since the objective of this part of the study is to explore the potential of using low-grade kaolin for performance and speciality applications, the sampling was targeted to areas with no intense kaolinisation, especially in the biotite granite. The sample set comprises a selection of hand samples and drill cores summarised in Table 4.1.

Table 4.1: List of rock samples collected in the St Austell Granite

Hand samples	
Pit	Quantity
Littlejohns	3
Melbur	15
Virginia	31

Drill core samples		
Pit	Location	Length
Melbur	CD003	6 m
Melbur	CD004	6 m
Melbur	CD007	6 m
Virginia	CD002	3 m
Virginia	CD004	6 m
Wheal Remfry	CD004	6 m

The collected hand samples tried to capture the transition between the parental granite and the kaolinised area, aiming to understand the mineralogy present in the kaolin ore. The samples were obtained from the mine faces at the Melbur and Virginia, in the peripheral parts of the altered areas, were the kaolinisation is rather low. For comparison with the parts of the deposit that are traditionally mined for performance and speciality applications, high-grade samples were collected at the Littlejohns pit (Li-mica granite). By comparing high-grade and low-grade samples it is possible to have a complete overview about the ore that is currently feeding the processing plant (high-grade), and the one that could potentially be incorporated to the process (low-grade). The hand samples were used for the exploratory data analysis that involved the identification of the dominant mineralogy and the determination of parameters for ore quality.

The drill cores were obtained from exploratory boreholes in more altered parts of the biotite granite in the Melbur, Virginia and Wheal Remfry pits. Drill core sections of depths between 10 and 30 m were used to identify textural patterns that can be relevant for the process and identify variations in the quality of the ore. The high moisture and friability of the material hindered the collection of high quality samples. It is worth to note that the sample set does not represent the entire variability of the deposit, but serves to have an overview of its mineralogical characteristics that can be analysed using infrared technology.

4.2.2. INFRARED SPECTRA COLLECTION AND PROCESSING

For the exploratory data analysis, the infrared reflectance spectra were collected using an ASD FieldSpec spectrometer (Table 2.2)Three measurements were taken at different spots in each sample. A preliminary interpretation of the data was conducted with The Spectral Geologist (TSG) software (CSIRO, 2007). Later, the TSG results were compared with the USGS spectral library (Clark et al., 2007). The TSG software was also used for the further processing and extraction of spectral parameters. The quality of the ore was assessed using the crystallinity of the kaolinite approach proposed by Pontual et al. (1997), which is based on the shape of the 2.2 µm feature.

The infrared analysis of the drill core and hand samples was carried out using image data collected with the SisuROCK spectral core logger (Table 2.3). The data processing was performed in the Matlab Environment. The spectral corrections included smoothing

using the Savitzky-Golay (SG) filter and spectra normalisation by removal of the convex hull using a continuum removal (CR) function. Minerals maps were created by using a decision tree classifier algorithm developed by Groenheide (2016), designed to identify Fe-bearing minerals and clay minerals. The decision tree uses the wavelength of the minimum, depth and slope as parameters for the classification. The quality of the ore was assessed using the same parameters as in the point data.

4.3. MINERAL ASSOCIATIONS AND TEXTURE

4.3.1. IDENTIFICATION OF INFRARED-ACTIVE MINERALOGY

The degree of kaolinisation of the samples was characterised based on the mineralogical and textural variations described by Mueller et al. (1999) and presented in Figure 4.4. The collected samples are medium altered, that is to say, the rock partially preserves the igneous texture, and there are relicts of rock-forming minerals (e.g. feldspars, biotite, and primary mica). Figure 4.5 shows the IR-active mineralogy that was detected in the samples using point spectral data. In general, three regions present the strongest spectral absorptions: around 1.40 µm, generated by the presence of water and OH bonds, around 1.90 µm, which is the characteristic water feature, and around 2.21 µm, related to Al–OH bonds. The water features have a particularly strong presence in the spectra, as revealed by the depth of the 1.90 µm feature, and the notable 1.45 µm hump that occurs in most of the spectra. It is likely that these water features are not related to the mineralogy of the samples but rather to the sampling conditions in the pits, where there is an abundant presence of water either from the environment or due to the mining style.

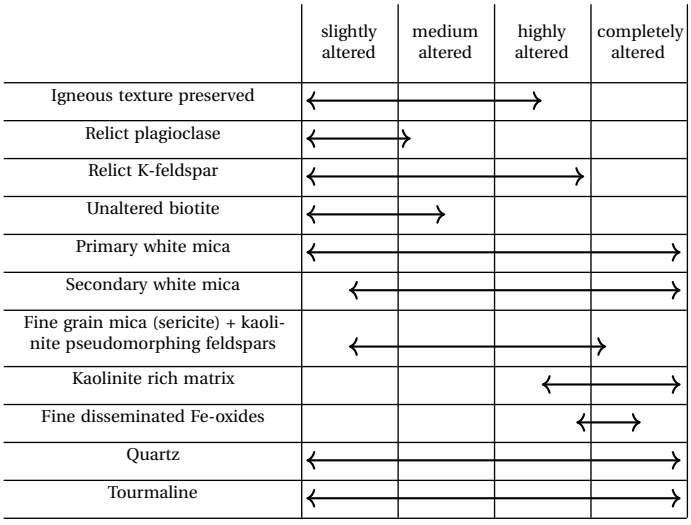

Figure 4.4: Mineralogical and textural changes with different degree of kaolinisation. Reproduced after Mueller et al. (1999), with permission

The region between 2.00 to 2.50 µm contains most of the features that describe the mineralogy of the samples. The most prominent feature at 2.21 µm, which is distinctive

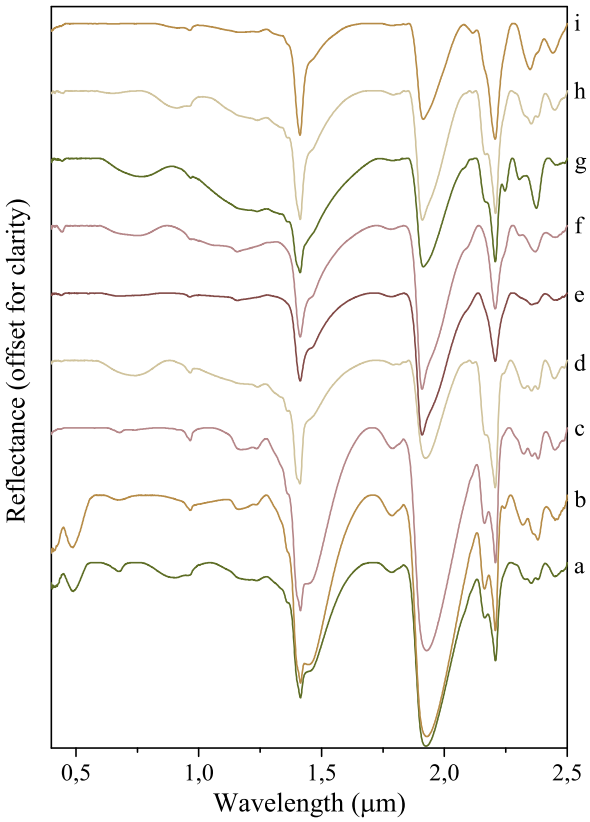

Figure 4.5: Minerals present in the kaolinised granite samples from the St Austel Granite that have characteristic spectral features in the SWIR range. The samples were collected at (**a**) Littlejons pit, (**b–d**) Melbur pit and (**e–i**) Virginia pit. (**a**) kaolinite, muscovite, illite, goethite, hematite; (**b**) kaolinite, goethite, biotite; (**c**) kaolinite, biotite; (**d**) kaolinite, biotite, muscovite; (**e**) montmorillonite, muscovite; (**f**) montmorillonite, muscovite, biotite; (**g**) tourmaline, biotite, montmorillonote, kaolinite; (**h**) kaolinite, montmorillonite, muscovite, hematite; (**i**) muscovite, goethite

for clay minerals, reveals the presence of kaolinite, evidenced by the kaolinite doublet, and muscovite, illite and montmorillonite, characterised by a single feature accompanied by other secondary absorptions between 2.25 to 2.50 µm. The iron-bearing mineralogy is mostly identified by the broad absorptions in the VNIR range and the short wavelengths of the SWIR range. These absorptions are characteristic of biotite (around 0.9 µm and 1.16 µm), hematite (0.66 µm and 0.88 µm) and goethite (0.66 µm and 0.93 µm). Another iron-bearing mineral that is particularly relevant in these samples is tourmaline, which is identified by the absorptions at 0.75 µm, 2.24 µm, 2.31 µm and 2.37 µm.

The samples from the Littlejohns pit (Figure 4.5a) contain kaolinite as dominant mineral, mixed with muscovite and illite. Iron oxides are also present in the form of coatings. In the samples from Melbur pit (Figure 4.5b, c and d) kaolinite is also the dominant mineral, which presents spectral mixtures with muscovite. The iron-bearing minerals are biotite, hematite, goethite and tourmaline. The mineralogical composition of the Virginia pit (Figure 4.5 e, f, g, h and i), is similar to that of the Melbur pit, but muscovite and montmorillonite are significantly more abundant, and the biotite occurrence is reduced.

4.3.2. MINERALOGICAL AND TEXTURAL VARIATIONS

The mineralogy detected in the IR hyperspectral images is the same as that detected using the point spectra, with the addition of halloysite. Figure 4.6 presents the mineral maps generated for some samples that serve as examples of the most relevant observations. Some samples present a porphyritic texture with a matrix of muscovite, illite and montmorillonite and with kaolinite as a pseudomorph of former K-feldspars (Figure 4.6a). Other samples have muscovite, illite and montmorillonite pseudomorphing plagioclase; in these cases, a gradation from muscovite to montmorillonite was observed from the inner part of the old crystal towards the rims, indicating phases of alteration (Figure 4.6b and c). The spectra of some samples show halloysite features, although this might as well correspond to a spectral mixture of kaolinite and montmorillonite. The halloysite spectrum occurs in the matrix or zones with fine grain. Its presence, if confirmed, might be an indication of recent weathering. The iron-bearing mineralogy consists of tourmaline phenocrysts visible to the naked eye, fine-grained biotite scattered in the matrix, and iron oxides (hematite and goethite) present as coatings or in a mixture with the clay minerals. Besides, topaz was also detected in few samples, always associated with muscovite. In the Littlejohns pit, tourmaline is the only iron-bearing mineral and has a smaller grain size than in the Virginia pit samples. In contrast, iron oxide coatings are more abundant in the Virginia pit (biotite granite) (Figure 4.6d). Topaz was only detected at this pit.

The samples collected from drill cores represent a more advanced grade of alteration than the rock samples, since the drill cores were obtained from central parts of the deposits, where the kaolinisation degree is higher. The structural integrity of the original granite is destroyed entirely, and the alteration minerals are contained in a fine-grain groundmass; the rock is extremely soft and has stains from dark purple to ochre/orange that might be the results of de-ferruginisation of biotite. According to Mueller et al. (1999), these features are characteristic of a completely altered granite. The preservation of the samples is poor given the high friability of the kaolinised granite. In the hyperspectral images (Figure 4.7), most of the samples are fully kaolinised, with a dominant presence

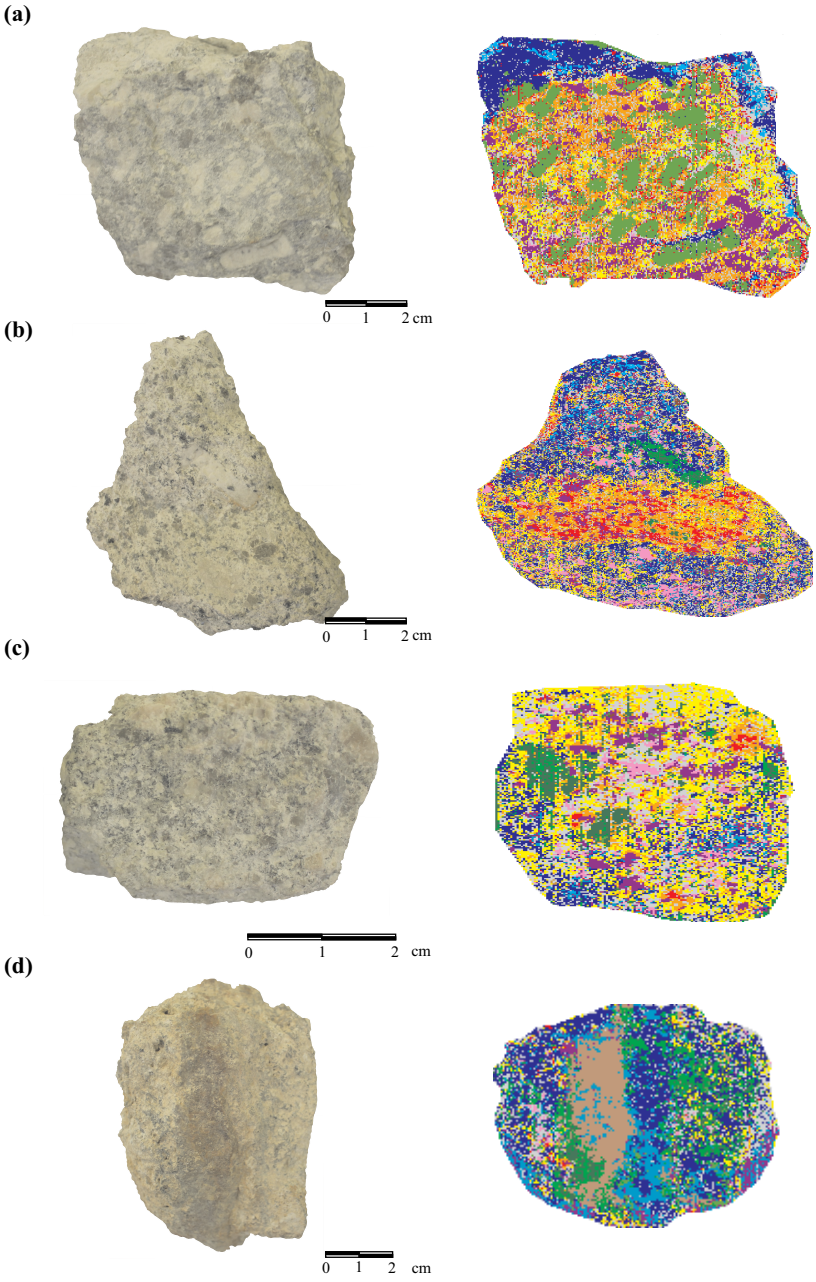

Figure 4.6: Photographs (left) and hyperspectral mineral maps (right) of samples collected in the St Austell granite: (**a**) [Littlejohns] Kaolinite as pseudomorph of K-feldspars, matrix of muscovite, illite and montmorillonite.(**b**) [Virginia] Muscovite-illite as plagioclase pseudomorphs and tourmaline phenocrysts embedded in a kaolinite-halloysite and biotite matrix. (**c**)[Virginia] Halloysite and montmorillonite matrix containing tourmaline, muscovite-illite and kaolinite. (**d**) [Virginia] Fine grain halloysite, kaolinite and montmorillonite with an iron oxide coating. Colour key: kaolinite (dark green, light green, light blue), halloysite (dark blue), muscovite (red), illite (orange), montmorillonite (yellow, purple), tourmaline (pink), biotite (dark purple), iron oxide (brown).

of kaolinite in some sections, halloysite presumably from secondary origin, or a mixture of kaolinite and montmorillonite. Muscovite, illite and montmorillonite are abundant in some samples and have iron oxide coatings (Figure 4.7b). Tourmaline is present as veins of 0.5 to 2 cm thickness, or phenocrysts disseminated in the clay matrix (Figure 4.7a and c). The veins were probably formed after the kaolinisation of the granite, whereas the disseminated grains might be relicts from the original granite. Alteration of biotite to other micas and iron oxides makes it scarce in the drill cores. The spectral mixtures of iron oxides and kaolinite are common (Figure 4.7c).

4.4. QUALITY OF THE KAOLIN ORE

The structural ordering of the kaolinite crystals partly defines the quality of the kaolin ore. This degree of crystal order can be measured with IR spectroscopy, by using the kaolinite crystallinity (Kx) index proposed by Pontual et al. (1997). The Kx index makes use of the shape of the 2.2 µm doublet of kaolinite based on the definition that a well-defined doublet is characteristic of well-ordered structures. The index uses the 2.164 slope parameter, calculated as the ratio of the reflectance at 2.164 µm over that at 2.177 µm from continuum removed corrected spectra, to assess the intensity of the doublet, and the 2.184 slope parameter, calculated as the ratio of the reflectance at 2.184 µm over that at 2.190 µm from continuum removed corrected spectra, to assess the definition of the main absorption (Figure 4.8). For the 2.164 slope parameter, values smaller than 1 (typically smaller than 0.99) indicate a strong doublet, thereby implying high kaolinite crystallinity, and vice versa; the lower the value, the stronger the doublet and hence higher crystallinity. For the 2.184 slope parameter, values close to 1 indicate a probably broad and weak absorption, whereas values higher than 1.02 indicate a sharp absorption characteristic of high structural order. Equal values for both slope parameters evidence the absence of a doublet, and therefore kaolinite is not detected in such spectrum (Figure 4.8c). The Kx index combines the slope parameters as follows:

$$\mathrm{Kx} = 2.184\mathrm{slope} - (2.164\mathrm{slope} - 2.184\mathrm{slope}) \tag{4.1}$$

The left side of the equation assesses the difference between the two parameters, producing a 0 value for the absence of a doublet, a positive value for a weak doublet and a negative value for a strong doublet. When the newly generated value is subtracted from the right side of the equation, negative values enhance the index, and positive values decrease it. In this way, Kx values greater than 1.05 indicate very highly crystalline kaolinite, values between 1.02 and 1.05 correspond to moderately highly crystalline kaolinite, and values smaller than 1.02 are characteristic of poorly crystalline kaolinite.

The slope parameters and the Kx index were calculated using the point data spectra. They were analysed taking into account the existence of the 2.2 µm doublet, the occurrence of the 1.45 µm water feature, and the distortions of the secondary features of kaolinite between 2.25 µm and 2.50 µm. The results are presented in Figure 4.9. The presence of the 2.2 µm doublet was used to confirm the presence of kaolinite in the spectra. Samples without a doublet have elevated 2.164 slope values, comparable in magnitude to the value of the 2.184 slope. The absence of a doublet indicates that these samples do not contain kaolinite, and therefore, were not taken into account for the

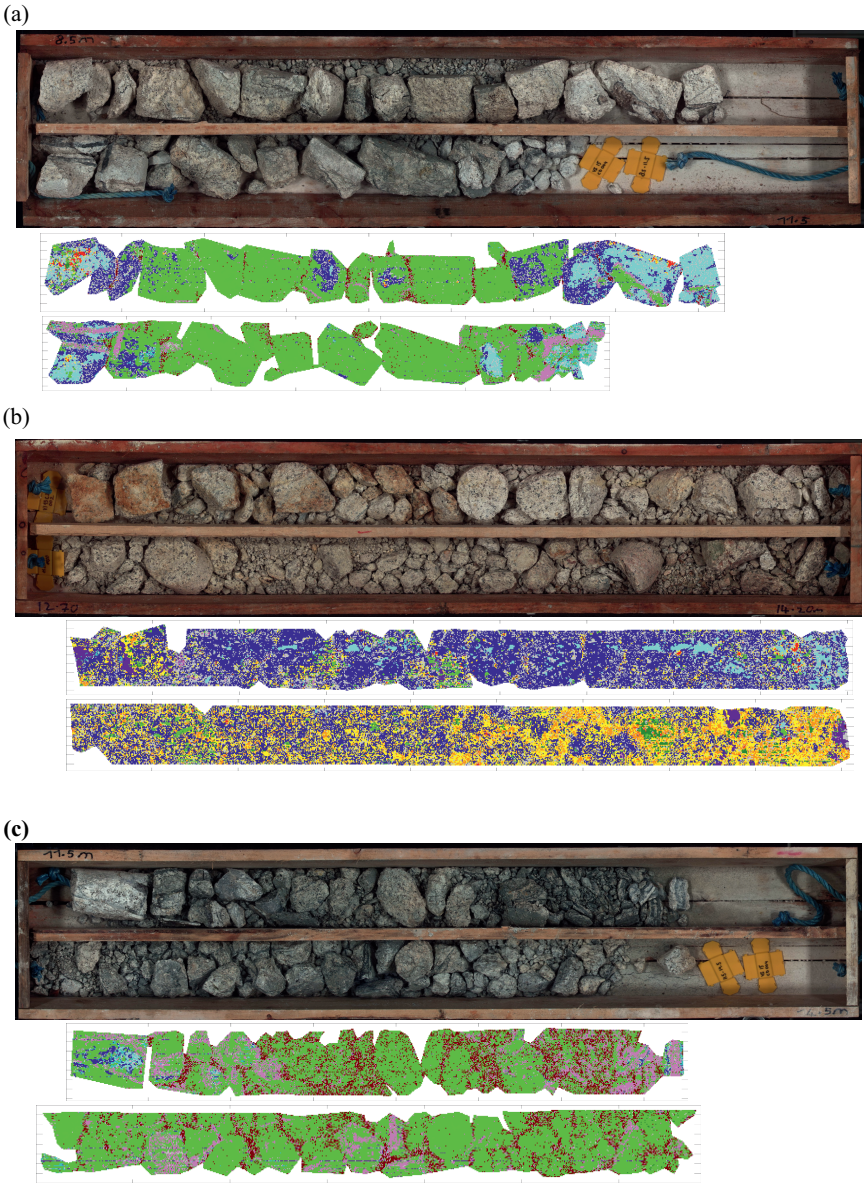

Figure 4.7: RGB images and hyperspectral mineral maps of drill cores sampled in the biotite granite: (**a**) Completely kaolinised granite with tourmaline veins and iron oxide coatings. (**b**) Kaolinised granite with abundant presence of halloysite, muscovite, illite, montmorillonite and iron coatings. (**c**) Kaolinised granite with tourmaline veins and iron staining. Colour key: kaolinite (light green, light blue), kaolinite mixed with iron oxide (dark green), halloysite (dark blue), muscovite (red), illite (orange), montmorillonite (yellow), montmorillonite mixed with iron oxide (purple), tourmaline (pink).

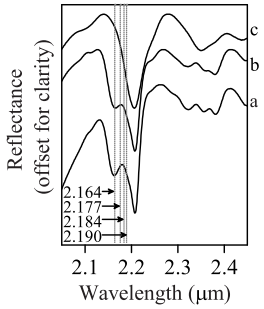

Figure 4.8: Position of the wavelengths at which the reflectance values are taken to calculate the slope parameters and the Kx index (**a**) Pure kaolinite, (**b**) impure kaolinite, (**c**) muscovite.

other analyses. Most of the kaolinite-bearing samples have a 2.164 slope between 0.95 and 1.00 and a 2.184 slope greater than 1.02, indicating high kaolinite crystallinity. The values of the Kx index range from 1.058 to 1.162, which according to the classification established by Pontual et al. (1997), describe very highly crystalline kaolinite. The second subject of analysis was the occurrence of the water feature at 1.45 μm. This peculiar water absorption raised questions about its possible influence on the quality of the kaolinite, which could presumably decrease its crystallinity. However, the water feature occurred at the entire range of Kx values. Furthermore, the feature was absent only in samples with the lower crystallinity, but this does not necessarily imply any causality. Consequently, the influence of abundant water in the sample environment does not seem to have any influence on the quality of the kaolinite.

Lastly, the effect of the possible spectral mixtures was determined. Other clay minerals such as muscovite, illite and montmorillonite, which are present in the samples, have their main absorption around 2.2 μm; their spectra can smoothen the kaolinite doublet generating imprecise lower crystallinity values. The spectral mixtures are more evident in the secondary features in the 2.25 to 2.50 μm range. Kaolinite has three small absorptions at 2.312 μm, 2.350 μm and 2.380 μm (Figure 4.8a), the presence of other minerals distorts these features (Figure 4.8b and c). The occurrence of such distortions was compared to the slope parameters and the Kx index, expecting that distorted-mixed spectra would be related to high a 2.164 slope and low Kx. However, as Figure 4.9 shows, there is no evidence of a relationship between mixed-spectra and degree of crystallinity. This suggests that, even in the presence of mineral mixtures, the Kx index gives a reliable estimation of the crystallinity of the kaolinite.

The Kx index of the rock and drill core samples was calculated using the hyperspectral images. Figure 4.10 displays some examples of the generated crystallinity maps. The Kx index values are of similar magnitude as those calculated from the point data, ranging from 1.04 to 1.10. In the rock samples, the kaolinite that pseudomorphs the feldspars has lower Kx values than the kaolinite that is present in the matrix (Figure 4.10a). Moreover, inside the pseudomorphs, the Kx index seems to gradually increase from the central part of the crystal towards the rims, possibly indicating the progression of the alteration. The higher Kx values in the matrix might indicate that due to the finer grain there is a higher

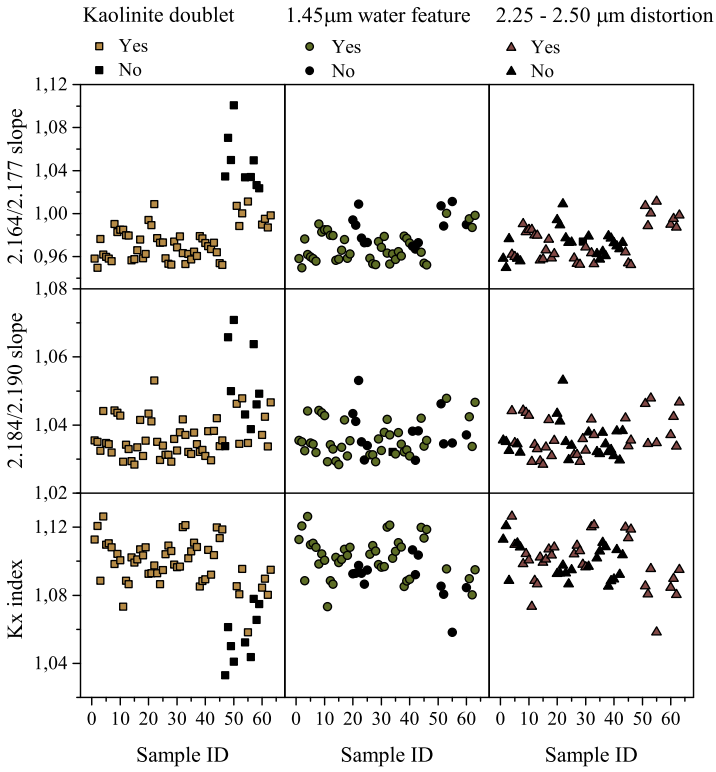

Figure 4.9: Slope parameters and Kx index values calculated from the point spectra, compared to the presence of the kaolinite 2.2 µm doublet, the 1.45 µm water absorption and the kaolinite spectral distortions in the 2.25 to 2.50 µm range. .

degree of alteration that has allowed the kaolinite crystals to develop a more ordered structure. The mixtures of kaolinite with iron oxides generate relatively low Kx values (Figure 4.10b, see also Figure 4.6d for reference). It is unclear whether the presence of iron oxide coating reduces the overall reflectance, hindering the detection of the kaolinite features, or whether the surplus of iron has reacted with the kaolinite producing Fe^{+3} for Al^{+3} cation exchange that modifies the crystal structure of the kaolinite, decreasing its crystallinity. The Kx values of the drill cores are higher than those of the rock samples, ranging from 1.06 to 1.2. As described in previous sections, the rock samples are described as moderately altered whereas the drill cores correspond to completely altered parts of the granite, indicating once again that stronger alteration has led to kaolinite with a well-ordered crystal structure. Despite the crystallinity variations, there is not any indication of alteration patterns along the drill cores. Unlike the crystallinity in the rock samples, the presence of iron does not seem to affect the Kx index values.

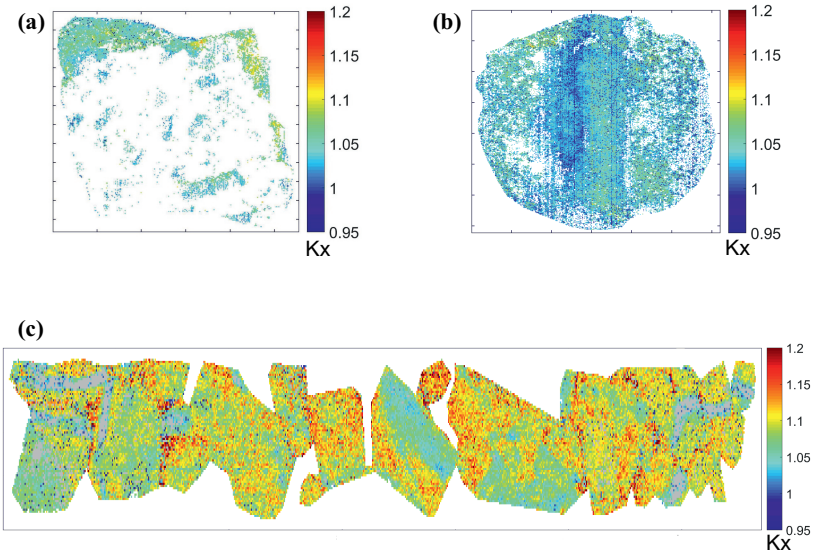

Figure 4.10: Kaolinite crystallinity maps of rock samples and drill cores based on the Kx index: (**a**) same sample as Figure 4.6a, (**b**) same sample as Figure 4.6b, (**c**) same drill core as Figure 4.7a, bottom row.

4.5. IMPLICATIONS FOR PROCESSING AND GENERATION OF HIGH QUALITY PRODUCTS

The kaolin deposits in the St Austell Granite have been extensively studied. The geological processes that led to the kaolinisation created a deposit of exceptional quality. Nevertheless, the properties that are characteristic of high-quality ores that are suitable for their use in performance and speciality applications are restricted only to some parts of the deposit. In particular, the variable presence of iron and iron-bearing mineralogy determines the parts of the deposit that host high-quality kaolin ores. Such ores should ideally have not only kaolinite with high crystallinity, but also it must be iron-free, or

the presence of iron should be linked to minerals that can be easily removed during the beneficiation process.

As a proof of concept, the IR spectroscopy analyses successfully detected the occurrence of iron in the high-grade and low-grade samples, which have different degree of kaolinisation. In the high-grade samples, where the most important iron-bearing mineral is tourmaline, only a few sections with iron oxide coatings were identified. In contrast, in the low-grade samples, the occurrence of iron revealed differences regarding the intensity of the alteration. In areas with moderate alteration, biotite is the dominant iron-bearing mineral, whereas in completely kaolinised areas the biotite seems to be altered producing secondary clays and iron oxides. From a beneficiation perspective, removal of biotite is more straightforward than the removal of iron oxides, which can become highly soluble.

Regarding the type of kaolinite, the high-grade samples establish the benchmark for crystallinity. As measured by the Kx index, the definition of a high-quality kaolin ore includes a Kx value higher than 1.05. In the low-grade samples, the higher Kx values occurred in the zones with more extensive alteration, whereas the zone with moderate alteration had lower Kx values of similar magnitude to those of the newly established threshold. Moreover, these moderate altered areas showed also a higher content of other clay minerals than the completely altered ones, which logically are composed mainly of kaolinite.

Based on these observations, the potential of the low-grade kaolin from the biotite granite pits faces the trade-off between a kaolin ore with iron content that can be easily removed, or an ore with high kaolinite crystallinity. In a broader picture, to meet the production standards, the quality specifications should be achieved using the raw ore, which entails a degree of intrinsic variability within a deposit. The control of such variability involves the blending of the material that passes through the different stages of the process. In this scenario, the different types of ore identified in the biotite granite could be treated similarly to maximise their potential. In particular, the generation of mineral and crystallinity maps built upon IR hyperspectral data could be used for this purpose given their demonstrated ability in the identification of the mineralogy of the kaolinised granite, with particular sensitivity to iron-bearing phases. Moreover, they facilitate the distinction between clay minerals that otherwise require extensive analyses for their identification. This distinction enables the determination of kaolinite abundance in different zones inside a pit, as well as its crystallinity and possible variations along the deposit. The spectral definition of the parameters for quality ore can certainly support the selection of mine targets and assist the further blending of different ores, ensuring the consistency and the quality of the processed ore.

4.6. CONCLUSIONS

This study explored the contrasts between different parts of the deposit that determine the advantages and the challenges that they impose for their usage as ore in the generation of certain products. For doing this, infrared (IR) spectroscopy was used as a tool that can identify the most relevant mineralogy in the kaolinised areas, as well as the rock textures. The results obtained generated a comprehensive overview of the content, quality and distribution of the kaolin ore in the sampled material.

The IR point data and hyperspectral images were successful in the identification of the mineral associations in the kaolin ore, including the occurrence of mineral impurities.

The observations on the mineralogy and the textures were correlated to the extent of the kaolinisation and the quality of the kaolin ore. Particularly, the use of the kaolinite crystallinity (Kx) index and the detection of iron impurities aided in the characterisation of parts of the kaolin deposit where the quality parameters vary considerably from the traditional targeted areas.

The insights of the present study contribute to the knowledge and the understanding of the of the kaolin deposits in the St Austell Granite, with practical implications for the mining industry. The results hereby presented can assist the mine planning and processing activities for the generation of kaolin products. The IR characterisation of the kaolin ore may be applied to other stages of the mining value chain, enabling the record of comparable data along the process.

REFERENCES

BGS (2009), 'Mineral planning factsheet: Kaolin', Online.
URL: *https://www.bgs.ac.uk/downloads [Accessed June 2018]*

Bray, C. J. and Spooner, E. T. C. (1983), 'Sheeted vein Sn-W mineralization and greisenization associated with economic kaolinization, Goonbarrow china clay pit, St. Austell, Cornwall, England; geologic relationships and geochronology', *Economic Geology* **78**(6), pp. 1064–1089. DOI: 10.2113/gsecongeo.78.6.1064

Bristow, C. M. (1993), The genesis of the china clays of south-west England – A multistage story, *in* H. H. Murray, W. M. Bundy and C. C. Harvey, eds, 'Kaolin Genesis and Utilization', The Clay Minerals Society, Boulder, Colorado, Chapter 8, pp. 171–204.

Bristow, C. M. and Exley, C. S. (1994), 'Historical and geological aspects of the china-clay industry of southwest England', *Transactions of the Royal Geological Society of Cornwall* **21**, pp. 247–314.

Bristow, C. M., Palmer, Q. , Witte, G. J. , Bowditch, I. and Howe, J. H. (2002), The ball clay and china clay industries of Southwest England in 2000, *in* P. W. Scott and C. M. Bristow, eds, 'Industrial Minerals and Extractive Industry Geology', The Geological Society, pp. 17–41.

Brown, L. G. (1953), 'Geological aspects of the St. Austell granite', *Clay Minerals* **2**(5), pp. 17–21.

Clark, R. N., Swayze, G. A. , Wise, R. , Livo, K. E. , Hoefen, T. M. , Kokaly, R. F. and Sutley, S. J. (2007), 'USGS Digital Spectral Library splib06a'.
URL: *http://speclab.cr.usgs.gov/spectral.lib06/ds231/datatable.html [Accessed 2016]*

CSIRO (2007), 'The Spectral Geologist software suite'.
URL: *http://www.thespectralgeologist.com/ [Accessed 2016]*

Exley, C. S., Floyd, P. A. and Styles, M. T. (1993), Igneous rocks of south-west England, *in* 'Igneous rocks of south-west England', number 5 *in* 'Geological Conservation Review', Springer Netherlands, Chapter 1, pp. 1–5.

Groenheide, S. (2016), Mapping the kaolin mineralization of the St. Austel granite (SW England) using VNIR and SWIR hyperspectral imaging, Master's thesis, Delft University of Technology.

Idoine, N, E., Bide, T. , Brown, T. J. and Raycraft, E. R. (2016), United Kingdom Minerals Yearbook 2015, Technical Report OR/16/021, British Geological Survey.
URL: *https://www.bgs.ac.uk/mineralsuk/statistics/ukStatistics.html [Accessed February 2019]*

Konta, J. (1969), Comparison of the proofs of hydrothermal and supergene kaolinisation in two areas of Europe, *in* 'Proceedings of the international clay conference', Vol. 1, Tokyo, pp. 281–291.

Manning, D. A. C., Hill, P. I. and Howe, J. H. (1996), 'Primary lithological variation in the kaolinized St Austell Granite, Cornwall, England', *Journal of the Geological Society* **153**(6), pp. 827–838. DOI: 10.1144/gsjgs.153.6.0827

Mueller, S., Scott, P. W. and Evans, M. J. (1999), 'Kaolinisation, mineralisation and structures in biotite granite at Bodelva, St. Austell, Cornwall', *Geoscience in South-West England* **9**(4), pp. 310–317.

Murray, H. H. (2006), Kaolin Applications, *in* H. H. Murray, ed., 'Applied Clay Mineralogy - Occurrences, Processing and Application of Kaolins, Bentonites, Palygorskite-Sepiolite, and Common Clays', Vol. 2 of *Developments in Clay Science*, Elsevier, Chapter 5, pp. 85–109. DOI: 10.1016/s1572-4352(06)02005-8

Murray, H. H. and Keller, W. D. (1993), Kaolins, kaolins, and kaolins, *in* H. H. Murray, W. M. Bundy and C. C. Harvey, eds, 'Kaolin Genesis and Utilization', The Clay Minerals Society, Boulder, Colorado, Chapter 1, pp. 1–24.

Pontual, S., Merry, N. and Gamson, P. (1997), Regolith Logging, *in* S. Pontual, N. Merry and P. Gamson, eds, 'Spectral Analysis Guides for Mineral Exploration', Vol. 1, AusSpec International, Chapter 8, pp. 8.1–8.62.

Psyrillos, A., Manning, D. A. C. and Burley, S. D. (1998), 'Geochemical constraints on kaolinization in the St Austell Granite, Cornwall, England', *Journal of the Geological Society* **155**(5), pp. 829–840. DOI: 10.1144/gsjgs.155.5.0829

5

CHARACTERISATION OF THE KAOLIN CALCINATION PROCESS USING INFRARED SPECTROSCOPY

This chapter assesses the suitability of IR spectroscopy as a potential technique for the online characterisation of the calcination of kaolin.

Parts of this chapter have been published in:
Guatame-Garcia, A., Buxton, M., Deon, F., Lievens, C. and Hecker, C. (2018). Toward an on-line Characterization of Kaolin Calcination Process Using Short-Wave Infrared Spectroscopy. *Mineral Processing and Extractive Metallurgy Review 39(6),* 420-431. doi: 10.1080/08827508.2018.1459617.

The processing of kaolin that is used for the manufacturing of paper, paint, rubber and other specialty applications involves thermal treatment at high temperatures in a process known as calcination. A primary concern in the production of calcined kaolin (trade name metakaolin) is the ability to monitor the extent of the mineral transformation on-site and in real-time, thus ensuring the generation of optimal products. The aim of this study was to assess the suitability of using infrared (IR) spectroscopy as a potential technique for the online characterisation of the calcination of kaolin. For this, samples calcined to different temperatures were first characterised in the laboratory using Mid- and Long-Wave Infrared ranges. Next, the observations were extrapolated to the Short-Wave Infrared (SWIR) range, which is more suitable for instruments that provide on-site use capabilities. The laboratory data showed changes in the kaolinite spectra related to dehydroxylation and changes in the adsorption of water during the recrystallisation stage. In the SWIR spectra, those variations were detected using the kaolinite crystallinity (Kx) index and the depth of the water spectral feature (1900D). A high correlation between the Standard Operational Procedure for the quality control of calcined kaolin and the Kx index was observed ($r = -0.89$), as well as with the 1900D parameter ($r = -0.96$). Overall, this study offers a new conceptual approach to the use of SWIR spectroscopy for the characterisation the calcination of kaolin, withdrawing the need of using extensive laboratory techniques. Besides, it serves as a foundation for the development of a spectroscopy-based online analytical tool for process control during the generation of calcined kaolin products.

5.1. INTRODUCTION

For industrial applications, natural kaolin clay is heated to temperatures above 900 °C. The purpose of this thermal treatment, also known as calcination, is to modify the chemical and physical properties and to enhance the value of the raw material. During the calcination, kaolinite [$Al_2Si_2O_5(OH)_4$], which is the main constituent in kaolin, is transformed first into metakaolinite [$Al_2Si_2O_7$] and further into mullite [Al_2SiO_8]. The industrial interest on calcined kaolin depends on the chemical and physical properties of the intermediate phases produced at various calcination stages. For example, the highly disordered and reactive metakaolinite is used as a pozzolanic additive in the cement industry. For other uses, such as in the pharmaceutical industry, the calcination time is increased to reduce the metakaolinite chemical reactivity and enhance the whiteness, yet keeping low abrasiveness (Thomas et al., 2009). The high-temperature mullite phase is whiter than metakaolinite, but highly abrasive, which is detrimental for the targeted markets. In order to ensure the production of calcined kaolin with optimum properties, the quality control strategies should involve techniques that enable a quick turnaround for timely operational feedback. It is then required that such techniques can be used in an online production environment and generate (near) real-time data. However, the study of calcined kaolin in the industry has focussed mostly on product development rather than in the monitoring and control of the calcination process.

The Standard Operating Procedure (SOP) in the industry for the quality control of calcined kaolin products is the chemical extraction of soluble Al_2O_3. This parameter is used to estimate the intermediate stages between the metakaolinite and mullite phases; however, the extraction of soluble Al_2O_3 is a time-consuming laboratory-based technique, which is contrary to the necessities of a production environment. Other techniques,

such as X-ray diffraction, struggle with the characterisation of the metakaolinite and the subsequent intermediate stages, due to their amorphous structure, as was already remarked by Brindley and Nakahira (1959) and Percival et al. (1974). For the consideration of an alternative characterisation technique, the capability of detecting both, crystalline and amorphous phases, and the possibility of implementation in an online environment are mandatory requirements.

Regarding the first condition, Infrared (IR) spectroscopy has been successfully used by multiple researchers to characterise the calcined kaolin reaction sequence (Drits et al., 2016; Freund, 1974; Frost et al., 2002; Frost and Vassallo, 1996; Miller, 1961; Percival et al., 1974). Using laboratory-based instruments, which commonly cover the wavelength range between 2.5 µm and 16.00 µm, known as Mid and Long-Wave infrared ranges (MWIR and LWIR, respectively), different spectral bands have been assigned to detect the kaolinite – metakaolinite and metakaolinite – mullite transitions. Concerning the second condition, IR spectroscopy in the wavelength range between 1.00 µm and 2.50 µm, known as Short-Wave Infrared or SWIR, has been used before in online applications in other mineral processing environments (Haavisto and Hyötyniemi, 2011). In these ranges, IR spectroscopy has been proven a suitable online technique because of the lower costs of the optics of the instruments and their commercial availability. However, for the online characterisation of the calcined kaolin reaction, the conditions to extrapolate the laboratory observations to a suitable online set-up in the SWIR have not been yet explored.

To be able to develop an online analysis tool that provides information along entire kaolin calcination reaction, it is necessary to identify the spectral features in the SWIR range that describe the kaolinite – metakaolinite – mullite transition. This study explores different spectral parameters that can be related to such processes, and assesses the suitability of using SWIR spectroscopy as a proxy for the determination of the industrial standard, with the objective of contributing to the development of a monitoring and control strategy for the production of calcined kaolin. This paper first presents a brief review of the known IR spectral features that characterise the calcined kaolin reaction sequence. Then, samples of Cornish kaolin calcined at different temperatures are analysed using laboratory and portable IR spectrometers in various spectral ranges. A special focus is given to the characterisation of the mineral transitions in the MWIR and LWIR ranges to improve the interpretation of the SWIR spectra, especially for the calcination stages that involve indirect observations. The results of the SWIR analyses are further compared with the standard soluble Al_2O_3 test, and the observations are discussed with a view towards their implications for the online characterisation of the calcined kaolin reaction.

5.2. INFRARED SPECTROSCOPY AND THE CALCINED KAOLIN REACTION

In the IR spectrum, the absorption features are a function of the wavelength and are related to the vibrations of molecular bonds in the minerals, thus giving information about their structure. In the study of the calcined kaolin reaction, previously described in Section 3.2.2, IR spectroscopy is particularly useful since it detects the structural changes between the mineral transitions, including the amorphous phases. In the IR spectrum, the MWIR and LWIR ranges contain the fundamental vibrations that describe minerals

thoroughly, whereas the VNIR and SWIR ranges contain overtones or combinations of the vibrations than contain OH-bonds. Traditionally, IR studies have focused on the MWIR and LWIR ranges to characterise the kaolinite – metakaolinite dehydroxylation process (Drits et al., 2016; Frost and Vassallo, 1996; Miller, 1961; Percival et al., 1974), and the re-crystallisation from metakaolinite to mullite (Percival et al., 1974; Ptáček et al., 2011).

KAOLINITE – METAKAOLINITE TRANSITION

Frost et al. (2002) Drits et al. (2016) and Percival et al. (1974) summarised the diagnostic spectral absorption bands of the kaolinite-metakaolinite transition (Figure 5.1). The aluminosilicate framework presents multiple absorptions related to Si–O bonds between 8.69 µm and 10.00 µm, and two Al–O features around 12.59 µm and 13.29 µm; absorption bands near 10.66 µm and 10.94 µm correspond to inner Al–OH bonds; the outer OH groups present features at lower wavelengths, between 2.70 µm and 2.77 µm. Presence of bonded molecular water, not from the kaolinite structure but due to atmospheric exposure, has absorption band near 2.78 µm and 6.13 µm (Johnston, 2017). In the SWIR range, the first overtone of the OH vibration is present at 1.41 µm, the combination tones of the OH and Al–OH generates a double absorption band at 2.16 µm and 2.21 µm, and the overtones of water are near 1.38 µm, 1.45 µm and 1.88 µm.

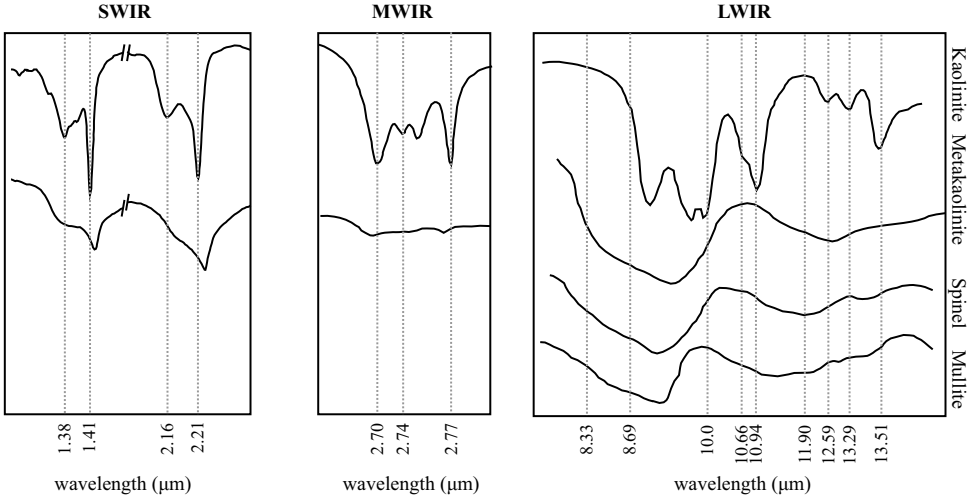

Figure 5.1: Main infrared spectral features that characterise the kaolin calcination process in the SWIR (Frost et al., 2002), MWIR (Drits et al., 2016) and LWIR (Percival et al., 1974) ranges

In the transformation towards metakaolinite, the main changes are related to the loss of OH groups. Miller (1961) described how in the dehydroxylation process, the bands near 2.77 µm merge and the Al–OH bands at 10.66 µm and 10.94 µm vanish indicating the destruction of the octahedral sheet. Percival et al. (1974) and Freund (1974) added that the Si–O bands merge and shift towards lower wavelengths, forming a broad absorption band around 9.35 µm and a new band emerges near 12.39 µm from the newly bonded Al–O.

METAKAOLINITE – MULLITE TRANSITION

The transition from metakaolinite to mullite is characterised by the abundance of amorphous material and the re-organisation of the crystal lattice, in particular of the Al^{+3} ions in the form of γ-alumina.In the IR spectrum (Figure 5.1), the amorphous phases typically have broad absorption bands that shift towards lower wavelengths, near 8.33 µm for the Si-spinel and towards 11.90 µm for the γ-alumina. Well-developed Si–O absorption bands near 8.55 µm and 11.10 µm and Al–O absorptions near 13.51 µm characterise the crystallisation of mullite.

5.3. METHODS

5.3.1. SAMPLES

This study used three commercial kaolin samples thermally treated to 500 °C from a kaolin processing plant in Cornwall (South-west England) (Wilson, 2003). The samples were taken from the production route after demagnetising, drying and milling, and they are they are representative of the typical feeds used for calcination. The samples were calcined in the laboratory using a muffle furnace attempting to emulate the conditions normally used in industrial operations where soft calcination is performed. Soft calcination involves exposing the kaolin to high temperatures for a prolonged amount of time to guarantee complete calcination. Each sample was calcined at temperatures from 500 to 1200 °C at 100 °C intervals. For each experiment, 360 g of kaolin were equally split into six fused-silica dishes and placed in the calciner and heated from ambient to the specified temperature at a rate of 15 °C per minute. The calciner was kept at the specified temperature for 15 minutes and then allowed to cool naturally. Once the temperature had cooled below 200 °C the sample was taken out and replaced with the next one. The samples were named Ka-b, with a being the sample number and b the calcination temperature. For this study, access was not granted to untreated samples; however, since the thermal behaviour or partially dehydroxylated kaolin samples are qualitatively similar to that of untreated samples (Drits et al., 2016), the samples calcined at 500 °C are regarded here as untreated kaolin. Table 5.1 shows the chemical composition of the reference kaolin determined with XRF data. According to semi-quantitative XRD analysis in combination with the bulk chemical analysis, the mineralogical content is aproximately 65% kaolinite and 35% illite.

Table 5.1: Chemical composition (XRF) of the three kaolinite samples (wt%)

Sample	Al_2O_3	SiO_2	K_2O	Fe_2O_3	TiO_2	CaO	MgO	Na_2O	P_2O_5	LOI
K1-500	37.0	48.0	1.45	0.65	0.03	0.08	0.31	0.06	0.11	12.3
K2-500	36.7	47.5	1.63	0.92	0.05	0.43	0.38	0.02	0.14	12.3
K3-500	37.2	47.0	1.15	1.43	0.04	0.06	0.26	0.01	0.16	12.6

5.3.2. X-RAY DIFFRACTION AND THERMOGRAVIMETRY ANALYSIS

The XRD patterns were collected with a Bruker D8 Advance diffractometer featuring Bragg Brentano geometry using a Cu – Kα radiation of 45 kV and 40 mA on powders placed on a PMMA holder L25. The XRD spectra were measured with a coupled $\theta - 2\theta$ scan ranging

from 10 to 110 °2θ (step size: 0.03 °2θ, time per step: 1 sec). The acquired XRD patterns were interpreted by using the Bruker software DIFFRAC.EVA V4.2. A further interpretation was attempted with the Rietveld Software EXPGUI.

Information on the thermal degradation of the reference kaolin samples was obtained by thermogravimetry analysis (TGA). The measurements were carried out with a Perkin Elmer TGA 8000. Samples of ± 10 mg were placed in an alumina pan and flushed with an N2 carrier gas (30 ml/min). The samples were heated at 15 °C per minute up to 1150 °C, with an isothermal period of 15 minutes. The experiments were performed in duplicates.

5.3.3. INFRARED SPECTROSCOPY

The kaolin calcination reaction was characterised with three spectroscopy methods: Attenuated Total Reflectance (ATR), Directional-Hemispherical Reflectance (DHR) and Bidirectional reflectance (Section 2.2.3). ATR data was used for identifying the fundamental absorption bands of the samples. Since the ATR spectrum tends to be weak at shorter wavelengths, only the LWIR segment was used in the analysis. The DHR spectra was used to complement the ATR fundamentals data, ensuring good quality information in the MWIR. Besides, this technique was selected because the instrument set-up emulates the measuring conditions present in remote sensing applications. The measurements were collected on loosely packed powders trying to emulate the type of samples found in a processing plant environment. Only the MWIR range was used in the analysis. Bidirectional reflectance was used as an intended on-site technique. The measurements were collected on compact powders with a rough surface as an alternative sample preparation for in-plant conditions. Only the SWIR range was used in the analyses.

Spectral data processing included removal of the continuum to normalise the reflectance spectra, thus enabling a better comparison of certain spectral features. The continuum, or background spectrum, is the overall albedo of the reflectance curve. It can be modelled as a mathematical function to isolate specific absorption bands, as explained by Clark and Roush (1984). The continuum was removed by using a built function in the ENVI software (ITT, 2008) that calculates straight-line segments tangential to the spectra. The continuum removal (CR) was done independently for the 1.30 to 1.50 µm, 1.80 to 2.10 µm, 2.10 to 2.30 µm, 5.50 to 6.50 µm, and 7.50 to 15.00 µm regions, and it was extracted for the spectral analysis of the sharpness of the LWIR Si–O and Al–O features, kaolinite crystallinity (Kx) index and 1900D parameter. Specific spectral values, such as reflectance and wavelength position were retrieved using the HypPy Hyperspectral Python Software Package developed by Bakker (2016). The general noise in the spectra was reduced using a Savitzky–Golay filter.

The sharpness of the Si–O absorption band around 9.50 µm was determined by calculating the changes in the full-width half maximum (FWHM) constrained from 7.70 to 10.90 µm. The development of an Al–O absorption band around 13.70 µm was determined using a slope parameter, named in this work as the *13.70 slope*. It represents the slope between 13.30 µm and 13.75 µm and it was calculated as the ratio of the reflectance value at 13.30 µm over that at 13.75 µm. The slope between these values denotes the intensity of the 13.70 µm absorption band.

The extraction of the Kx index was based on the parameters defined by Pontual et al. (1997). This index makes use of the characteristic doublet of kaolinite around 2.20 µm

to assess its degree of crystallinity. The determination of the Kx index is based on the formula:

$$\mathrm{Kx} = (R_{2.184}/R_{2.190}) - ((R_{2.164}/R_{2.177}) - (R_{2.184}/R_{2.190})) \tag{5.1}$$

where R_x is the reflectance value at the given x wavelength, extracted from continuum removed spectra (Figure 5.2a). Well-defined doublets with steep slopes produce Kx ≥ 1.02, characteristic of highly crystalline kaolinites, whereas for smooth doublets Kx ≤ 1.02 defining those that are poorly crystalline.

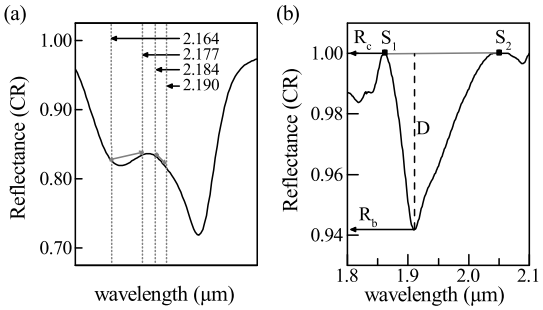

Figure 5.2: Definition of the spectral feature characteristics used in the extraction of the (**a**) Kx index and the (**b**) 1900D parameter (Spectra were taken from sample K1-500).

The 1900D parameter in this work is defined as the relative absorption depth of the minimum point in the 1.86 to 2.06 μm region. The parameter was calculated on continuum removed spectra according to the definition of van der Meer (2004) as:

$$\mathrm{D} = 1 - (R_b/R_c) \tag{5.2}$$

where R_b is the reflectance at the bottom of the absorption band, and R_c is the reflectance of the continuum at the same wavelength as R_b, as represented in Figure 5.2b. The S1 and S2 points represent the shoulders that constrain the width of the absorption band at 1.86 μm and 2.06 μm respectively. The 1900D parameter represents the intensity of the water absorption feature.

Soluble Al_2O_3 was used as reference data to estimate the extent of the calcination reaction. It was chosen since it is the standard method utilised for quality control in some of the kaolin processing plants, such as the operations in Cornwall. This parameter measures the amount of Al_2O_3 extracted from the γ-alumina in the spinel phase and, therefore, it is an indication of the stability of the mineral's crystal structure. The soluble Al_2O_3 was extracted by leaching using nitric acid following the procedure presented by Thomas (2010). The Al_2O_3 content was measured using XRF analysis and is reported in Table 5.2.

The amount of environmentally adsorbed water (Table 5.2) was assessed by drying the samples overnight in an oven at 105 °C and later exposing them to ambient conditions. The weight increase between the dry and exposed samples is taken as the relative amount of adsorbed water. This procedure was followed to ensure that the environmental conditions and time of exposure would be equal for all the samples.

Table 5.2: Soluble Al_2O_3 values and mass increase due to environmentally adsorbed water of the calcined samples

Sample	**Soluble Al_2O_3** (wt%)	**Mass increase** (wt%)
K1-500	0.51	0.41
K1-600	2.99	0.32
K1-700	13.3	0.42
K1-800	19.7	0.31
K1-900	23.5	0.21
K1-1000	18.8	0.29
K1-1100	10.2	0.31
K1-1200	1.58	0.46
K2-500	0.45	0.39
K2-600	3.51	0.45
K2-700	15.3	0.39
K2-800	16.3	0.32
K2-900	20.6	0.20
K2-1000	18.3	0.10
K2-1100	9.92	0.28
K2-1200	3.24	0.36
K3-500	0.54	0.36
K3-600	3.28	0.40
K3-700	9.52	0.40
K3-800	15.5	0.20
K3-900	21.6	0.11
K3-1000	21.0	0.30
K3-1100	8.15	0.38
K3-1200	1.25	0.42

5.4. RESULTS AND DISCUSSION

5.4.1. CHARACTERISATION OF CALCINED KAOLIN

The XRD patterns of the calcined kaolin samples, summarised in Figure 5.3, enabled the identification of the mineralogical content along the calcination stages. In the low temperatures (500 to 800 °C), kaolinite is identified by the diffraction peaks at 25 °2θ (d(002) = 0.36 nm), 20 °2θ (d(020) = 0.44 nm) and 12 °2θ (d(001) = 0.71 nm); in the reference kaolin, aproximately 65 % consists of kaolinte. The diffraction peaks around 9, 18 and 27 °2θ are assigned to illite based on the chemical composition of the samples. From 500 to 800 °C, the reducing intensity of the kaolinite's diffraction peaks indicates breakdown of the crystal structure. Besides, increasing lump from 15 to 35 °2θ indicates the formation of an amorphous phase, attributed to metakaolinite. The presence of other diffraction peaks indicates the occurrence of crystalline phases attributed to illite and quartz, which remain present along the entire calcination sequence in an amount that varied from 35 to 45 % for illite and from 10 to 15 % for quartz. After 900 °C, the diffraction peaks of kaolinite are completely absent, indicating complete dehydroxylation. At 1100 °C the development of new crystalline phases becomes evident by the emerging diffraction peaks characteristic of γ-alumina (37, 46 and 67 °2θ) and mullite (16, 33, 41,

61 and 74 °2θ), following the reaction presented in Equations (3.4) and (3.5) although possibly amorphous γ-alumina already occurs at slightly lower temperatures, namely around 1000 °C.

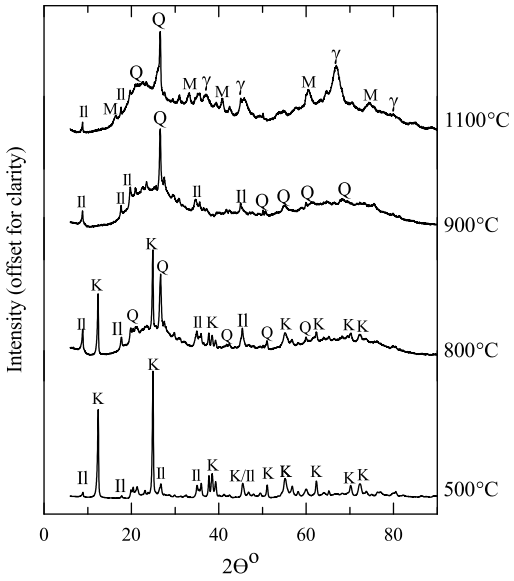

Figure 5.3: XRD patterns of calcined kaolin at 500 °C, 800 °C, 900 °C and 1100 °C where the most relevant mineralogical changes are detected. K = kaolinite, Il = illite, Q = quartz, γ = γ-alumina, M = mullite. (Patterns from K1 samples)

In order to characterise the thermal transformations of the studied samples, TGA and DTA analyses were conducted for the reference kaolin, as Figure 5.4 shows. Since the reference kaolin has been already calcined to 500 °C, the mass loss related to dehydration and pre-dehydroxylation is lower than that of natural kaolins. However, according to Drits et al. (2016), the patterns along the rest of the heating sequence are qualitatively similar. The dehydroxylation of kaolinite occurs from 420 to 730 °C, with the endothermic peak around 550 °C, characteristic of high-crystallinity kaolinites. The exothermic peak that indicates the formation of γ-alumina around 985 °C is weak suggesting mild recrystallisation, probably due to the heating rate and good crystallinity of the kaolinite. The asymmetry of the 550 °C endothermic peak indicates the presence of illite, as previously indicated by the XRD analysis.

5.4.2. KAOLIN CALCINATION REACTION IN THE MWIR AND LWIR RANGES

The MWIR and LWIR measured spectra of the kaolin calcination are displayed in Figure 5.5. The spectra are divided into three regions to highlight the main absorption bands that characterise the reaction sequence. The first region (2.60 to 3.00 µm) shows the variation in the outer hydroxyls (Figure 5.5a); the second region (5.5 to 6.50 µm) displays the spectral absorption bands of molecular water (Figure 5.5b); the third one (8.00 to

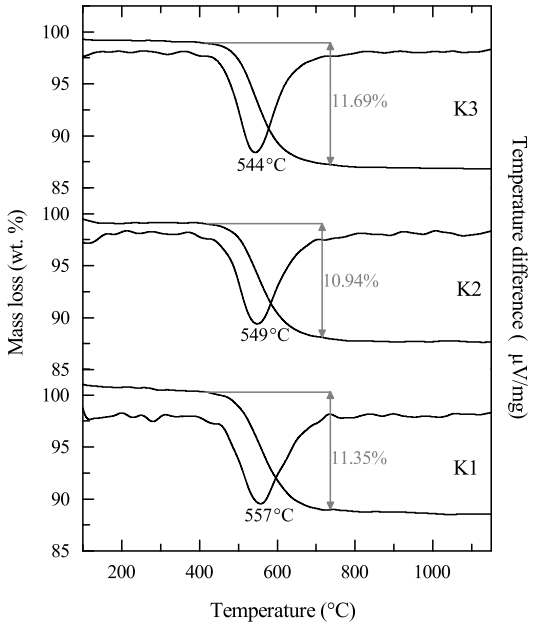

Figure 5.4: TGA and DTA curves of kaolin partially dehydroxylated to 500 °C

14.00 µm) shows the aluminosilicate and the Al-hydroxyl absorption bands (Figure 5.5c-d). The most notorious change in the overall spectra occurs between 800 °C and 900 °C with a considerable reduction in the number of troughs, resulting in a transformation in the shape of the absorption bands.

The spectral changes in the low-temperature domain (500 to 800 °C) clearly describe the dehydroxylation process that occurs in the kaolinite – metakaolinite transition. Most of the spectral absorption bands weaken as a result of the gradual breakdown of the kaolinite structure. The biggest changes occur in the MWIR range, where multiple bands between 2.70 µm and 2.77 µm become gradually shallower and suddenly fuse to a single and broad absorption band between 800 °C and 900 °C, reflecting the loss of OH groups. Similarly, the Si–O absorption bands in the LWIR range merge into a single band with minimum at 9.66 µm, indicating the transition towards an amorphous phase. The Al–O and water absorption bands become shallower, nearly flat, with the increasing temperature as a consequence of the water loss described in Equation (3.3). Furthermore, the complete fading of the Al–OH absorption band between 800 °C and 900 °C indicates that the dehydroxylation is complete, giving place to the metakaolinite phase.

In the high-temperature domain, from 900 to 1200 °C, broad and smooth bands that are particular of amorphous phases prevail. In the MWIR range, a weak hydroxyl band is constant at 2.74 µm, as indication of the presence of illite previously identified with XRD. Besides, a new weak trough develops at 2.78 µm, which is attributed by Aines and Rossman (1984) to the presence of molecular water; in addition, the deepening of the

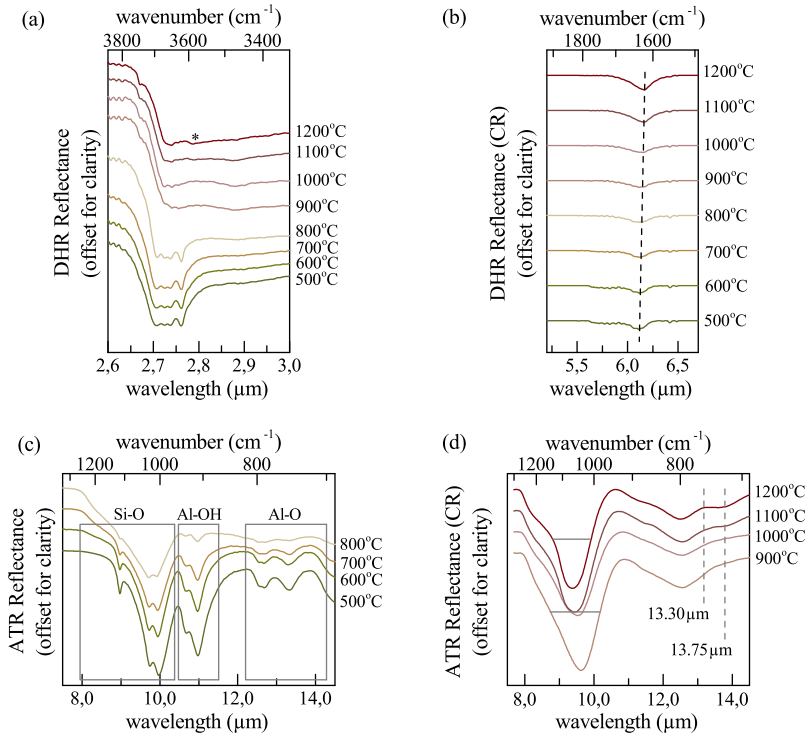

Figure 5.5: Infrared spectra of the calcined kaolin (sample K1). (**a**) Outer hydroxyls in the MWIR range at 2.63 to 3.13 µm in DHR reflectance (the * symbol indicates the through at 2.78 µm); (**b**) diagnostic water absorption band in the MWIR range at 5.63 to 6.77 µm in CR DHR reflectance; (**c**) aluminosilicate and Al-hydroxyl absorption bands in the LWIR range at 7.50 to 14.50 µm in ATR reflectance between 500 °C and 800 °C; (**d**) enhanced CR ATR spectra between 900 °C and 1200 °C; horizontal bars in the Si–O band denote differences in the FWHM, vertical dashed lines indicate the wavelengths used in the 13.70 slope for the Al–O feature.

characteristic water absorption band at 6.13 µm at higher temperatures (Figure 5.5b) reinforces this interpretation. The most prominent bands appear in the LWIR range (Figure 5.5d) where the Si–O single absorption band is dominant. This feature shifts to shorter wavelengths, and it constantly narrows towards the highest temperature, as the decrease in the FWHM values indicates (Figure 5.6a); besides, a shoulder appears at 9.09 µm in the 1200 °C spectrum. Even though the presence of illite (9.2 µm) and quartz (9.7 µm) in the high-temperature domain should be reflected in the Si–O feature, it seems that the amorphous fraction masks these absorptions. The Al–O feature keeps a weak band around 12.63 µm, which becomes mildly better defined at 1100 °C and 1200 °C. After 1100 °C, the emergence of a new absorption band at 13.76 µm is denoted by the 13.70 slope parameter, shown in Figure 5.6b, which indicates the continuous increasing intensity around this wavelength.

The redefinition of the Si–O and Al–O absorption bands at the highest temperatures suggest the beginning of the re-crystallisation of the spinel phase, described in Equa-

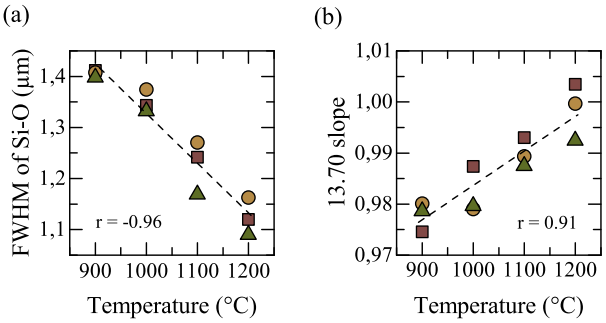

Figure 5.6: Spectral parameters that describe the redefinition of the Si–O and Al–O features in the high-temperature domain. (a) FWHM of the Si–O feature around 9.50 µm; (b) 13.70 slope parameter that indicates the formation of the Al–O absorption band. (⊠ = K1, ● = K2, ▲ = K3).

5

tion (3.5). These results are consistent with data obtained by Percival et al. (1974), who described the spinel as Si-spinel and γ-alumina. However, in Figure 5.5d, the band centers for the Si–O and Al–O features are located at longer wavelengths than those reported in the literature (Section 3.2.2), indicating in the studied samples that the amorphous phase is dominant, which is in agreement with the TGA resulst that suggested that only mild recrystallisation takes place. For the given experimental design, the temperature range where the metakaolinite and spinel phase are developed is also consistent with the time-temperature-transformation diagrams for kaolinite presented by Onike et al. (1986).

MacIver et al. (1963) indicated that γ-alumina strongly adsorbs molecular water on its surface. Moreover, Liu (2008) attributes the presence of a broad 2.84 µm absorption band to adsorbed water in hydrated γ-alumina. Since the studied samples were exposed to environmental conditions, it is expected that the presence of the γ-alumina phase formed from the metakaolinite is responsible for the re-adsorption of water once the sample has cooled down, and consequently, for the changes in the 2.78 µm and 6.13 µm absorption bands in the high-temperature domain. Therefore, the changes in the water absorption band are attributed to environmental conditions and not to the actual mineral transition. Most of the studies that characterise the metakaolinite – mullite transition focus on the description of the aluminosilicate bands. However, the evidence presented here supports the use of water-related absorption bands for the identification of γ-alumina, in conditions where the samples are exposed to the environment.

5.4.3. KAOLIN CALCINATION REACTION IN THE SWIR RANGE

The overtones and combination of the hydroxyl bands in the SWIR reflectance spectra are presented in Figure 5.7. In this range, the doublets at 1.41 µm and 2.21 µm are diagnostic for the identification of kaolinite. In the low-temperature domain, these doublets gradually smoothen with the temperature rise, illustrating the extent of the dehydroxylation reaction and the transition towards the metakaolinite phase. Based on the 2.21 µm double absorption band, the Kaolinite crystallinity (Kx) index has been commonly used to characterise different types of kaolinite. Since this band is a combination of all the

hydroxyl-related fundamentals, it might also give a good representation of the kaolinite dehydroxylation process. The Kx index makes use of the sharpness of the 2.21 µm doublet as a measure of the structural ordering in the kaolinite. Since the kaolinite – metakaolinite transition involves precisely a change in the crystal structure, the Kx index seems adequate to characterise these process.

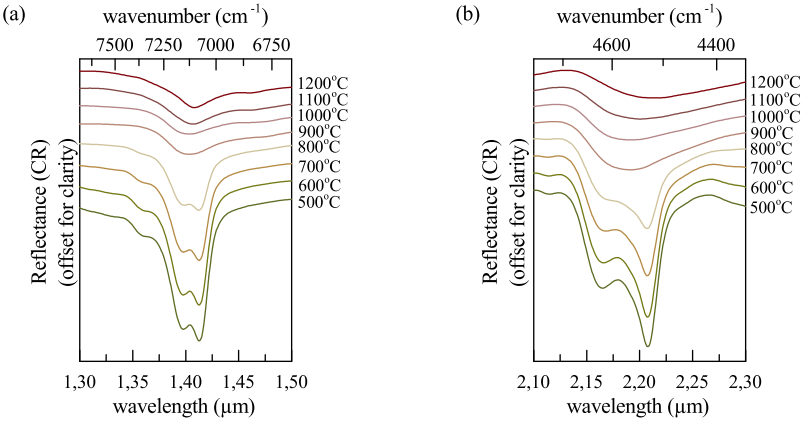

Figure 5.7: Hydroxyl overtones and combinations in the SWIR bidirectional reflectance spectra of the calcined kaolin (sample K1). (**a**) 1.30 to 1.50 µm range; (**b**) 2.10 to 2.30 µm range.

In Figure 5.8, the Kx index is used to characterise the kaolinite – metakaolinite transition. The Kx vs temperature plot (Figure 5.8a) shows the changes in crystallinity in relation to the temperature. According to the classification of Pontual et al. (1997), the kaolinite at 500 °C is a very highly crystalline kaolinite, at 700 °C has degraded to a poorly crystalline kaolinite, and at 800 °C is a very poorly crystalline kaolinite. The scatter plot reveals that dehydroxylation is rather a linear process, even though between 700 to 800 °C there is a sudden decrease of the Kx index. According to the XRD data, at 800 °C the proportion of illite (~ 48%) is higher than that of kaolinite (~ 40%). Illite presents a single sharp absorption band at 2.21 µm that smoothens the kaolinite doublet and decreases the Kx index values. Consequently, the crystallinity of kaolinite at this point should be slightly higher than indicated by the index. The XRD Hinckley Index (HI), which is commonly taken as the standard test in the analysis of the crystal structure of kaolinite (Plançon et al., 1988), was used to assess the influence of illite on the kaolinite analysis. The Pearson product moment correlation coefficient computed between the Kx and HI indices, displayed in Figure 5.8b, shows a strong positive correlation (r = 0.95), thus indicating that the presence of illite does not substantially influence the Kx values. In this way, the use of the Kx could probably offer a quantitative analysis of the dehydroxylation process.

In order to assess the suitability of the Kx index as a parameter to monitor the calcination reaction, a Pearson product-moment correlation coefficient was computed again to determine the relationship between the Kx values and the industrial standard, which is soluble Al_2O_3. The scatterplot in Figure 5.8c shows how, in the low-temperature domain, the amount of soluble Al_2O_3 increases with the temperature, as previously shown in Table 3. Consequently, the Kx vs Soluble Al_2O_3 plot illustrates a negative yet nearly linear

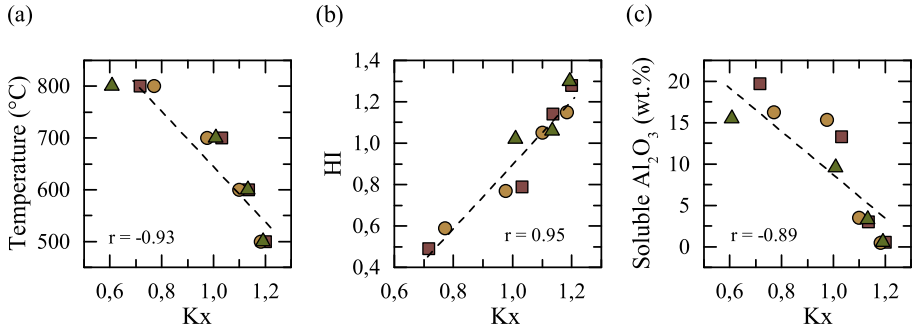

Figure 5.8: Relationship of the SWIR Kx index with (**a**) temperature, (**b**) Hinckley index (HI) and (**c**) Soluble Al_2O_3 (⊠ = K1, ● = K2, ▲ = K3) (Error bars smaller than plot symbol).

5

correlation between these parameters. For the highly crystalline kaolinite (Kx > 1.02), the release of soluble Al_2O_3 is very low, given that the crystal structure is still very stable. In the poorly (0.80 < Kx < 1.02) and very poorly (Kx < 0.80) crystalline kaolinite, the soluble Al_2O_3 strongly increases, since the crystal lattice weakens, and the kaolinite becomes more susceptible to chemical attack. However, the precise aluminium values vary among the three samples. This variation can be due to impurities in the chemical composition of the primary kaolinite, which might have greater influence on the structural stability at higher temperatures. Nevertheless, a Pearson's r value of −0.89 indicates that there is a good correspondence between kaolinite crystallinity and soluble Al_2O_3. The soluble Al_2O_3 measurements for this study have an accuracy of 0.1 %, although routine industrial checks lower the accuracy to 0.5 %. These data must be interpreted with caution since with the limited amount of samples it is not possible to estimate how accurate the Kx index would be as a proxy for soluble Al_2O_3. Moreover, the typical cut-off values of soluble Al_2O_3 are between 15 % and 20 %, where the correlation with the Kx index is less clear. However, these results serve as a conceptual approach for the further development of the Kx index as a proxy for the measurement of soluble Al_2O_3 in the kaolin calcination reaction.

The variations in the SWIR water absorption feature are shown in Figure 5.9. This feature tends to disappear in the kaolinite – metakaolinite transition, identical to what was observed in the MWIR spectra. Between 900 °C and 1200 °C, the deepening of the 1.90 µm feature is remarkable. Similarly, the 1.41 µm absorption band in Figure 6.1 sharpens in the same temperature range, and a new trough emerges near 1.45 µm. From the MWIR spectral characterisation, the patterns of these absorption bands are attributed to the increasing presence of molecular water adsorbed by the γ-alumina phase. Given that the aluminosilicate fundamentals do not present secondary absorption bands in the SWIR range, the spectral detection of water in calcined kaolin samples could be used as a parameter to detect the presence of γ-alumina that has been generated in the recrystallisation phase from metakaolinite to mullite. Therefore, the depth of the 1.90 µm water absorption band, defined as the 1900D parameter, seems to be convenient for the determination of the intermediate phases in the high-temperature domain.

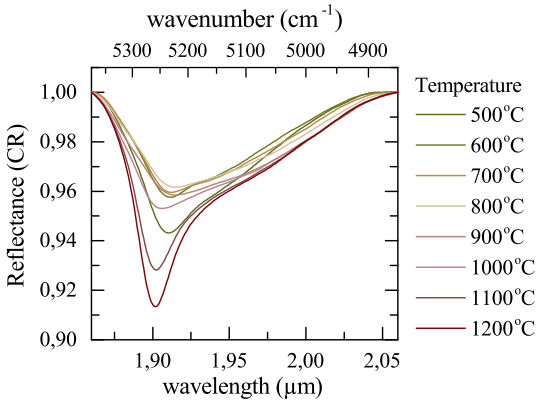

Figure 5.9: Changes in the depth of the water absorption feature (at 1.90 µm) in the SWIR bidirectional reflectance spectra of the calcined kaolin (Sample K1)

Akin to the Kx index analysis, Pearson product-moment correlation coefficients were computed to assess the relationship between the 1900D parameter and the relevant variables in the high-temperature domain. First, in order to ensure that the 1.90 µm absorption band is related to surface water, the correlation between the 1900D parameter and the adsorbed water measurement was assessed. Figure 5.10a shows that there is a positive correlation between these two variables, which indicates that the 1900D parameter is indeed related to water environmentally adsorbed in the material's surface. However, the coefficient value r = 0.72 suggests that the water absorption feature does not fully explain the amount of absorbed water. The error of the absorbed water measurements is 0.01 %; therefore it does not significantly affect the analysis. The mismatch indicates that the amount of surface water is a more complex function that involves not only the exposition to the environment (i.e. time of exposure, humidity), but also the powder properties (i.e. particle size, packing density of the sample). All these variables would affect the 1900D parameter and therefore must be taken into account to improve its reliability as a proxy for the measurement of the soluble Al_2O_3, and for establishing the level of accuracy of the method. These topics should be a matter of further research.

Figure 5.10b presents the variation of the 1900D with the treatment temperature. The lowest 1900D values correspond to the metakaolinite phase between 900 °C and 1000 °C, and the depth increase is related to the transition from amorphous to crystalline γ -alumina, which corresponds to the process presented in Equations (3.4) and (3.5). The scatterplot shows that the deepening of the water absorption band has a strong positive correlation (r = 0.93) with the temperature increment. Figure 5.10c illustrates the relationship between the 1900D parameter and soluble Al_2O_3; the correlation is negative yet strong (r = −0.96). Low 1900D values correspond to a high amount of soluble Al_2O_3, which fits well with the metakaolinite phase. With an increase in the water content, there is a drop in the soluble Al_2O_3 values due to the gradual incorporation of alumina into the spinel phase. The good correlation between the 1900D parameter and the soluble Al_2O_3 values indicates that the depth of the water absorption band measured in the SWIR

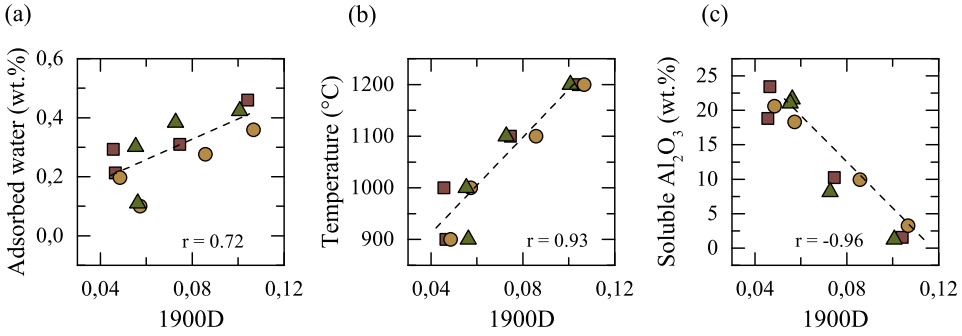

Figure 5.10: Variation in the depth of the 1.9 µm absorption band (1990D parameter) compared with the changes in (**a**) adsorbed water, (**b**) temperature and (**c**) soluble Al_2O_3 (⊠ = K1, ● = K2, ▲ = K3) (Error bars smaller than plot symbol).

5

spectra could be used as a proxy for the amount of soluble Al_2O_3, and therefore, for the formation of γ -alumina. For a more accurate quantification of soluble Al_2O_3 using the 1900D parameter, it would be needed to perform more refined statistical analysis.

5.4.4. IMPLICATIONS FOR ONLINE CHARACTERISATION OF THE CALCINED KAOLIN REACTION

Numerous researchers have studied the calcined kaolin reaction sequence. This continuous interest has been driven by the industrial importance of the products derived from the various calcination stages. Nevertheless, most of the published work focusses on the development of products with certain properties, rather than in the monitoring and control of the calcination process. For these applications, it is necessary to use techniques that can perform online measurements and provide information in real time. This study has taken advantage of the broad knowledge of the kaolin calcination process to make a step forward to the development of a monitoring and control strategy. More precisely, it has focused on the use of infrared spectroscopy in the MWIR and LWIR range to explore the feasibility of using the SWIR range as an alternative to estimate the extent of the calcination reaction in an online environment, offering a conceptual approach for the further development of this method.

The results of the MWIR and LWIR characterisation agree with those of reference works, such as Frost (1998) and Percival et al. (1974) . Furthermore, it also provides evidence of the presence of adsorbed water related to the γ-alumina phase, which can be used as a parameter for spectrally characterising the high-temperature phases in the calcined kaolin sequence. The extrapolation of the MWIR and LWIR results to the SWIR range demonstrates that the kaolin calcination reaction can be entirely characterised by using SWIR spectroscopy. On the one hand, the kaolinite – metakaolinite transition is directly described by the variations in the 2.21 µm band and can be quantified using the Kx index. On the other hand, the metakaolinite – γ -alumina transition can be indirectly estimated by using the water absorption feature depth at 1.90 µm. The good correlation of both, the Kx and the 1900D parameters with the soluble Al_2O_3 values shows that

these spectral parameters could be used as a proxy to quantify the extent of the kaolin calcination reaction.

The present study raises the possibility of using SWIR spectroscopy as a technique for the monitoring and control of calcined kaolin process. The results presented in this work, offer the criteria needed to refine the Kx and 1900D parameters and transform them into a tool capable of quantifying the amount of soluble Al_2O_3. For this, specific Kx and 1900D thresholds that comply with the optimum soluble Al_2O_3 values must be determined. Besides, the conditions for the implementation of an online analysis system should also be considered. In a kaolin processing plant, the calcination is performed in a Multiple Hearth Furnace (MHF), in which the temperature increases from hearth to hearth. The online spectral analysis would ideally be implemented by taking measurements of the feed for the calciner and at every hearth to track the evolution of the kaolin transformation sequence and establish the optimum point for the desired product.

5.5. CONCLUSIONS

This study has shown that the calcined kaolin reaction sequence can be entirely characterised using SWIR spectroscopy. The spectral changes are in good agreement with the XRD and TGA data, although quantitative analyses are required to verify the accuracy of the spectral characterisation. Based on the results, the kaolinite crystallinity (Kx) index and the depth of the water absorption feature (1900D) were defined as spectral parameters that describe different steps in the calcination of kaolinite. The results were analysed towards an assessment of the possibility of using SWIR spectroscopy as a technique for the online analysis of the calcination reaction.

The analysis of the MWIR and LWIR spectra of the calcined samples revealed the extent of the calcination reaction. In the first part of the reaction, the breakdown of the kaolinite structure is evidenced by the general weakening of the spectral absorption bands. Between 800 °C and 900 °C, the kaolinite dehydroxylation was complete giving place to the metakaolinite phase. The sharpening of the spectral absorption bands in the second part of the reaction indicated the formation of the spinel phase. The latter was accompanied by an increase in the intensity of the water spectral absorption band. This was attributed to physically absorbed water after exposure to the environment, which is a consequence of the γ-alumina presence. The spectral detection of adsorbed water accompanying the γ-alumina phase is one of the most significant findings that emerged from this study.

In the SWIR range, the changes in the 2.21 µm band described the dehydroxylation of kaolinite; at this wavelength, the Kx index was used to measure the transition from kaolinite towards the amorphous metakaolinite, by showing the gradual loss of hydroxyl groups. The metakaolinite – spinel transition was indirectly interpreted from the 1900D parameter, which measures the increase in the water content, previously related to the formation of γ-alumina with the help of MWIR spectra.

The relevance of the utilisation of the Kx index and 1900D parameter in the characterisation of the calcined kaolin reaction is supported by their good correlation with the industry standard soluble Al_2O_3 measurements. The results indicate that the SWIR spectrum could be used to estimate the extent of the calcination reaction. In this sense, this research ultimately provides a framework for the development of an online analysis

system based on SWIR spectroscopy, which ultimately would increase the consistency and quality of the calcined kaolin products. Such system would drastically reduce the turn-around time required for quality control, by minimising the use of off-line measurements. Moreover, the type of samples and instruments support the practicality of using the proposed approach. Last but not least, the technology readiness would foster the tailoring and implementation of the technique in the kaolin production environment.

REFERENCES

Aines, R. D. and Rossman, G. R. (1984), 'Water in minerals? A peak in the infrared', *Journal of Geophysical Research* **89**, pp. 4059–4071. DOI: 10.1029/JB089iB06p04059

Bakker, W. (2016), 'HypPy Hyperspectral Python software package'.
URL: *https://www.itc.nl/personal/bakker/hyppy.html [Accessed May 2015]*

Brindley, G. W. and Nakahira, M. (1959), 'The kaolinite-mullite reaction series: I, A survey of outstanding problems', *Journal of the American Ceramic Society* **42**, pp. 311–314. DOI: 10.1111/j.1151-2916.1959.tb14314.x

Clark, R. N. and Roush, T. L. (1984), 'Reflectance spectroscopy: Quantitative analysis techniques for remote sensing applications', *Journal of Geophysical Research* **89**, pp. 6329–6340. DOI: 10.1029/JB089iB07p06329

Drits, V. A., Derkowski, A. , Sakharov, B. A. and Zviagina, B. B. (2016), 'Experimental evidence of the formation of intermediate phases during transition of kaolinite into metakaolinite', *American Mineralogist* **101**, pp. 2331–2346. DOI: 10.2138/am-2016-5776

Freund, F. (1974), Ceramics and thermal transformation of minerals, *in* V. C. Farmer, ed., 'The Infrared Spectra of Minerals', Vol. Monograph 4, Mineralogical Society, London, book section 20, pp. 465–482.

Frost, R. L. (1998), 'Hydroxyl deformation in kaolins', *Clays and Clay Minerals* **46**, pp. 280–289. DOI: 10.1346/ccmn.1998.0460307

Frost, R. L., Makó, É. , Kristóf, J. and Kloprogge, J. T. (2002), 'Modification of kaolinite surfaces through mechanochemical treatment - A mid-IR and near-IR spectroscopic study', *Spectrochimica Acta - Part A: Molecular and Biomolecular Spectroscopy* **58**, pp. 2849–2859. DOI: 10.1016/S1386-1425(02)00033-1

Frost, R. L. and Vassallo, A. M. (1996), 'The dehydroxylation of the kaolinite clay minerals using infrared emission spectroscopy', *Clays and Clay Minerals* **44**, pp. 635–651. DOI: 10.1346/CCMN.1996.0440506

Haavisto, O. and Hyötyniemi, H. (2011), 'Reflectance spectroscopy in the analysis of mineral flotation slurries', *Journal of Process Control* **21**, pp. 246–253. DOI: 10.1016/j.jprocont.2010.10.015

ITT, Visual Information Solutions (2008), 'ENVI –Environment for Visualizing Images– software application'.
URL: *https://www.harrisgeospatial.com/Software-Technology/ENVI [Accessed April 2019]*

Johnston, C. T. (2017), Infrared studies of clay mineral-water interactions, *in* W. P. Gates, J. T. Kloprogge, J. Madejová and F. Bergaya, eds, 'Infrared and Raman Spectroscopies of Clay Minerals', Vol. 8 of *Developments in Clay Science*, Elsevier, Chapter 9, pp. 288–309. DOI: 10.1016/b978-0-08-100355-8.00009-6

Liu, X. (2008), 'DRIFTS study of surface of gamma-alumina and its dehydroxylation', *Journal of Physical Chemistry C* **112**, pp. 5066–5073. DOI: 10.1021/jp711901s

MacIver, D. S., Tobin, H. H. and Barth, R. T. (1963), 'Catalytic aluminas I. Surface chemistry of eta and gamma alumina', *Journal of Catalysis* **2**, pp. 485–497. DOI: 10.1016/0021-9517(63)90004-6

Miller, J. G. (1961), 'An infrared spectroscopic study of the isothermal dehydroxylation of kaolinite at 470', *The Journal of Physical Chemistry* **65**, pp. 800–804. DOI: 10.1021/j100823a023

Onike, F., Martin, G. D. and Dunham, A. C. (1986), 'Time-temperature-transformation curves for kaolinite', *Kinetics and Mass Transport in Silicate and Oxide Systems* **7**, pp. 73–82. DOI: 10.4028/www.scientific.net/MSF.7.73

Percival, H. J., Duncan, J. F. and Foster, P. K. (1974), 'Interpretation of the kaolinite-mullite reaction sequence from infrared absorption spectra', *Journal of the American Ceramic Society* **57**, pp. 57–61. DOI: 10.1111/j.1151-2916.1974.tb10813.x

Plançon, A., Giese, R. F. and Snyder, R. (1988), 'The Hinckley Index for kaolinites', *Clay Minerals* **23**, pp. 249–260. DOI: 10.1180/claymin.1988.023.3.02

Pontual, S., Merry, N. and Gamson, P. (1997), Regolith Logging, *in* S. Pontual, N. Merry and P. Gamson, eds, 'Spectral Analysis Guides for Mineral Exploration', Vol. 1, AusSpec International, Chapter 8, pp. 8.1–8.62.

Ptáček, P., Šoukal, F. , Opravil, T. , Nosková, M. , Havlica, J. and Brandštetr, J. (2011), 'Mid-infrared spectroscopic study of crystallization of cubic spinel phase from metakaolin', *Journal of Solid State Chemistry* **184**(10), pp. 2661–2667. DOI: 10.1016/j.jssc.2011.07.038

Thomas, R. (2010), High temperature processing of kaolinitic materials, PhD thesis, University of Birmingham.
URL: *http://etheses.bham.ac.uk/6075/ [Accessed July 2013]*

Thomas, R., Grose, D. , Obaje, G. , Taylor, R. , Rowson, N. and Blackburn, S. (2009), 'Residence time investigation of a multiple hearth kiln using mineral tracers', *Chemical Engineering and Processing: Process Intensification* **48**(4), pp. 950–954. DOI: 10.1016/j.cep.2009.01.003

van der Meer, F. (2004), 'Analysis of spectral absorption features in hyperspectral imagery', *International Journal of Applied Earth Observation and Geoinformation* **5**, pp. 55–68. DOI: 10.1016/j.jag.2003.09.001

Wilson, I. R. (2003), 'Current world status of kaolin from south-west England', *Geoscience in South-West England* **10**, pp. 417–423.

6

INFRARED-BASED PREDICTION OF SOLUBLE AL_2O_3 FOR PRODUCT QUALITY CONTROL

This chapter uses multivariate calibration methods to predict the soluble Al_2O_3 content in calcined kaolin.

Parts of this chapter have been published in:
Guatame-Garcia, A. and Buxton, M. (2018). Prediction of Soluble Al_2O_3 in Calcined Kaolin Using Infrared Spectroscopy and Multivariate Calibration. *Minerals 8(4)*, 136. doi: 10.3390/min8040136.

In the production of calcined kaolin, the soluble Al_2O_3 content is used as a quality control criterion for some speciality applications. The increasing need for automated quality control systems in the industry has brought the necessity of developing techniques that provide (near) real-time data. Based on the results presented in Chapter 5 regarding the relationship between the absorption of water and the soluble Al_2O_3 content, in this study, a hand-held infrared spectrometer was used to analyse a set of calcined kaolin samples obtained from a production plant. The spectra were used to predict the amount of soluble Al_2O_3 in the samples by implementing partial least squares regression (PLS-R) and support vector regression (SVR) as multivariate calibration methods. The presence of nonlinearities in the dataset and the different types of association between water and the calcined kaolin represented the main challenges for developing a good calibration. In general, SVR showed a better performance than PLS-R, with root mean squared error of the cross-validation (RMSECV) = 0.046 wt% and R^2 = 0.87 for the best-achieved prediction. This accuracy level is adequate for detecting variation trends in the production of calcined kaolin which could be used not only as a quality control strategy, but also for the optimisation of the calcination process.

6.1. INTRODUCTION

High-grade kaolin is mainly composed of the mineral kaolinite [$Al_2Si_2O_5(OH)_4$], and is commonly thermally treated for industrial purposes (Murray, 2006). This process aims to tailor the physical and chemical properties of the original mineral to specific market specifications. The kaolin calcination process was explained in detailed in Chapter 3. When kaolinite is calcined to high temperatures (above 600 °C), it dehydroxylates and transforms into amorphous metakaolinite [$Al_2Si_2O_7$] (Equation (3.3)), which has typically high chemical reactivity. Calcination to temperatures around 980 °C transforms the metakaolinite into the spinel phase (Al-spinel [Al_2O_3] and Si-spinel [SiO_2]) (Equation (3.4)), followed by the nucleation of the spinel and transformation into mullite (Equation (3.5)), which is characteristically hard and abrasive (Chakraborty, 2003; Gualtieri and Bellotto, 1998; Ptáček et al., 2011).

For applications in the pharmaceutical industry, natural kaolin is calcined to temperatures around 1100 °C in industrial furnaces, such as the Multiple Hearth Furnace (MHF) (Section 3.2.1), to generate a product in an intermediate stage between the amorphous and crystalline spinel phase. This stage marks the balance point between low reactivity and low abrasiveness that is required for calcined kaolin products (Thomas et al., 2009). In the industry, one of the criteria to assess the extent of the calcination reaction is the chemical extraction of soluble Al_2O_3. This method makes use of the solubility of Al_2O_3 in the spinel phase (γ-alumina) in strong acids (Hulbert and Huff, 1970; Phillips and Wills, 1982; Ruíz-Santaquiteria and Skibsted, 2015) to estimate the reactivity of the calcined kaolin (Taylor, 2005; Thomas, 2010). Consequently, the extraction of soluble Al_2O_3 is employed as the standard operational procedure (SOP) to determine the quality of the calcined product. However, this is a laboratory and time-consuming method that restricts timely operational feedback, thus limiting the opportunities for the online optimisation of the calcination process.

The development of an on-site and (near) real-time method that can support the SOP and can be used as an on-site quality control measurement would benefit the production

of calcined kaolin (Glass, 2016). Other researchers have developed different strategies for controlling the extent of the calcination process inside an MHF calciner. For example, Thomas et al. (2009) investigated the residence time of kaolin in the calciner to improve the consistency of the properties of the calcined product; Eskelinen et al. (2015) modelled some of the furnace's variables and related them to the physical-chemical phenomena taking place during calcination. However, these studies did not address a mechanism for direct quality control of the calcined product. The relationship between the infrared spectra of the kaolin calcination reaction and the changes in the calcined clay's reactivity, measured as soluble Al_2O_3 were investigated in Chapter 5. Infrared spectroscopy is particularly useful in the characterisation of the kaolin calcination reactions. The spectral features describe changes in the mineral structure related to the kaolinite dehydroxylation (Equation (3.3)) and recrystallisation of the spinel and mullite phases (Equations (3.4) and (3.5)) (Drits et al., 2016; Frost et al., 2002; Percival et al., 1974). Besides these transformations, the results reported in Chapter 5 showed an inverse correlation between the adsorption of water by the calcined clay as detected by the water-related spectral features, and the soluble Al_2O_3 content. Since the spectral ranges that exhibit the spectrum of water can be measured by using portable and hand-held spectrometers, infrared spectroscopy could be used as an on-site and (near) real-time proxy for the SOP.

To be able to correlate the spectra of calcined kaolin samples—and in particular the water-related spectral features— with the soluble Al_2O_3 content and establish quantitative predictions for unknown samples, it is necessary to use a chemometric approach (Chryssikos and Gates, 2017). Chemometrics has been used, for example, in applications for mineral processing and control of zinc (Haavisto and Hyötyniemi, 2009), coal (Andrés and Bona, 2005; Bona and Andrés, 2007), and petroleum oil (Filgueiras et al., 2014). The correlation between spectral data and the mineral characteristics is commonly done by using multivariate calibration methods, among which partial least squares regression (PLS-R) (Wold et al., 2001) is often used as the standard methodology. However, in the presence of nonlinearities or complex datasets, it is not possible to implement PLS-R. In these cases, multivariate nonlinear models such as support vector regression (SVR) should be used along with spectral processing strategies (Devos et al., 2009; Li et al., 2009). SVR models operate in a kernel-induced feature space that facilitates nonlinear modelling with a good performance, even for relatively small datasets, leading to more robust and accurate predictions (Brereton and Lloyd, 2010; Filgueiras et al., 2014). The use of PLS-R and SVR calibrations can generate a method for the quantification and prediction of soluble Al_2O_3 in calcined kaolin products based on their infrared spectra.

In this study, spectral processing strategies such as standard normal variate (SNV) and continuum removal (CR), combined with PLS-R and SVR regression are applied to the infrared spectra of calcined kaolin samples to determine their soluble Al_2O_3 content. Different combinations of spectral processing strategies and model calibration parameters are tested on the spectral regions that exhibit water features. The performance of the generated models is compared and discussed with respect to the use of an infrared-based prediction model as a quality control strategy in the production of calcined kaolin.

6.2. METHODS

6.2.1. CALCINATION OF KAOLIN AND SAMPLES

The samples used in this study were obtained from a kaolin processing plant where natural kaolin is calcined in a (MHF) calciner. The production of calcined kaolin for pharmaceutical applications is performed using the soft calcination method, which involves exposing the kaolin to high temperatures for a prolonged amount of time to guarantee complete calcination. The collected calcined powders are cumulative and homogenised samples taken over a period of 12 h (one shift) after blast-cooling. Since the water content in the samples was one of the critical parameters investigated for analysis, two sampling campaigns were conducted during different seasons to ensure that the possible influence of environmental factors was also considered in the measurements. The first sampling campaign occurred during the summertime under local high precipitation and humidity conditions, whereas the second campaign was carried out in autumn, when the precipitation levels are low. In the first period, only samples from the day shift were collected over 23 consecutive days. In the second period, samples from both day and evening shifts were collected during 17.5 consecutive days, for a total of 56 samples. Approximately 1 kg of sample was taken for every shift. Table 6.1 presents the average chemical composition of the samples.

Table 6.1: Chemical composition determined by X-ray fluorescence (XRF) and the soluble Al_2O_3 content of the calcined kaolin samples (wt%).

	Al_2O_3	SiO_2	K_2O	Fe_2O_3	TiO_2	CaO	MgO	Na_2O	LOI	Soluble Al
Mean	42.27	54.41	1.58	0.69	0.11	0.11	0.31	0.09	0.26	0.41
Standard Deviation	0.33	0.20	0.14	0.07	0.07	0.21	0.03	0.02	0.05	0.08
Minimum	41.07	53.85	1.25	0.58	0.04	0.04	0.26	0.05	0.17	0.26
Median	42.23	54.47	1.61	0.67	0.07	0.05	0.32	0.09	0.27	0.43
Maximum	42.91	54.69	1.80	0.78	0.32	1.31	0.35	0.13	0.37	0.64

X-ray diffraction (XRD) analysis was performed to identify the mineral phases that can influence the infrared spectra. The XRD patterns were collected with a Bruker D8 Advance diffractometer featuring Bragg Brentano geometry using a Cu-Kα radiation of 45 kV and 40 mA on powders placed on a PMMA holder L25. The XRD spectra were measured with a coupled $\theta - 2\theta$ scan ranging from 10 to 110° 2θ (step size: 0.03 °2θ, time per step: 1 s). The XRD patterns displayed in Figure 6.1 show that the calcined kaolin is mostly amorphous, with crystalline phases related to illite and quartz. Diffraction peaks characteristic of Al-spinel (γ-alumina) and mullite are also present.

6.2.2. SOLUBLE AL_2O_3

The amount of soluble Al_2O_3 present in the calcined samples was measured following the conventional method used in the industry, as reported by Taylor (2005) and Thomas (2010). The extraction of soluble Al_2O_3 was done by diluting 0.1 g of sample into 10 mL of concentrated (16M) nitric acid (Analar grade) for 4 h. Inductively coupled plasma atomic emission spectroscopy (ICP-AES) determined the concentration of Al_2O_3 in solution. These analyses were performed at the plant's laboratory using a Thermo Electron Iris-AP emission spectrometer; the overall error of the method is reported as 0.015 wt%.

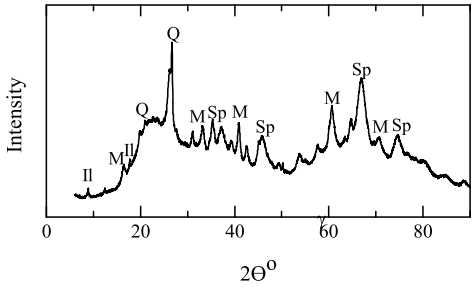

Figure 6.1: XRD patterns of the calcined kaolin samples identifying the main mineral phases. Il = illite, Q = quartz, Sp = Al-spinel, M = mullite.

6.2.3. INFRARED SPECTRA COLLECTION AND PROCESSING

Diffuse reflectance infrared spectra were collected using the Agilent 4300 instrument (Section 2.2.3). A petri dish was filled with each of the powder samples; the surface was first compacted and flattened with a spatula to minimise void spaces and then slightly roughened to maximise the direction of the reflections. Five spectral measurements per sample were taken at different spots of the surface. For every sample, the respective five spectral measurements were averaged as means of noise reduction, generating one spectrum per sample. The resulting spectra were smoothed using the Savitzky–Golay (SG) filter (Savitzky and Golay, 1964) with polynomial order of 3 and windows size of 55 data points. Spectral subsets were made on the regions that exhibit features of molecular water, namely between 2.60 to 3.30 µm and 5.70 to 6.50 µm.

The spectral processing strategies used in this study are standard normal variate (SNV) and continuum removal (CR). SNV removes multiplicative interferences caused by scattering and particle size, and corrects shifts in the baseline of the reflectance spectra of powders using a second-degree polynomial regression (Barnes et al., 1989). CR normalises the albedo of the reflectance curve, which is also known as continuum. It can be modelled as a mathematical function to isolate specific absorption bands (Clark and Roush, 1984). Both signal processing strategies were computed independently for each spectral subset in the R environment using the prospectr package (Stevens and Ramirez-Lopez, 2014).

6.2.4. REGRESSION METHODS

PARTIAL LEAST SQUARES REGRESSION

Partial least squares regression (PLS-R) was developed with the aim of maximising the correlation between the information variables and the parameters to be quantified (Höskuldsson, 1988). In regression problems where the variables largely exceed the number of observations, PLS-R decomposes the variables into orthogonal scores and loadings and performs the regression to the scores. The PLS-R latent variables (LVs), which are analogous to the components in principal component analysis (PCA), describe the variability of the input data that is relevant for the determination of the parameters to be predicted (Wold et al., 2001). Cross-validation determines the number of LVs that are optimal for the regression. Even though PLS-R is best suited to linear systems, it is also able to cope

with mild nonlinearities.

For the development of the PLS-R models in this study, the information variables or predictors corresponded to the reflectance value for each wavelength in the infrared spectra, whereas the parameter to be quantified corresponded to the laboratory measurement of soluble Al_2O_3. In a second experiment, chemical components of the samples (K_2O, Fe_2O_3, and MgO) were also added as input variables. The number of LVs was determined by using 10-fold cross-validation.

SUPPORT VECTOR REGRESSION

Cortes and Vapnik (1995) initially established support vector machines (SVMs) to perform binary classification and pattern recognition. After further developments, SVMs have demonstrated to be a powerful technique, particularly in nonlinear systems. For solving regression problems, SVMs are implemented via support vector regression (SVR) using the epsilon-insensitive SVR (ε-SVR) application, which is extensively described in the literature (Devos et al., 2009; Li et al., 2009; Smola and Schölkopf, 2004). ε-SVR aims to find a function *f(x)* where the errors or deviations from a target in the training data are not larger than a given ε value, and that is as flat or smooth as possible. For solving the regression problem, the input data is first mapped into a high dimensional feature space, and kernel functions are used to impart linearity to the dataset. The ε-SVR function makes use of an ε-tube that defines the margins where deviations are tolerated; a constant C represents the cost parameter, which determines the trade-off between the flatness of the function and the tolerance in the deviations, assigning greater penalty on the error of the samples outside the ε-tube. The ε-insensitive loss function ignores the errors inside the ε-tube and calculates the loss for the data points outside the ε-tube based on the distance between the data point and the ε boundary. All the data points that contribute to the regression are the support vectors (SVs). The analyst should optimise the parameters ε and C.

For the development of the ε-SVR models, the input vectors corresponded to the spectra of the samples, and the response vector corresponded to the measured soluble Al_2O_3. The ε-SVR models were developed using the RBF (radial basis function) kernel function. The parameters ε and C were optimised using a grid search and 10-fold cross-validation.

In this study, for developing the PLS-R and SVR multivariate calibration models, the samples were split into a calibration set ($n = 46$) and a validation set ($n = 10$) by random selection. Each spectral subset (2.6 to 3.3 µm and 5.7 to 6.5 µm) was tested under raw, SNV, and CR spectra, for a total of six different test scenarios. All the analyses were performed in the R environment. PLS-R was carried out with the built-in routines in the PLS-R package (Mevik and Wehrens, 2007). The SVR regression was carried out with the interface to LIBSVM (open source machine learning library for SVM) (Chang and Lin, 2011) in the package e1071 (functions for SVM, among others) (Meyer, 2017). The performance of the models was assessed using the root mean squared error of the cross-validation (RMSECV), the root mean squared error of the calibration (RMSEC), and the root mean squared error of the prediction (RMSEP). The RMSECV corresponds to the results of the 10-fold cross-validation used for the selection of the parameters in the PLS-R and SVR models using the calibration set. The RMSEC was measured as the difference between the predicted

and measured soluble Al_2O_3 values using the calibration set, whereas the RMSEP was measured as the difference between the predicted and measured soluble Al_2O_3 values using the validation set.

6.3. RESULTS

The calcined kaolin samples used in this study had soluble Al_2O_3 content from 0.26 to 0.54 wt% (Table 6.1). Figure 6.2 shows that the samples collected in the first period (samples 1 to 23) generally had lower soluble Al_2O_3 content—average 0.35 wt%—than those obtained in the second period (samples 24 to 56), with an average of 0.46 wt%. The variation in the average values between the two periods might reflect differences in the quality of the raw kaolin used as a feed for calcination, volume of material fed into the calciner, or variations in the calciner's temperature profile. Nevertheless, according to the plant's historical data, the soluble Al_2O_3 content in the produced calcined kaolin typically varies from 0.3 to 0.6 wt%. Despite the differences between the two production periods, the sample set covers the production range continuously, ensuring the data representability. These data are the actual values used for developing the calibration PLS-R and SVR models.

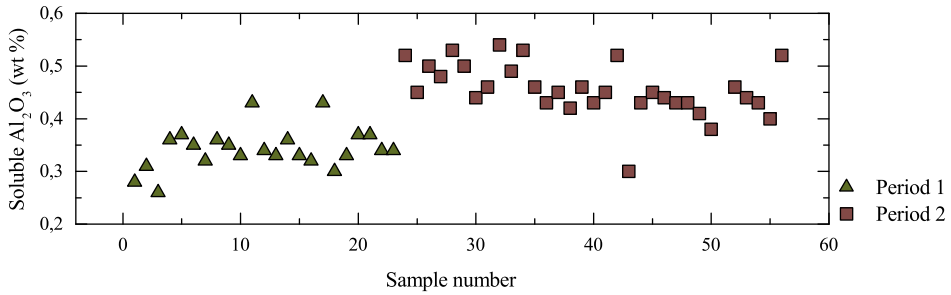

Figure 6.2: Soluble Al_2O_3 content of the calcined kaolin samples from the two periods. The numbering of the samples refers to the collection chronology (error bars are smaller than plot symbols).

6.3.1. SPECTRAL PROCESSING

The average spectrum of the calcined kaolin clay after SG smoothing is presented in Figure 6.3. The adsorbed water on the surface of γ-alumina from the spinel phase exhibits spectral features in two regions. The first region ranges from 2.6 to 3.3 µm and corresponds to the stretching H–O–H vibrations (νH_2O); the second region extends from 5.7 to 6.5 µm, where the O–H bending vibrations (δH_2O) are located (Aines and Rossman, 1984; Johnston, 2017; Liu, 2008). From the minerals detected by XRD analysis, only illite is expected to have spectral features at 2.74 µm, 3.48 µm and 5.56 µm (Yitagesu et al., 2011); mullite and quartz are featureless in the presented spectral range. Even though the sample preparation sought to minimise the effect from the environment on the spectra, the CO_2 in the air induced artefacts around 4.2 µm. The analysis of the spectra of water in γ-alumina was then constrained to the spectral regions previously described to reduce the influence of the features of illite and CO_2.

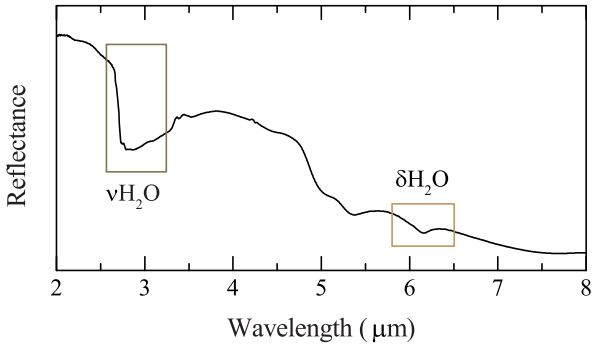

Figure 6.3: Average infrared spectra of the calcined kaolin samples. The boxes highlight the spectral regions where the water features are located.

Figures 6.4 and 6.5 display the spectra of the 2.6–3.3 µm and 6.5–7.5 µm subsets after Savitzky–Golay (SG) smoothing (hereafter referred to as raw spectra), SNV, and CR processing. In the 2.6 to 3.3 µm range, spectral processing using SNV and CR (Figure 6.4b,c) enhances the 2.78 µm peak, attributed to the adsorption of water (Aines and Rossman, 1984). The other two peaks at 2.73 µm and 2.75 µm are also better resolved; however, they can be indistinctly attributed to the presence of water or the surface hydroxyls in illite. The 5.7 to 6.5 µm region contains only the δH_2O spectral feature (Figure 6.5). In this range, SNV and CR processing enhance the depth at the centre of the feature at 6.15 µm, apparently separating the spectra into two groups. Besides, the type of spectral processing influences the shape of the spectra. The CR spectra appear to be symmetric, whereas the SNV one is biased towards longer wavelengths, also having a difference in the shoulder position to the deeper spectra at 6.24 µm, and that in the shallower one at 6.27 µm.

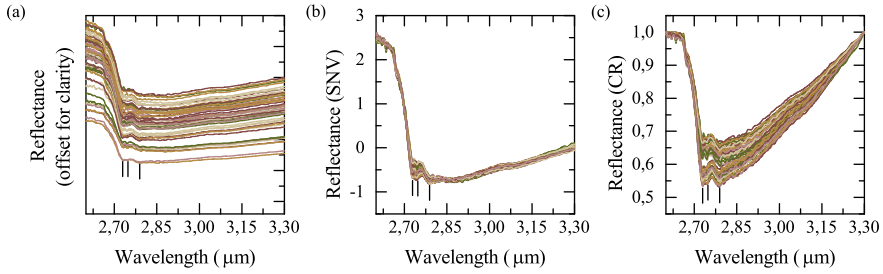

Figure 6.4: (**a**) Raw; (**b**) standard normal variate (SNV); and (**c**) continuum removal (CR) processed infrared spectra of calcined kaolin in the 2.6 to 3.3 µm region. The markers indicate wavelength positions at 2.73 µm, 2.75 µm and 2.78 µm.

Following the approach proposed in a previous study (Guatame-García et al., 2018), the depth of the water feature was used to investigate the general behaviour of the spectra of the calcined kaolin samples in relation to the soluble Al_2O_3 content. Figure 6.6 shows

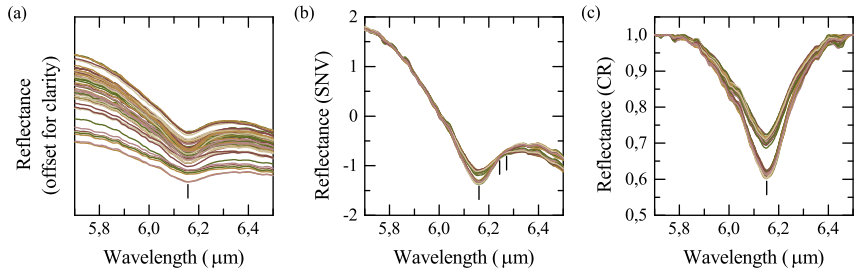

Figure 6.5: (**a**) Raw; (**b**) SNV; and (**c**) CR processed infrared spectra of calcined kaolin in the 5.7 to 6.5 μm region. The markers indicate the center of the wavelength of the water feature at 6.15 μm and the right shoulders in the SNV spectra at 6.24 μm and 6.27 μm.

these parameters using the depth of the δH_2O feature at 6.15 μm extracted from CR spectra. The most remarkable aspect of this plot is that the feature depth separates the samples collected in the first and the second period. The samples of the first period—which have the lowest soluble Al_2O_3—have a deep water feature, whereas in samples of the second period (with higher soluble Al_2O_3), this feature is shallower, as was expected from former studies. However, in an individual assessment of every period, it is difficult to describe a pattern of correlation between the depth of the water feature and the soluble Al_2O_3 content. A proper assessment of the spectral features of water in relation to the amount of soluble Al_2O_3 in calcined kaolin samples should include not only the depth, but also the overall shape of the spectral feature. Besides, the clustering of data points in Figure 6.6 and lack of trends make it clear that the relationship between the spectra and the soluble Al_2O_3 is not linear. As a consequence, a multivariate approach that can cope with nonlinearities is more appropriate than a univariate one.

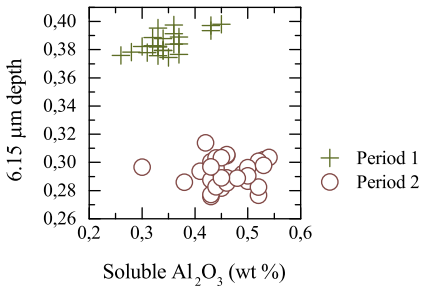

Figure 6.6: Depth of the δH_2O feature at 6.15 μm compared with the soluble Al_2O_3 content, highlighting the differences between samples collected in the first and second periods.

6.3.2. MULTIVARIATE CALIBRATION

Table 6.2 presents the results of the PLS-R models developed for the six scenarios by using only the infrared spectra as the information variables. In general, the difference in the performance of the models is minimal. Since the RMSECV for all the scenarios is

in principle the same, the selection of the best model was based on the lowest RMSEC and RMSEP, which is the model generated from the 5.7 to 6.5 µm SNV processed spectra, using two LVs and with a prediction error RMSECV = 0.050 wt %. For this model, the coefficient of determination is $R^2 = 0.64$. The measured vs predicted plot (Figure 6.7a) shows clustering rather than an even distribution along the regression line. The same is true for the predicted values from the validation set. In addition, the residuals plot (Figure 6.7b) shows large residuals—particularly for the extremes, where low and high values have respectively strong negative and positive residuals. These results suggest that in this case, the PLS-R calibration is not able to cope entirely with the nonlinearity of the dataset.

Table 6.2: Summary of the parameters and performance indicators of the best partial least squares regression (PLS-R) calibrations. LV: latent variable; RMSEC: root mean squared error of the calibration; RMSECV: root mean squared error of the cross-validation; RMSEP: root mean squared error of the prediction.

Scenario		**LV**	**RMSECV**	**RMSEC**	**RMSEP**	R^2
Range	**Processing**		(wt %)	(wt %)	(wt %)	
2.6 to 3.3 µm	raw	3	0.051	0.044	0.046	0.62
	SNV	3	0.051	0.040	0.054	0.62
	CR	2	0.050	0.044	0.055	0.57
5.7 to 6.5 µm	raw	3	0.051	0.047	0.053	0.60
	SNV	2	0.050	0.041	0.046	0.64
	CR	1	0.050	0.047	0.051	0.52

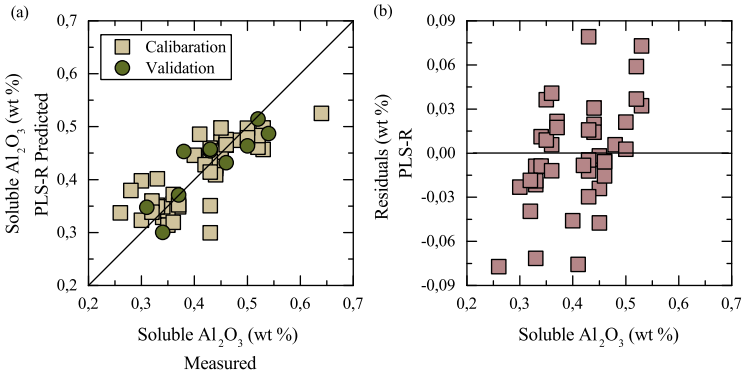

Figure 6.7: (**a**) Measured vs Predicted plot of the PLS-R model for the 5.7 to 6.5 µm range after SNV processing. LV = 3 in the calibration and validation samples. (**b**) Residuals plot of the PLS-R calibration.

A possible cause of the nonlinearity might be related to the mineralogical content of the samples. The interpretation of the XRD and infrared spectra revealed that the samples also contain illite. Even though the relative amount of illite is low, its presence can contribute to the variability of the spectra. In order to consider the influence of illite in the performance of the PLS-R calibration, the chemical contents associated exclusively to illite—i.e., K_2O, Fe_2O_3, and MgO—were included as information variables. The results of

the calibration for the six scenarios are presented in Table 6.3. Compared to the previous results, when taking illite into account, the performance indicators of the new models are slightly better. Moreover, in the measured vs predicted plot (Figure 6.8a), the data points are more evenly distributed along the regression line than those presented in Figure 6.7, suggesting that the inclusion of illite as a variable can improve the performance of the model. However, Figure 6.8 also shows a poor prediction for high soluble Al_2O_3 values and larger residuals for some data points, leading to a low coefficient of determination ($R^2 = 0.53$). Even though the consideration of illite seems to correct for the nonlinearities in the dataset, the overall result of the calibration is not optimal.

Table 6.3: Summary of the parameters and performance indicators of the best PLS-R calibrations, including K_2O, Fe_2O_3, and MgO as variables.

Scenario		**LV**	**RMSECV**	**RMSEC**	**RMSEP**	R^2
Range	**Processing**		**(wt %)**	**(wt %)**	**(wt %)**	
2.6 to 3.3 µm	raw	3	0.053	0.034	0.046	0.62
	SNV	4	0.053	0.036	0.061	0.62
	CR	3	0.050	0.036	0.056	0.57
5.7 to 6.5 µm	raw	3	0.053	0.036	0.052	0.57
	SNV	2	0.050	0.036	0.039	0.53
	CR	1	0.050	0.036	0.043	0.54

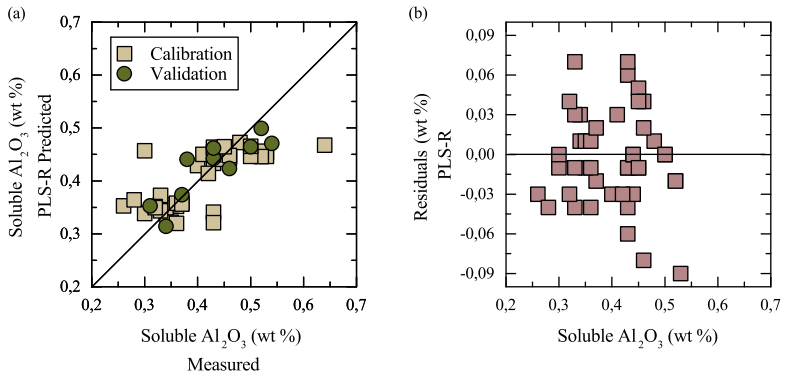

Figure 6.8: (**a**) Measured vs Predicted plot of the PLS-R model for the 5.7 to 6.5 µm range after SNV processing, including K_2O, Fe_2O_3, and MgO as variables. LV = 2 in the calibration and validation samples. (**b**) Residuals plot of the PLS-R calibration.

Another strategy for coping with nonlinearities is the implementation of SVR models. The results of the SVR calibration for the six scenarios are presented in Table 6.4. The SVR cross-validation errors do not differ significantly from those reported by the PLS-R models; however, the RMSECs of the SVR are considerably smaller than the PLS-R ones, indicating better performance. The performance of the SVR models improved after applying spectral processing; however, the most notorious improvement occurred in the 5.7 to 6.5 µm spectra using CR (RMSECV = 0.046 wt %), which was consequently

selected as the best model. The coefficient of determination for this model is $R^2 = 0.87$, which confirms its good performance. The measured vs predicted plot (Figure 6.9a) shows that even though the data points seem to separate into two groups, there is an even distribution along the regression line for the entire dataset. Moreover, the predicted values from the validation set are also evenly distributed, except for the values above 0.5 wt%. The magnitude of the residuals (Figure 6.9b) is remarkably smaller than those of the best PLS-R model; however, their spread shows that the low values are generally over-estimated, whereas the highest values are under-estimated.

Table 6.4: Summary of the optimisation parameters and performance indicators of the best support vector regression (SVR) calibrations.

Scenario		***C***	***ε***	**SV**	**RMSECV**	**RMSEC**	**RMSEP**	R^2
Range	**Processing**				**(wt %)**	**(wt %)**	**(wt %)**	
2.6 to 3.3 µm	raw	15.0	0.80	20	0.055	0.048	0.050	0.57
	SNV	3.5	0.40	21	0.052	0.023	0.050	0.86
	CR	3.5	0.50	22	0.048	0.031	0.048	0.71
5.7 to 6.5 µm	raw	5.0	0.31	30	0.056	0.045	0.047	0.59
	SNV	4.0	0.53	17	0.048	0.027	0.047	0.80
	CR	3.1	0.46	19	0.046	0.025	0.044	0.87

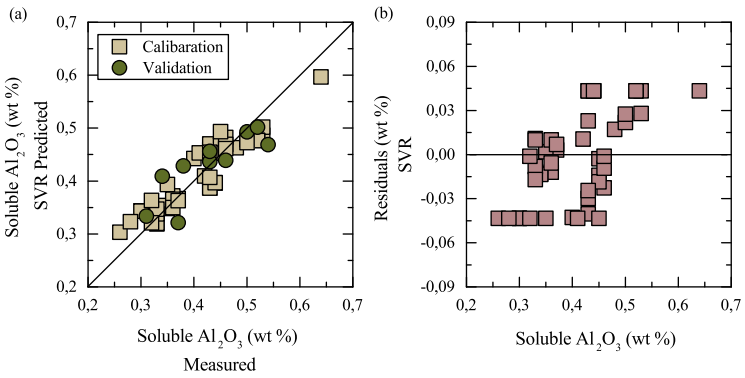

Figure 6.9: (**a**) Measured vs Predicted plot of the SVR model for the 5.7 to 6.5 µm range after CR processing. $C = 3.1$, $\varepsilon = 0.46$, SV = 19 in the calibration and validation samples. (**b**) Residuals plot of the SVR calibration.

6.4. DISCUSSION

The resulst presented in Chapter 5 noted the correlation between the reactivity of calcined kaolin and the hydration of γ-alumina when the calcination reaches the spinel phase. Such a relationship was also assessed by the amount of extracted soluble Al_2O_3 and the infrared spectral features of water adsorbed by γ-alumina in the calcined clay. In this chapter, infrared spectroscopy was used to determine the soluble Al_2O_3 content in the calcined clay utilising a combination of spectral processing strategies and multivariate

calibration. Even though in Chapter 5 it was suggested that the depth of the water spectral features could predict the soluble Al_2O_3 content, the results of this work showed that such direct prediction is not possible. Since the depth of the water feature captures not only the water physically adsorbed on the surface of γ-alumina but also all the water present in the system (i.e., chemically bound and free water), the depth parameter is influenced by the γ-alumina properties as well as the sample's environmental conditions. In Figure 6.6, the separation of the two sampling periods by the water parameter indicates differences in the total amount of water present in the samples, where those with a larger exposure to water from the environment have the deepest features. Therefore, the proper assessment of the relationship between soluble Al_2O_3 and adsorbed water requires the analysis of the complete spectral features of water, that is to say, not only the wavelength of the deepest point but also the width and the shape of the feature. In such a way, the spectral characteristics that relate to physically adsorbed water would have more relevance than those that are related to chemically bound or free water.

Since the spectral analysis must take the shape of the water feature into account, it is relevant to select an appropriate spectral processing strategy. The main difference between the strategies used in this study is that CR exaggerates the spectral features for a more precise discrimination. As a consequence, CR processing enhances the depth differences in the spectra of the water feature, thus increasing variations that are not relevant to the calibration. Using CR in the PLS-R modelling influenced the number of LVs required for the prediction, making only one or two LVs necessary for achieving a low prediction error. However, the calibration assigns high loadings to the peak of the feature enhancing the influence of the feature's depth, hindering a good prediction. Consequently, the RMSEC of the calibrations using CR-processed spectra were consistently larger than those processed with SNV, given that SNV assigned relatively small loadings to the feature's depth. In contrast, for the SVR modelling, the performances of the calibrations generated from CR spectra are better than those from SNV. The SVs used in these models seem to reduce the influence of the depth differences, although they are not eliminated, while giving more importance to features that are related to water adsorption.

Aside from the spectral processing, the selection of a spectral range also influenced the performance of the multivariate calibrations. In general, the errors of the models in the 2.6 to 3.3 µm range are higher than those in the 5.7 to 6.5 µm. Even though both ranges represent water features related to water adsorption, the presence of illite produces a mixed spectrum around 2.7 µm that explains the underperformance of the calibrations. Since the feature in the 5.7 to 6.5 µm range is exclusive for water, the calibrations in this part of the spectrum are more reliable. However, illite itself can also host water, inducing error to the predictions. The results of the PLS-R calibrations that included the chemical components of illite as variables show that there is indeed an influence of this mineral in the performance of the predictions. However, the inclusion of these variables can make the models more sensitive to errors induced by other types of impurities. To achieve more reliable calibrations, it would be necessary to quantify the amount of illite in the calcined clay and estimate its actual influence on the spectra.

Overall, the performance indicators in all the assessed scenarios indicate that the SVR calibrations are more accurate than the PLS-R ones. However, the most evident difference in the performance between SVR and PLS-R models is shown by the residuals

of the different achieved models. The size and the distribution of the PLS-R residuals are evidence of a poor calibration, and suggest that a nonlinear approach should be used. The smaller SVR residuals indicate a better calibration; however, the model struggles with the high and low values by systematically over-estimating values lower than 0.3 wt% and under-estimating values higher than 0.5 wt%. As a consequence, a note of caution is due here for the interpretation of new predictions that result in values lower than 0.3 wt% or higher than 0.5 wt%, since they might be considered as over-calcination in the first case, and under-calcination in the latter.

Even though the accuracy of the model with the best performance (5.7 to 6.5 µm spectra after CR processing) which has an RMSECV = 0.046 wt% is lower than the one of the SOP (0.015 wt%), it is enough for detecting variations in the soluble Al_2O_3 content in the calcined clay. For this sort of application, the lower performance of the prediction at extreme values—i.e., around 0.3 wt% and 0.5 wt%—is not of great consequence, since the over- or under-predicted values are still an indication of general variation trends in the calcination output. These factors encourage the use of the SVR predictions based on infrared spectra as part of a control system.

For an on-site and (near) real-time implementation scenario, the fact that the prediction model is based on spectra collected with a hand-held instrument increases the likelihood that such a system can be used in a mineral production environment. Moreover, the delimitation of the spectral range that is useful for the prediction optimises the required time for spectral collection and data processing. This approach enables the analysis of a larger volume of material than the one that could be possibly measured by the SOP. Therefore, the predicted soluble Al_2O_3 values could assist a more efficient utilisation of the SOP by performing the laboratory analysis in specifically determined samples. Furthermore, the infrared-based predicted values for soluble Al_2O_3 could be used to support the in-plant monitoring by improving operational feedback, thus making an impact on the performance of the calciner and the quality of the calcined product.

6.5. CONCLUSIONS

Soluble Al_2O_3, as an industrial parameter for quality control in calcination, is related to the formation of γ-alumina and consequently to the reactivity of the calcined clay. In the infrared spectra, the presence of γ-alumina is evidenced by the spectral features related to water adsorption. However, the nature of the water spectra (which captures not only adsorbed but also chemically bound and free water) hinders a univariate or linear relation with the amount of soluble Al_2O_3.

This study developed multivariate calibration models for the prediction of the content of soluble Al_2O_3 in calcined kaolin clays by using infrared spectroscopy. A combination of factors that affect the achievement of a good prediction was used to develop testing scenarios: (1) spectral regions where the water features are present between 2.6 to 3.3 µm and 5.7 to 6.5 µm; (2) standard normal variate (SNV) and continuum removal (CR) as spectral processing strategies to improve the discrimination among the different forms in which water is present in the samples; (3) partial least squares regression (PLS-R) and support vector regression (SVR) as multivariate calibration methods that cope with nonlinearity.

In general, the SVR models demonstrated a better ability to relate the water features

to the soluble Al_2O_3 parameter than the PLS-R ones. The best-performing model was achieved by using SVR in the 5.7 to 6.5 µm range after CR processing. The SVR model predicts the soluble Al_2O_3content in the calcined clay with RMSECV = 0.046 wt% and $R^2 = 0.87$. Even though this level of accuracy is lower than that one of the standard operational procedure (SOP), it is suitable for detecting variation trends in the production of calcined kaolin. These results encourage the use of infrared spectroscopy as a technique for (near) real-time quality control that supports the optimisation of the calcination process.

REFERENCES

Aines, R. D. and Rossman, G. R. (1984), 'Water in minerals? A peak in the infrared', *Journal of Geophysical Research* **89**, pp. 4059–4071. DOI: 10.1029/JB089iB06p04059

Andrés, J. M. and Bona, M. T. (2005), 'Analysis of coal by diffuse reflectance near-infrared spectroscopy', *Analytica Chimica Acta* **535**(1), pp. 123–132. DOI: 10.1016/j.aca.2004.12.007

Barnes, R. J., Dhanoa, M. S. and Lister, S. J. (1989), 'Standard normal variate transformation and de-trending of near-infrared diffuse reflectance spectra', *Applied Spectroscopy* **43**(5), pp. 772–777. DOI: 10.1366/0003702894202201

Bona, M. T. and Andrés, J. M. (2007), 'Coal analysis by diffuse reflectance near-infrared spectroscopy: Hierarchical cluster and linear discriminant analysis', *Talanta* **72**(4), pp. 1423–1431. DOI: 10.1016/j.talanta.2007.01.050

Brereton, R. G. and Lloyd, G. R. (2010), 'Support Vector Machines for classification and regression', *The Analyst* **135**(2), pp. 230–267. DOI: 10.1039/b918972f

Chakraborty, A. K. (2003), 'New data on thermal effects of kaolinite in the high temperature region', *Journal of Thermal Analysis and Calorimetry* **71**(3), pp. 799–808. DOI: 10.1023/a:1023318008031

Chang, C. and Lin, C. (2011), 'LIBSVM: A library for support vector machines', *ACM Transactions on Intelligent Systems and Technology* **2**, pp. 27.1–27.27.
URL: *http://www.csie.ntu.edu.tw/ cjlin/libsvm [Accessed September 2017]*

Chryssikos, G. D. and Gates, W. P. (2017), Spectral manipulation and introduction to multivariate analysis, *in* W. P. Gates, J. T. Kloprogge, J. Madejová and F. Bergaya, eds, 'Infrared and Raman Spectroscopies of Clay Minerals', Vol. 8 of *Developments in Clay Science*, Elsevier, pp. 64–106. DOI: 10.1016/b978-0-08-100355-8.00004-7

Clark, R. N. and Roush, T. L. (1984), 'Reflectance spectroscopy: Quantitative analysis techniques for remote sensing applications', *Journal of Geophysical Research* **89**, pp. 6329–6340. DOI: 10.1029/JB089iB07p06329

Cortes, C. and Vapnik, V. (1995), 'Support-vector networks', *Machine Learning* **20**(3), pp. 273–297. DOI: 10.1007/bf00994018

Devos, O., Ruckebusch, C. , Durand, A. , Duponchel, L. and Huvenne, J. P. (2009), 'Support vector machines (SVM) in near infrared (NIR) spectroscopy: Focus on parameters optimization and model interpretation', *Chemometrics and Intelligent Laboratory Systems* **96**(1), pp. 27–33. DOI: 10.1016/j.chemolab.2008.11.005

Drits, V. A., Derkowski, A. , Sakharov, B. A. and Zviagina, B. B. (2016), 'Experimental evidence of the formation of intermediate phases during transition of kaolinite into metakaolinite', *American Mineralogist* **101**, pp. 2331–2346. DOI: 10.2138/am-2016-5776

Eskelinen, A., Zakharov, A. , Jämsä-Jounela, S. L. and Hearle, J. (2015), 'Dynamic modeling of a multiple hearth furnace for kaolin calcination', *AIChE Journal* **61**(11), pp. 3683–3698. DOI: 10.1002/aic.14903

Filgueiras, P. R., Sad, C. M. S. , Loureiro, A. R. , Santos, M. F. P. , Castro, E. V. R. , Dias, J. C. M. and Poppi, R. J. (2014), 'Determination of API gravity, kinematic viscosity and water content in petroleum by ATR-FTIR spectroscopy and multivariate calibration', *Fuel* **116**(Supplement C), pp. 123–130. DOI: 10.1016/j.fuel.2013.07.122

Frost, R. L., Makó, É. , Kristóf, J. and Kloprogge, J. T. (2002), 'Modification of kaolinite surfaces through mechanochemical treatment - A mid-IR and near-IR spectroscopic study', *Spectrochimica Acta - Part A: Molecular and Biomolecular Spectroscopy* **58**, pp. 2849–2859. DOI: 10.1016/S1386-1425(02)00033-1

Glass, H. J. (2016), Geometallurgy – Driving innovation in the mining value chain, *in* 'The Third AusIMM International Geometallurgy Conference (GeoMet) 2016', Vol. 3, The Australasian Institute of Mining and Metallurgy: Melbourne, pp. 21–28.
URL: *https://www.ausimm.com.au/publications/epublication.aspx?ID=16947 [Accessed June 2018]*

Gualtieri, A. and Bellotto, M. (1998), 'Modelling the structure of the metastable phases in the reaction sequence kaolinite-mullite by X-ray scattering experiments', *Physics and Chemistry of Minerals* **25**, pp. 442–452. DOI: 10.1007/s002690050134

Guatame-García, A., Buxton, M. , Deon, F. , Lievens, C. and Hecker, C. (2018), 'Toward an on-line characterization of kaolin calcination process using short-wave infrared spectroscopy', *Mineral Processing and Extractive Metallurgy Review* **39**(6), pp. 420–431. DOI: 10.1080/08827508.2018.1459617

Haavisto, O. and Hyötyniemi, H. (2009), 'Recursive multimodel partial least squares estimation of mineral flotation slurry contents using optical reflectance spectra', *Analytica Chimica Acta* **642**(1-2), pp. 102–109. DOI: 10.1016/j.aca.2008.11.017

Höskuldsson, A. (1988), 'PLS regression methods', *Journal of Chemometrics* **2**(3), pp. 211–228. DOI: 10.1002/cem.1180020306

Hulbert, S. F. and Huff, D. E. (1970), 'Kinetics of alumina removal from a calcined kaolin with nitric, sulphuric and hydrochloric acids', *Clay Minerals* **8**(337), pp. 337–345. DOI: 10.1180/claymin.1970.008.3.11

Johnston, C. T. (2017), Infrared studies of clay mineral-water interactions, *in* W. P. Gates, J. T. Kloprogge, J. Madejová and F. Bergaya, eds, 'Infrared and Raman Spectroscopies of Clay Minerals', Vol. 8 of *Developments in Clay Science*, Elsevier, Chapter 9, pp. 288–309. DOI: 10.1016/b978-0-08-100355-8.00009-6

Li, H., Liang, Y. and Xu, Q. (2009), 'Support vector machines and its applications in chemistry', *Chemometrics and Intelligent Laboratory Systems* **95**(2), pp. 188–198. DOI: 10.1016/j.chemolab.2008.10.007

Liu, X. (2008), 'DRIFTS study of surface of gamma-alumina and its dehydroxylation', *Journal of Physical Chemistry C* **112**, pp. 5066–5073. DOI: 10.1021/jp711901s

Mevik, B. and Wehrens, R. (2007), 'The pls Package: Principal Component and Partial Least Squares Regression inR', *Journal of Statistical Software* **18**(2), pp. 1–23. DOI: 10.18637/jss.v018.i02

Meyer, D. (2017), 'Support Vector Machines: The interface to libsvm in package e1071', R package Vignette.
URL: *https://cran.r-project.org/web/packages/e1071/index.html [Accessed September 2017]*

Murray, H. H. (2006), Kaolin Applications, *in* H. H. Murray, ed., 'Applied Clay Mineralogy - Occurrences, Processing and Application of Kaolins, Bentonites, Palygorskite-Sepiolite, and Common Clays', Vol. 2 of *Developments in Clay Science*, Elsevier, Chapter 5, pp. 85–109. DOI: 10.1016/s1572-4352(06)02005-8

Percival, H. J., Duncan, J. F. and Foster, P. K. (1974), 'Interpretation of the kaolinite-mullite reaction sequence from infrared absorption spectra', *Journal of the American Ceramic Society* **57**, pp. 57–61. DOI: 10.1111/j.1151-2916.1974.tb10813.x

Phillips, C. V. and Wills, K. J. (1982), 'A laboratory study of the extraction of alumina of smelter grade from China clay micaceous residues by a nitric acid route', *Hydrometallurgy* **9**(1), pp. 15–28. DOI: 10.1016/0304-386X(82)90050-0

Ptáček, P., Šoukal, F. , Opravil, T. , Nosková, M. , Havlica, J. and Brandštetr, J. (2011), 'Mid-infrared spectroscopic study of crystallization of cubic spinel phase from metakaolin', *Journal of Solid State Chemistry* **184**(10), pp. 2661–2667. DOI: 10.1016/j.jssc.2011.07.038

Ruíz-Santaquiteria, C. and Skibsted, J. (2015), Reactivity of heated kaolinite from a combination of solid state NMR and chemical methods, *in* K. Scrivener and A. Favier, eds, 'Calcined clays for sustainable concrete', Proceedings of the 1st International Conference on Calcined Clays for Sustainable Concrete, Springer Netherlands, pp. 125–132.

Savitzky, A. and Golay, M. J. E. (1964), 'Smoothing and differentiation of data by simplified least squares procedures.', *Analytical Chemistry* **36**(8), pp. 1627–1639. DOI: 10.1021/ac60214a047

Smola, A. J. and Schölkopf, B. (2004), 'A tutorial on support vector regression', *Statistics and Computing* **14**(3), pp. 199–222. DOI: 10.1023/b:stco.0000035301.49549.88

Stevens, A. and Ramirez-Lopez, L. (2014), 'An introduction to the prospectr package', R package Vignette.
URL: *https://cran.r-project.org/web/packages/prospectr/index.html [Accessed December 2016]*

Taylor, R. J. (2005), 'Treatment of metakaolin - patent number WO2005108295 A1'.
URL: *https://patents.google.com/patent/WO2005108295A1/en [Accessed February 2017]*

Thomas, R. (2010), High temperature processing of kaolinitic materials, PhD thesis, University of Birmingham.
URL: *http://etheses.bham.ac.uk/6075/ [Accessed July 2013]*

Thomas, R., Grose, D. , Obaje, G. , Taylor, R. , Rowson, N. and Blackburn, S. (2009), 'Residence time investigation of a multiple hearth kiln using mineral tracers', *Chemical Engineering and Processing: Process Intensification* **48**(4), pp. 950–954. DOI: 10.1016/j.cep.2009.01.003

Wold, S., Sjöström, M. and Eriksson, L. (2001), 'PLS-regression: a basic tool of chemometrics', *Chemometrics and Intelligent Laboratory Systems* **58**(2), pp. 109–130. DOI: 10.1016/s0169-7439(01)00155-1

Yitagesu, F. A., van der Meer, F. , van der Werff, H. and Hecker, C. (2011), 'Spectral characteristics of clay minerals in the 2.5–14 μm wavelength region', *Applied Clay Science* **53**(4), pp. 581–591. DOI: 10.1016/j.clay.2011.05.007

7

FRAMEWORK FOR MONITORING AND CONTROL OF THE PRODUCTION OF CALCINED KAOLIN

This chapter proposes an infrared-based framework for online monitoring and quality control of the kaolin feed and the calcination products.

In the previous chapters of this Thesis, infrared (IR) spectroscopy has been used to characterise the quality parameters of kaolin feed and calcination products. The main purpose of using IR sensors in this work has been to appraise the opportunities for the collection and generation of on-site and real-time data that can influence the processing of calcined kaolin. The purpose of this chapter is to propose a framework for the online monitoring and quality control of the kaolin feed and calcination products utilising IR spectroscopy. For this, kaolin feed and calcination products were obtained from the production route with determined sampling intervals. The spectra of the feed samples were used to estimate the quality of the kaolin based on the results presented in Chapters 4 and 5. The spectra of the product samples were used to improve and validate the Support Vector Regression (SVR) models developed in Chapter 6 for the determination of the soluble Al_2O_3 content. A framework for monitoring and control based on two systems was proposed. The first system focuses on feed monitoring, seeking to ensure the consistency of the kaolin quality. The second system is applied to quality control of the calcined products, using a 2-step determination of the soluble Al_2O_3 content. An assessment of the integration of monitoring and control based on IR spectroscopy with the current control strategy showed how the proposed framework would significantly reduce the operational feedback and allow timely advice to the system regarding the tuning of the feed rate and the gas flow to the calciner. Such an approach would lead to the optimisation of the resource utilisation and the energy consumption by the calciner.

7.1. INTRODUCTION

In the stages involved in the processing of kaolin for speciality applications, calcination is the stage that has the highest consumption of energy (Glass, 2016). Nevertheless, the focus of the minerals industry in recent years has been towards the sustainable extraction and processing of raw materials. As a consequence, mining companies are developing and implementing practices that include, among others, reduction of energy consumption and reduction of CO_2 emissions (Kogel et al., 2014). In this scenario, the optimisation of the calcination process during the generation of kaolin products is of increasing importance.

As estated in Section 3.2.1, the industrial calcination of kaolin typically occurs in a Multiple Hearth Furnace (MHF). According to Jämsä-Jounela et al. (2018), in ideal conditions, the transformation from kaolinite to metakaolinite occurs at the fourth hearth, and the transformation of metakaolinite into Al-Si spinel occurs at the sixth hearth. As part of the process control strategy, the temperature at hearth six is manipulated to facilitate the absorption of Al into the spinel phase. Since the optimum calcination stage is defined by a point where kaolin has been fully but not excessively calcined, this step is a critical part of the process. At this specific point, over-heating would result in the nucleation of abrasive mullite, whereas under-heating would prevent the absorption of Al in the spinel phase, resulting in a product with high soluble Al_2O_3. Both mullite and soluble Al_2O_3 are deleterious in the calcined kaolin products for some speciality applications (Thomas et al., 2009).

The current control strategy, described by Jämsä-Jounela et al. (2018), is based on the online measurements of the operating conditions of the calciner, that is to say, temperature, gas flow and feed rate for the calciner. Additionally, the expected feed for calcination

is analysed in the laboratory to detect the Fe_2O_3 and K_2O levels, which account for the impurities in the raw kaolin. The quality control of the generated product takes place in the laboratory with analyses of soluble Al_2O_3, particle size and brightness. An apparent drawback of this approach is that the laboratory-based nature of the characterisation of feed and product prohibit consistent and timely feedback for process control. Buxton and Benndorf (2013) stated that, in this scenario, on-site sensor-based material characterisation has the potential to increase the performance of the process by ensuring the quality and homogeneity of the feed material. In addition, it ensures the adherence of the product to the quality specifications, reduces the necessity of off-line analyses and provides reconciliation data for real-time monitoring and control. For this type of applications, infrared (IR) spectroscopy is increasingly becoming as an established technique. Regarding the analysis of kaolin, the use of IR spectroscopy is common for the online analysis of kaolinite (Goetz et al., 2009), mineral mixtures that include kaolinite (de Souza et al., 2017; Yitagesu et al., 2011) and the kaolin calcination reaction (Frost et al., 2002; Guatame-García et al., 2018). Furthermore, in this Thesis, Chapter 6 proposed the use of infrared (IR) sensors to predict the soluble Al_2O_3 content in calcined kaolin by using a Support Vector Regression (SVR) model.

The primary objective of this study is to propose a framework for the online monitoring and quality control of feed and products in the generation of calcined kaolin using infrared spectroscopy. The feed control makes use of the quality grade parameters described in Chapters 4 and 5, which focus on the purity and crystallinity degree of the raw kaolinite. The product control follows the measurement of the soluble Al_2O_3 content using infrared spectroscopy proposed in Chapter 6, including an update of the support vector regression (SVR) model. The integration of the online monitoring of kaolin feed and calcination products with the current control strategy would improve its performance having a direct impact on the optimisation of the calcination process.

7.2. METHODS

7.2.1. SAMPLES

The feed and product samples used in this work were obtained from the calciner facilities located at the Devon County (south-west England). In this plant, the calcination process follows the soft calcination method in an MHF calciner (Section 3.2.1), in which kaolin undergoes exposure to high temperatures for an extended period. Ideally, the calcination reaction stops before the formation of mullite, generating a calcined product with minimised abrasion, hence the term “soft calcined”. The kaolin that serves as feed for the MHF calciner is composed mainly by kaolinite ($> 90\,\%$), with small amounts of muscovite/illite and quartz. Inside the MHF furnace, the kaolin feed suffers the calcination reactions described in Section 3.2.2.

This study comprises samples from two different sampling campaigns. In the first campaign, feed and product samples were obtained from the production route in the time span of 26 hours in sampling intervals of 2 hours. The feed samples were collected at the feed silo, before transfer to the calciner, whereas the product samples were obtained after blast cooling. In this campaign, it was noted that the soluble Al_2O_3 content of the products was lower than the one of the samples used to generate the SVR model for the

prediction of soluble Al_2O_3 in Chapter 6. Therefore, it was decided to use these samples to update the model and perform a new sampling campaign as a final test. In the second campaign, only product samples were collected, also after blast cooling. In this case, one sample was collected every hour in a time span of six hours for four consecutive days.

7.2.2. DATA COLLECTION AND PROCESSING

For the collection of the infrared spectra, each sample was placed in a sample cup where the powder was compacted and flattened with a spatula to minimise void spaces. The infrared spectra of kaolin feed and product samples were collected using an Agilent 4300 handheld FTIR spectrometer (Section 2.2.3). The spectra of the feed samples were recorded in the short-wavelength (SWIR) range, from 5200 to 4000 cm^{-1} (1.9 to 2.5 µm), whereas the spectra of the product samples were recorded in the mid-wavelength (MWIR) range, from 1800 to 1538 cm^{-1} (5.5 to 6.5 µm).

The spectral processing and analysis were carried out in the R environment using the prospectr package (Stevens and Ramirez-Lopez, 2014). First, the average of the five spectral measurements corresponding to each sample was computed; the resulting spectra were subsequently smoothened using the Savitzky-Golay filter with a polynomial order of 3 and windows size of 101 data points for the SWIR and 55 data points for the MWIR. Both datasets were subject to continuum removal (CR).

The feed control is based on some of the parameters used on the kaolin processing operations to determine its quality. Those parameters are kaolinite crystallinity, K_2O and Fe_2O_3. First, all these parameters were measured using the standard methods used in the operation plant, which are X-ray fluorescence (XRF) for determination of the oxides and the X-ray diffraction (XRD) for the computation of the Hinckley Index (HI). The following step consisted of the assessment of these parameters in combination with the IR spectra. This required the calculation of the kaolinite crystallinity index (Kx), previously described in Equation (5.1) (Chapter 5), which estimates the degree of structural order in kaolinite based on the shape of the 2.2 µm feature (Figure 5.2).

The analysis of the product quality is based on the soluble Al_2O_3 content. Such value can be estimated from the IR spectra of the calcined clay by using the SVR model proposed in Chapter 6. As mentioned above, the samples of the first campaign were used to update the model, extending its scope to lower soluble Al_2O_3 values; the samples from the second campaign were used for final validation of the model. The reference soluble Al_2O_3 measurements were obtained using the method used by Taylor (2005) and Thomas (2010) described in Chapter 6. The update of the SVR model followed the same methodology used in the calibration of the original model: using the R environment, interface to LIBSVM (open source machine learning library for SVM) (Chang and Lin, 2011), package e1071 (functions for SVM) (Meyer, 2017), and an RBF (radial basis function) kernel function. The optimisation of the parameters ε and C used a grid search and 10-fold cross-validation. Likewise, the assessment of the model performance used the root mean squared error of the cross-validation (RMSECV), root mean squared error of the calibration (RMSEC), and root mean squared error of the prediction (RMSEP). Additionally, the root mean squared error of the validation (RMSEV) assessed the performance of the final validation test.

7.3. RESULTS

7.3.1. FEED CHARACTERISATION AND CONTROL

DESCRIPTION OF THE FEED QUALITY PARAMETERS

The crystallinity, or degree of structural order, is an indicator of the stability of the crystal structure of kaolinite. Well-ordered kaolinites have an almost perfect stacking of the basic crystal unit and strong molecular bonds. Triggering the dehydroxylation reaction in such structures requires a higher temperature and has a lower calcination rate compared to poorly-ordered kaolinites (Murray and Lyons, 1959). The kaolinite that is calcined to produce aids for fillers and speciality applications should be of the well-ordered type. The Hinckley Index (HI) (Plançon et al., 1988) is measured regularly in the laboratory to ensure the input of such kaolinite in the calciner. Based on the HI values, the kaolinite is classified as very highly crystalline (0.5 < HI < 1.78), moderately highly crystalline (0.3 < HI < 0.5) and poorly/very poorly crystalline (HI < 0.3).

The calculated HI values for the feed samples, shown in Table 7.1, indicate that all the samples are classified into the very highly crystalline kaolinite group, evidencing the high-quality of the feed. The HI values vary in a narrow range from 0.9 to 1.23 also indicating that all the samples are similar and that the feed to the calciner is fairly consistent.

Table 7.1: Chemical composition (XRF) of the feed samples (wt %) and XRD Hinckley Index

Sample time (hours)	Al_2O_3	SiO_2	K_2O	Fe_2O_3	TiO_2	CaO	MgO	Na_2O	LOI	Hinckley Index
2	37.21	47.72	1.28	0.56	0.04	0.04	0.3	0.06	12.69	0.91
4	37.14	47.61	1.26	0.54	0.03	0.28	0.31	0.06	12.68	1.2
6	37.14	47.57	1.27	0.53	0.03	0.32	0.31	0.06	12.68	1.14
8	37.26	47.62	1.34	0.54	0.04	0.05	0.3	0.06	12.69	1.12
10	37.27	47.58	1.32	0.55	0.03	0.14	0.31	0.07	12.7	1.1
12	37.15	47.55	1.36	0.55	0.03	0.24	0.31	0.06	12.65	1.23
14	37.28	47.62	1.31	0.55	0.03	0.11	0.3	0.06	12.65	1.19
16	37.26	47.64	1.32	0.56	0.03	0.09	0.31	0.06	12.65	1.05
18	37.21	47.58	1.33	0.53	0.03	0.19	0.3	0.06	12.66	1.18
20	37.27	47.69	1.29	0.55	0.03	0.06	0.31	0.06	12.65	1.17
22	37.32	47.62	1.33	0.55	0.04	0.04	0.31	0.05	12.65	1.17
24	37.31	47.43	1.33	0.53	0.03	0.25	0.31	0.06	12.65	1.04
Mean	37.23	47.6	1.31	0.55	0.03	0.15	0.31	0.06	12.67	1.13
SD	0.06	0.07	0.03	0.01	0.004	0.1	0.004	0.004	0.02	0.09
Min	37.14	47.43	1.26	0.53	0.03	0.04	0.3	0.05	12.65	0.91
Max	37.32	47.72	1.36	0.56	0.04	0.32	0.31	0.07	12.7	1.23

The second quality parameter is the K_2O content of the feed. Since kaolinite does not contain K_2O, the determination of this parameter indicates the purity of the feed. At this stage of the processing, potasium is an indicator of the presence of illite and muscovite. From the XRF results in Table 7.1, K_2O accounts in average for a 1.3 % of the samples. According to the stoichiometric proportions of K_2O in illite and muscovite, also taking into account the Fe_2O_3 and MgO content, it is likely that the samples contain approximately 5 % of muscovite and 10 % of illite. Similarly to the crystallinity results, the small variations in the K_2O content give an account of the consistency of the feed.

The presence of iron is detrimental in the kaolin feed since its oxidation during

calcination produces pink shading on the calcined product, which reduces the brightness and the whiteness. The average iron content of the kaolin ore in the current production pits in Cornwall does not exceed 2 % ((Manning et al., 1996)). After the beneficiation of the ore, iron can still be present in the feed as isomorphous substitution of Fe^{+3} for Al^{+3} in kaolinite, adhered to the kaolinite's surface, or as a constituent in residual illite. The iron content in the feed samples, measured with XRF as Fe_2O_3, is in average 0.55 %, which despite being very low, can still influence the optical properties of the calcined product.

When iron is present as an isomorphous substitution in kaolinite, such substitution causes a defect that influences the ordering of the mineral's structure. Therefore, higher iron content normally results in lower crystallinity values compared to iron-free kaolinite. The correlation coefficient between the HI crystallinity values and the Fe_2O_3 content was calculated to assess whether the presence of iron is displayed as variations in crystallinity. A coefficient of $R^2 = -0.31$ indicates no correlation between these parameters. Consequently, it is unlikely that the kaolinite hosts iron as part of its crystal structure. Given the presence of illite in the samples, part of the iron might be hosted by this mineral. According to the previous illite estimate, the amount of iron present in the samples contained in the illite fraction would not exceed 0.2 %. It is therefore likely that most of the iron in the feed samples occurs as residual iron adhered to the surface of the kaolinite.

DETECTION OF THE FEED QUALITY PARAMETERS WITH INFRARED SPECTROSCOPY

The IR spectra in the SWIR range were studied to assess whether the kaolinite crystallinity, iron and potassium content of the feed for calcination can be inferred using IR spectroscopy. For this, the Kx index of the samples was computed. The spectra and the results are presented in Figure 7.1. The Kx index of the feed varies from 1.07 to 1.09. According to the HI–Kx correspondence established by Pontual et al. (1997), these Kx values are attributed as well to highly crystalline kaolinite. Figure 7.2 compares the response of the Kx values and the parameters for feed quality assessment. The scale of the plots corresponds to the maximum and minimum values for each parameter.

In Figure 7.2 (top) there is a comparison between the Kx and the HI indices. The calculated coefficient of correlation between the indices is $R^2 = 0.65$, which suggests a moderately good correlation. In the plot, it is possible to see that the sample corresponding to 22h, in which the Kx differs notoriously from the HI, affects the coefficient. Despite this sample, both measurements follow a similar trend regarding the variations in crystallinity. In this part of the spectra, the spectral features of kaolinite are dominant and can give a reliable estimation of kaolinite crystallinity.

The differences between the HI and Kx indices could be due to mineral mixtures with illite and muscovite. Since the presence of these two minerals is related to the K_2O content, the comparison of this parameter with the crystallinity indices could explain whether there is an influence of the mineral impurities in the Kx index. In Figure 7.2 (centre) the Kx is compared to the K_2O content. It would be expected that the dissimilarities between the indices would coincide with high levels of K_2O and vice versa. However, there is not a clear trend that can explain these variations consistently.

Regarding the detection of iron content using the IR spectra, it would be presumed that high Fe_2O_3 content would result in a lower Kx index due to: (1) an eventual Fe–Al replacement in kaolinite that destabilises the crystal structure, (2) Fe present in illite, which

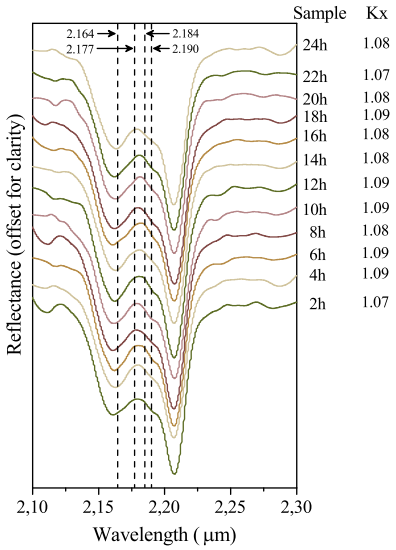

Figure 7.1: Stackplot with the collected SWIR spectra of the kaolin feed samples and their correspondent Kx index. The vertical lines indicate the wavelengths that are used for the calculation of the Kx index.

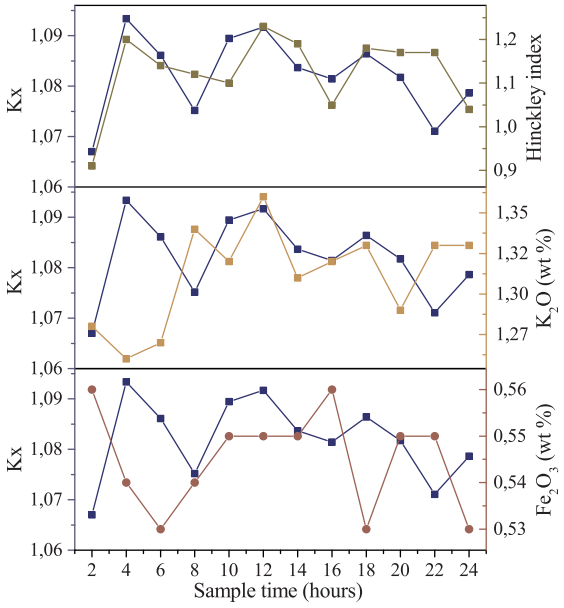

Figure 7.2: Comparison of the Kx index with the standard parameters used for quality control of the feed for calcination (**top**) HI index, (**middle**) K_2O, (**bottom**) Fe_2O_3.

in spectral mixture with kaolinite affects the shape of the kaolinite spectral absorptions. However, the previous observations made evident that there are not apparent crystallinity changes due to iron replacement and that it is not possible to provide conclusive evidence of the influence of mineral mixtures in the spectra. Therefore it is difficult to establish a relationship between the iron content in the feed and the spectra. This is also noticeable in Figure 7.2 (bottom), where the Kx index and Fe_2O_3 do not show any similar trends.

7.3.2. PRODUCT CONTROL

MODEL UPDATE

Chapter 6 presented the development of an SVR model for the prediction of soluble Al_2O_3 values in calcined kaolin samples. Such model was built in a soluble Al_2O_3 content ranging from 0.26 to 0.64 wt%. As Table 7.2 shows, the soluble Al_2O_3 values of the samples of the first campaign used in this chapter range from 0.23 to 0.32 wt% and have a mean of 0.27 wt%, which indicates that a significant part of the sample set lies outside the range of the SVR model. Despite this, the IR spectra were used to calculate the soluble Al_2O_3 content on these samples using the SVR model. A comparison with the reference laboratory measurements evidenced the poor performance of the prediction, as noted by an RMSE = 0.14 wt%, which is three times as high as the error that the model allows.

Table 7.2: Soluble Al_2O_3 content of the product samples (wt%) of the first and second campaigns. The samples of the second campaign are labelled as x-y, where x = sampling day and y = sampling time.

First sampling campaign		**Second sampling campaign**			
Sample time	**Soluble Al_2O_3**	**Sample ID**	**Soluble Al_2O_3**	**Sample ID**	**Soluble Al_2O_3**
0	0.3			3-0	0.27
2	0.26			3-1	0.27
4	0.29	1-2	0.21	3-2	0.27
6	0.25	1-3	0.24	3-3	0.26
8	0.24	1-4	0.24	3-4	0.28
10	0.24	1-5	0.24	3-5	0.29
12	0.23	1-6	0.54	3-6	0.32
14	0.23	2-0	0.29	4-0	0.26
16	0.27	2-1	0.29	4-1	0.25
18	0.31	2-2	0.26	4-2	0.27
20	0.32	2-3	0.27	4-3	0.26
22	0.32	2-4	0.28	4-4	0.26
24	0.25	2-5	0.28	4-5	0.26
26	0.28	2-6	0.30	4-6	0.27
Mean	0.27				0.28
SD	0.03				0.06
Min	0.23				0.21
Max	0.32				0.54

These results made evident that the SVR model does not adequately represent the entire range of soluble Al_2O_3 values of the calcined kaolin products. In order to create a more robust model that can cope with a broader range of values, the sample set used initially in the development of the SVR model was merged with the sample set of the first

campaign. The new dataset consisted of 70 samples, with soluble Al_2O_3 values that range from 0.23 to 0.64 wt% and a mean value of 0.38 wt%. The merged sample set was split into a training set of 55 samples and a test set of 15 samples using random selection. The spectral processing followed the same procedures used for the original model.

Table 7.3 summarises the calibration and performance parameters of the original and updated models. Regarding the calibration parameters, the ε value is smaller in the updated model, and the required number of support vectors (SV) is proportionally larger. A smaller ε value implies that, in order to compensate for the variation added by the low soluble Al_2O_3 values, this model became more rigid than the original one. Consequently, the model requires a larger proportion of the dataset as support vectors. Nevertheless, the number of SV guarantees that the model does not over-fit the data. The adjustment of the model comes with the cost of a decreased accuracy, reflected in the RMSECV, RMSEC and R^2, which are larger than in the original model.

Table 7.3: Summary of the optimisation parameters and performance indicators of the original (Chapter 6) and updated support vector regression (SVR) calibrations

Model	**Samples**			***C***	***ε***	**SV**	**RMSECV**	**RMSEC**	**RMSEP**	R^2
	Total	**Training**	**Test**				**(wt %)**	**(wt %)**	**(wt %)**	
Original	56	46	10	3.1	0.46	19	0.046	0.025	0.044	0.87
Updated	70	55	15	3.0	0.3	30	0.057	0.040	0.039	0.77

A representation of the results in Figure 7.3 shows that, despite the increased errors, the updated model produces reasonably good predictions that do not differ significantly from those of the original model, as previously shown in Figure 6.9. Similarly to the original model, the updated one seems to under-predict high soluble Al_2O_3 values (above 0.5 wt%) and over-predict low values (below 0.3 wt%), although in a bigger magnitude than the original model, as evidenced by the residuals plot. These results indicate that even though the updated model compromises the accuracy to cover a more extensive range of soluble Al_2O_3 values, the model is nonetheless valid.

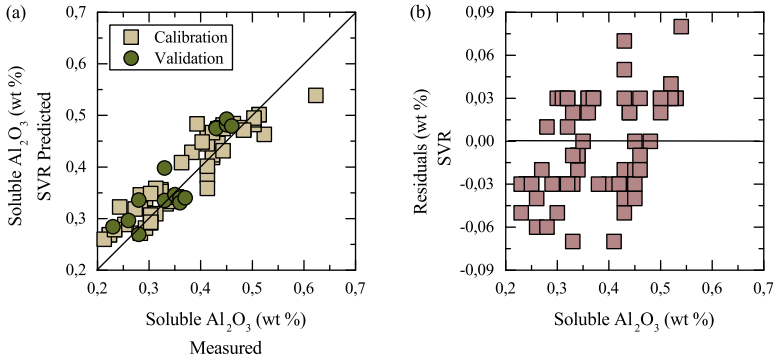

Figure 7.3: (**a**) Measured vs Predicted plot of the updated SVR model in the calibration and validation samples, and (**b**) their respective residuals.

MODEL VALIDATION

The final validation of the updated SVR model was done using a completely new sample set collected in the second campaign. This set, presented in Table 7.2, consists of 26 samples with soluble Al_2O_3 values that vary from 0.21 to 0.54 wt%. This time, only one sample lies slightly outside the range of the updated SVR model, which was used to calculate the soluble Al_2O_3 content of the sample from the IR spectra. Figure 7.4 displays the IR-predicted and measured soluble Al_2O_3 values of the validation samples. In general, there seems to be an acceptable match between the IR-predicted and the measured values, with a reported error RMSE = 0.059 wt%. This error is similar to the RMSECV of the updated model (RMSE = 0.057 wt%), which indicates that the model is adequate for this set of samples. Despite this, there are two remarkable differences between the predicted and the measured values that deserve more detailed analysis.

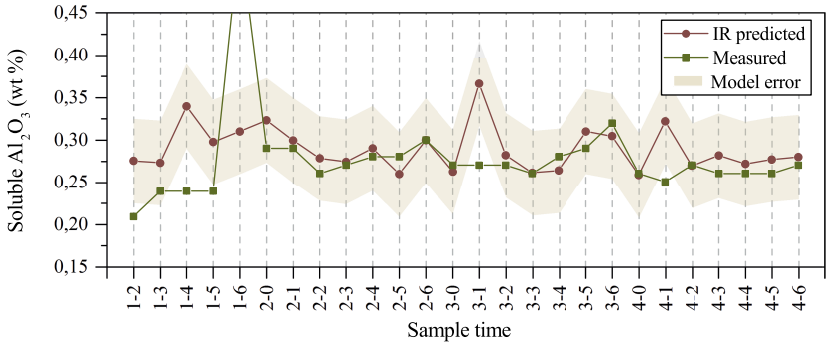

Figure 7.4: IR-predicted values of the validation sample set using the updated SVR calibration model, compared to the measured values. Sample 1-6 (measured) not displayed for purposes of scale (measured value = 0.54 wt%)

The most striking difference between the measured and predicted values occurs in the sample labelled as 1-6, namely the last sample collected on day one. The measured soluble Al_2O_3 value of this sample is 0.54 wt%, whereas the predicted value is 0.31 wt%, a difference almost four times as big as the error of the model. Observing the trends of the samples on day 1 (samples 1-2 to 1-6), all the predicted and measured values fluctuate in a narrow range, with the only exception of the measured data point of sample 1-6. Given these trends, and taking into account the operation of the calciner and the consistency of the feed – as shown previously in Section 7.3.1 –, an error in the laboratory measurement is more likely than the error in the prediction, which suggests a value between 0.26 and 0.37 wt%. Without this data point, the RMSEV drops to 0.039 wt%, which is similar to the RMSEC and RMSEP in the model.

The second difference also occurs in the samples collected on day one. Except for sample 1-6, explained above. In the remainder samples, the soluble Al_2O_3 values are strongly over-predicted, with the measured values lying outside or close to the margin of error. The over-prediction of low values was already observed in the calibration set

(Figure 7.3), and in this validation set, most of the samples have also over-estimated predictions. However, these results indicate that the discrepancy between measured and predicted values becomes stronger at very low values. Nonetheless, taking into account that very low soluble Al_2O_3 is not critical for the control of the calcined product, the updated SVR model can be considered adequate for quality control purposes.

7.4. FEED AND PRODUCT MONITORING

The study of Thomas et al. (2009) established that, with a standard feed throughput of $5.3\,t\,h^{-1}$, the residence time of the kaolin inside the MHF calciner is 42 minutes. However, that study also indicated that the operating conditions and design of the furnace difficult the calculation of the kaolin residence time with precision. Moreover, the feed rates to the calciner can be adjusted from time to time to optimise the production capacity of the furnace. All these factors hinder the possibility of making a direct link between feed and product samples. For this reason, the monitoring and control strategies for feed and products should be handled as independent systems. This study proposes a twofold infrared-based monitoring scheme for calcination feed and products, which features include:

1. A system for the feed monitoring that supervises the quality and consistency of the feed regarding the kaolinite crystallinity, composed by:
    - An IR sensor that collects spectra in the SWIR range
    - An algorithm that measures the crystallinity of kaolinite in the feed using the measured spectra
2. A system for the quality control of the product that estimates the soluble Al_2O_3 content of the calcined kaolin product, composed by:
    - An IR sensor that collects the spectra in the MWIR range
    - 2 SVR models that predict the soluble Al_2O_3 in calcined kaolin using the measured spectra

The system for feed monitoring aims to guarantee the consistency of the feed for calcination, and is based on the infrared Kx index. The results presented in Section 7.3.1 noted that the raw kaolin coming from the current production pits has remarkable high crystallinity. However, the possible blending of ores from different pits or even from different mines can affect the consistency of the feed. In this case, which is likely to be the trend in the industry (Imerys Minerals, Ltd., personal communication May 24, 2017), the feed monitoring system would allow detecting changes in the ore that affect the crystallinity of the kaolinite. Furthermore, the system could also facilitate the smart blending of ores from different sources to generate a regular feed that meets the production needs.

The system for product monitoring aims to provide soluble Al_2O_3 measurements that give timely feedback to the operation of the calciner. The system is based on the soluble Al_2O_3 SVR-estimation using the IR spectra. The results presented in Section 7.3.2 indicated that there is a trade-off between a robust model that has a broad range of soluble Al_2O_3 detection but a reduced accuracy, that is to say, the updated SVR model,

and a model limited to a narrower detection range but with better accuracy, namely the original SVR model. Nevertheless, both models can estimate the amount of soluble Al_2O_3 in the calcined kaolin with a level of accuracy that is acceptable for practical applications, as in the monitoring of the process.

The SVR models can be incorporated and become an integral part of the enhanced quality control strategy for the MHF proposed by Jämsä-Jounela et al. (2018). The control strategy seeks to optimise the capacity of the furnace and minimise its energy consumption while maintaining the quality standards of the calcined product. The parameters that the control strategy can influence are the tempeature of the furnace, regulated by the gas flow, and the feed rate to the calciner. Figure 7.5 presents a proposal for the integration of the the IR-based soluble Al_2O_3 measurement into the enhanced control strategy. In practice, the quality requirements for soluble Al_2O_3 specify a threshold of 0.55 wt% as the maximum amount allowed in the product. Therefore, that threshold is the critical value that the monitoring and control system should focus. In this scenario, a combination of the updated and original models would give a more reliable estimation of the quality of the samples.

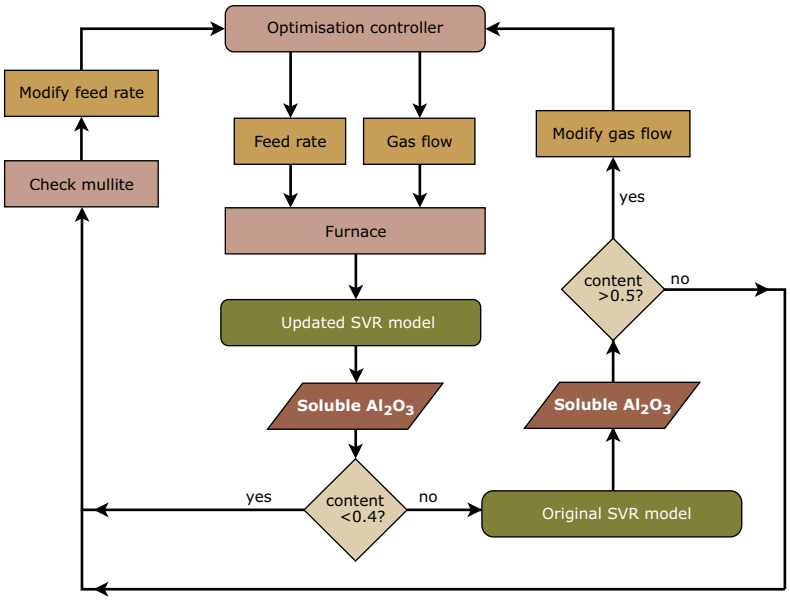

Figure 7.5: Proposed monitoring scheme for the quality control of the production of calcined kaolin based on the IR estimation of soluble Al_2O_3 to be integrted into the enhanced control strategy proposed by Jämsä-Jounela et al. (2018).

At first instance, the updated SVR model can provide with an initial estimation of the soluble Al_2O_3 content in the product, and discriminate low or high values. Based on the response of both models, as observed in Figure 6.9 and Figure 7.3, a low–high threshold can be set at 0.4 wt%. Low values do not impose a warning for the process, and therefore,

precise estimation is not highly relevant. Nevertheless, low soluble Al_2O_3 might suggest over-calcination of the kaolin, in which case, the mullite content of the calcined product should be considered. A balance between low mullite content and aceptable soluble Al_2O_3 dictates changes in the feed rate.

In the case of high values, the soluble Al_2O_3 content can be re-calculated using the original model that would generate a more accurate estimation. Since the accuracy of the original model is 0.046 wt%, a threshold at 0.50 wt% can be set as the point where action needs to be taken to increase the temperature in the furnace and avoid under-calcination of the kaolin.

The implementation of an IR-based monitoring strategy for feed and products would enable the frequent collection of data, also creating permanent records. The integration of these data with other historical plant records could be used to perform trend analysis, develop soft-sensors and explore the opportunities for detecting other properties. Furthermore, the routine collection of data would serve to periodically recalibrate the models with the laboratory measurements that are regularly taken for official reporting.

With the existing instrumentation, the system can be used in a semi-offline mode, that is to say, on-site but with the intervention of an operator who collects the sample and manipulates the instrument. The feed monitoring could be performed at any point required between the feed silo and the feeder bin. The product monitoring could be carried out at earliest after blast cooling when the temperature of the calcined material allows its manipulation, representing a delay of the measurements between 30 to 45 minutes, which is still adequate for operational feedback. The implementation of the system does not require extensive knowledge of chemometrics or infrared spectroscopy. A regular plant operator with minimal training could perform the measurements. Nevertheless, with some modifications of the instrument, the system has the potential to become automated.

7.5. CONCLUSIONS

The increasing demand for generating calcined kaolin products together with the increasing economic and energy concerns related to the calcination process itself has created the need to generate strategies to optimise the process. The current control strategy for the Multiple Hearth Furnace (MHF) is based on the operational setup and laboratory measurements. This study proposed the integration of on-site monitoring of the material that serves as feed for calcination and the calcined kaolin product to optimise the current control strategy. The monitoring of the feed and products uses a sensor-based approach that employs infrared (IR) spectroscopy.

The monitoring of the kaolin feed for calcination aims to ensure the consistency of the feed and support proactive control of the calcination process. From the three parameters that are relevant for feed characterisation (Fe_2O_3, K_2O and kaolinite crystallinity), the infrared system can determine the crystallinity of kaolinite using the Kx index. The measurement can be used to detect variations in the feed, especially relevant in foreseeable scenarios that would involve ore blending from different sources.

The monitoring scheme for product control is based on the estimation of soluble Al_2O_3 using Support Vector Regression (SVR). The system uses a combination of two SVR models: a first model that discriminates low and high soluble Al_2O_3 values, and a second

model that has better accuracy at predicting values near to the threshold for quality specifications. The integration of this monitoring scheme into the general control strategy for the MHF furnace influences the decision parameters for feed rate and temperature control, with direct repercussions on the optimisation the resource utilisation and energy consumption of the calcination process.

REFERENCES

Buxton, M. and Benndorf, J. (2013), The use of sensor derived data in optimization along the mine-value-chain: An overview and assessment of techno-economic significance, *in* 'Proceedings of the 15th International ISM Congress, Aachen, Germany', pp. 324–336.

Chang, C. and Lin, C. (2011), 'LIBSVM: A library for support vector machines', *ACM Transactions on Intelligent Systems and Technology* **2**, pp. 27.1–27.27.
URL: *http://www.csie.ntu.edu.tw/ cjlin/libsvm [Accessed September 2017]*

de Souza, M. K., Veronez, M. R. , Tognoli, F. M. W. , Gonzaga, L. , de Souza, L. V. , Kochhann, M. V. L. , da Silva, N. G. , Marson, F. P. and Cagliari, J. (2017), Identification and quantification of kaolinite in mixtures with goethite using short-wave infrared (SWIR) reflectance spectroscopy, *in* '2017 IEEE International Geoscience and Remote Sensing Symposium (IGARSS)', IEEE, pp. 4882–4885. DOI: 10.1109/igarss.2017.8128097

Frost, R. L., Makó, É. , Kristóf, J. and Kloprogge, J. T. (2002), 'Modification of kaolinite surfaces through mechanochemical treatment - A mid-IR and near-IR spectroscopic study', *Spectrochimica Acta - Part A: Molecular and Biomolecular Spectroscopy* **58**, pp. 2849–2859. DOI: 10.1016/S1386-1425(02)00033-1

Glass, H. J. (2016), Geometallurgy – Driving innovation in the mining value chain, *in* 'The Third AusIMM International Geometallurgy Conference (GeoMet) 2016', Vol. 3, The Australasian Institute of Mining and Metallurgy: Melbourne, pp. 21–28.
URL: *https://www.ausimm.com.au/publications/epublication.aspx?ID=16947 [Accessed June 2018]*

Goetz, A. F. H., Curtiss, B. and Shiley, D. A. (2009), 'Rapid gangue mineral concentration measurement over conveyors by NIR reflectance spectroscopy', *Minerals Engineering* **22**(5), pp. 490–499. DOI: 10.1016/j.mineng.2008.12.013

Gomez-Fuentes, J., Guatame-Garcia, A. , Jämsä-Jounela, S. L. , Moseley, D. , Skuse, T. and Buxton, M. (2019), 'Control strategy of a calciner enhanced by mineralogy driven machine learning algorithms'. Submitted manuscript.

Guatame-García, A., Buxton, M. , Deon, F. , Lievens, C. and Hecker, C. (2018), 'Toward an on-line characterization of kaolin calcination process using short-wave infrared spectroscopy', *Mineral Processing and Extractive Metallurgy Review* **39**(6), pp. 420–431. DOI: 10.1080/08827508.2018.1459617

Jämsä-Jounela, S. L., Gomez-Fuentes, J. , Hearle, J. , Moseley, D. and Smirnov, A. (2018), 'Control strategy for a multiple hearth furnace in kaolin production', *Control Engineering Practice* **81**, pp. 18–27. DOI: 10.1016/j.conengprac.2018.08.020

Kogel, J. E., Trivedi, N. and Herpfer, M. A. (2014), 'Measuring sustainable development in industrial minerals mining', *International Journal of Mining and Mineral Engineering* **5**(1), pp. 4–18. DOI: 10.1504/ijmme.2014.058921

Manning, D. A. C., Hill, P. I. and Howe, J. H. (1996), 'Primary lithological variation in the kaolinized St Austell Granite, Cornwall, England', *Journal of the Geological Society* **153**(6), pp. 827–838. DOI: 10.1144/gsjgs.153.6.0827

Meyer, D. (2017), 'Support Vector Machines: The interface to libsvm in package e1071', R package Vignette.
URL: *https://cran.r-project.org/web/packages/e1071/index.html [Accessed September 2017]*

Murray, H. H. and Lyons, S. C. (1959), Further correlations of kaolinite crystallinity with chemical and physical properties, *in* A. Swineford, ed., 'Eighth National Conference on Clays and Clay Minerals', Clays and Clay Minerals, Elsevier Science, pp. 31–40. DOI: 10.1346/CCMN.1959.0080104

Plançon, A., Giese, R. F. and Snyder, R. (1988), 'The Hinckley Index for kaolinites', *Clay Minerals* **23**, pp. 249–260. DOI: 10.1180/claymin.1988.023.3.02

Pontual, S., Merry, N. and Gamson, P. (1997), Regolith Logging, *in* S. Pontual, N. Merry and P. Gamson, eds, 'Spectral Analysis Guides for Mineral Exploration', Vol. 1, AusSpec International, Chapter 8, pp. 8.1–8.62.

Stevens, A. and Ramirez-Lopez, L. (2014), 'An introduction to the prospectr package', R package Vignette.
URL: *https://cran.r-project.org/web/packages/prospectr/index.html [Accessed December 2016]*

Taylor, R. J. (2005), 'Treatment of metakaolin - patent number WO2005108295 A1'.
URL: *https://patents.google.com/patent/WO2005108295A1/en [Accessed February 2017]*

Thomas, R. (2010), High temperature processing of kaolinitic materials, PhD thesis, University of Birmingham.
URL: *http://etheses.bham.ac.uk/6075/ [Accessed July 2013]*

Thomas, R., Grose, D. , Obaje, G. , Taylor, R. , Rowson, N. and Blackburn, S. (2009), 'Residence time investigation of a multiple hearth kiln using mineral tracers', *Chemical Engineering and Processing: Process Intensification* **48**(4), pp. 950–954. DOI: 10.1016/j.cep.2009.01.003

Yitagesu, F. A., van der Meer, F. , van der Werff, H. and Hecker, C. (2011), 'Spectral characteristics of clay minerals in the 2.5–14 μm wavelength region', *Applied Clay Science* **53**(4), pp. 581–591. DOI: 10.1016/j.clay.2011.05.007

III

PROCESS AIDS: FILTERS AND ABSORBENTS

8

PERLITE AND DIATOMITE

This chapter presents perlite and diatomite as the major industrial minerals used as process aids, particularly as filters and absorbents. Their properties, the mining and processing techniques that they undergo, as well as their uses are reviewed.

Industrial minerals that are used as process aids are those which facilitate the attainment of the desired results in a process. The main processes assisted by process aid minerals are filtration and absorption. Filter aids are used to clarify, purify and clean liquids by removing the dissolved and particulate matter that is present in suspension, while absorbents are used to clean up liquid wastes or spills (Mathers and Scott, 2002; Mathur and Ravishankar, 2006). The most common applications of process aids are for the filtration of liquid food products, water treatment, petroleum and chemicals, and pharmaceuticals and drugs. For these uses, industrial minerals are wanted to form filters that enable a high flow rate of filtration, at the time that generate a filtrate with high clarity. Given the type of uses, the presence of the process aids or their residues in the finished product should be avoided or limited, taking especial care that they will not present any health risk or will not have any unwanted effect on the final product. The major minerals used as filter aids and absorbents are perlite and diatomite.

8.1. MINERALOGY AND PROPERTIES

The minerals used for filtration purposes belong to the silica group, which is characterised by its chemical stability. The silica contained in perlite and diatomite is a variety of opal ($SiO_2 \cdot H_2O$), which is amorphous and essentially inert (Chang, 2002*a*). In addition, perlite and diatomite have particular crystal structures that form microscopic voids, which impart high porosity; this enables the flow of liquids and the retention of solid particulate matter.

Perlite is a form of hydrated volcanic glass of rhyolitic composition with 2 to 5 % of combined water (Barker and Santini, 2006). It has pearly lustre and onionskin texture as a consequence of the devitrification that leads to the formation of the perlite. As a filtration aid, perlite is desired due to its chemical inertness, low density (1.750 to 1.875 $kg\,m^{-3}$) and expansion capability (from 4 to 20 times its original volume) (Kadey, 1983). In the perlite deposits, volcanic glass is commonly associated with zeolites and clay minerals.

Diatomite is a sedimentary rock formed primarily by fossilised diatom frustules. The composition of recent frustules resembles that of silica gel, whereas the silica in the fossil frustules is opaline, which has a lower solubility (Kamatani, 1971) and 1.9 to 9.6 % of combined water. The intricate structure of the diatom frustules imparts low density and high porosity (10 to 30 %) to the diatomite rock. Besides these characteristics, diatomite has a mild abrasiveness, high absorption capacity, high brightness and low thermal conductivity.

8.2. GEOLOGICAL OCCURRENCE

Perlite and diatomite deposits are associated to active continental margins, where arc-cordillera volcanics occur along present-day or earlier subduction zones, as Figure 8.1 shows (Mathers and Scott, 2002; Scott, 2011). The presence of these deposits is restricted to the circum-Pacific region and southern Europe.

Perlite usually occurs in steep-sided domes or the centre of bedded rhyolitic tuffs (Scott, 2011). Its genesis is related to the hydration of volcanic glass in association with high-silica lava flows. The hydration is the result of the chemical weathering of obsidian at or near the earth's surface produced by hydrothermal, meteoric or phreatic waters.

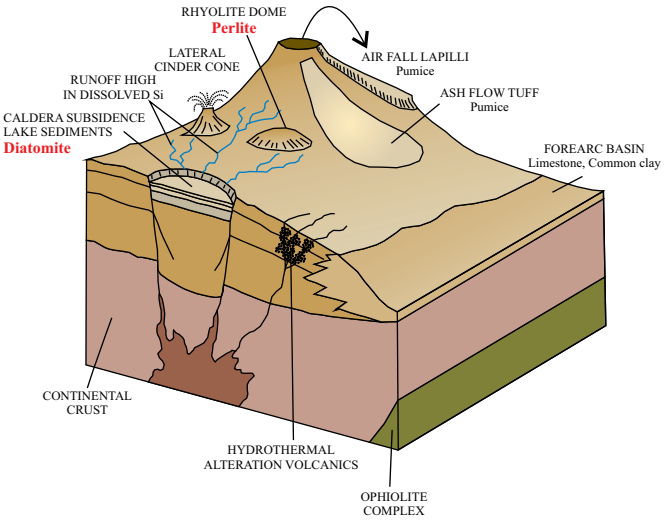

Figure 8.1: Generalized block diagram showing the geological setting for the formation of perlite and diatomite deposits (Modified after Mathers and Scott (2002))

The dimensions of a perlite deposit depend upon the eruptive history of the parent volcano; likewise, different types of perlite –defined by its texture– depend upon the level of alteration within the volcanic dome (Barker and Santini, 2006). Preservation of perlite is unusual in rocks older than the Cenozoic era (66 Ma) since the alteration and devitrification process continues, transforming the perlite into zeolites and other aluminosilicates (Chang, 2002*b*).

Diatomite deposits take place in shallow sedimentary basins with an abundant supply of silica in solution from volcanism that fosters the diatom growth (Scott, 2011). Additionally, the basin should not have a steady influx of terrigenous material. Marine deposits are associated with regions of upwelling that bring nutrients to the surface (Barron, 1987). Lacustrine basins can be formed, for example, as the result of the subsidence of a caldera and the blocking of drainage by volcanic deposits, as shown in Figure 8.1 (Mathers and Scott, 2002; Scott, 2011). The sources of silica can be external (runoff water, groundwater seepage, and hot or cold springs) or internal (silica released from bottom sediments) (Hurley et al., 1985). Depending on the sedimentation history of the deposit, clay minerals, volcanic ash, carbonates and organic matter are deposited together or interbedded with the diatom frustules. The deposition of thick layers of diatomite requires a stable environment and stable depositional conditions for long periods. The preservation of the deposit is subject to protection from erosion and to slow diagenesis that prevents the dissolution of silica or its transformation to higher crystalline forms (e.g. cristobalite/tridymite). Because of this, only diatomite deposits from the Cenozoic era are still preserved (Breese and Bodycomb, 2006).

8.3. MINING AND PROCESSING

In the mining and processing of perlite and diatomite, the most critical aspect is to maintain the integrity of the crystal structure that imparts high porosity. The degree of processing depends on the desired properties by the end-users in the industry. In some cases, perlite and diatomite are subjected to calcination to reduce the amount of combined water and modify the pore size and surface area. As a consequence, the calcined products have less dense particles with a larger particle size, which results in an increased flow rate. Variations in the calcination temperature and the residence time inside the furnace result in calcined products with different specifications (Mathur and Ravishankar, 2006).

Perlite is usually mined using open pit techniques. Figure 8.2 shows a simplified flowsheet for the mining and processing of perlite. Due to the softness and friability of the rock, only ripping is needed. Blasting is only used in particular cases if the ore is particularly hard; however, its use is avoided since it increases the amount of fine particles. In some operations, selective mining aids to minimise the amount of rhyolite or obsidian. After primary crushing, the ore is loaded to the processing plant. If the deposit is not homogeneous, or if the feed to the plant comes from different deposits, the ore is blended to produce consistent milling that can meet the end-user specifications (Barker and Santini, 2006).

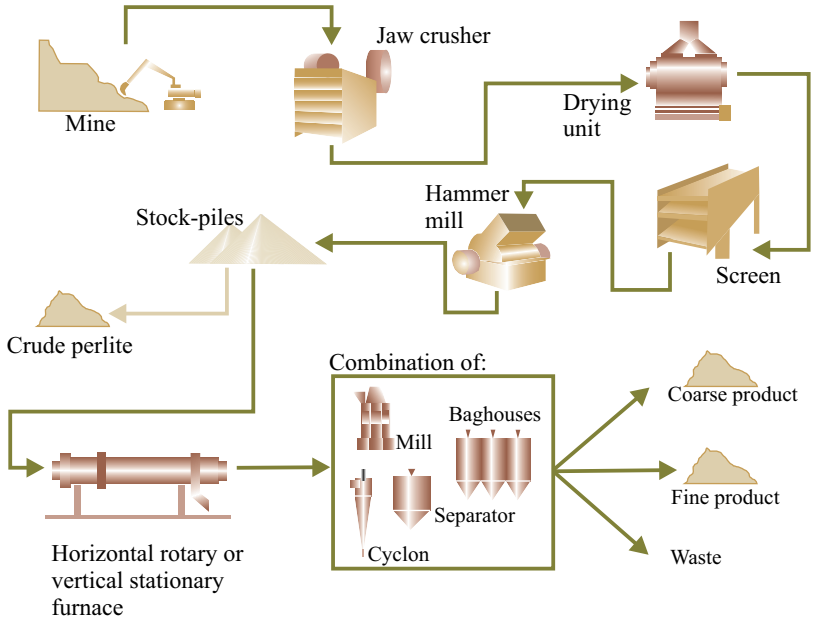

Figure 8.2: Simplified flowsheet for the processing of expanded perlite (Reproduced with permission from Imerys Minerals, Ltd.)

Depending on the market demands, a perlite processing plant can produce different kinds of perlite products, namely crude perlite or expanded. Crude perlite only undergoes particle size reduction, whereas expanded perlite is subject to calcination. The aimed

product determines the particle size range generated after crushing and the conditions required for calcination (Chang, 2002*b*). In the first sizing step, the ore is reduced to approximately 1.6 cm using jaw or roller crushers. After drying, the particle size is further reduced with vibratory screens, air classification and hammer or rod mills. Then, the ore is blended and stored in stockpiles upon specifications (Kadey, 1983). If the intended product is expanded perlite, calcination is undertaken in rotary or vertical furnaces. The calcination temperature varies between 480 to 1160 °C. A final particle size separation is carried on with a combination of cyclones, mills, separators and baghouses.

The flow diagram for the mining and processing of diatomite is presented in Figure 8.3. The most common method for the mining of diatomite is open-pit quarrying. Before mining, each stratum must be characterised to determine the options for further ore blending. Depending on the thickness of the diatomite layers, mining is performed using benches from 1.5 to 15 m. Likewise for the mining of perlite, due to the softness of the diatomite rocks the extraction of the material is done by ripping the mine face. If the climate is favourable, the ore is stockpiled and exposed for natural-solar drying aiming to reduce the moisture (Breese and Bodycomb, 2006).

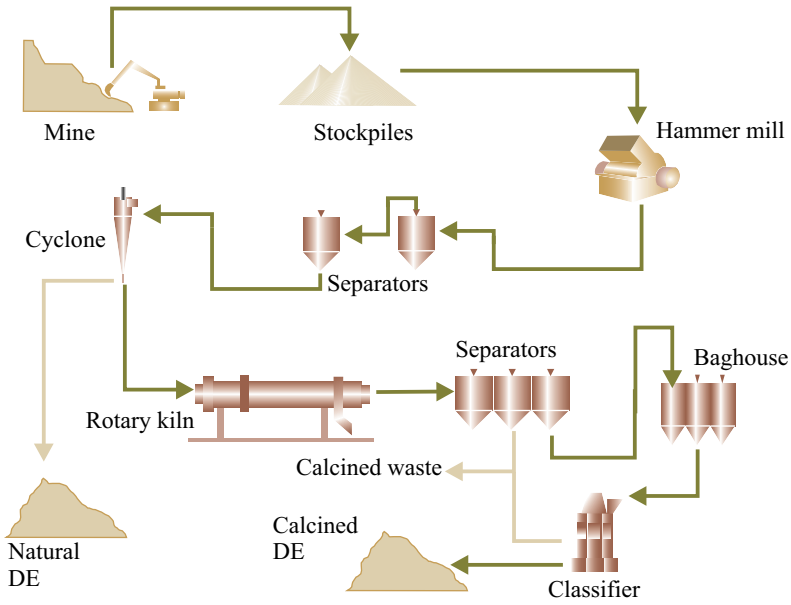

Figure 8.3: Simplified flowsheet for the processing of diatomite (Reproduced with permission from Imerys Minerals, Ltd.)

In the processing plant, the ore is lightly crushed using hammer mills to reduce the particle size to 1.3 cm. If the ore is not dry, it should undergo a further low-temperature moisture reduction. Then the particles are separated based on particle size. If the intended product is natural diatomaceous earth, the material can go at this point to storage. Else, the material is sent to the calciner. For some applications, a flux is added before calcination. The calcination occurs in a rotary kiln, with temperatures that range from

870 to 1100 °C. The (flux) calcined diatomaceous earth product is finally classified based on particle size and then stored.

8.4. USES

Perlite and diatomite are employed as filter-aids in the filtration of liquids. Their primary use is for cake filtration, where liquids are separated from solids by forcing the liquid through a porous medium, and the solids are trapped to form a filter cake (Mathur and Ravishankar, 2006). The main applications of expanded perlite and calcined diatomaceous earth are the industrial filtering of vegetable oil, fruit juice, beer and wine. They are also used for the filtration of solvents, industrial water, industrial waste, swimming pools and pharmaceuticals. Diatomite, in particular, is good for the absorption of acids, liquid fertilisers, alcohol and water (Kamatani, 1971).

For such applications, the critical requirements are high porosity –adjusted with the thermal treatment-, low density and absence of soluble impurities. The mineral filters should produce a clear filtrate, have a high-flow rate, and long cycle duration (Mathur and Ravishankar, 2006). The American Society of Testing Materials (ASTM) and the perlite institute established the standards for determination and specification of the properties of expanded perlite (Breese and Bodycomb, 2006). In general, the performance of diatomite is better than that of perlite, although perlite is less dense, which yields to additional filtering capacity. Perlite is preferred in rotary vacuum filters and filter-aid applications that require high flow-rates and where high clarity of the filtrate is not essential (Mathur and Ravishankar, 2006).

Some substitutes for perlite and diatomite as filter aids include sand, garnet, asbestos, cellulose and carbon, although they are only considered for niche applications (Breese and Bodycomb, 2006). Even though there are notorious advances in the development of synthetic membranes, they are not yet considered as a threat for the perlite and diatomite markets due to the high costs for their production (Crossley, 2000). Moreover, according to Mathur and Ravishankar (2006), since the mineral filter-aids are effective an economic, their demand in the market will persist.

REFERENCES

Barker, J. M. and Santini, K. (2006), Perlite, *in* J. E. Kogel, N. C. Trivedi, J. M. Barker and S. T. Krukowski, eds, 'Industrial Minerals and Rocks', 7th edn, Society for Mining, Metallurgy, and Exploration, pp. 685–702.

Barron, J. A. (1987), Diatomite: environmental and geologic factors affecting its distribution, *in* J. R. Hein, ed., 'Siliceous sedimentary rock-hosted ores and petroleum', Vol. 21 of *Evolution of ore fields*, Van Nostrand Reinhold Co, Chapter 7, pp. 164–178.

Breese, R. O. Y. and Bodycomb, F. M. (2006), Diatomite, *in* J. E. Kogel, N. C. Trivedi, J. M. Barker and S. T. Krukowski, eds, 'Industrial Minerals and Rocks', 7th edn, Society for Mining, Metallurgy, and Exploration, pp. 433–450.

Chang, L. (2002*a*), Diatomite, *in* S. L. Snavely, ed., 'Industrial mineralogy: materials, processes and uses', Prentice Hall, Chapter 10.

Chang, L. (2002*b*), Perlite and pumice, *in* S. L. Snavely, ed., 'Industrial mineralogy: materials, processes and uses', Prentice Hall, Chapter 28.

Crossley, P. (2000), 'Clarifying matters - World diatomite reviewed', *Industrial Minerals* **390**(March), pp. 119–141.

Hurley, J. P., Armstrong, D. E. , Kenoyer, G. J. and Bowser, C. J. (1985), 'Ground water as a silica source for diatom production in a precipitation-dominated lake', *Science* **227**(4694), pp. 1576–1578. DOI: 10.1126/science.227.4694.1576

Kadey, Jr. F. L. (1983), Perlite, *in* S. J. Lefond, ed., 'Industrial Minerals and Rocks', 5th edn, Society of mining engineers, AIME, pp. 997–1015.

Kamatani, A. (1971), 'Physical and chemical characteristics of biogenous silica', *Marine Biology* **8**(2), pp. 89–95. DOI: 10.1007/bf00350922

Mathers, S. J. and Scott, P. W. (2002), Models and domains: tools to help realize the industrial mineral potential of the developing world, *in* C. M. Scott, P. W. Bristow, ed., 'Industrial minerals and extractive industry geology', The Geological Society, pp. 205–220.

Mathur, S. and Ravishankar, S. A. (2006), Filters and process aids, *in* J. E. Kogel, N. C. Trivedi, J. M. Barker and S. T. Krukowski, eds, 'Industrial Minerals and Rocks', 7th edn, Society for Mining, Metallurgy, and Exploration, pp. 1337–1352.

Scott, P. W. (2011), The geological setting for industrial mineral resources, *in* G. E. Christidis, ed., 'Advances in the characterization of industrial minerals', Vol. 9 of *European Mineralogical Union notes in mineralogy*, Mineralogical Society of Great Britain and Ireland, Chapter 2, pp. 13–34. DOI: 10.1180/emu-notes.9.2

9

INFRARED DETECTION OF THE VARIABILITY IN PERLITE ORE THAT INFLUENCES THE QUALITY OF ITS CALCINED PRODUCTS

This chapter identifies the variability in the perlite ore that is related to the generation of fine particles and to the presence and concentration of heavy metals with a tool that can be used routinely in the pit.

Parts of this chapter have been published in:
Guatame-Garcia, A. and Buxton, M. (2017). Infrared Detection of Ore Variability that Influences the Environmental Risks During Perlite Mining and Processing. *Environmental Earth Sciences 76(21)*, 741. doi: 10.1007/s12665-017-7074-y.

During the mining of perlite deposits, the control the generation of fine particles and the concentration of metals is of outstanding importance to meet environmental and market requirements (e.g. chemical purity, emission of pollutants). Particle size and chemical purity are conventionally manipulated during the processing of the ore to achieve high product specifications. However, the current practices do not consider a proactive approach that focuses on the in-pit characterisation of the ore that could minimise the environmental impact and optimise the mining process since its early stages. This chapter presents a method for the in-pit detection of the variability in perlite ore that is related to the generation of fine particles and the elevated concentration of metals. Particle size and chemical purity showed to be dependent on the mineralogical variations of the ore, specifically opal and montmorillonite. Using a portable infrared spectrometer, an index that establishes the relative proportions of these minerals in the perlite ore was created. Such an index provided insight into the correlation between mineralogy, fine particles and concentration of metals. Consequently, the index could be used not only for mineralogical determination but also as a predictor of the presence of the main impurities in the perlite ore. These results can be implemented in perlite mining to reduce the generation of waste, and can influence the production of high-quality perlite products.

9.1. INTRODUCTION

Perlite is a versatile material with unique properties, and it is used in numerous industrial applications. In particular, the chemical inertness and expansion capabilities of perlite make it a preferred filter aid in the food, pharmaceutical and chemical industries (Shackley and Allen, 1992). Natural perlite is a form of hydrated volcanic glass emplaced in the top of high-silica rhyolite lava domes (Allen, 1988; Fink, 1983). In such an environment, the mineralogy and the chemistry of the ore body vary according to the geological features of the perlite deposit (Noh and Boles, 1989). Examples of such variations are those caused by hydrothermal alteration, as described by Clarke (1989) and Silberman and Berger (1985) . The particular characteristics of the deposit have a direct impact on the mining of perlite deposits, by affecting the generation of mine waste and the quality of commercial perlite products. Therefore, it is fundamental to understand and control the variability of the ore since the early stages of the mining activities.

The environmental regulations and the perlite market conditions define the quality parameters that mining companies must meet. Authorities such as the United States Environmental Protection Agency (USEPA, 1995) and the United States Pharmacopeial Convention (USPC, 2012) describe the fine particles generated during mineral processing and the content of metals in the ore as potential environmental risks and therefore are considered as cost penalties, which must be below certain thresholds. The fine particles are generally treated as nuisance dust; what is more, evidence provided by Elmes (1987) and Maxim et al. (2014) suggests that, in large amounts, these particles represent a component of air pollution and a potential health risk for workers. Regarding the chemical purity, even though perlite is deemed to be an inert material, it has been mentioned before that the chemical composition of the ore can still be altered by the particular geological features of the deposit, which might result in an enrichment of elements that ultimately contaminate the ore.

Due to the simplicity of the extraction and processing methods and the relative abun-

dance of chemically-pure perlite deposits, there has been limited systematic research into the opportunities for optimisation on the mining and processing of perlite. However, Bennett (2015) remarked that the increasing demand for perlite products, as well as the development of novel applications, might result in a depletion of reserves. Therefore, new challenges in the mining and processing of perlite ores are arising. Strategies that aim for early detection of potential environmental risks involved in perlite mining and processing are of considerable interest for the industry. To enable this, the identification of the contaminants, such as fine particles and metals, can be addressed from a mineralogical perspective, by analysing the composition of the ore and its different size fractions. This approach involves identification of the mineralogical content of the different size fractions of the perlite, and the determination of the metals–bearing mineral phases. Sensor technologies that allow on-site and real-time mineralogical characterisation of the ore would aid in the in-pit identification of perlite impurities, assisting the decision-making process during mineral extraction and processing.

The purpose of this study is to create a method for characterising perlite ores in-pit, with a focus on the determination of the likelihood of generating fine particles, and the assessment for the presence of chemical impurities. This chapter presents the characteristics of perlite samples from a mine in the Dikili area in west-Turkey regarding particle size analysis, chemistry and mineralogy. Infrared spectroscopy was used to create a mineralogical index that estimates the proportion of the mineral content in the ore, which can be used to determine the ore variability in relation to the environmental risks. The chapter also discusses the potential for implementing the results of this work in realistic in-pit conditions.

9.2. ZEYTINDAĞ PERLITE DEPOSITS

The Zeytindağ perlite deposits (Dikili – İzmir area, western Turkey) are associated with the Western Anatolian Miocene volcanism. In this area, the widespread magmatism related to the tectonic evolution produced a variety of plutonic and volcanic rocks. The volcanic associations range from dacite-rhyolite to basaltic andesites (Karacik et al., 2007). During the Late Miocene – Early Pliocene, a tectonic extensional regime favoured the extrusion of rhyolitic domes and basaltic trachyandesite lava dykes, which are structurally controlled along NE-SW trending fault systems (Figure 9.1). At the top of the rhyolitic domes, obsidian and perlite are common. In such an environment, the perlite formed as the result of the interaction between volcanic glass with hydrothermal fluids or with meteoric water percolated through the faults, which led to the hydration of the silica phase. As a consequence, there was formation of opal, in paragenesis with smectites, zeolites, quartz and feldspars (Allen, 1988; Fink, 1983; Noh and Boles, 1989). Depending on the alteration of the glass, different perlite facies range from classical, with characteristical onion skin texture that indicates low degree of alteration, to granular and finally pumiceous, as the highly altered facies (Barker and Santini, 2006).

The volcanic activity and active tectonics in the Dikili – İzmir area served as a suitable environment for the presence of metal enrichment in some areas of the Zeytindağ perlite deposits(Karacik et al., 2007; Yilmaz, 2002). This environment enabled the circulation of hydrothermal fluids through major faults and fracture zones that interacted with the

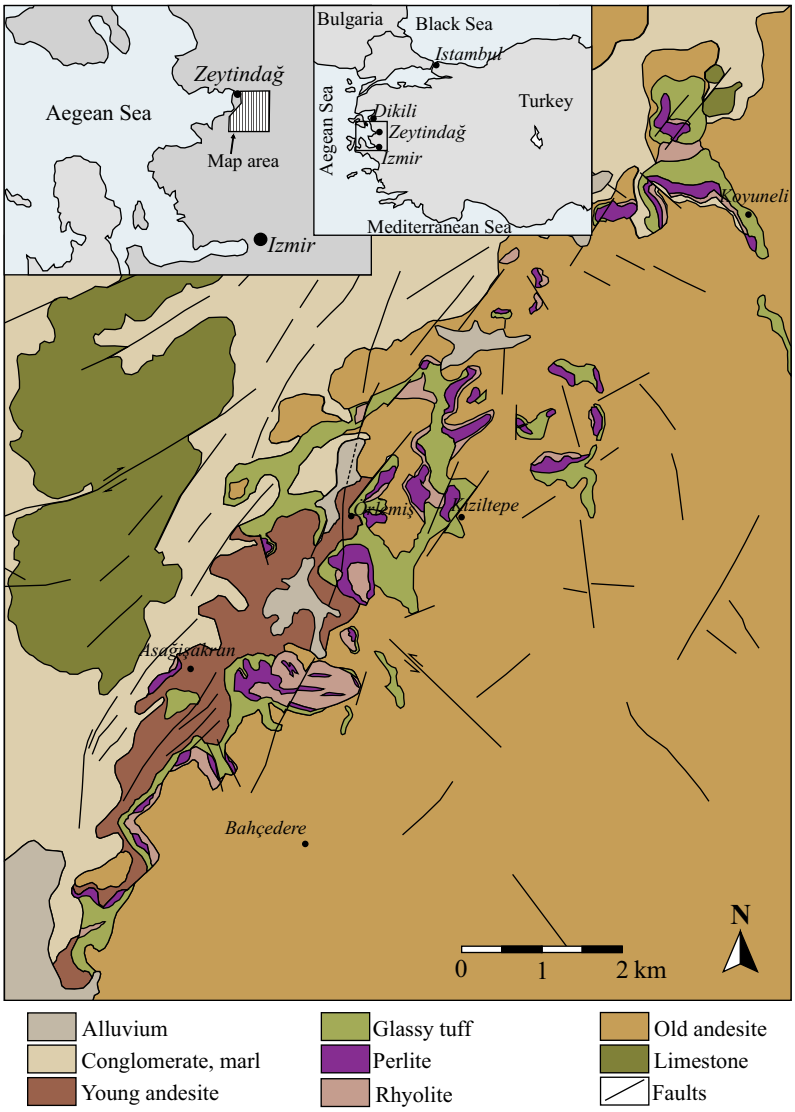

Figure 9.1: Distribution of the Zeytindağ perlite deposits in the Dikili – İzmir area (Reproduced after Özgenç (2012), with permission)

perlite, leading to the adsorption of metals at the glass surface (Baba and Sozbilir, 2012; Petit et al., 1990). One scenario that might have permitted such interaction was the process of perlitisation of the volcanic glass, where the alteration fluids could have carried metals. Another scenario was the presence of fluids at a stage posterior to the perlite formation, where the emplacement of younger epithermal mineralisation systems, such as those presented by Yilmaz (2002), cross-cut the perlite domes. These intrusions generated new hydrothermal pathways that altered the perlite bodies, creating outcrop-scale alteration halos, following the patterns described by Yanev (2008). In both scenarios, the attribution of elevated contents of metals is given to ascending hydrothermal fluids of magmatic origin and to the percolation of ground water that leached metals from the host rocks by oxidation of sulphides (Baba and Sozbilir, 2012). Such metals are those commonly present in epithermal environments, e.g. As, Fe, Zn, Pb, Cu, Nd, Co, Hg and Sb, which are usually associated with Mn, Ba, Rb and Ti (Clarke, 1989; Silberman and Berger, 1985).

9.3. ENVIRONMENTAL RISKS ASSOCIATED WITH PERLITE ORES

The type of perlite that is used as filter aid is the one known as classical perlite, which has a characteristic onion skin texture. The main applications of perlite filter aids include the filtration of liquids in the beverage, food and pharmaceutical industries. For these applications, filters containing perlite must not impart any colours or odours to the filtered media, or contain any contaminant that could be hazardous to human or animal health or the environment. To deem perlite products as safe for their intended use, they should meet the standards listed by the Food and Agriculture Organization of the United Nations (FAO, 2006), the Food Chemicals Codex (USPC, 2012), the Oenological Codex (OIV, 2017) and other market-specific purity acceptance criteria set by perlite customers. As previously mentioned, depending on the particularities of the geological setting, the perlite body can be exposed to potential contaminants that affect the chemical inertness, and therefore, the acceptability for the use of perlite filters.

Along with chemical inertness, the expansion capability is the most interesting property of perlite. The production of lightweight filter aids consist of open-pit mining, particle size reduction (comminution and sizing) and thermal expansion. In this last step, the ore is thermally treated at temperatures between 480 and 1160 °C, causing expansion up to twenty times the original particle size (Blunt, 1994; Shackley and Allen, 1992). Stein and Murdock (1955) pointed out that the success of the expansion process greatly depends upon the capacity of a processing plant to generate particles conforming to the specifications for size distribution, which normally varies between 50 µm and 5.00 mm. For this reason, comminution (crushing and milling) and sizing are the main steps before thermal expansion. However, since perlite is quite friable, the reduction of the particle size inevitably produces large quantities of dust and excessively fine material that, in most of the cases, are dumped as a waste (Ray et al., 2007).

By the end of the last century it was considered that the particles produced during perlite comminution could be treated as a nuisance dust since they do not contain quartz or fibrous minerals and dismissed them as a significant health risk (Cooper and Sargent, 1986; Elmes, 1987). However, more recent studies suggest that excess of exposure to perlite dust without the necessary protective equipment has an adverse effect on human health, and it is related in particular to respiratory diseases (Maisanaba et al., 2015; Maxim

et al., 2014; Sampatakakis et al., 2013). Furthermore, there is evidence that shows that particulate material generated during mineral processing of perlite is a matter of concern since it greatly contributes to air pollution in mining regions (Davidson et al., 2005).

The mining style for perlite and the facilities that are commonly available at the processing plants make difficult to monitor the potential environmental risks proactively. The laboratory facilities in the perlite processing plants are rather small and are not capable of performing detailed chemical or mineralogical analyses.

9.4. METHODS

9.4.1. SAMPLE COLLECTION

The samples for this study were collected from three different pits (named Pit 1, Pit 2 and Pit 3) in the Zeytindağ perlite deposit (the exact location of the pits cannot be disclosed due to commercial sensitivity). Even though classical and granular perlite are present in the deposit, only classical perlite is sold to the filtration market; therefore, only this perlite type was surveyed.

The samples used for particle size analysis come from Pits 1 and 2. The ore in these pits, which are currently active, is deemed uniform. The samples come from run-of-mine (ROM) stockpiles that normally serve as feed for the processing plant. At each pit, the ore was extracted along cross-sections using mobile ripping; the material was then transported to the processing plant where dumps from aleatory parts of the pit were combined and homogenised to form the stockpiles. Three random stockpiles were chosen per pit, from which 5 kg were collected with a shovel at the centre of the volume of every stockpile. This sample collection strategy, which combines random and clustering sampling, ensures the good representativity of the collected material. In the normal processing operations, the stockpiles are blended before crushing to homogenise the ore. For this study, the samples from every pit were treated separately to identify the ore variability between pits.

In Pit 3, enrichment of chemical impurities was expected due to a local rhyolitic intrusion. For this reason, Pit 3 is not exploited for commercial use, but can be used to study the impact of hydrothermal alteration in the ore, which is detrimental to the perlite quality. Therefore, this pit cannot be regarded as representative of the entire volume of the ore, but rather of undesired ore conditions. The samples were systematically collected in a radius of 10 meters from the vein in two opposite directions (north and south) in segments of 1 meter wide to assess the distribution of the elements of interest and the mineralogical variation of the perlite. The sample set included one additional sample from the rhyolite vein. Figure 9.2 shows the pit face used for sampling and the location of the samples. The material was collected from the surface of the pit face by ripping with peak and shovel. The naming of the samples corresponds to the location of the sample (north = N, south = S) and the distance from the vein.

9.4.2. MINERALOGY

The mineralogical content was estimated using infrared spectroscopy. The selection of the technique was due to its ability to detect amorphous phases of minerals, which provides an advantage for the detection of opaline silica, which is the major constituent

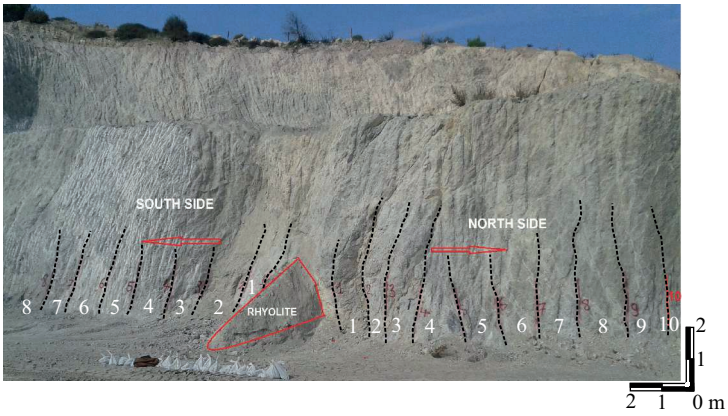

Figure 9.2: Mine face of Pit 3, including the sample's location

in perlite (Chester and Elderfield, 1968). Furthermore, the availability of infrared field devices facilitates an in-pit implementation of the results (Thompson et al., 1999). Spectra were first collected in the laboratory for spectral characterisation, and later new spectra were collected using a field portable device to assess the opportunities for on-site implementation. Data were collected first in the laboratory using Attenuated Total Reflectance (ATR) in the MWIR-LWIR range. The field set-up was tested on loose powder samples using bidirectional reflectance with the ASD FieldSpec spectrometer in the SWIR range (Section 2.2.3).

In the MWIR-LWIR range, opaline silica can be identified by the strong Si–O features at 10.00 µm, water absorptions at 6.13 µm and free-hydroxyl bands between 2.60 and 2.90 µm (Parke, 1974). Quartz and feldspars have absorptions in the between 9.50 and 13.00 µm (Moenke, 1974). Clay minerals have characteristic metal-hydroxyl bands around 10.00 and 12.00 µm and the free hydroxyls bands around 2.60 and 2.90 µm (Farmer, 1974). In the SWIR range, only minerals that bear metal-hydroxyl bonds are identifiable. In opaline silica (Si–OH) and clay minerals (Al–OH), this absorption is present around 2.22 µm. The molecular water has a characteristic absorption at 1.90 µm (Hunt, 1977).

9.4.3. PARTICLE SIZE

For particle size analysis, the samples from Pits 1 and 2 were sieved at ten different size fractions. Per every stockpile sample, 600 grammes were divided in a laboratory mechanical shaker during 15 minutes with a nest of sieves between 6.30 and 0.06 mm. The aperture of the mesh was selected based on the typical particle sizes produced during the perlite processing. The coarser size corresponds to the feed for the comminution, whereas particle gradations between 4.00 and 0.06 mm correspond to the size fractions generated for different applications. The finest particles (<0.06 mm) correspond to the dust fraction, which is dumped as a waste. These samples were named as Px-#, where x corresponds to the pit source (1 or 2), and # makes reference to the particle size.

9.4.4. CHEMICAL IMPURITIES

The chemical composition of the samples was determined using laboratory X-ray fluorescence. The measurements were collected using a Panalytical Axios Max WD-XRF spectrometer. The major elements were used to validate the mineralogical interpretation, whereas the criteria for selection of the elements regarded as chemical impurities were based on the standards mentioned in Section 9.3. Table 9.1 lists the chemical impurities as well as the accepted maximum concentration level established by the accepted authorities, which is taken as a reference level in this study (Imerys Minerals, Ltd., personal communication January 21, 2015). The characterisation of the chemical impurities was firstly done in the samples from Pit 3. Then those observations were used to analyse such impurities in the size fraction samples of Pits 1 and 2.

Table 9.1: Elements regarded as chemical impurities in perlite products and their respective accepted maximum concentration level as per established by authorities and perlite customers (Imerys Minerals, Ltd., personal communication)

Element	Threshold	Element	Threshold
As	1 to 12 ppm	**Nd**	20 ppm
Ba	Report	**Ni**	10 ppm
Cd	1 to 2 ppm	**Pb**	5 to 30 ppm
Co	1 ppm	**Rb**	Report
Cr	5 ppm	**Sb**	2 ppm
Cu	Report	**Se**	Report
F	150 ppm	**Ti**	Report
Fe	300 ppm	**Zn**	Report
Hg	0.1 to 1.0 ppm		

9.5. RESULTS AND DISCUSSION

9.5.1. MINERALOGICAL VARIABILITY OF THE PERLITE ORE

CHEMICAL AND MINERALOGICAL CHARACTERISATION USING LABORATORY INSTRUMENTS

The mineralogical variability of the perlite ore was determined using ATR spectroscopy. Figure 9.3 shows the spectra of representative samples for every pit in the MWIR and LWIR regions where the relevant features for mineral identification are present. The absorption at 10.00 µm was common to all samples. Thus, the preliminary mineral identification was based on other smaller yet detectable features. In general, the perlite samples were characterised as mineral mixtures containing mainly opal (feature at 12.5 µm) and montmorillonite (features from 2.6 to 3.0 and 9.0, 10.9 and 11.9 µm), and minor amount of quartz (feature at 14.3 µm) as main components. Minerals of the zeolite group, usually associated with perlite, were not detected. Complementary XRD analysis suggested the presence of small amounts of plagioclase and did not detect other clay minerals. The plagioclase was not detected in the ATR spectra since the dominant absorptions of opal and montmorillonite between 9.50 and 13.00 µm overlap its spectral features.

From the infrared spectra in Figure 9.3 it is evident that the abundance of the containing minerals in perlite ore varies among samples. For an unambiguous determination

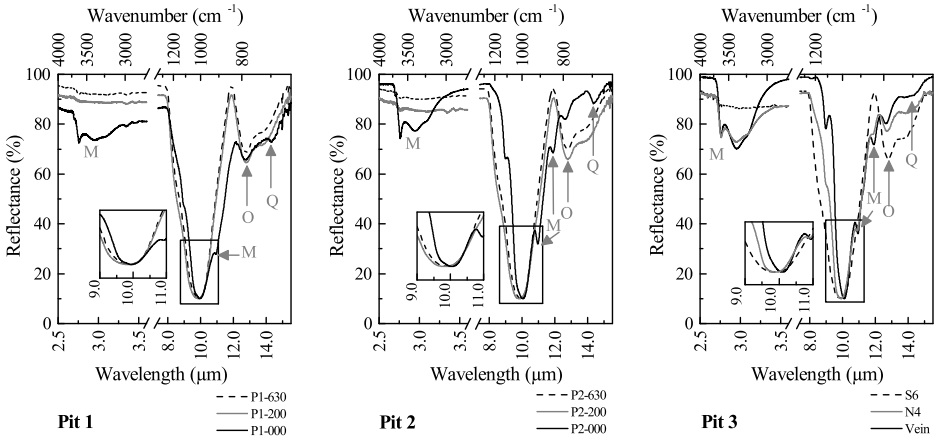

Figure 9.3: ATR (MWIR and LWIR) spectra of the perlite samples that represent the mineralogical variability of the ore. The identification of minerals is based on the absorptions at 2.6 to 3.0 µm, 9.0, 10.9 and 11.9 µm for montmorillonite (M), 12.5 µm for opal (O) and 14.3 µm for quartz (Q). The inset enlarges the shape and wavelength position differences in the 10.0 µm absorption

of the prevalence of one or the other mineral, it was necessary to establish spectral parameters that make a distinction of opal from montmorillonite. Figure 9.3 shows that the 10.0 µm absorption is narrower in the montmorillonite-like spectrum, and therefore it is expected that the overall area of the absorption band is smaller than the one in the opal-like spectrum. Moreover, the inset figure highlights an apparent shift in the wavelength position of the deepest point of the absorption. According to Milkey (1960), this shift is caused by changes in the Al:Si ratio, in a way that the deepest point of the band moves towards larger wavelengths as Al increases. In this context, it would imply an increment in the montmorillonite content.

Based on these observations, the spectral parameters for opal – montmorillonite differentiation were defined as the area and the wavelength of the minimum point of the 10.0 µm spectral feature. The parameters were computed using built-in functions in The Spectral Geologist software (CSIRO, 2007) in continuum removed spectra. The "area" parameter was calculated as the relative area of the absorption bounded by the maximum reflectance between 7.69 to 11.9 µm. The "wavelength of the minimum" parameter was calculated as the parabolic interpolation of the wavelength at the lowest point of the absorption in the same given range, using a fit of 7 channels. Table 9.2 presents the calculated values.

In order to confirm that the observed spectral changes were due to the presence of montmorillonite, the spectral parameters were compared with the major elements composition (Table 9.2). Statistical analyses of these data were computed using the Pearson's product-moment correlation coefficients to assess linear relationship between the spectral parameter and the major elements. The results indicated that Al_2O_3, MgO and CaO correlated strongly with the area parameter ($r_{Al} = -0.88$, $r_{Mg} = -0.92$ and $r_{Ca} = -0.87$); whereas the correlations with wavelength of minimum were smaller ($r_{Al} = 0.77$, $r_{Mg} = 0.75$ and $r_{Ca} = 0.73$), but the trend remained. Figure 9.4 shows the correlation

Table 9.2: Calculated spectral parameter values and major element chemistry (XRF) of the perlite samples

Sample ID	**Spectral parameters**		**Major elements composition**				
	Area	Wavelength*	Al_2O_3	CaO	MgO	Na_2O	SiO_2
		µm	wt%	wt%	wt%	wt%	wt%
P1-630	98.6	9.89	14.1	0.84	0.39	3.95	74.8
P1-400	101.35	9.88	12.4	0.91	0.24	3.20	77.0
P1-200	101.08	9.87	13.7	0.76	0.28	4.08	76.0
P1-118	102.01	9.91	13.1	0.75	0.25	4.02	76.7
P1-060	103.29	9.89	13.1	0.74	0.24	4.01	77.0
P1-043	98.22	9.94	13.1	0.72	0.25	3.95	76.6
P1-021	98.99	9.93	13.4	0.76	0.35	3.71	76.5
P1-013	96.48	9.95	14.5	0.91	0.46	3.55	74.3
P1-006	96.12	9.94	14.5	1.00	0.62	3.10	74.4
P1-000	94.47	9.94	15.4	1.37	1.38	1.77	74.4
P2-630	96.73	9.92	13.9	0.83	0.56	3.48	75.9
P2-400	98.39	9.93	13.8	0.85	0.62	3.34	76.2
P2-200	101.42	9.81	13.7	0.79	0.57	3.52	76.1
P2-118	98.19	9.85	13.4	0.83	0.53	3.49	76.7
P2-060	99.08	9.88	13.7	0.97	0.62	3.53	75.9
P2-043	97.08	9.92	13.8	0.84	0.62	3.77	75.7
P2-021	96.28	9.94	14.3	0.92	0.87	3.33	75.4
P2-013	90.33	10.01	16.5	1.25	1.54	2.89	72.3
P2-006	88.19	9.99	16.9	1.54	2.27	2.14	71.8
P2-000	79.22	10.05	19.4	2.32	3.79	0.76	70.1
S8	79.56	10.09	13.6	1.25	0.79	2.19	75.2
S7	97.37	9.86	13.5	1.17	0.79	2.28	75.9
S6	76.87	10.02	13.2	1.07	0.54	2.61	76.2
S5	76.67	9.99	14.3	1.29	1.44	1.91	74.9
S4	86.80	9.96	15.3	1.55	2.14	1.49	73.7
S3	90.82	9.89	14.3	1.22	1.34	1.95	75.1
S2	95.22	9.89	13.7	1.16	0.90	2.13	75.7
S1	104.78	9.81	15.6	1.50	2.22	1.59	73.6
Vein	101.33	9.89	16.0	5.27	2.41	0.43	63.5
N1	103.28	9.87	18.4	2.17	3.06	0.89	70.6
N2	94.56	9.86	19.1	2.59	3.42	0.72	70.1
N3	88.93	9.90	17.1	1.76	2.21	1.41	72.6
N4	90.60	9.90	15.6	1.70	2.17	1.41	73.4
N5	87.32	9.92	14.2	1.19	1.16	2.00	75.2
N6	85.22	9.90	13.6	1.03	0.71	2.46	76.0
N7	88.91	9.90	13.7	1.02	0.57	2.70	76.0
N8	99.73	9.91	13.6	1.02	0.53	2.74	76.3
N9	99.14	9.90	13.9	1.08	0.81	2.40	75.8
N10	93.24	9.90	13.6	0.99	0.56	2.67	76.2
Mean	94.25	9.91	14.6	1.28	1.10	2.60	74.6
SD	7.45	0.06	1.7	0.78	0.92	1.02	2.6
Min	76.64	9.81	12.4	0.72	0.24	0.43	63.5
Max	104.78	10.09	19.4	5.27	3.79	4.08	77.0
Error			0.1	0.03	0.02	0.05	0.1

*Wavelength of the minimum

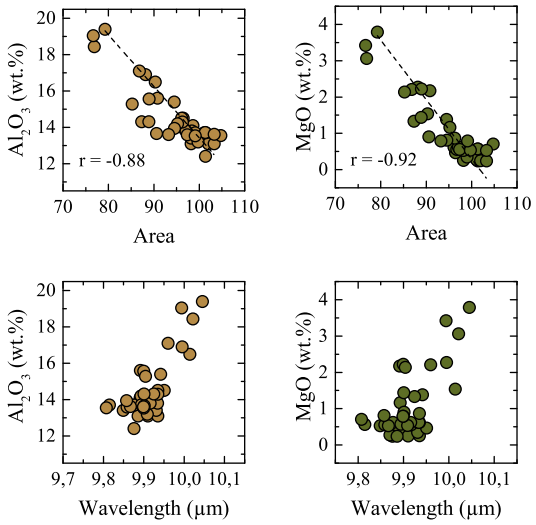

Figure 9.4: Correlation between spectral parameters and Al_2O_3 and MgO indicating that small area and long wavelength values indicate the presence of montmorillonite (Error bars smaller than plot symbol)

between the spectral parameters and Al_2O_3 and MgO; high concentrations of Al_2O_3 and MgO correspond to spectra with a relatively narrow area and long wavelength, thus confirming that these parameters indicate the presence of montmorillonite. As expected from the correlation coefficients, the area parameter explains better the relationship between spectral and mineralogical changes, whereas for the wavelength of minimum only the high values show a clear correlation pattern.

MINERALOGICAL CHARACTERISATION USING THE FIELD SPECTROMETER

Likewise in the MWIR and LWIR ranges, in the SWIR range, the main features of opal and montmorillonite are located at the same wavelength (Figure 9.5). However, significant differences in the shape of the spectra are due to the low crystallinity of the opal, and the way that both minerals host water in their structure. In order to establish a frame of end-members that define the differences in the spectral signatures of opal and montmorillonite, reference data from minerals deemed as spectrally pure were acquired from the USGS spectral library (Clark et al., 2007). Figure 9.5 displays the spectral differences of the reference opal and montmorillonite end-members. Three main absorptions at 1.40, 1.90 and 2.22 µm describe the variability of the spectra. The 1.40 µm feature is related to chemi-adsorbed water, which typically presents a deeper feature in montmorillonite than in opal, due to stronger bonding. The 2.22 µm absorption is related to hydroxyl-metal bonds, which are Si-OH for opal and Al-OH for montmorillonite; this variation in composition results in a spectral band wide and asymmetrical for opal, and a narrow and symmetric for montmorillonite. The absorption at 1.90 µm corresponds to molecular water (Hunt, 1977).

The combination of the spectral absorptions can be used to discriminate between the

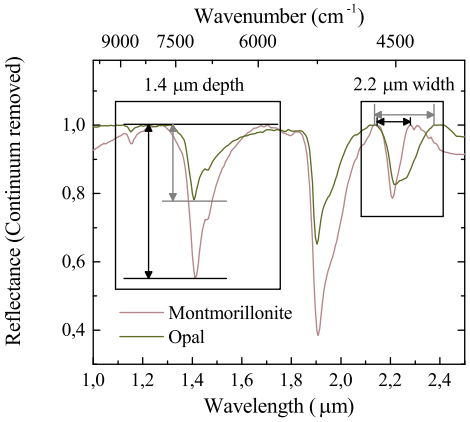

Figure 9.5: Reference SWIR spectra of opal and montmorillonite from the USGS spectral library (samples Opal TM8896 and Montmorillonite CM20). Variations in the absorptions at 1.40 and 2.22 µm permit to make a distinction between the two end-members

dominant mineralogy in the perlite ore. The narrowing of the 2.22 µm and the deepening of the 1.40 µm features indicate the enrichment from opal to montmorillonite. To visualise this transition, the Opal-Montmorillonite (OM) Index was defined, as follows:

$$\text{OM} \quad \text{Index} = 2.2w/1.4d \tag{9.1}$$

where $2.2w$ is the width at 2.22 µm, measured as the distance between the shoulders of the absorption, and $1.4d$ is the depth at 1.40 µm. These parameters were calculated using built-in functions in The Spectral Geologist software (CSIRO, 2007), with the reflectance spectrum in micrometres and continuum removed. Calculation of the OM index for the reference samples gave OM values of 0.97 for opal and 0.21 for montmorillonite.

The calculated OM index values for the perlite ore samples are presented in Table 9.3. Extreme OM values indicate the presence of almost pure end-members. Major element chemistry validated the robustness of the index. In Figure 9.6, the OM index is compared to the Al_2O_3 and MgO content, showing that in general there is an inverse correspondence between the spectral index and the Al and Mg enrichment, which confirms the presence of montmorillonite at low OM values.

In Pit 3, the changes in texture and colour of the pit face expose the rhyolite intrusion, as shown in Figure 9.2. However, it was difficult to assess the impact of the alteration in the surrounding ore without the use of more sophisticated techniques. In this case, the OM index aided in the characterisation of the mineralogical variation associated with the intrusion. As seen in Table 9.3, the lowest OM values are from the samples located in the vicinity of the vein, and they increase with increasing distance from the intrusion. The variations in the OM index mean that in the zone of intense hydrothermal influence, the ore is strongly altered to montmorillonite. With increasing distance from the intrusion, the perlite ore is gradually less disturbed, and therefore the mineralogy becomes dominated by opal. Even though these considerations might be self-evident in an epithermal alteration setting, on-site observations (i.e. colour or textural differences)

Table 9.3: Calculated OM index values for the particle size fractions samples (Pit 1 and 2) and for the the alteration profile samples (Pit 3)

Pits 1 and 2			Pit 3		
Sample ID	**Particle Size (mm)**	**OM Index**	**Sample ID**	**Distance (m)**	**OM Index**
P1-630	6.30	0.81	S8	-8	0.54
P1-400	4.00	0.85	S7	-7	0.79
P1-200	2.00	0.86	S6	-6	0.95
P1-118	1.18	0.86	S5	-5	0.61
P1-060	0.60	0.88	S4	-4	0.32
P1-043	0.43	0.81	S3	-3	0.62
P1-021	0.21	0.81	S2	-2	0.64
P1-013	0.13	0.76	S1	-1	0.44
P1-006	0.06	0.75	Vein	0	0.23
P1-000	<0.06	0.65	N1	1	0.23
P2-630	6.30	0.77	N2	2	0.25
P2-400	4.00	0.78	N3	3	0.33
P2-200	2.00	0.85	N4	4	0.5
P2-118	1.18	0.80	N5	5	0.65
P2-060	0.60	0.80	N6	6	0.82
P2-043	0.43	0.77	N7	7	0.71
P2-021	0.21	0.73	N8	8	0.74
P2-013	0.13	0.58	N9	9	0.69
P2-006	0.06	0.52	N10	10	0.69
P2-000	<0.06	0.46			
Mean		0.75	Mean		0.56
SD		0.12	SD		0.21
Min		0.45	Min		0.23
Max		0.88	Max		0.95

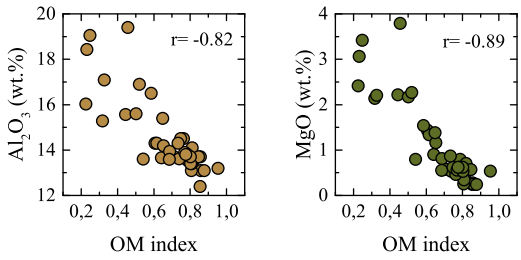

Figure 9.6: Correlation between the OM index and Al_2O_3 and MgO content that confirms the presence of montmorillonite at low OM values. (Error bars smaller than plot symbol)

only permit distinction of the area next to the rhyolitic vein. The detection of a gradual transition from the altered area to unaltered perlite ore can be only evident by means of more sophisticated techniques, even more in scenarios where the alteration is not uniform in all directions. In this context, the OM index is important since it enables the establishment of spatial trends and the dimensions of the altered zone, which are not visually apparent in the pit.

In Pits 1 and 2, the size fraction samples present the same mineralogical variability as the samples from Pit 3. The calculated OM index for Pits 1 and 2, presented in Table 9.3, reproduces the observations made previously for the MWIR and LWIR spectra (Figure 9.8). The OM values for Pit 1 vary between 0.65 and 0.88, reflecting a limited mineralogical variation in the samples, which is opal-dominant. In contrast, the OM values for Pit 2 fluctuate in a broader range indicating that the mineralogical variability includes both opal and montmorillonite dominance.

9.5.2. PARTICLE SIZE ANALYSIS

The cumulative and range particle size distribution (PSD) curves of Pits 1 and 2 are displayed in Figure 9.7. The cumulative PSD curves show in general a similar pattern for both pits, with a good representation of all the size fractions thus indicating a well-graded material. However, subtle yet relevant differences were detected, particularly in the small size fraction up to 0.60 mm. In this range, the volume of particles was larger in Pit 2 than in Pit 1, with the greatest contribution at the 0.21 mm mm fraction; this trend changed at 0.60 mm where Pit 1 produced a larger volume of particles than Pit 2, as the range PSD curve shows. The differences in small size fraction between the two pits are relevant for the determination of the source of fine particles, as is further discussed in Section 9.5.4.

Figure 9.3 makes evident the variation in mineralogy related to the particle size. The coarse and medium fractions (samples P1-630, P1-200, P2-630 and P2-200) have only spectral features characteristic of opal, whereas in the fine fraction (samples P1-000 and P2-000) the spectral absorptions of montmorillonite prevail. It is also noticeable that the variations in mineralogy differed in Pits 1 and 2, particularly for the fine fraction.

Based on those observations, Figure 9.8 shows a comparison of the spectral parameters, presented previously in Table 9.2, and the particle size fractions. In order to facilitate the interpretation, arbitrary thresholds were established to determine the dominance of opal, montmorillonite or a mixture. The thresholds were not only based on the spectral parameters but also on the secondary features and the correlation coefficients. There are remarkable differences between Pit 1 and 2. In general, Pit 1 presents less spectral variation than Pit 2, indicating a more homogeneous mineralogy. A closer inspection of the size fractions shows that in Pit 2, montmorillonite is dominant at the smaller particles, from >0.06 to 0.13 mm, whereas in Pit 1 this is the case only for the finest fraction. In contrast, indicators of opal dominance are more frequent in Pit 1, from 0.60 to 4.00 mm, whereas in Pit 2 opal is only clearly dominant at 2.00 mm.

An integrated analysis of the particle size distribution (Figure 9.7) and the mineralogical variations permit the understanding of their relationship. The perlite ore is essentially a mineral mixture of opal and montmorillonite. The grinding and sieving rapidly liberate the montmorillonite, which due to its physical properties turns into the main constituent of the small size fraction. Because of this, in the medium size fraction the montmorillonite

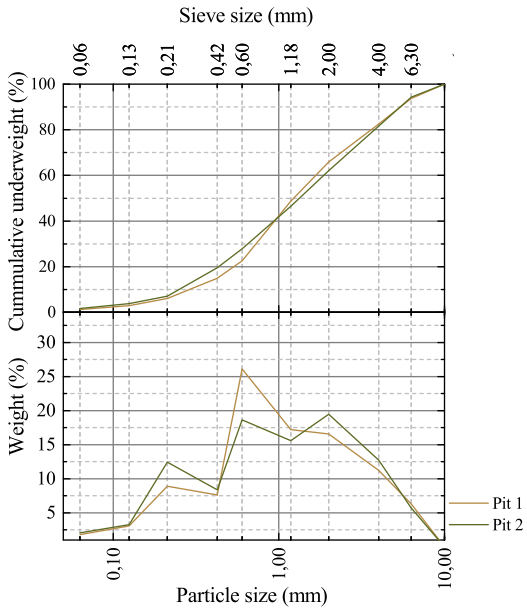

Figure 9.7: Particle size distribution curves of Pits 1 and 2: Cumulative distribution (**top**) and range distribution (**bottom**)

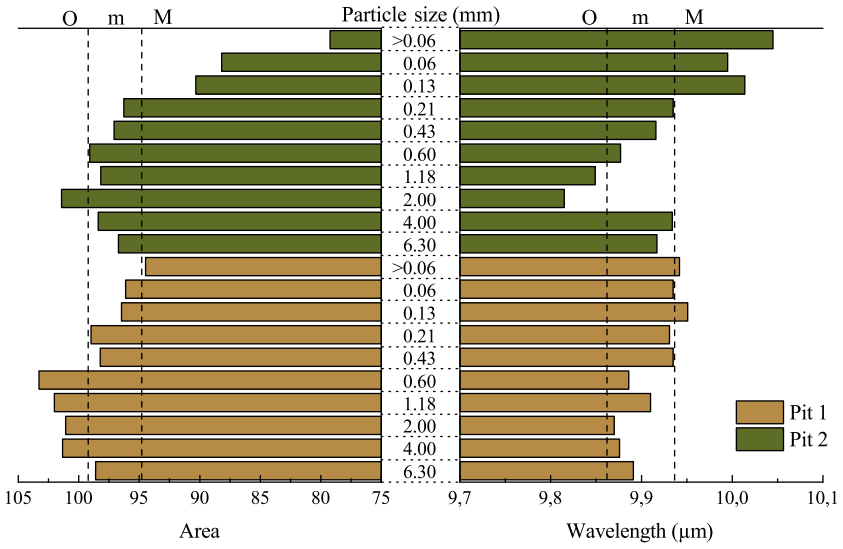

Figure 9.8: Comparison of spectral parameters and the particle size fractions. Broad area and short wavelength indicate that opal (O) is dominant, whereas narrow area and long wavelength indicate dominance in montmorillonite (M). Intermediate features are deemed as mixtures (m). The thresholds are arbitrary

content is minimised, and therefore the ore is richer in opal. As indicated by the mineral content of the coarsest size fractions, the raw ore of Pit 2 has more montmorillonite than that of Pit 1; therefore, it has a higher potential of producing small particles. Moreover, in Pit 2 remains of montmorillonite along the entire size distribution hinder the production of other size fractions consistently dominant in opal. In contrast, the reduced proportion of montmorillonite in the raw ore of Pit 1 limits the generation of large volumes of fine particles; Furthermore, it favours the production of particles with a nearly opal-dominant mineralogy in a broader size fraction range. These observations have direct implications for mineral processing and quality control, as it will be further discussed.

9.5.3. CHEMICAL IMPURITIES

The rhyolite intrusion in Pit 3 provided an interesting opportunity for the analysis of impurities in the perlite ore. The samples coming from this pit were expected to have a higher content of chemical impurities compared to the rest of the perlite deposit, and therefore they were used as a pilot test to assess their relationship with the ore. Table 9.4 provides the concentration of the chemical impurities detected by XRF. The interpretation of high or low concentration values of a given analyte was based on the standards reported in Table 9.1. It is apparent from Table 9.4 that the Fe concentration is remarkably high along the sample set; the Nd, Pb and Sb concentrations are slightly over the accepted threshold; As, Co and Hg are within the acceptance criteria, and Cr and Ni have very low levels. Moreover, from the overall list of chemical impurities Cd, F and Se are not reported. The concentration values are higher at the hydrothermal vein for most of the elements, except for As, Ba and Rb, for which the vein has the lowest concentration values, and for Cr, Hg and Pb, for which no striking values are noted.

A preliminary analysis using Pearson's product-moment correlation coefficients highlighted the expected elemental associations between As–Ba (r = 0.89), As–Rb (r = 0.93) and Ba–Rb (r = 0.89) on the one hand, and between Fe–Ti (r = 0.86), Fe–Zn (r = 0.94) and Ti–Zn (r = 0.77) on the other hand. Principal Component Analysis (PCA) was carried out to understand the nature of such associations in the perlite pit and to elucidate any other possible correlations. From the elements reported in Table 9.4, Co, Cr and Ni were excluded from the analysis due to the frequent presence of values below the XRF detection limit; the "vein" sample was also excluded since its extreme values represent an anomaly in the data set.

Figure 9.9a shows the loadings of the first and second principal components, while Figure 9.9b presents the geochemical transects of the elements with the higher loadings to support the PCA interpretation. PC1 depicts the correlations already described by the Pearson's correlation. Specifically, it establishes a negative correlation between the elements that have a higher concentration in proximity to the rhyolite vein (represented by negative loadings), from those which concentrations are lower at that location (represented by positive loadings). There are thus apparent opposite spatial trends for the concentration of As–Ba–Rb and Fe–Ti–Zn. Moreover, the geochemical transect shows that Fe–Ti–Zn are constrained to the central part of the system, whereas As–Ba–Rb have increased values in the peripheral areas. For the elements with positive loadings in PC2, the values at the vein are the highest; even though there are spiky values in the rest of the transect, as the Nd plot shows (Figure 9.9b), they lack any spatial trend and do not seem

Table 9.4: X-ray fluorescence (XRF) concentration of the chemical impurities in samples from Pit 3. The values of the rhyolitic vein samples are in bold. All the values initially reported as oxides were converted into ppm to facilitate comparison with the standards

Sample ID	Distance	As	Ba	Co	Cr	Cu	Fe	Hg	Nd	Ni	Pb	Rb	Sb	Ti	Zn
	m	ppm	ppm	ppm	ppm	ppm	ppm	ppm	ppm	ppm	ppm	ppm	ppm	ppm	ppm
Threshold*		1-12	Report	1	5	Report	300	0.1-1.0	20	10	5-30	Report	2	Report	Report
S8	−8.0	9	1350	<1	2	2	5204	0.05	23	<1	36	130	6	671	37
S7	−7.0	8	1338	1	2	1	5567	0.05	17	<1	35	123	4	665	34
S6	−6.0	9	1359	<1	<1	2	4581	0.04	25	<1	51	122	5	689	32
S5	−5.0	7	1236	<1	1	2	4973	0.03	21	<1	36	121	5	701	37
S4	−4.0	7	1116	2	1	2	6057	0.02	23	1	40	114	4	737	39
S3	−3.0	9	1242	1	1	2	4539	0.05	25	<1	36	121	5	671	35
S2	−2.0	9	1324	1	<1	2	4812	0.03	23	<1	58	124	4	677	34
S1	−1.0	7	1073	1	1	2	6169	0.14	25	<1	37	110	5	761	42
Vein	**0.0**	**2**	**757**	**3**	**1**	**4**	**11086**	**0.10**	**33**	**2**	**42**	**16**	**6**	**935**	**69**
N1	1.0	5	750	1	2	1	9009	0.06	20	1	42	77	5	899	47
N2	2.0	5	618	1	1	1	6819	0.03	21	1	44	60	6	953	41
N3	3.0	6	1004	1	2	3	6917	0.07	24	1	37	89	5	839	39
N4	4.0	7	1191	<1	1	2	5868	0.07	19	<1	36	109	5	743	37
N5	5.0	8	1266	1	1	2	5658	0.03	30	<1	40	125	6	773	41
N6	6.0	10	1336	2	3	1	5428	0.06	21	<1	37	124	6	671	36
N7	7.0	9	1339	1	<1	2	4903	0.06	24	<1	36	123	6	671	33
N8	8.0	8	1342	<1	2	2	4784	0.02	22	<1	35	121	5	647	32
N9	9.0	9	1355	1	<1	2	5050	0.05	27	<1	36	123	4	671	34
N10	10.0	9	1357	<1	<1	2	4707	0.03	21	<1	34	124	5	653	32
Mean		7.5	1176.5	1.3	1.5	1.9	5901.6	0.05	23.4	0.32	39.4	108.2	5.1	738.3	38.5
SD		1.95	233.92	0.63	0.65	0.7	1627.2	0.03	3.76	0.58	6.1	28.91	0.74	98.23	8.4
Min		2	618	<1	<1	1	4539	0.02	17	0	34	16	4	647	32
Max		10	1359	3	3	4	11086	0.14	33	2	58	130	6	953	69
Error		1	70	1	1	1	230	0.01	5	1	10	15	1	60	15

*Threshold values for chemical impuriries as specified in Table 9.1

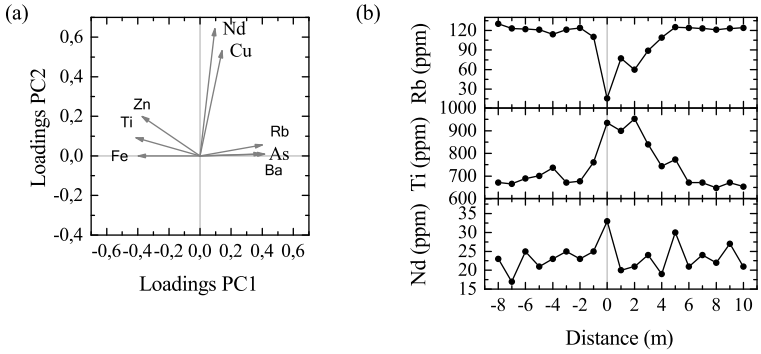

Figure 9.9: (**a**) Loadings of the first and second principal components of the chemical impurities in perlite at Pit 3 to establish correlations among elements; (**b**) Geochemical transects in relation to the position of the rhyolitic vein of the elements with meaningful correlations and higher PC1 and PC2 loadings

to have a correlation with a specific sample location. The spatial distribution of Hg, Pb and Sb does not seem to be related to the rhyolitic intrusion since neither striking values nor spatial trends are detected.

The alteration in Pit 3 involves displacement of Si, which leads to Al enrichment next to the intrusion with the subsequent formation of montmorillonite. Following the methodology used by Christidis (1998), the metals regarded as chemical impurities were compared with the Al_2O_3 content to assess the element mobility during the alteration caused by the hydrothermal intrusion. The sample regarded as opal-dominant according to the OM (Section 9.5.1) index was used as a reference for relative enrichment towards the Si phase. In Figure 9.10a, Ti has a linear relationship with the regression line passing through the origin, indicating that Ti is immobile and is enriched in the montmorillonite by residual behaviour. Zn and Fe also have a positive linear correlation (Figure 9.10 b-c), but the shift in the intersection of the regression line in respect of the origin means that the alteration fluid phase introduced these elements. In the Rb, Ba and As plots (Figure 9.10 d-f) the samples lie below the origin-to-opal line, and the regression line has a negative slope indicating leaching of these elements along with the Si phase, leading to their enrichment in the opal-dominant ore. Lack of patterns and scattering in the Nd and Cu plots (Figure 9.10 g and h) suggest that their mobility is not related to residual behaviour.

Table 9.5 presents the chemical impurities of the size fractions samples. There are a number of significant differences between the size fractions samples (Pits 1 and 2) and the hydrothermally influenced samples (Pit 3). First, As, Co, Hg and Sb are not reported for Pits 1 and 2; the values for these elements were very low already in Pit 3, and it is possible that they are not present, or their concentrations are below the XRF detection limit. Second, Cu and Nd are only present at certain size fractions. Interestingly, the reported levels of these two elements along with those of Cr and Ni are remarkably higher than in Pit 3.

The relationships in the chemical impurities for Pits 1 and 2 were analysed following the same PCA approach as for Pit 3; Cu and Nd were excluded from the analysis due to the

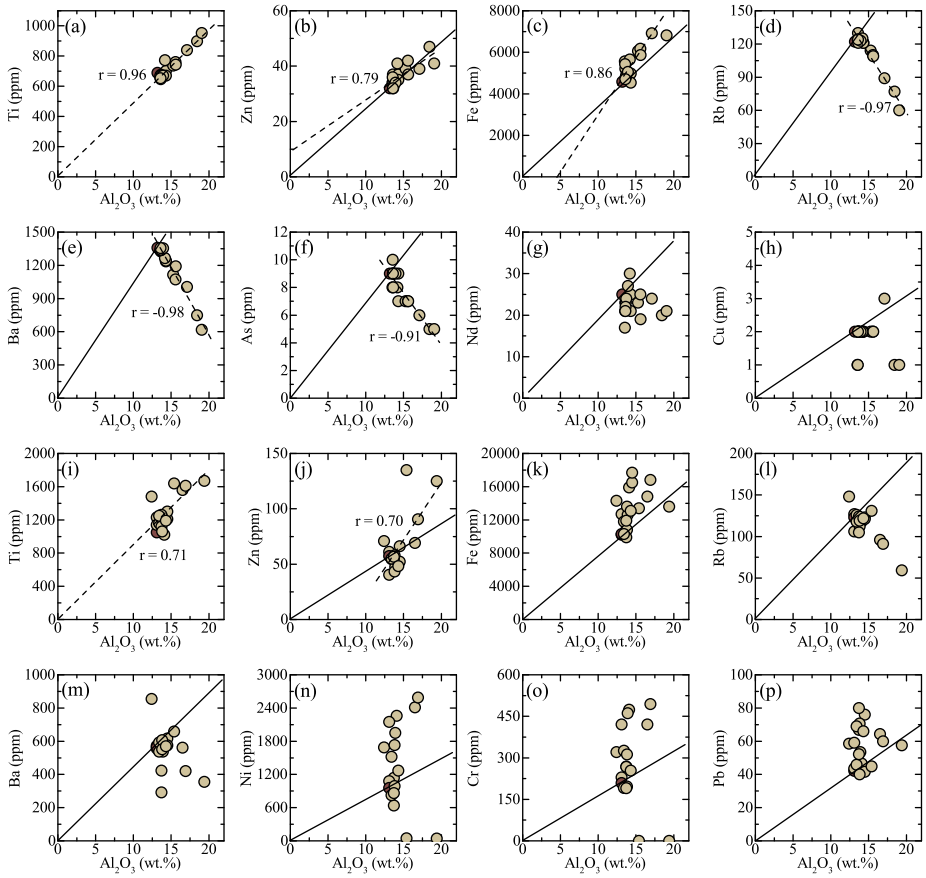

Figure 9.10: Projection of perlite's chemical impurities (ppm) over Al_2O_3 (wt%) to assess their relative mobility due to hydrothermal alteration in Pit 3 (**a** to **h**), and due to perlite formation or groundwater percolation in Pits 1 and 2 (**i** to **p**). The brown circle is the most opal-dominant sample according to the OM index, the full lines are the origin-to-opal as a reference for relative enrichement, and the dashed line is linear regression

Table 9.5: XRF concentration of chemical impurities in samples from the size fractions of samples from Pits 1 and 2

Sample ID	Particle size	As	Ba	Co	Cr	Cu	Fe	Hg	Nd	Ni	Pb	Rb	Sb	Ti	Zn
	mm	ppm	ppm	ppm	ppm	ppm	ppm	ppm	ppm	ppm	ppm	ppm	ppm	ppm	ppm
Threshold*		1-12	Report	1	5	Report	300	0.1-1.0	20	10	5-30	Report	2	Report	Report
P1-630	6.30	–	526	–	324	–	11121	–	–	1776	45	108	–	612	39
P1-400	4.00	–	766	–	220	–	10002	–	–	1328	57	135	–	887	57
P1-200	2.00	–	527	–	183	24	7554	–	–	896	65	112	–	743	45
P1-118	1.18	–	498	–	157	547	7134	–	183	849	58	116	–	737	49
P1-060	0.60	–	513	–	143	–	7204	–	–	753	41	112	–	629	46
P1-043	0.43	–	506	–	288	458	8883	–	–	1690	42	97	–	683	32
P1-021	0.21	–	531	–	223	–	8253	–	–	1194	45	115	–	695	44
P1-013	0.13	–	552	–	450	51	11541	–	111	2986	74	112	–	725	42
P1-006	0.06	–	516	–	430	–	12380	–	–	2790	40	111	–	779	53
P1-000	<0.06	–	590	–	–	–	9372	–	–	37	44	120	–	983	108
P2-630	6.30	–	481	–	315	38	8813	–	–	1532	52	109	–	731	38
P2-400	4.00	–	543	–	134	–	7554	–	–	778	69	102	–	719	47
P2-200	2.00	–	261	–	183	52	6924	–	–	504	78	96	–	755	44
P2-118	1.18	–	481	–	131	–	7204	–	–	647	67	108	–	749	44
P2-060	0.60	–	379	–	130	–	8323	–	–	678	51	113	–	671	46
P2-043	0.43	–	493	–	213	555	9512	–	–	1360	39	109	–	635	35
P2-021	0.21	–	510	–	174	38	9163	–	94	998	64	112	–	713	39
P2-013	0.13	–	503	–	288	26	10352	–	–	1894	63	88	–	935	56
P2-006	0.06	–	377	–	338	36	11750	–	–	2035	58	83	–	965	73
P2-000	<0.06	–	318	–	–	388	9512	–	–	34	56	54	–	1001	100
Mean		–	493.51	–	240.19	201.32	9127.6	–	129.46	1237.9	55.38	105.63	–	767.67	51.87
SD		–	104.11	–	100.23	230.86	1664.2	–	47.48	794.79	11.83	16.55	–	120.4	20.07
Min		–	261	–	130	24	6924	–	94	34	39	54	–	612	32
Max		–	766	–	450	555	12380	–	183	2986	78	135	–	1001	105
Absolute Error		–	68	–	38	16	230	–	29	15	21	27		60	18

*Threshold values for chemical impuriries as specified in Table 9.1

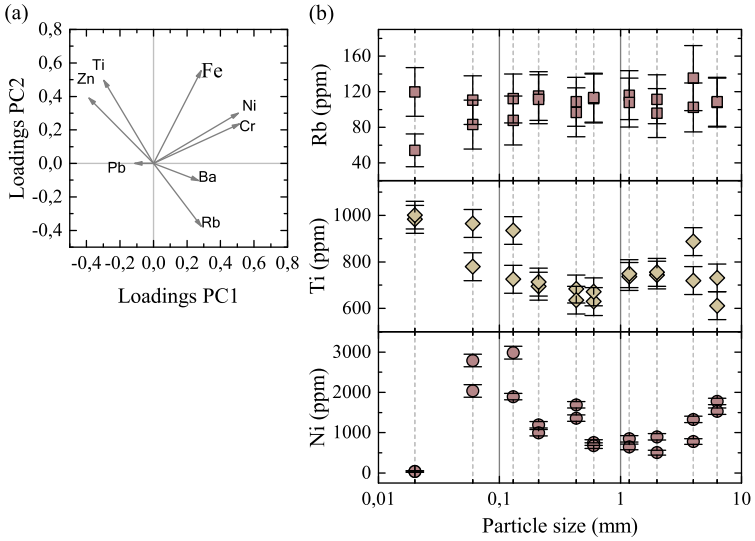

Figure 9.11: (**a**) Loadings of the first and second principal components of the chemical impurities in perlite at Pits 1 and 2 to establish correlations among elements and differences with Pit 3; (**b**) Variation in the concentration of Rb, Ti and Ni related to the size fraction. No apparent correlations are found

missing values. The loadings of PC1 and PC2, shown in Figure 9.11a, present similarities with the Pit 3 analysis regarding the correlations between Ti-Zn and Rb–Ba. For these four elements, the respective geochemical plots (Figure 9.10 i-j, l-m) suggest similar enrichment mechanisms to those in Pit 3, that is to say, in-situ enrichment of Ti and Zn is due to immobility in respect of Al, and Rb and Ba are leached along with Si. In this case, the alteration phase might be related to the perlite genesis, which leads to the formation of montmorillonite and opal, rather than a posterior process. However, all the elements analysed in Pits 1 and 2 (Figure 9.10 i-p) present more scattering that the geochemical plots of Pit 3; moreover, in the PCA plot it is notorious that Fe does not correlate anymore with Ti and Zn, but instead presents more similarities with Ni and Cr. The increased scattering in the geochemical plots might indicate a possible uptake of metals from an external source, given either by the alteration fluid responsible for the perlitisation or by percolation of groundwater that leached the metals from the surrounding rock units.

A comparison between the chemical impurities and the particle size permitted a first assessment of their relationship. Figure 9.11b displays plots for Rb, Ti and Ni, which represent the most extreme PC loadings and ease the comparability with the results from Pit 3, against the size particle. The elevated concentrations of Ti and Ni seem to be associated with the fine particles, except for the smallest size fraction where Ni is at its lowest. For this element, the rest of the particles show a gradual change from high to low concentrations in the middle size fraction, and again towards relatively high levels in the coarsest particles. However, it is not possible to establish a clear relationship between the variations of the chemical impurities and the size fractions. A probable reason for this is that the analysis ignores the fact that particles of the same size fraction might have

different mineralogy, depending on the source of the ore, as indicated in Section 9.5.2. Therefore, for explaining the variations in the chemical impurities, it is more appropriate to consider mineralogical variables, as presented in Section 9.5.4.

9.5.4. ORE VARIABILITY AS DETECTOR OF ENVIRONMENTAL RISKS

The particle size analysis indicated that the mineralogical content of the perlite ore could play a major role as a controlling factor for some of the properties of perlite. Additionally, the presence of hydrothermal alteration in Pit 3 suggests that changes in the ore mineralogy and the variations in the presence of chemical impurities might be related. Therefore, the OM index calculated in Section 9.5.1 was used to check the validity of those observations.

Integration of the OM index and XRF data suggested a possible correlation between the mineralogical variations in the perlite ore and the chemical impurities. The integration approach included only the PCA results from Pit 3. Figure 9.12a displays the scores and loadings of the PC1 and PC2; every point represents a sample, and the colouring corresponds to the respective OM index value. The plot presents the likelihood of a montmorillonite- or opal-dominant phase to have elevated concentrations of chemical impurities. The scores in PC1 describe well the variations in mineralogy, where negative scores represent the montmorillonite-dominant samples, and opal-dominant samples are those with positive scores. From the PC loadings, previously described in Figure 9.9a, it can be seen that the elevated Fe-Ti-Zn concentrations correspond to the montmorillonite-dominant samples, whereas the high As–Ba–Rb are characteristic of the opal-dominant ones. The high Cu and Nd values, explained by the PC2 loadings, confirm not to have a clear correlation to the dominant mineralogy.

As mentioned before, the distribution of the alteration is not uniform; therefore, the intrusion per se does not fully explain the variations in the concentration of a particular element. Other factors such as the composition of the parental rock, the perlitisation process or percolation of groundwater should also be considered. This was beyond the scope of the present study. In any case, the mechanisms of enrichment are constant for some elements, which appear frequently related to a particular mineral phase. Based on these observations, a mineralogical-based approach could be used to estimate the concentration of the target elements in similar samples.

Section 9.5.3 showed that the differences in element concentration are not strictly related to the variations in particle size. The mineralogical analysis revealed that the mineral composition of a particular fraction size is not the same in the two pits. The PCA results for chemical impurities and the OM index of the size fraction samples were integrated taking those observations into account. The PCA scores and loadings of PC1 and PC2 are shown in Figure 9.12b. The spreading of the data points, coloured according to their respective OM values, shows a separation between the montmorillonite- and opal-dominant mineralogy. With comparable results as those for Pit 3, the loadings of the chemical impurities indicate that the montmorillonite-dominant samples have higher Ti and Zn concentrations, and the opal-dominant ones have a higher amount of Ba and Rb. The Cr, Fe and Ni loadings lie perpendicular to the direction of the mineralogical variation. Therefore, they cannot relate with certainty to a mineral phase.

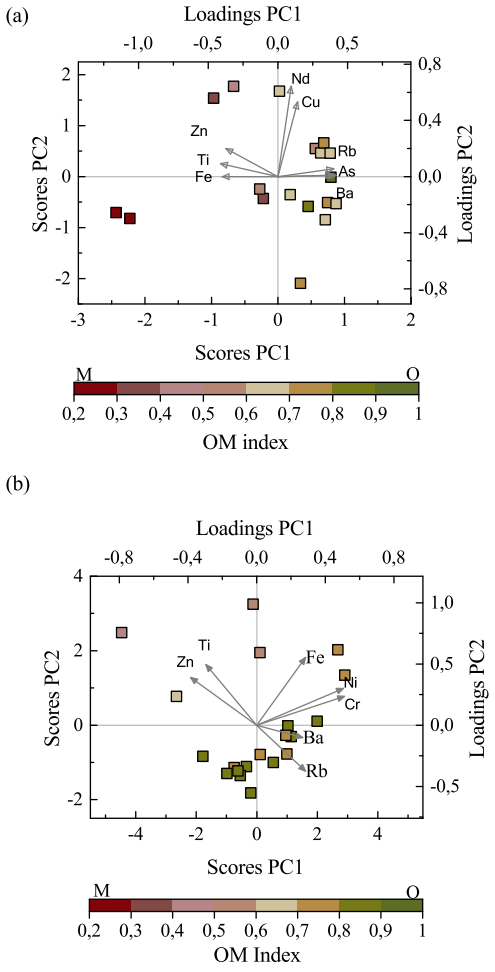

Figure 9.12: (**a**) Pit 3 integration of the OM index with the variability of chemical impurities as analysed with PCA (scores and loadings of the PC1 and PC2). The PC1 scores are related to the variations in mineralogy, whereas the loadings indicate the likelihood of elevated concentrations of the chemical impurities. Pb, Hg and Sb not shown for readability; (**b**) Pits 1 and 2 integration of the OM index with the variability of chemical impurities as analysed with PCA (scores and loadings of the PC1 and PC2). The loadings indicate the likelihood of elevated concentrations of the chemical impurities. Pb not shown for readability

9.5.5. OPPORTUNITIES FOR IMPLEMENTATION OF INFRARED SENSORS AS A TOOL FOR THE DETECTION OF THE VARIABILITY IN PERLITE ORE

Throughout the analyses, several differences were detected between Pits 1 and 2. Even though it was anticipated that the main factor affecting the quality of the perlite ore was the presence of intrusions from a felsic epithermal system, the elevated concentration of Fe, Ni, and Cr, especially in Pit 1, indicated an additional source of contaminants. Such a source is likely to be related to the andesitic rocks that preceded the formation of the perlite deposit (Figure 9.1). Moreover, the reduced content of montmorillonite in Pit 1 indicated that locally the influence of the felsic hydrothermal intrusions was limited, which resulted in a lower content of the associated chemical impurities. In the absence of evident in-pit features, such as fractures or changes in colour and texture of the ore, it is difficult to determine the extent of the influence of the identified sources of contaminants in different areas of the perlite deposit.

In such geological context, the characterisation of the perlite ore using the OM index can be used as a tool to determine the mineralogical composition of the ore, enabling to focus further analysis in the more likely contaminants. The determination of the dominant mineralogy in the perlite ore can be used to estimate the presence of chemical impurities and the expected proportion of fine particles generated during mineral processing. Perlite ores with low OM index can be regarded as influenced mainly by the hydrothermal intrusions, and thus they will be possibly enriched in elements characteristic of felsic epithermal systems; such ores will also produce a larger amount of fine particles due to the increased clay minerals content. In contrast, perlite ores with high OM index will indicate no secondary alteration, with a consequent homogeneous and opal-dominant mineralogy, which during mineral processing will generate a smaller volume of fine particles. In these ores, the type of chemical impurities would be related only to the genesis of the deposit.

These observations provide a framework for the in-pit characterisation of perlite ores, by offering parameters for monitoring and control during the mining and processing activities. As a result, a sensor-based in-pit or online approach using of SWIR spectroscopy as a mineral identification technique could be practically implemented. Portable SWIR devices permit the retrieval of data on-site and in real time. Even though the samples used for this study were measured as pressed powders, the results are still valid for on-site point measurements. On the one hand, the segment of the spectra used in the analysis is not influenced by environmental conditions. On the other hand, on-site measurements have the ease of collecting several data points in the form of grids or transects to provide a complete overview of the mine face, becoming even more meaningful than the powder samples.

The OM index should be interpreted and used taking into account the overall description of the mine face and the pit. The calculation of the OM index gives a quick estimation of the dominant mineralogy based on spectral data. Its implementation could influence decision making prior to mining, aiming to minimise the associated environmental risks by identification and preferential extraction of low-montmorillonite ores. Moreover, it could assist in the creation of a smart processing program to maximise resource extraction efficiency, optimise the use of the exploited ore and reduce the generation of waste. That would ensure the production of safe perlite products and a reduction in the environmental

impact and the health risks associated with the perlite mining and processing.

9.6. CONCLUSIONS

This study has presented a method for the in-pit characterisation the ore variability of perlite in order to predict factors that are deemed as environmental risks in mining and processing. Based on the results, the mineralogical variations in the ore were found to be a major controlling factor in the presence of an epithermal system. The mineralogical analysis based on infrared (SWIR, MWIR and LWIR) spectroscopy, identified opal and montmorillonite as the major constituents in the ore. By establishing the relative proportion of one or the other in the crude ore, it was possible to predict the generation of fine particles and to estimate the concentration of chemical impurities.

The results of particle size analysis and mineralogy showed that perlite ores with an opal-dominant composition produced particles mainly in a preferred size fraction, leading to a smaller volume of fine particles. In contrast, ores composed of a mixture of opal and montmorillonite produced particles distributed more homogeneously along the entire size fraction range. As a consequence, the amount of fine particles was greater than in the opal-dominant ore. With regard to the presence of chemical impurities, montmorillonite-dominant ores hosted an elevated concentration of elements characteristic of felsic epithermal systems, whereas the impurities in opal-dominant ores seem to be related to elements from rocks of mafic composition.

The development of the Opal-Montmorillonite (OM) index assisted in the determination of the dominant mineralogy in the ore. This index makes use of infrared spectral data in the SWIR range to indicate whether a perlite sample is opal-dominant or montmorillonite-dominant. Based on this estimation, it could be assessed if the ore is prone to the generation of large volumes of fine particles and the type of chemical impurities likely to be present. This result could be implemented during mining and processing of perlite ores. With the widespread commercial availability of portable infrared devices, in-pit mineralogical characterisation of the ore could be readily and routinely achieved. This could be utilised for selective mining and as a mechanism for monitoring and control of the process. This approach would have a positive impact on reduction of generation of waste and the production of safe perlite products.

REFERENCES

Allen, R. L. (1988), 'False pyroclastic textures in altered silicic lavas, with implications for volcanic-associated mineralization', *Economic Geology* **83**(7), pp. 1424–1446. DOI: 10.2113/gsecongeo.83.7.1424

Baba, A. and Sozbilir, H. (2012), 'Source of arsenic based on geological and hydrogeochemical properties of geothermal systems in Western Turkey', *Chemical Geology* **334**, pp. 364–377. DOI: 10.1016/j.chemgeo.2012.06.006

Barker, J. M. and Santini, K. (2006), Perlite, *in* J. E. Kogel, N. C. Trivedi, J. M. Barker and S. T. Krukowski, eds, 'Industrial Minerals and Rocks', 7th edn, Society for Mining, Metallurgy, and Exploration, pp. 685–702.

Bennett, S. M. (2015), Perlite, *in* '2013 Minerals yearbook', USGS, pp. 55.1–55.5.
URL: *https://minerals.usgs.gov/minerals/pubs/commodity/perlite/myb1-2013-perli.pdf [Accessed January 2019]*

Blunt, W. G. (1994), Characteristics of perlite filter aids, *in* 'Industrial Minerals '94: Sixth Canadian Conference on Markets for Industrial Minerals', Canadian conference on markets for industrial minerals, Blendon Information Services, Willowdale, Ont.

Chester, R. and Elderfield, H. (1968), 'The infrared determination of opal in siliceous deep-sea sediments', *Geochimica et Cosmochimica Acta* **32**(10), pp. 1128–1140. DOI: 10.1016/0016-7037(68)90113-0

Christidis, G. E. (1998), 'Comparative study of the mobility of major and trace elements during alteration of an andesite and a rhyolite to bentonite, in the islands of Milos and Kimolos, Aegean, Greece', *Clays and Clay Minerals* **46**(4), pp. 379–399. DOI: 10.1346/CCMN.1998.0460403

Clark, R. N., Swayze, G. A. , Wise, R. , Livo, K. E. , Hoefen, T. M. , Kokaly, R. F. and Sutley, S. J. (2007), 'USGS Digital Spectral Library splib06a'.
URL: *http://speclab.cr.usgs.gov/spectral.lib06/ds231/datatable.html [Accessed 2016]*

Clarke, Donald S. (1989), The trace element geochemistry of vein material in epithermal systems: significance for exploration, *in* '11th New Zealand Geothermal Workshop', University of Auckland, pp. 139–142.

Cooper, W. C. and Sargent, E. N. (1986), 'Study of chest radiographs and pulmonary ventilatory function in perlite workers', *Journal of Occupational and Environmental Medicine* **28**(3), pp. 199–206.

CSIRO (2007), 'The Spectral Geologist software suite'.
URL: *http://www.thespectralgeologist.com/ [Accessed 2016]*

Davidson, C. I., Phalen, R. F. and Solomon, P. A. (2005), 'Airborne particulate matter and human health: A review', *Aerosol Science and Technology* **39**(8), pp. 737–749. DOI: 10.1080/02786820500191348

Elmes, P. C. (1987), 'Perlite and other 'nuisance' dusts', *Journal of the Royal Society of Medicine* **80**(7), pp. 403–404. DOI: 10.1177/014107688708000703

FAO (2006), Inorganic components, *in* 'Combined compendium of food additive specifications', Vol. 4 of *Analytical methods, test procedures and laboratory solutions used by and referenced in the food additive specifications*, Food and Agriculture Organization of the United Nations, Rome, pp. 51–75.
URL: *http://www.fao.org/3/a-a0691e.pdf [Accessed June 2017]*

Farmer, V. C. (1974), The layer silicates, *in* V. C. Farmer, ed., 'The Infrared Spectra of Minerals', Vol. Monograph 4, Mineralogical Society, book section 15, pp. 331–364.

Fink, J. H. (1983), 'Structure and emplacement of a rhyolitic obsidian flow: Little Glass Mountain, Medicine Lake Highland, northern California', *Geological Society of America Bulletin* **94**(3), pp. 362–380. DOI: 10.1130/0016-7606(1983)94<362:saeoar>2.0.co;2

Hunt, G. R. (1977), 'Spectral signatures of particulate minerals in the visible and near infrared', *Geophysics* **42**, pp. 501–513. DOI: 10.1190/1.1440721

Karacik, Z., Yilmaz, Y. and Pearce, J. (2007), 'The Dikili-Candarli volcanics, Western Turkey: Magmatic interactions as recorded by petrographic and geochemical features', *Turkish Journal of Earth Sciences* **16**, pp. 493–522.

Maisanaba, S., Pichardo, S. , Puerto, M. , Gutiérrez-Praena, D. , Cameán, A. M. and Jos, A. (2015), 'Toxicological evaluation of clay minerals and derived nanocomposites: A review', *Environmental Research* **138**, pp. 233–254. DOI: 10.1016/j.envres.2014.12.024

Maxim, L. D., Niebo, R. and McConnell, E. E. (2014), 'Perlite toxicology and epidemiology - A review', *Inhalation Toxicology* **26**(5), pp. 259–270. DOI: 10.3109/08958378.2014.881940

Milkey, R. G. (1960), 'Infrared spectra of some tectosilicates', *American Mineralogist* **45**(9-10), pp. 990–1007.

Moenke, H. H. W. (1974), Silica, the three-dimensional silicates, borosilicates and beryllium silicates, *in* V. C. Farmer, ed., 'The Infrared Spectra of Minerals', Vol. Monograph 4, Mineralogical Society, book section 16, pp. 365–382.

Noh, J. H. and Boles, J. R. (1989), 'Diagenetic alteration of perlite in the Guryongpo area, Republic of Korea', *Clays & Clay Minerals* **37**(1), pp. 47–58. DOI: 10.1346/Ccmn.1989.0370106

OIV (2017), Products used in œenology – Sheet E-COEI-1-PERLIT, *in* 'International Œnological Codex', International Organization of Vine and Wine, pp. 427–429.
URL: *http://www.oiv.int/public/medias/5121/codex-2017-en.pdf [Accessed June 2017]*

Özgenç, Ismet (2012), 'Geologic map of the Zeytindag (Dikili – Izmir) perlite deposits', Dokuz Eylül University, Faculty of Engineering, Department of Geology.

Parke, S. (1974), Glasses, *in* V. C. Farmer, ed., 'The Infrared Spectra of Minerals', Vol. Monograph 4, Mineralogical Society, book section 21, pp. 513–583.

Petit, J. C., Dellamea, G. , Dran, J. C. , Magonthier, M. C. , Mando, P. A. and Paccagnella, A. (1990), 'Hydrated-layer formation during dissolution of complex silicate-glasses and minerals', *Geochimica Et Cosmochimica Acta* **54**(7), pp. 1941–1955. DOI: 10.1016/0016-7037(90)90263-K

Ray, A., Sriravindrarajah, R. , Guerbois, J. P. , Thomas, P. S. , Border, S. , Ray, H. N. , Haggman, J. and Joyce, P. (2007), 'Evaluation of waste perlite fines in the production of construction materials', *Journal of Thermal Analysis and Calorimetry* **88**(1), pp. 279–283. DOI: 10.1007/s10973-006-8107-z

Sampatakakis, S., Linos, A. , Papadimitriou, E. , Petralias, A. , Dalma, A. , Papasaranti, E. S. , Christoforidou, E. and Stoltidis, M. (2013), 'Respiratory disease related mortality and morbidity on an island of Greece exposed to perlite and bentonite mining dust', *International Journal of Environmental Research and Public Health* **10**(10), pp. 4982–4995. DOI: 10.3390/ijerph10104982

Shackley, D. and Allen, M. J. (1992), 'Perlite and the perlite industry', *Minerals Industry International* **1008**, pp. 13–22.

Silberman, M. L. and Berger, B. R. (1985), Relationship of trace-element patterns to alteration and morphology in epithermal precious-metal deposits, *in* B. R. Berger and P. M. Bethke, eds, 'Geology and Geochemistry of Epithermal Systems', Vol. 2 of *Reviews in Economic Geology*, Society of Economic Geologist, El Paso, USA, book section 9, pp. 203–232.

Stein, H. A. and Murdock, J. B. (1955), 'The processing of perlite', *California Journal of Mines and Geology* **51**(2), pp. 105–116.

Thompson, A. J. B., Hauff, P. L. and Robitaille, A. J. (1999), 'Alteration mapping in exploration: Application of short-wave infrared (SWIR)spectroscopy', *SEG Newsletter* **1**(39), pp. 15–27.

USEPA (1995), Mineral products industry, *in* 'Compilation of Air Pollutant Emissions Factors (AP-42)', 5th edn, Vol. 1, United States Environmental Protection Agency, pp. 11.30.1–11.30.5.
URL: *https://www3.epa.gov/ttnchie1/ap42/ch11/ [Accessed November 2016]*

USPC (2012), Food Chemicals Codex, *in* 'FCC 8', 8th edn, The United States Pharmacopeial Convention, pp. 861–862.
URL: *http://app.knovel.com/hotlink/toc/id:kpFCCE001Q/food-chemicals-codex/food-chemicals-codex [Accessed October 2015]*

Yanev, Y. (2008), Geology of the Eastern Rhodopes perlite deposits (Bulgaria): a review, *in* '6th International Conference and Exhibition on Perlite', pp. 177–195.

Yilmaz, H. (2002), 'Ovacik gold deposit: An example of quartz-adularia-type gold mineralization in Turkey', *Economic Geology and the Bulletin of the Society of Economic Geologists* **97**(8), pp. 1829–1839. DOI: 10.2113/97.8.1829

10

INFRARED DETERMINATION OF THE QUALITY OF CARBONATE-RICH DIATOMITE ORES

This chapter identifies the types of carbonate impurities present in diatomite ore and their associations with the silica phase.

Parts of this chapter have been published in:
Guatame-Garcia, A. and Buxton, M. (2018). The Use of Infrared Spectroscopy to Determine the Quality of Carbonate-Rich Diatomite Ores. *Minerals 8(3)*, 120. doi: 10.3390/min8030120.

Diatomite, a rock formed by the accumulation of opaline diatom frustules, is a preferred raw material for the manufacturing of filters. Its uniqueness relies on the high porosity and inertness of the frustules. The presence of carbonates in some diatomite ores hinders these properties. The purpose of this chapter was to identify the type of carbonates and their association with the ore in a diatomite deposit, and to assess the suitability of determining the quality of the ore using techniques with potential for in-pit implementation. For this, run-of-mine samples were analysed using Environmental Scanning Electron Microscopy (ESEM) and infrared spectroscopy. The ESEM images showed that carbonate is present as cement and laminae. The infrared data revealed that the carbonate minerals correspond to aragonite and calcite, and that their occurrence is linked to the total amount of carbonate in the sample. By using a portable spectral instrument that uses diffuse reflectance, it was possible to classify the spectra of the ore samples based on the carbonate content. These results indicate that infrared technology could be used on-site for determining the quality of the ore, thus providing relevant information to assist the optimisation of mining and beneficiation activities.

10.1. INTRODUCTION

Diatomite is a sedimentary rock formed mainly by the accumulation of the skeletal remains of diatoms. Diatoms are unicellular algae that have a rigid cell wall (frustule) made of amorphous opaline silica with an intricate porous structure (Breese and Bodycomb, 2006; Korunic, 1998). These characteristics make diatomite a unique material with high porosity, low density and low chemical reactivity. Due to these properties, diatomite has great importance as an industrial raw material and is widely used as filtration media, adsorbent, filler and functional mineral additive. From these applications, filtration represents the majority of the consumption of the diatomite production (Crangle, 2016).

The purity of diatomite is especially important to ensure the adequate performance of filter grade products. Industry standards, such the Food Chemical Codex (FCC), determine that the amount of non-siliceous substances in diatomite filters should not be more than 25 wt % (USPC, 2016). Filters used for beverages pay particular attention to impurities that can be soluble in the filtered media (Braun et al., 2011). However, during the formation of diatomite deposits, other minerals deposit along with the diatom frustules, among which carbonate minerals are common (Bellanca et al., 1989). The high reactivity of CO_3 in these minerals affects the chemical purity of the diatomite ore. Furthermore, the intimate association of the frustules and carbonates can affect the porosity of diatomite. Conventionally, to generate filter-grade diatomite products, diatomite deposits are mined through open-pit methods, the extracted ore is then treated by disagglomeration, drying, degritting and sizing. Especial care is taken through all these processes to preserve the delicate diatom structure (Breese and Bodycomb, 2006). Finally, to adjust the adjust the pore structure and particle size required for filtration, the beneficiated ore is calcined in a rotary kiln (Ediz et al., 2010; Martinovic et al., 2006). At this stage, the presence of CO_3 in the ore is also detrimental to the process, since it increases the energy consumption for the kiln and increases the CO_2 emissions (Moffat and Walmsley, 2005).

In the processing of filter-grade diatomite products, the objective is to generate a grade or blend with a controlled amount of impurities. Such product must provide an acceptable flow-rate and clarity by the industrial standards and customers' requirements, at the time

that maintains the essential pore structure of the diatom frustules. In this context, a considerable number of beneficiation techniques have been developed to remove the carbonate minerals and improve the purity of the diatomite finished products. Some methods use physical separation of ore and impurities such as sequential classification (Al-Wakeel, 2009), electric field-based separation (Jung et al., 2014; Moradi et al., 2017) and centrifugal separation (Sun et al., 2017). These are sometimes complemented with enrichment methods such as flotation (Rezai, 2005) and acid leaching (Şan et al., 2009; Zhang et al., 2013). Even though these techniques have proven successful in increasing the purity of diatomite products, they are not ideal for the beneficiation process. The physical techniques can destroy the diatom structure (Şan et al., 2009; Zhang et al., 2013), reducing the porosity of the diatomite, whereas acid leaching and flotation generate large amounts of acid wastewater, increasing the environmental impact of the process. As a consequence, it is relevant to reduce the effect of the beneficiation techniques in the quality of the diatomite products and the environment. This could be achieved by feeding the processing with a pre-upgraded ore, allowing the optimisation of the beneficiation techniques.

The in-pit classification of the diatomite ore based on the carbonate content could support a controlled feed to the processing plant. Prior knowledge about the characteristics of the diatom frustules and their association with the type and amount of carbonate minerals would also influence the decision-making for the beneficiation process. For this information to be useful for operational feedback, it is necessary to be able to acquire the data of the ore synchronously with the mining and processing activities, that is to say, on-site and in (near) real-time. In this context, infrared (IR) spectroscopy can detect the minerals present in the diatomite ore (opal and carbonates) and has the technology maturity to be used as an on-site technique.

In this work, the diatomite deposit in Elche de la Sierra (Spain) was chosen to perform a detailed characterisation of a carbonate-rich diatomite ore. This study analyses how the characteristics of the ore are related to the carbonate content and how this information can be used for optimising mining and processing. For this, microscopic techniques were used to characterise the morphology and preservation of the diatom frustules and their association with the carbonate minerals and to analyse their possible influence in the porosity of the ore. Additionally, laboratory and portable infrared spectroscopy techniques were used to determine the type and amount of carbonate minerals in the ore. The observations focused on the capability of the portable techniques to be used as an on-site sensor for the characterisation of the diatomite ore. The results are further discussed in the context of offering new insights for the optimised beneficiation of diatomite ores.

10.2. DIATOM MORPHOLOGY

Diatom cells have a rigid wall, known as frustule, composed by amorphous silica. As shown in Figure 10.1a, the frustule is made of two valves (epivalve and hypovalve) that are held together by several rings, denoted as girdle bands, resembling the shape of a pillbox (Zurzolo and Bowler, 2001). In the surface of the valves, there are a series of pores which impart an intricate structure. The arrangement of the pores is distinctive of individual species (Breese and Bodycomb, 2006). The size of the frustules ranges from 0.75 to 1000 µm, although most of them are in the range from 10 to 150 µm. Based on the

shape of the frustules, the class *Diatomae* is subdivided into two orders: centric diatoms (order *Centrales*) which is radially symmetric, and pennate diatoms (order *Pennales*) which are elongated and bilaterally symmetric (Figure 10.1b) (Zurzolo and Bowler, 2001).

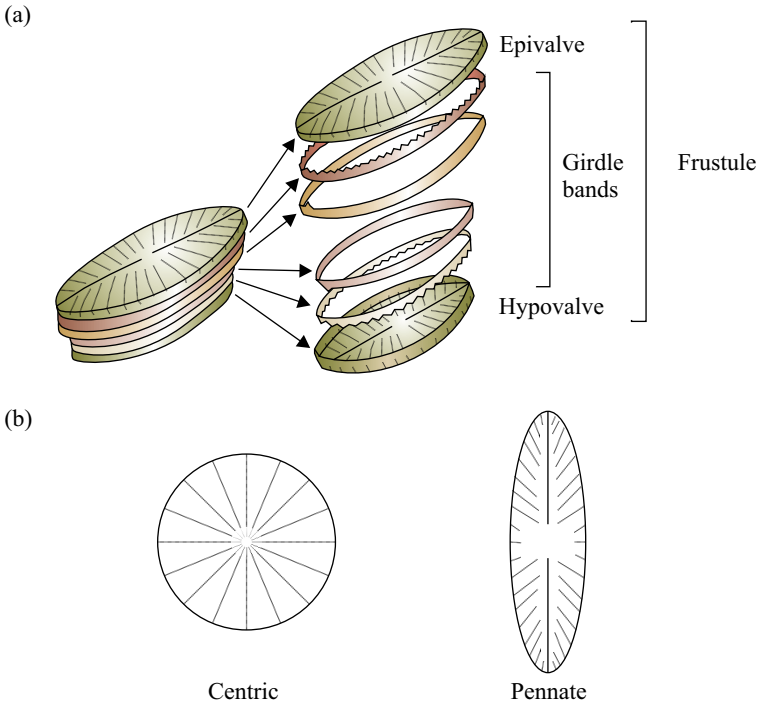

Figure 10.1: (**a**) Schematic overview of the components of diatoms shells (Reproduced after Zurzolo and Bowler (2001), with permission); (**b**) Schematic representation of the morphology of centric diatoms (left) and pennate diatoms (right)

10.3. ELCHE DE LA SIERRA DIATOMITE DEPOSIT

The samples for this study were obtained from the diatomite deposit in the Elche de la Sierra basin (south-east Spain) (Figure 10.2). The deposit forms part of a system of continental Neogene basins located on the external side of the Betic Ranges (Bellanca et al., 1989). During the Upper Miocene, the basins were filled mainly with lacustrine sediments. Towards the end of the evolution of the basins, active volcanism generated a surplus of silica in the water, favouring the thriving of diatoms. The deposition of diatomites occurred together with marls and carbonates (Elizaga and Calvo, 1988), generating diatomite deposits with a variable amount of carbonates and some terrigenous intercalations through the stratigraphic sequence (Foucault et al., 1987). The formation of the carbonate minerals and the type and abundance of diatoms was affected by seasonal variations of composition and volume of the water in the lakes (Bellanca et al., 1989). The diatom flora indicates a depositional environment in a shallow lacustrine basin with sporadic marine inputs (Servant-Vildary et al., 1990).

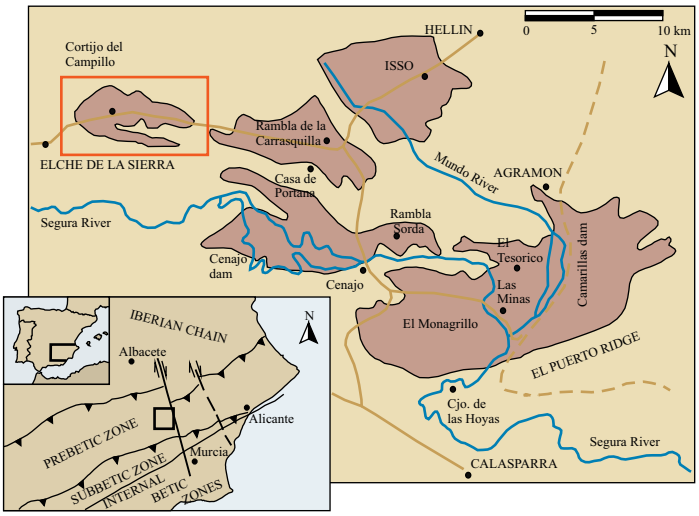

Figure 10.2: Neogene basins on the external side of the Betic Ranges, and location of the Elche de la Sierra basin (red rectangle in the upper-left corner) (Modified from Ortí et al. (2014), with premission)

Locally, Jurassic and Tertiary limestones and faulted Quaternary alluvium enclose the Elche de la Sierra diatomite deposit. Northwards, diatomite transforms progressively to clays, marls and conglomerate. Southwards, the edge of the body thins and transforms into opal-CT (cristobalite/tridymite). In the central part of the basin, the diatomite deposit has a maximum thickness of 80 meters. The stratigraphic sequence consists of a basal conglomerate, overlain by the diatomaceous ore body, lacustrine limestones, and a Quaternary polymictic conglomerate in the top. The diatomaceous ore body consists of 8 to 11 tabular diatomite layers, interbedded with limestones, marls, sand and clay horizons.

10.4. MATERIALS AND METHODS

10.4.1. SAMPLES

The material for this study was composed of run-of-mine (ROM) samples collected from a mine face in the deposit at different stratigraphic positions. Figure 10.3 shows a section of the deposit where diatomite layers of 1 m to 3 m thickness are recognisable by their white colour, whereas a light grey colour identifies the limestone layers. Intercalation of thin layers of diatomite, limestones, marls and clay horizons are also present in this part of the deposit. Only diatomite layers thicker than 1 meter are mineable. From these layers, 13 samples (named D1 to D13) were taken at different stratigraphic positions and different points in the pit upon accessibility, taking special care that all the diatomite layers were represented in the sample set.

Based on the threshold established by the FCC of maximum 25 wt % of non-siliceous substances in diatomite filters, for this research, a cut-off value of 25 wt % $CaCO_3$ was established as the maximum threshold for a sample to be regarded as diatomite ore. For

an analogue with the actual processing of diatomite ore, the samples were classified into different quality grade (QG) levels based on the $CaCO_3$ content. The cut-off values for every QG assigned in this study do not exactly correspond to those used in the industry (disclosure not possible due to commercial sensitivity), but yet they attempt to resemble the classification used by some mining companies. The cut-off values used in this study are as follows: QG1 < 10 wt %, Q2 = 10−16 wt %, QG3 = 16−22 wt % and QG4 = 22−25 wt %. To ensure that all the QG levels were represented in the sample set, four samples with known $CaCO_3$ values were added, namely samples D14 to D17.

Figure 10.3: Active mine face section of the diatomite deposit where some of the ore samples were obtained: (**a**) limestone layer with small intercalations of diatomite, (**b**) diatomite layer with small intercalations of limestones, (**c**) limestone layer, (**d**) intercalation of diatomite, limestones, marls and clay horizons, (**e**) diatomite layer with small intercalations of limestones.

10.4.2. ANALYTICAL METHODS

The association between carbonates and diatom frustules as well as the variations in the diatom morphology and preservation were investigated using Environmental Scanning Electron Microscopy (ESEM). The observations were conducted on rock chips to avoid any alteration of the diatom frustules induced by sample preparation. The instrument used was a Philips XL30 ESEM and supported with element analysis. The amount of $CaCO_3$ and the concentration of major elements in the samples to support the mineralogical analyses, were determined using X-ray fluorescence (XRF) using a PANalytical Magix Pro.

The mineralogical content of the samples was identified by using infrared (IR) spectroscopy. This technique was used firstly due to its ability to detect amorphous phases in minerals, which is adequate for the detection of opaline silica (Chester and Elderfield, 1968), and secondly due to its demonstrated capabilities for operating in mining and industrial environments. The samples used for all the spectral analyses were gently powdered using pestle and mortar, trying to preserve the delicate diatom structure, and later homogenised. Laboratory data were collected using Attenuated Total Reflection (ATR) (Section 2.2.3) in the spectral range 7.5 to 15 µm.

Spectra were also collected using portable spectrometers to assess the optimum

conditions for measurement and analysis required for an actual on-site application. Bidirectional reflectance spectra were collected using the ASD FieldSpec spectrometer (Section 2.2.3) covering the 0.3 to 2.5 µm range. The measuring time per spectrum (50 scans) was in average 60 seconds. Diffuse reflectance spectra were measured with the Agilent 4300 hand-held FTIR spectrometer (Section 2.2.3), ranging from 1.9 to 15 µm. The measuring time per spectrum (128 scans) was in average 90 seconds.

The bidirectional and diffuse spectral measurements were carried out using Petri dishes as sample containers. The surface was first compacted and flattened with a spatula to minimise void spaces and then slightly roughened with the edge of the spatula to maximise the direction of the reflections. It is important to note that with this method it is not possible to achieve the same roughness in all samples, causing variations in the overall reflectance from sample to sample. Five spectral measurements per sample were recorded. The spectral files were processed in the R environment. First, noise reduction was conducted by averaging the spectra recorded for every sample. The bidirectional reflectance spectra were processed using continuum removal and derivatives. The diffuse reflectance spectra were smoothed using the Savitzky-Golay filter with polynomial order of 3 and window size of 55 data points. Further Principal Component Analysis (PCA) was also performed in the R environment using the Chemometrics With R package (Wehrens, 2011).

10.5. RESULTS

10.5.1. ORE ESEM MICROSCOPY

Environmental Scanning Electron Microscope images, displayed in Figure 10.4, were used to characterise the texture of the diatomite ore. These images allowed the identification of the morphological characteristics of the frustules, as well as their relationship with the carbonate minerals. Most of the observed frustules are centric and a variable size between 10 to 40 µm. They correspond to the genus *Cyclotella*, as Foucault et al. (1987) and Servant-Vildary et al. (1990) reported previously. In Figure 10.4, *Cyclotella* diatoms can be identified by the circular pillbox-like shape; the differences in size and pore distribution correspond to different species and stages of maturity. Sporadic occurrences of pennate frustules were also observed, they correspond to the genera *Navicula* (Figure 10.4b) and *Cocconeis* (Figure 10.4g). The microscopic images showed that most of the valves are separated but complete, and occur together with fragments of the loose girdle bands (Figure 10.4b,d,f).

The carbonate was determined to be cement, coating the diatom frustules and in some cases filling the pores (Figure 10.4d), but also occurs as carbonate laminae in sharp contact with diatom laminae (Figure 10.4e). Biogenic aragonite with rod-like structure (Gopi and Subramanian, 2012) was also present in some samples mixed with the diatoms frustules (Figure 10.4h,i) or forming the carbonate laminae (Figure 10.4j). In addition to the diatom frustules and the carbonate minerals, sponge spicules (Figure 10.4a,c) and detrital fragments were found in a very small proportion.

In order to identify any relationship between the previous observations and the QG levels, the samples from the same quality grade were compared. As Figure 10.4 shows, the morphological characteristics of the diatoms do not show any particular pattern regarding

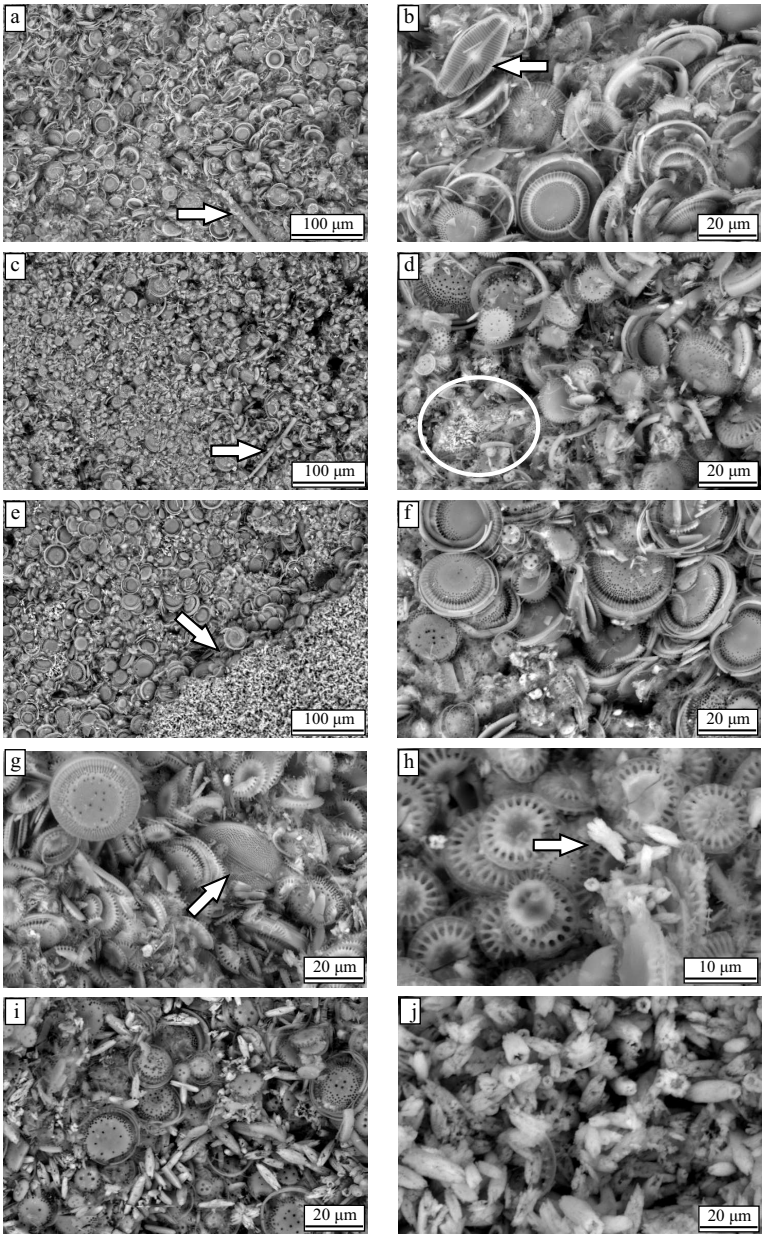

Figure 10.4: Environmental scanning electron microscopy (ESEM) microphotographs of the diatomite ore: (**a**) QG1 with fragments of sponge spicules, (**b**) QG1 with the occurrence of the genus *Navicula*, (**c**) QG2 with fragments of sponge spicule, (**d**) QG2 with carbonate cement (**e**) QG3 with sharp contact between silica and carbonate laminae, (**f**) QG3 composed almost exclusively by the genus *Cyclotella*, (**g**) QG3 with the occurrence of the genus *Cocconeis*, (**h - i**) QG4 with rod-like aragonite crystals, (**j**) carbonate lamina composed mainly of rod-like aragonite crystals (zoom in from microphotograph **e**)

the QG level. *Cyclotella*, the most common of the diatoms, appears in all the QG levels. The other types of diatoms seem to occur randomly regardless of the type or amount of impurities in the samples. Concerning the amount and type of carbonate, it was found that in samples from QG1 and QG2 the carbonate is most commonly found as cement whereas laminae were almost exclusive from QG3 and QG4. Moreover, the occurrence of rod-like aragonite was also restricted to the levels with high amount of carbonate.

10.5.2. XRF CHARACTERISATION

The chemical composition of the samples, summarised in Table 10.1, reveals that the most abundant component in the samples is SiO_2, comprising an average of 80 % in the samples. Based on the ESEM microphotographs, most of the SiO_2 can be attributed to the diatom frustules which are made of opaline silica ($SiO_2 \cdot H_2O$). The second component in abundance, and therefore the principal impurity in the ore, is $CaCO_3$, which constitutes on average 18 % of the composition of the samples. It can be assigned to calcite, aragonite or vaterite, which are calcium carbonate polymorphs. The remaining 2 % consist of Al_2O_3, Cl, Na_2O, SrO and SO_3, indicating that the other mineral impurities correspond to clay minerals and evaporites, such as halite, celestine and gypsum, expected from evaporitic shallow lacustrine environments, as is the case of the Elche de la Sierra basin (Ortí et al., 2014).The Mg content in the samples could be either associated with clay minerals, such as montmorillonite, or with carbonates, in the form of dolomite. However, the low concentration of Mg in the samples makes, for this study, the likely presence of dolomite negligible.

10.5.3. MINERALOGICAL CHARACTERISATION USING LABORATORY INFRARED SPECTROSCOPY

The infrared spectra provide a more precise characterisation of the mineralogical content in the diatomite ore. Figure 10.5 presents the spectra of the ore reference samples with different amounts of $CaCO_3$. The most prominent spectral features are those that are characteristic of opaline silica. The main feature, centred at 9.4 µm, is caused by the asymmetric stretching of the [SiO_4] tetrahedron; the feature around 12.6 µm is associated to the Si–O–Si bending vibration mode; and the shoulder at 10.2 µm is due to Si–OH molecular vibrations (Gendron-Badou et al., 2003); this feature is in particular distinctive for diatoms (Chester and Elderfield, 1968; Goryniuk, 2004; Moenke, 1974). Because the silica polymorphs have similar spectra in the analysed range, it was not possible to identify any other silica minerals besides opal. A particular feature of quartz at 14.4 µm (Moenke, 1974) was not detected in any of the samples, suggesting that quartz is either absent or in a very low concentration.

The identification of carbonate minerals was based first on the spectral feature at 14.0 µm, caused by the OCO bending (in-plane deformation) mode. Calcite and aragonite are differentiated by the CO_3 out-of-plane deformation mode feature located at 11.4 µm for calcite and 11.7 µm for aragonite; besides, aragonite present as well a second feature associated to the OCO bending mode at 14.3 µm (Andersen and Brečević, 1991; Gunasekaran et al., 2006). The characteristic feature of vaterite at 13.4 µm (Gopi and Subramanian, 2012) was not detected in any of the samples. It is expected that the intensity of the spectral features of the carbonate minerals decreases with lower $CaCO_3$

Table 10.1: X-ray fluorescence (XRF) analysis of the diatomite ore samples (concentrations expressed in wt %)

Sample ID	Al_2O_3	$CaCO_3$	Cl	Fe_2O_3	K_2O	MgO	Na_2O	P_2O_5	SiO_2	SO_3	SrO	TiO_2
D1	0.56	19.9	0.06	0.43	0.10	0.19	0.12	0.07	68.4	0.04	0.17	0.03
D2	0.42	18.6	0.07	0.14	0.06	0.16	0.08	0.07	70.9	0.03	0.17	0.04
D3	0.46	10.9	0.09	0.33	0.08	0.14	0.12	0.04	82.2	0.08	0.08	0.05
D4	0.64	16.4	0.07	0.34	0.11	0.19	0.09	0.06	73.7	0.05	0.10	0.03
D5	0.45	22.1	0.07	0.14	0.07	0.16	0.09	0.06	65.5	0.04	0.17	0.06
D6	0.54	22.1	0.04	0.22	0.09	0.16	0.08	0.06	65.3	0.05	0.22	0.06
D7	0.77	22.2	0.03	0.34	0.13	0.28	0.06	0.08	64.7	0.04	0.14	0.07
D8	0.67	20.8	0.04	0.69	0.14	0.21	0.08	0.08	66.7	0.03	0.13	0.05
D9	0.67	24.3	0.06	0.25	0.12	0.20	0.14	0.04	61.8	0.04	0.19	0.08
D10	0.96	23.1	0.12	0.40	0.18	0.45	0.13	0.07	62.7	0.05	0.21	0.04
D11	0.38	9.61	0.03	0.47	0.04	0.16	0.04	0.04	84.3	0.02	0.07	0.03
D12	0.68	10.4	0.02	0.32	0.09	0.25	0.06	0.05	82.8	0.02	0.02	0.05
D13	0.84	21.5	0.03	0.50	0.15	0.32	0.05	0.08	65.5	0.03	0.13	0.06
D14	0.51	6.29	0.03	0.28	0.07	0.17	0.05	0.04	89.3	0.02	0.02	0.04
D15	0.73	10.9	0.02	0.45	0.11	0.25	0.06	0.07	81.8	0.02	0.05	0.06
D16	0.74	16.4	0.05	0.50	0.11	0.29	0.11	0.07	73.3	0.03	0.12	0.07
D17	0.72	24.4	0.03	0.42	0.10	0.28	0.05	0.07	61.4	0.05	0.17	0.01
Mean	0.63	17.6	0.05	0.36	0.10	0.23	0.08	0.06	80.6	0.04	0.13	0.05
SD	0.16	5.9	0.03	0.14	0.03	0.08	0.03	0.01	6.08	0.02	0.06	0.02
Min	0.38	6.3	0.02	0.14	0.04	0.14	0.04	0.04	73.6	0.02	0.02	0.01
Max	0.96	24.2	0.12	0.69	0.18	0.45	0.14	0.08	92.4	0.08	0.22	0.08
Error	0.02	0.08	0.006	0.02	0.009	0.01	0.008	0.007	0.10	0.006	0.009	0.007

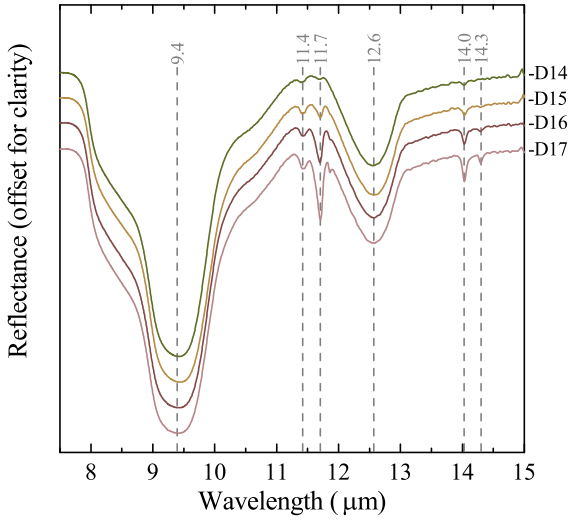

Figure 10.5: Attenuated total reflection (ATR) infrared (IR) spectra of diatomite ore samples with variable content of $CaCO_3$: D14 = 6.29 wt%, D15 = 10.9 wt%, D16 = 16.4 wt%, D17 = 24.4 wt%. The dashed lines indicate position of the spectral features opal (9.4 and 12.6 μm), calcite (11.4 and 14.0 μm) and aragonite (11.7, 14.0 and 14.3)

content. However, it is noticeable that the calcite features, even if weak, are present in the spectra of all the samples, whereas the aragonite features are only present at relatively high $CaCO_3$ content (above ~ 11 wt%). The IR spectra did not detect any other minerals likely to be present in the samples as suggested by the XRF analyses, namely clays (Al_2O_3) and evaporites (SrO), since their concentration in the samples is too low.

10.5.4. MINERAL IDENTIFICATION USING PORTABLE INFRARED DEVICES

Two portable spectral techniques and ranges were tested to assess the suitability of detecting on-site the purity of the diatomite ore in relation to the carbonate content. Each technique makes use of a different type of infrared reflection and a different spectral range. The potential of these techniques for an on-site implementation was assessed based on their ability to differentiate the carbonate minerals from the opaline silica and to make a qualitative assessment of the amount of impurities in the ore.

The spectra recorded using bidirectional reflectance were constrained to the 1.9 to 2.5 μm wavelength range, where the absorption features of opaline silica and carbonates occur. In this range, opaline silica presents features at 2.21 and 2.26 μm caused by the stretching mode of isolated Si–OH and bending mode of the H-bound silanol (Goryniuk, 2004). Aragonite and calcite present strong absorption features at 2.33 and 2.26 μm due to the combination tones of the carbonate vibrations; for these two minerals, the features occur at the same or slightly shorter wavelengths (Gaffey, 1986). Other carbonate features are present between 1.7 to 2.1 μm, but there are usually not present in mixed spectra. In Figure 10.6 (top), the spectra of the diatomite ore were processed using the Continuum Removal (CR) technique to enhance the differences between spectral features. However, only the features of opaline silica are visible. The overlap of opal and carbonate features at

2.26 µm hinders the use of this wavelength as a diagnostic mark, and the 2.33 µm feature is masked. To amplify the possible differences in the spectra, the first derivative was calculated. Figure 10.6 (bottom) reveals the 2.33 µm carbonate feature in the D16 and D17 samples (CO_3 = 16.4 wt% and 24.4 wt%, respectively) but not in the D15 sample ($CaCO_3$ = 10.9 wt%). Based on this observation, it can be said that the limit of detection for carbonates in this type of samples using bidirectional reflectance lies approximately between 11 to 16 wt%.

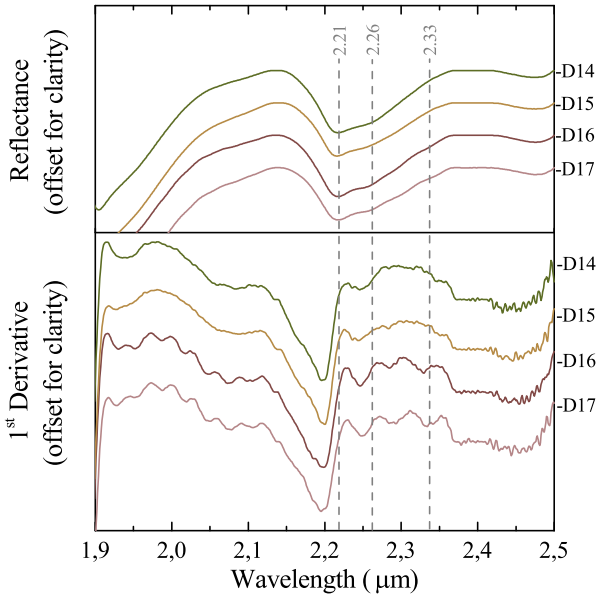

Figure 10.6: Bidirectional reflectance spectra of diatomite ore samples with variable content of $CaCO_3$ after continuum removal (**top**) and 1^{st} derivative (**bottom**): D14 = 6.29 wt%, D15 = 10.9 wt%, D16 = 16.4 wt%, D17 = 24.4 wt%. The dashed lines indicate position of the spectral features opal (2.21 and 2.26 µm) and calcite and aragonite (2.26 and 2.33 µm)

In the diffuse reflectance, the spectra were noisier than using bidirectional reflectance, and long wavelengths were influenced by the volume scattering of the diatomite powders (Cooper et al., 2002), generating low-quality spectra. For these data, the most useful spectral region was the one that covers the opal and carbonate between 6.0 to 8.0 µm. In this range, the features of opaline silica are detected at 6.1 µm, caused by the H–O–H bend in isolated molecular water, and at 7.4 µm, corresponding to the Christiansen Feature (CF) for silicates (Goryniuk, 2004). The features for carbonate minerals in this region are due to the asymmetric C–O stretching; absorptions at 6.4 and 6.6 µm are characteristic of aragonite, whereas those at 6.9 and 7.2 µm correspond to calcite (Andersen and Brečević, 1991; Gunasekaran et al., 2006). In the spectra of the diatomite ore, shown in Figure 10.7, the opal Christiansen Feature in the D14 sample is broadened to shorter wavelengths due

to the 7.2 µm calcite feature. With the increasing $CaCO_3$ content in the other samples, the calcite absorptions of calcite become better defined along with the aragonite ones. In the particular case of aragonite, the broad bands in Figure 10.7 are an indication of a distorted amorphous lattice (Andersen and Brečević, 1991).

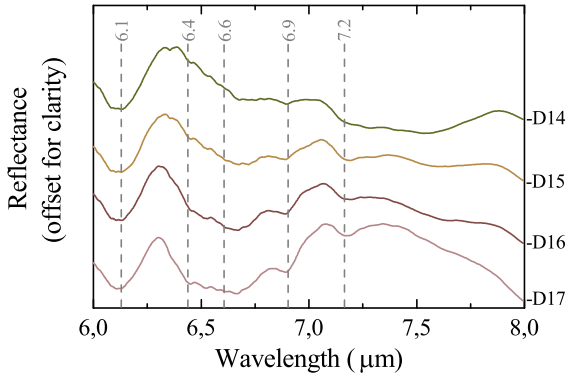

Figure 10.7: Diffuse reflectance spectra of diatomite ore samples with variable content of $CaCO_3$: D14 = 6.29 wt%, D15 = 10.9 wt%, D16 = 16.4 wt%, D17 = 24.4 wt%. The dashed lines indicate position of the spectral features opal (6.1 and 7.2 µm), calcite (6.9 and 7.2 µm) and aragonite (6.4 and 6.6 µm)

The results of the characterisation of the diatomite ore using diffuse reflectance spectra are in agreement with those achieved by using the laboratory ATR data. Furthermore, they provide more complete information than that acquired by using the bidirectional reflectance set-up. Based on this outcome, further analysis was carried out for the diffuse reflectance data. Principal Component Analysis (PCA) was used to assess whether it is possible to classify the ore according to the QG levels using the infrared spectra. PCA analysis presents the advantage of identifying the largest possible variance in the sample set, giving the most meaningful information in the first components. Other sources of variability related to noise, for example, are relegated to other components. In the case of the spectra used in this study, the PCA analysis is convenient since it identifies not only the spectral variability related to the mineral composition but also because it minimises the influence of spectral variations in the overall reflectance due to the sample preparation.

Figure 10.8 shows the scores and loadings plots of the first Principal Component (PC1). The scores plot is coloured based on the quality grade levels. Even though the size of the sample set is rather small, it is possible to identify trends in the PCA scores. Positive scores are associated with QG1 and QG2, whereas negative scores are related to QG3 and QG4. Moreover, the dimension of the positive scores separates QG1 from QG2. In contrast, in the negative scores, there is not a clear separation between QG3 and QG4. The variability in the spectra described by PC1 is related to the silica and the carbonate features, as the loadings plot shows. Positive loadings belong to the region between 6.3 to 6.8 µm, where the aragonite features occur. In contrast, negative loadings correspond to the regions that host the opal features, between 6.0 to 6.3 µm and 7.0 to 7.7 µm. It is not surprising that the PCA does not differentiate sharply between quality grade levels since, on the one hand

the cut-off values for the quality grades are arbitrary; on the other hand, the composition and consequently the spectra of the samples varies continuously along quality grades.

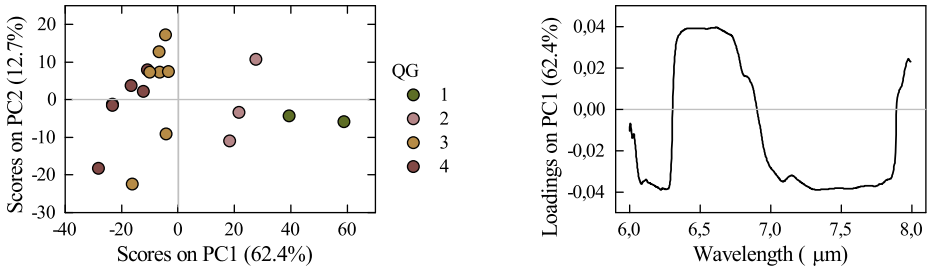

Figure 10.8: Principal component analysis (PC1 vs PC2) of diatomite ores (**left**) and corresponding loadings plot (**right**).

10.6. DISCUSSION

10.6.1. INFLUENCE OF THE ORE CHARACTERISTICS IN MINERAL PROCESSING

The observations about the texture of the diatomite ore revealed that, even though the girdles are commonly detached from the diatom frustule, complete valves and complete shells make up the majority of the diatom remains. This implies that the natural porosity of the diatomite ore is not affected by the disaggregation of the frustules. However, it was also observed that the carbonate present as cement fills the pores of some of the frustules, decreasing the natural porosity of the ore, as shown in Figure 10.4d. In contrast, biogenic aragonite crystals do not affect the porosity, due to their particle size (10 to 20 μm), and carbonate laminae have a reduced surface of contact with the frustules.

The association between the carbonate and the frustules, together with the type of carbonate present in the ore, might influence the performance of certain beneficiation techniques (Moradi et al., 2017). Removal of carbonate present as cement would be more effective by using wet beneficiation techniques that dissolve the $CaCO_3$, whereas large aragonite crystals and carbonate laminae, in general, could be removed by using physical beneficiation techniques. Since the presence of carbonate as a cement is usually found in ores of higher quality (QG1 and QG2), and laminae and aragonite crystals are more common in high carbonate ores (QG3 and QG4), high and low quality ores could be beneficiated separately using adequate methods for the type of mineral association.

10.6.2. POTENTIAL FOR THE USE OF INFRARED SENSORS AS A TOOL FOR OPTIMISING THE MINING AND PROCESSING OF DIATOMITE ORES

The characterisation using infrared spectroscopy enabled the identification of calcite and aragonite as the main ore impurities. Moreover, it established a correspondence between the type of carbonate mineral and the quality of the diatomite ore, where high-grade ores contain only aragonite whereas low-grade ores have aragonite and calcite. The identification of the type of carbonate was possible by using not only the traditional laboratory infrared technique, but also by using a portable instrument that uses diffuse

reflectance spectroscopy. Even though the quality of the data collected with the device equipped with diffuse reflectance is lower than the laboratory one, the acquired spectra were shown to be adequate to perform a qualitative analysis of the composition of the diatomite ore.

The main advantage of the diffuse over the bidirectional reflectance is based on the possibility of using a spectral range where the features of carbonates and opal do not overlap, enabling a unambiguous identification of the two mineral phases present in the ore. Moreover, in the spectral range used, it was also possible to differentiate the features of calcite from those of aragonite. Given these factors, it was feasible to perform a qualitative analysis using principal component analysis (PCA). The PCA results demonstrated that, by using the spectra above, it is possible to classify the diatomite ore based on the carbonate content. These results also open up the opportunity for conducting more precise quantitative analysis with the aid of chemometric tools, such as partial least squares regression (PLS), as suggested by Meyer-Jacob et al. (2014), or relational models based on the inherent parameters of the carbonate absorption features (e.g., wavelength position, depth) and the actual $CaCO_3$ content following the approach used by Zaini et al. (2016) .

Besides the analytic advantages provided by the use of diffuse reflectance spectroscopy, this technique also represents a suitable sensor for the in-pit characterisation of the diatomite ore. The spectral range used is not affected by particle size, and, therefore, can be used either for rock or powder samples. The availability of portable instruments that work in the mentioned spectral range enables the collection of data on-site, with little or no sample preparation. The spectral acquisition takes only a few minutes per sample, and the data does not require extensive processing or high computing capabilities, making it possible to generate information in (near) real-time.

Despite these advantages, to the knowledge of the author, the technological advances to date in the 6.0 to 8.0 µm range allow collecting point data only, leaving applications such as sample and face imaging out of reach. Hyperspectral imagers are available only in the Short Wavelength IR (SWIR) (1.0 µm to 2.5 µm) and in the thermal IR (TIR) (8.0 µm to 12.0 µm). The results of this study discouraged the use of the SWIR range due to the overwhelming spectral response of opal (Figure 10.6) and the use of the TIR range due to issues related to particle size. Nevertheless, for the applications that work for whole rock rather than for powders, this constraint is not valid anymore. In this case, the features that were studied in this work using laboratory spectra (Figure 10.5) could be possibly used to establish the relationship between the spectra and the $CaCO_3$ content. However, unlike the diffuse reflectance data, the collection and processing of spectral images, either as mine face or drill core scanners, are time-consuming, and therefore, they could not be considered for processes that require real-time data.

The use of diffuse reflectance spectroscopy, using a portable device sensitive to wavelengths betwee 6.0 and 8.0 µm, would enable the on-site determination of the quality grade of the diatomite ore. Even though it works as a point measurement technique, results can be obtained on-site and (near) real-time offering the possibility of collecting several data points that characterise either a section of the pit or high volumes of stocked piled ore. The results of the spectral analysis could be used, for example, to aid selective mining, by discriminating sections of the pit with a given quality grade. The spectral

classification of the ore could also assist with the upgrading of the ore before mineral processing, aiding in the selection of convenient and optimised beneficiation techniques.

10.7. CONCLUSIONS

This study presented the main characteristics of the diatomite ore that are relevant for generating filter-grade finished products. In addition, it assessed the potential of using infrared spectroscopy as a technique for the on-site characterisation of the diatomite ore with a view to the optimisation of mining and beneficiation.

The textural observations of the ore revealed that the diatom frustules are excellently preserved and the disaggregation state does not diminish the porosity of the diatomite. The presence of carbonate minerals was identified as the only factor that affects the quality of the ore. For this case study, carbonate was found as calcite cement in ores with relatively low carbonate content, and as cement, loose aragonite crystals and laminae in ores with relatively high carbonate content. These minerals were identified by using laboratory and portable infrared spectroscopy. From the portable techniques tested, diffuse reflectance using the 6.0 to 8.0 µm spectral range provided a better mineral identification that could be used for classifying the diatomite ore according to the pre-determined quality grades.

These results show that the quality of the diatomite ore can be determined by using infrared spectroscopy. This information integrated with the acquired knowledge about the type of associations between the carbonate and opaline silica phases can be used for optimising the beneficiation process. Consequently, this study offers insights on the advantages and the potential of using infrared spectroscopy as an on-site tool for the characterisation of the diatomite ore. An infrared-based determination of the quality of the ore would provide relevant and timely information at mining and pre-beneficiation stages that can support proactively the decision-making process. Ultimately, the implementation of infrared ore characterisation would result in a more efficient use of the diatomite resources, optimised mineral processing and generation of high-quality diatomite products.

REFERENCES

Al-Wakeel, Mohamed I. (2009), 'Characterization and process development of the Nile diatomaceous sediment', *International Journal of Mineral Processing* **92**(3-4), pp. 128–136. DOI: 10.1016/j.minpro.2009.03.008

Andersen, F. A. and Brečević, L. (1991), 'Infrared spectra of amorphous and crystalline calcium carbonate.', *Acta Chemica Scandinavica* **45**, pp. 1018–1024. DOI: 10.3891/acta.chem.scand.45-1018

Bellanca, A., Calvo, J. P. , Censi, P. , Elizaga, E. and Neri, R. (1989), 'Evolution of lacustrine diatomite carbonate cycles of Miocene age, Southeastern Spain: Petrology and isotope geochemistry', *Journal of Sedimentary Petrology* **59**(1), pp. 45–52. DOI: 10.1306/212f8f12-2b24-11d7-8648000102c1865d

Braun, F., Hildebrand, N. , Wilkinson, S. , Back, W. , Krottenthaler, M. and Becker, T. (2011), 'Large-scale study on beer filtration with combined filter aid additions to cellulose

fibres', *Journal of the Institute of Brewing* **117**(3), pp. 314–328. DOI: 10.1002/j.2050-0416.2011.tb00475.x

Breese, R. O. Y. and Bodycomb, F. M. (2006), Diatomite, *in* J. E. Kogel, N. C. Trivedi, J. M. Barker and S. T. Krukowski, eds, 'Industrial Minerals and Rocks', 7th edn, Society for Mining, Metallurgy, and Exploration, pp. 433–450.

Chester, R. and Elderfield, H. (1968), 'The infrared determination of opal in siliceous deep-sea sediments', *Geochimica et Cosmochimica Acta* **32**(10), pp. 1128–1140. DOI: 10.1016/0016-7037(68)90113-0

Cooper, B. L., Salisbury, J. W. , Killen, R. M. and Potter, A. E. (2002), 'Mid infrared spectral features of rocks and their powders', *Journal of Geophysical Research E: Planets* **107**(E4), pp. 1.1–1.17. DOI: 10.1029/2000JE001462

Crangle, R. D. (2016), Diatomite, *in* '2015 Minerals yearbook', USGS, pp. 22.1–22.5.
URL: *https://minerals.usgs.gov/minerals/pubs/commodity/diatomite/myb1-2015-diato.pdf [Accessed January 2019]*

Ediz, N., Bentli, İ. and Tatar, İ. (2010), 'Improvement in filtration characteristics of diatomite by calcination', *International Journal of Mineral Processing* **94**(3-4), pp. 129–134. DOI: 10.1016/j.minpro.2010.02.004

Elizaga, E. and Calvo, J. P. (1988), 'Evolución sedimentaria de las cuencas lacustres neógenas de la zona prebética (Albacete, España). Relación, posición y efectos del vulcanismo durante la evolución. Interés minero', *Boletín Geológico y Minero* **99**(6), pp. 837–846.

Foucault, A., Calvo, J. P. , Elizaga, E. , Rouchy, J. M. and Servant-Vildary, S. (1987), 'Situation of the late Miocene lacustrine deposits from Hellin - Province of Albacete, Spain - in the geodynamic evolution of the Betic Cordilleras. (Pace des depots lacustres d'age Miocene superieur de la region de Hellin (Province de Albacete, Espagne) dans l'evolution geodynamique des Cordilleres Betiques.)', *Comptes Rendus - Academie des Sciences, Serie II* **305**(13), pp. 1163–1166.

Gaffey, S. J. (1986), 'Spectral reflectance of carbonate minerals in the visible and near infrared (0.35-2.55 microns): calcite, aragonite, and dolomite.', *American Mineralogist* **71**(1-2), pp. 151–162.

Gendron-Badou, A., Coradin, T. , Maquet, J. , Frölich, F. and Livage, J. (2003), 'Spectroscopic characterization of biogenic silica', *Journal of Non-Crystalline Solids* **316**(2-3), pp. 331–337. DOI: 10.1016/s0022-3093(02)01634-4

Gopi, S. P. and Subramanian, V. K. (2012), 'Polymorphism in CaCO3 — effect of temperature under the influence of EDTA (di sodium salt)', *Desalination* **297**, pp. 38–47. DOI: 10.1016/j.desal.2012.04.015

Goryniuk, M. C. (2004), 'The reflectance spectra of opal-A (0.5–25 microns) from the Taupo Volcanic Zone: Spectra that may identify hydrothermal systems on planetary surfaces', *Geophysical Research Letters* **31**(24), pp. L24701.1–L24701.4. DOI: 10.1029/2004gl021481

Gunasekaran, S., Anbalagan, G. and Pandi, S. (2006), 'Raman and infrared spectra of carbonates of calcite structure', *Journal of Raman Spectroscopy* **37**(9), pp. 892–899. DOI: 10.1002/jrs.1518

Jung, K., Jang, D. and Ahn, K. (2014), 'A novel approach for improvement of purity and porosity in diatomite (diatomaceous earth) by applying an electric field', *International Journal of Mineral Processing* **131**, pp. 7–11. DOI: 10.1016/j.minpro.2014.08.002

Korunic, Z. (1998), 'Review - Diatomaceous earths, a group of natural insecticides', *Journal of Stored Products Research* **34**(2-3), pp. 87–97. DOI: 10.1016/s0022-474x(97)00039-8

Martinovic, S., Vlahovic, M. , Boljanac, T. and Pavlovic, L. (2006), 'Preparation of filter aids based on diatomites', *International Journal of Mineral Processing* **80**(2-4), pp. 255–260. DOI: 10.1016/j.minpro.2006.05.006

Meyer-Jacob, C., Vogel, H. , Boxberg, F. , Rosén, P. , Weber, M. E. and Bindler, R. (2014), 'Independent measurement of biogenic silica in sediments by FTIR spectroscopy and PLS regression', *Journal of Paleolimnology* **52**(3), pp. 245–255. DOI: 10.1007/s10933-014-9791-5

Moenke, H. H. W. (1974), Silica, the three-dimensional silicates, borosilicates and beryllium silicates, *in* V. C. Farmer, ed., 'The Infrared Spectra of Minerals', Vol. Monograph 4, Mineralogical Society, book section 16, pp. 365–382.

Moffat, W. and Walmsley, M. R. W. (2005), Understanding lime calcination kinetics for energy cost reduction, *in* 'Proceedings of the 59th Appita Conference, Auckland, New Zealand', pp. 487–494.

Moradi, S., Moseley, D. , Hrach, F. and Gupta, A. (2017), 'Electrostatic beneficiation of diatomaceous earth', *International Journal of Mineral Processing* **169**, pp. 142–161. DOI: 10.1016/j.minpro.2017.11.008

Ortí, F., Rosell, L. , Gibert, L. , Moragas, M. , Playà, E. , Inglès, M. , Rouchy, J. M. , Calvo, J. P. and Gimeno, D. (2014), 'Evaporite sedimentation in a tectonically active basin: The lacustrine Las Minas Gypsum unit (Late Tortonian, SE Spain)', *Sedimentary Geology* **311**, pp. 17–42. DOI: 10.1016/j.sedgeo.2014.06.004

Rezai, B. (2005), The beneficiation studies of diatomite by flotation and hydrocyclone, *in* R. Venugopal, T. Sharma, V. K. Saxena and N. R. Mandre, eds, 'Mineral Processing Technology Mpt-2005', McGraw Hill, pp. 214–227.

Şan, O., Gören, R. and Özgür, C. (2009), 'Purification of diatomite powder by acid leaching for use in fabrication of porous ceramics', *International Journal of Mineral Processing* **93**(1), pp. 6–10. DOI: 10.1016/j.minpro.2009.04.007

Servant-Vildary, S., Rouchy, J. M. , Pierre, C. and Foucault, A. (1990), 'Marine and continental water contributions to a hypersaline basin using diatom ecology, sedimentology and stable isotopes: an example in the Late Miocene of the Mediterranean (Hellin Basin, southern Spain)', *Palaeogeography, Palaeoclimatology, Palaeoecology* **79**(3-4), pp. 189–204. DOI: 10.1016/0031-0182(90)90017-2

Sun, Z., Mao, J. , Hu, Z. and Zheng, S. (2017), 'Study on pilot-scale centrifugal separator for low-grade diatomite purification using response surface methodology', *Particulate Science and Technology* **35**(1), pp. 119–126. DOI: 10.1080/02726351.2015.1131794

USPC (2016), Monographs, *in* 'Food Chemical Codex – FCC 10', 10th edn, The United States Pharmacopeial Convention, pp. 410–411.
URL: *https://app.knovel.com/hotlink/toc/id:kpFCCE0031/food-chemicals-codex/food-chemicals-codex [Accessed November 2016]*

Wehrens, R. (2011), Principal Component Analysis, *in* R. Gentleman, K. Hornik and G. Parmigiani, eds, 'Chemometrics with R', Multivariate data analysis in the natural sciences and life sciences, Springer Berlin Heidelberg, Chapter 4, pp. 43–66. DOI: 10.1007/978-3-642-17841-2

Zaini, N., van der Meer, F. , van Ruitenbeek, F. , de Smeth, B. , Amri, F. and Lievens, C. (2016), 'An alternative quality control technique for mineral chemistry analysis of Portland cement-grade limestone using shortwave infrared spectroscopy', *Remote Sensing* **8**(12), pp. 950. DOI: 10.3390/rs8110950

Zhang, G., Cai, D. , Wang, M. , Zhang, C. , Zhang, J. and Wu, Z. (2013), 'Microstructural modification of diatomite by acid treatment, high-speed shear, and ultrasound', *Microporous and Mesoporous Materials* **165**, pp. 106–112. DOI: 10.1016/j.micromeso.2012.08.005

Zurzolo, C. and Bowler, C. (2001), 'Exploring bioinorganic pattern formation in diatoms. A story of polarized trafficking', *Plant physiology* **127**(4), pp. 1339–1345. DOI: 10.1104/pp.010709

IV

Epilogue

11

Discussion

This chapter provides a general discussion about the key findings in the thesis, indicating the links between the research objectives and the results achieved.

11.1. SYNTHESIS

This Thesis addresses the detection of factors that determine the quality parameters of some industrial minerals by using data derived from infrared sensors. The research was motivated by the needs in the mining industry of generating products that meet the strict market demands, and by the embracement of the concept of sustainable development by mining companies. In particular, this study focuses on three commodities that make use of calcination as part of the mineral processing, namely kaolin, perlite and diatomite. As presented in Chapter 1, the calcination process for these commodities is highly relevant in that it enhances the properties of the minerals and adds considerable value to the final product. From the operational standpoint, the optimisation of the calcination process can impact the efficiency of the mineral resources and the energy consumption of the calciner. Improvement of resource efficiency for calcined industrial minerals can be carried out at the extraction of the ore or around the calcination process. Consequently, the investigation of the detection of factors that affect the quality of the products should focus on these stages.

Table 11.1 recapitulates the characteristics of the kaolin, perlite and diatomite as raw ore, feed for calcination and calcined product, along with the quality parameters that are relevant at every stage. Table 11.1 also re-estates the objectives of using infrared-based characterisation and indicates the quality parameters that can be detected from the results of this work.

Kaolin is an example of the performance and speciality minerals. For this commodity, calcination aims to modify the crystal structure of kaolinite to create new compounds, in which colour, chemical reactivity and abrasiveness are some of the required quality parameters. Infrared spectroscopy aids in the identification of (1) iron, clay minerals and kaolinite crystallinity in the raw ore, (2) in the determination of the kaolinite crystallinity in the feed for calcination, and (3) in the development of a proxy for the quality standard for reactivity in the final product.

Perlite and diatomite are examples of process aids for filtration and absorption. In these commodities, calcination aims to modify the pore and particle size to enable their use as filter aids. In perlite, the presence of heavy metals that might be soluble in the filtered fluid hinders its performance for this application. Additionally, the generation of small particles as part of the particle size reduction process has also been pointed out as an environmental hazard and health risk. In this case, the analysis of the infrared spectra enables the detection of the associated mineralogy responsible for the generation of small particles. It also permits the establishment of a relationship between the mineralogy and the heavy metal content. Similarly to perlite, in diatomite, the presence of carbonates that can become soluble in the filtered media affects the performance of the product as a filter aid. The infrared analysis enables not only the detection of the carbonate associated with the diatomite ore but also the classification of the ore according to quality grade content. The subsequent sections discuss these findings in the view of the scope of this research.

Table 11.1: Summary of the characteristics and quality parameters of kaolin, perlite and diatomite as raw ore, feed for calcination and calcined product, and the used of infrared-based characterisation for these commodities

Process	**Material**	**Use of infrared sensors**	**Kaolin**	**Perlite**	**Diatomite**
Extraction	Raw ore	Determine the quality of the ore in the pit	**Ore description:** Kaolinised granite composed by kaolinite, muscovite, illite, biotite, quartz and feldspars. **Quality parameters:** Presence of iron-bearing minerals, presence of clay minerals different than kaolinite, kaolinite crystallinity (detected with IR)	**Ore description:** Perlitised volcanic glass containing opaline silica and clay minerals. **Quality parameters:** Presence of montmorillonite and heavy metals (detected with IR)	**Ore description:** Diatomite rock composed by diatom frustules (opaline silica), clay minerals, carbonates and evaporites **Quality parameters:** Presence of carbonate minerals (detected with IR)
Calcination	Feed	Monitor the consistency of the feed for calcination	**Feed description:** Beneficiated kaolin ore containing more than 90 % of kaolinite. **Quality parameters:** Kaolinite crystallinity (measured with IR), Fe content, presence of other clay minerals (no detected with IR)	**Feed description:** Crushed perlite ore **Quality parameters:** Particle size (no measured with IR)	**Feed description:** Beneficiated diatomite ore classified according to quality grades **Quality parameters:** Carbonate content measured with IR)
Calcination	Product	Support quality control and process feedback	**Product description:** Calcined kaolin in the amorphous γ-alumina phase. **Quality parameters:** Soluble Al_2O_3 content (predicted based on IR), mullite content, brightness (no measured with IR)	**Product description:** Expanded perlite **Quality parameters:** Particle and pore size (no measured with IR)	**Product description:** Calcined diatomaceous earth **Quality parameters:** Particle and pore size (no measured with IR)

11.2. USE OF INFRARED SENSOR DATA IN THE MINING AND PROCESSING OF INDUSTRIAL MINERALS

11.2.1. GENERATION OF PERFORMANCE AND SPECIALITY MINERALS FROM KAOLIN

One of the aims of this research was to create methods to detect factors that reduce the quality of the kaolin ore. Some of such factors are the presence of iron-bearing mineralogy and clay minerals distinct from kaolinite, and the crystallinity of kaolinite itself. All of these minerals have characteristics spectral features in the SWIR range, and therefore, it was expected that they could be detected or measured. Moreover, there are well-established methods based on infrared spectroscopy to identify these minerals that were directly used. Consequently, it was not required to developed new methods since the existing ones provided all the relevant data for analysis. The importance of this study relies on the interpretation of the obtained results from the existing methodology and their implications for the mining of the kaolin ore. These results make an important contribution to the corpus of knowledge about kaolin mineralisation in the St Austell granite.

The study of samples from different parts of the kaolin deposit with various degrees of alteration shows correlation among the factors that determine the quality of the ore. The observations reveal that, unlike the current production pits, the extraction of kaolin from parts of the deposit with a lesser quality set different priorities for the beneficiation of the ore, depending mainly on the type of occurrence of iron and the kaolinite crystallinity. Based on this, the use of infrared data could assist on the identification of mining targets or modifications to the beneficiation process.

The use of hyperspectral images permits the recognition of distribution patterns of the ore, such as texture and surface abundance, and impurities along drill core sections. From these results, one might think on the possibilities of upscaling these findings for face mapping, or even aerial surveying for mapping the mineralogy of the deposit for the definition of extraction areas. A study carried out by Ellis and Scott (2004) mapped the same part of the biotite granite that is subject of this study using airborne hyperspectral imagery. Surprisingly, this study did not report any iron-bearing minerals. This fact raises the question of whether, due to the lower spectral resolution of the airborne images, the spectra of the clay minerals mask those of iron oxides or biotite. If this is the case, that will hinder the upscaling of the results of this study.

Regarding the calcination stage, one of the aims of this study is to generate infrared-based tools to monitor the quality and the consistency of the feed for calcination. The same factors used in the characterisation of the kaolin ore are also of importance at this stage. After the beneficiation and upgrading of the ore, the spectra of the feed for calcination correspond to that of pure kaolinite. However, complementary analyses reveal that other clay minerals and iron are still present, although in a reduced proportion. A study carried out in a similar set of samples showed that in mixtures with kaolinite, iron oxides become detectable in the spectra in concentrations higher than 0.9 wt% (Guatame-García and Buxton, 2015). After going through the beneficiations steps, the kaolin feed typically has iron concentrations below this value, and consequently, it is not captured in the spectra. However, if the iron content increases it will be undoubtedly noticed.

Contrary to expectations, the presence of other clay minerals does not seem to affect the spectral determination of the kaolinite crystallinity using the Kx index, supporting its use in the characterisation of the feed for calcination. The index provides with a qualitative measure that can be easily used to establish quality thresholds to inform the process.

In the samples obtained from the processing plant, it is observed that after beneficiation there is a limited range of feed variability. This finding suggests that there is not a real need for implementing online monitoring for the feed, especially when the ore that feeds the processing plant comes from the same section of a deposit. A tool to guarantee consistency would be more useful in cases where the feed for calcination is made by the blending of ores extracted from different deposits or beneficiated at different processing plants. Even though that is not the current situation, it is expected that in the future the blending of ores will become a common practice (Imerys Minerals, Ltd., personal communication May 24, 2017).

For the final stage of the process, the aim is to develop a measurement that could serve as a proxy to the parameters that determine the quality of the product. One of the quality parameters for calcined kaolin products is the reactivity as per measured by the solubility of Al_2O_3. After the characterisation of the calcination reaction, it is possible to ascertain the features and regions of the spectra that hold a correlation with the quality standard. From those results and by implementing chemometric strategies, it is feasible to develop predicting models for the indirect measurement of soluble Al_2O_3 content. This measurement does not seek to replace the standard procedure, but to enable operational feedback. Although the method was only tested off-line, the expectation is that its implementation would reduce the feedback from days to less than an hour. Additionally, the result can be integrated into the furnace control strategy to influence operational decision-making. This result is a clear example of how the use of real-time sensor-based data can have an actual impact on the process.

All the final product samples were obtained from a stream in a processing plant. It is noticed that the soluble Al_2O_3 content in most of the samples goes far below the accepted threshold for this parameter. This fact limits the opportunity of getting production data that genuinely reflects the critical window for calcination, and limits the possibilities of generating a better solution, that is to say, a more representative model. Nevertheless, this situation evidences the magnitude of the concern regarding the soluble Al_2O_3 problem, where the production decisions are risking the over-calcination of the product, rather than generating one that is under-calcined and too reactive. This situation highlights the importance of this study and the need for its implementation.

11.2.2. GENERATION OF PROCESS AIDS FOR FILTRATION AND ABSORPTION FROM PERLITE AND DIATOMITE

Even though perlite and diatomite share the same properties for the final product, their origin is totally different. Therefore, the factors that affect the quality of the raw ore differ considerably. Consequently, the methods for the characterisation of the ore should be particular for each commodity.

The main factor that degrade the quality of the studied perlite ore is the presence of heavy metals. In addition, although not directly related to the quality of the perlite products, the generation of fine particles during processing is problematic for the pro-

cessing activities. These two issues are addressed from a mineralogical perspective with the aid of the infrared spectra. Opal, which is the main constituent of the ore, has a characteristic infrared response as well as the minerals typically associated with it (e.g. smectites, zeolites). Despite these associations, the aspect of the perlite mine face is homogeneous. The infrared spectra make detectable mineralogical changes that otherwise were not considered before for this deposit. Moreover, the discrimination of the dominant mineralogy by the developing of a spectral index gives insights on the likelihood of the ore of producing fine particles and enables the correlation between mineralogy and chemical impurities by implementing chemometric methods.

The concept of monitoring of quality of the feed for calcination does not apply to the perlite ore. The material fed into the calciner is mostly opal since the clay fraction is discarded as waste after the particle size reduction. With a mono-mineral phase, it is not possible to give further insights about the heavy metal content based solely on the infrared spectra. Likewise, the quality parameters for the calcined product are related to the physical expansion of the perlite, which cannot be measured using infrared spectroscopy.

It should be noted that the occurrence of the factors addressed here and their relationship with the ore are specific for this deposit. Their occurrence does not correspond to a phenomenon common to perlite ores in general. Therefore these results cannot be directly extrapolated to other perlite deposits. However, the fact that the minerals typically associated with perlite ores (e.g. zeolites and other clay minerals) have also a positive spectral response in the same infrared region would permit to follow the same methodology used in this study for other deposits.

In the diatomite ore, the main factor that reduces the quality of the product is the presence of carbonates, which are also have characteristic features in the infrared spectrum. In this case, the observations of the infrared spectra are accompanied by chemical analyses that permit to develop qualitative correlations and microscopic techniques that enable the establishment of textural relationships with the carbonate content. By using multivariate statistics, it is possible to classify the ore in quality grades according to the carbonate content and associate the grades with textural associations. These last results, in particular, have the most significant potential to improve the rest of the value chain since such information can be used to influence the decisions made in further processing stages.

The quality grade classification could also be used for ensuring the consistency of the feed of the calciner. Moreover, due to the spectral characteristics of the opaline and carbonate phases it is possible to develop quantitative analyses, should a more precise determination of carbonate content is required. Meyer-Jacob et al. (2014) developed quantitative measurements for mixtures of carbonate and biogenic silica using Partial Least Squares regression (PLS-R). Such an approach would be certainly applicable to this diatomite ore enabling the systematic analysis for the consistency of the feed for calcination by, for example, assisting the blending of ores with different qualities. Depending on the precision of a quantitative prediction, it could be useful to check the quality of the calcined product in regards to the carbonate content as well. Likewise to the perlite case, the infrared spectra cannot infer the pore and particle size quality parameters.

11.2.3. USE OF DATA DERIVED FROM INFRARED SPECTROSCOPY TO IMPROVE THE RESOURCE EFFICIENCY IN THE MINING AND PROCESSING OF INDUSTRIAL MINERALS

The use of data derived from infrared sensors in the three proposed case studies enables the identification of factors that can hinder the quality of calcined products directly at the deposit, prior to mining, as well as at the calcination stage. The use of infrared sensors permits the timely detection of those factors creating opportunities to improve the resource efficiency in the mining and processing of kaolin, perlite and diatomite. The results from this research also open new possibilities for the optimisation of such processes in other industrial minerals.

The possibilities of detecting factors that reduce the quality of the ores using infrared sensors depend in the relationship that they can bear with the infrared spectra. Most of the mineral impurities that are problematic in the case studies are captured in the infrared spectra (e.g. clay minerals in kaolinite and perlite, carbonates in diatomite). The successful identification of the mineral impurities depends upon the proportion or concentration of the mineral species, the possible spectral mixtures with the mineral that describes the ore, and the selection of an adequate spectral range that facilitates their differentiation. The creation of a method for the systematic pinpointing of mineral impurities from the infrared spectra includes the extraction of mineral indices, extraction of individual features and multivariate calibration.

For the identification of impurities related to chemical elements, it is necessary to assess their possible associations with the mineralogy of the ore. For doing this, it is required to integrate data derived from other analytical techniques. Data integration is also indispensable when a qualitative association between ore and impurities wants to be determined. To establish a link between the infrared spectra and data from other sources it is necessary to implement multivariate calibration techniques. Regarding the determination of the ore attributes, quality parameters can be extracted from the infrared spectra as long as they are directly or indirectly related to the crystal structure of the mineral.

The determination of quality parameters of the ore directly at the pit can be executed by characterising run-of-mine samples, drill cores and mine faces. At the deposit, where exploration and mining planning tasks are carried out, the real-time concept enables the use of techniques that require some time for data collection and processing, as is the case of hyperspectral images. The use of images is particularly useful in the cases where high texture variability is expected. In less complex ores with less or predictable variability, only point data is sufficient.

The aim of developing infrared-based tools for the monitoring of the feed for calcination is to ensure high quality and consistency. At this stage, the parameters that determine the quality are similar to those identified in the raw ore. However, since the ore has passed through various stages of beneficiation, the concentration of mineral impurities is drastically reduced. Moreover, beneficiation plants generate feeds that are mostly homogeneous. For this reason, the characterisation of the feed for calcination is more convenient when it is composed by ores coming from different deposits or different beneficiation plants. In this situation, rather than implementing a monitoring tool, a sensor-based assisted blending programme would add more value to the process.

The development of infrared-based measurements that serve as a proxy to quality parameters of the calcined product has two major requirements. First, an understanding of the ore transformations occurred during the thermal processing. Second, an interpretation of how the infrared spectrum registers such transformations. In the kaolin case, even though the ore has well defined spectral features, the spectral response of the calcined product as a consequence of the thermal transformation is entirely different. Moreover, the quality parameter itself is not detectable in the infrared spectrum. In this case, less obvious correlations need to be established between the quality parameter, properties associated with it, and their response in the spectra. The result is an indirect measurement that requires advanced chemometric techniques to establish reliable correlations. In such a relationship, it is necessary to assess other factors that can influence the measurements to avoid misinterpretations of the data.

In perlite and diatomite, the quality parameters of the calcined product cannot be directly measured in the infrared spectra either. Based on the approach used for the calcined kaolin, it would be possible to explore opportunities for creating proxies. For example, the amount of water lost during thermal expansion could be used as an indicator of the calcination extent and be indicative of the structure of the calcined product. However, in this case, the techniques that are already implemented for the detection of these parameters are sufficient, and there is not a real need for the development of new ones.

Unlike metallic ores, in many industrial minerals the ore itself is active in the infrared spectrum. Consequently, the present study raises the possibility of using the various approaches used in the investigation of kaolinite, perlite and diatomite ores for the optimisation of processes in other industrial mineral commodities. For calcined industrial minerals, in particular, the methods for extracting information from infrared data can be used for the development of tools that measure the quality of ores and calcination products. The industrial minerals that are more suitable for the implementation of infrared techniques are those that contain hydroxyl, carbonate or sulphate groups in the structure of the minerals that integrate the ore, which are the structural units that are more sensitive to thermal transformations. Examples of these are the calcination of bauxite for the production of alumina (Hill and Sehnke, 2006), clay minerals to produce fuller's earth and refractory clays (Harvey et al., 2006; Pickering and Heivilin, 2006), carbonates such as calcite and dolomite for the production of lime, and magnesite to generate magnesium oxide (Fulton, 2006), and gypsum and anhydrite for the production of plaster (Sharpe and Cork, 2006). There is also a particular interest for the analysis of non-calcined minerals regarding the availability of alumina in bauxite (Eyer, 1999) and in natural kaolin.

Essentially, the detection of factors that affect the quality of industrial mineral ores in the generation of calcined products seeks to improve the efficiency of the resource. Such an improvement is made not only by targeting the production of a high-quality product but also by optimising the performance of the processes carried out at different stages in the value chain. The implementation of sensor-based techniques as proposed by this research would have a positive impact in the industrial minerals sector regarding the following aspects:

- Better use of the natural resource, by supporting selective mining that enables the preferable extraction of ores with the desired properties, enabling the use of low-

grade or sub-economic deposits, therefore expanding the resource, and limiting the amount of waste material.

- The pre-selection or upgrading of the ore optimises the beneficiation steps by reducing the throughput to the processing plant and reducing the consumption of other resources, most importantly of water
- The minimisation of health risks generated by the by-products of mineral processing, such as small particles
- The optimisation of the energy consumption in the calciner, by timely reporting changes in the quality of the calcined product
- The reduction of the CO_2 emissions in the calciner, not only by the improvement of energy consumption but also by avoiding the unnecessary calcination of minerals that produce CO_2.

11.3. METHODS EMPLOYED IN THIS WORK: SOME CONSIDERATIONS

Three main arguments motivated the use of infrared spectroscopy as the core technique of this research. First, the potential that it has to be used directly at mining and processing operations. Second, the ability to extend the observations almost seamlessly from laboratory data to portable spectrometers and hyperspectral imagers. Third, the capability of not only identify several mineral specimens but also to retrieve information about their crystal structure, including amorphous phases. The latter aspect had particular throughout this work. In two of the commodities subject of this study, perlite and diatomite, the ore rather than a crystalline material is an amorphous substance that is difficult to characterise with other techniques. Regarding the calcination process, the thermal treatment implies transformations where the material passes through amorphous phases, as is the case of the transformation of kaolinite into metakaolinite.

Other analytical techniques that have been developed for online or and-site mineral identification include X-ray diffraction (XRD), laser-induced fluorescence (LIF) and Raman (Dalm, 2018). X-ray diffraction is perhaps one of the most used laboratory techniques for mineral identification, and the development of portable devices has extended its capabilities for in-the-field operations (XPLOREX, 2017). However, the use of XRD is mostly limited to crystalline materials, and the analysis of amorphous phases requires complex calibration sets and careful data processing. Laser-induced fluorescence measures the fluorescence spectrum of minerals that are irradiated with an ultraviolet (UV) laser; the spectrum has structure-specific fingerprints that enable mineral identification. Different LIF spectrometers, drill-core scanners and imagers have been developed mostly for coal applications. The LIF spectrum, and therefore the distinction of features, is more complex than the reflectance one; the LIF technique is also very sensitive to impurities and often requires site-specific calibrations (Kauppinen et al., 2014). Raman spectroscopy is a powerful tool for mineral analysis; the Raman spectrum is similar to the reflectance one in that both of them are based on vibrational spectroscopy. However, the Raman spectrum can be easily overwhelmed by the fluorescence of the material depending on the

wavelength of the laser used as energy source. As a point-wise measurement technique, Raman can be used for imaging (SciAps, 2013) although it is slow and not suitable for online scanning (Kauppinen et al., 2014).

This research also shows the advantage of exploring broad spectral ranges. Traditionally, due to the availability of commercial instruments, on-site applications for infrared spectroscopy are limited to the short-wavelength infrared (SWIR) range, where there is overlapping of secondary spectral features. This research also uses also the mid-wavelength infrared (MWIR) range extensively, which so far has been a less explored technique for on-site applications. Unlike the SWIR, the MWIR range captures fundamental features, some of them located at different wavelengths. The selection of the spectral range should depend upon the purpose of the analysis. For example, in the diatomite case, the opal features in the SWIR range mask completely those of the carbonate making it not possible to detect it. In the MWIR range, the features of the two minerals occur at different wavelengths facilitating the analysis. In contrast, in the perlite case, the overlapping of opal and montmorillonite features in the SWIR enables the visualisation of the transition from one mineral to the other, which can be measured by an index. A similar index developed in the MWIR would have to be more elaborated since montmorillonite presents multiple fundamental features in a narrow wavelength range making the analysis more complex.

In many cases, the parameters of interest can be directly retrieved from the infrared spectra, for example, mineral impurities that have characteristic spectral features. For them, the interpretation of the data can be deemed reliable. In other situations, it is necessary to construct more elaborated correlations between the parameters and the spectra, by using data from other sources. To this end, it is essential to understand the spectra and the phenomena that are under study. Only by having this knowledge as a fundamental part of the analysis it is possible to extract meaningful information by the implementation of chemometric techniques such as Principal Component Analysis (PCA), Partial Least Squares regression (PLS-R) or Support Vector Machine methods (SVM). Chemometrics is the most useful approach to relate the spectra to other parameters; it also has the advantage of enabling the development of models to utilise or replicate the information generated from the spectral analyses.

Even though this research used data from other sources only for laboratory calibration, it is also possible to generate more robust methods by integrating the infrared data with measurements retrieved from other online sensors through data fusion (Desta and Buxton, 2018; Khajehzadeh et al., 2017). The mineralogical characterisation is usually enhanced by integrating information related to the chemical composition of the material. Some of the techniques that can complement online and on-site infrared reflectance measurements are X-ray diffraction (XRF), laser-induced breakdown spectroscopy (XRF) and neutron activation analysis (NAA) (Dalm, 2018). From these techniques, XRF is the one that has had more significant development, more instruments that range from hand-held devices and drill-core scanners (Sjöqvist et al., 2015). The development online LIBS analysers, which includes hand-held instruments and imagers, is currently proliferating (Kuhn et al., 2016; Rifai et al., 2018). LIBS offers semi-quantitative analysis and enables the identification of a broader range of elements than XRF. The neutron analysis techniques, prompt gamma neutron activation analysis (PGNAA) and pulsed fast thermal neutron

activation (PFTNA), are in nature similar to XRF, although they offer the advantage of collecting volume rather than surface data (PANalytical, 2009).

For mining and processing operations, the use of infrared spectroscopy –and the models or measurements derived from it– as part of the analytical routines would offer the advantages of creating permanent records of samples that inevitably will be destroyed, transformed or transferred to customers. These records can be revisited when needed for quality checks, detection of trends in a defined period, or for the extraction of new information that was not considered during the initial analyses.

11.4. PERSPECTIVES AND LIMITATIONS

Even though the results presented in this Thesis provide a contribution for the industrial minerals sector, they do not offer universal solutions for all the commodities. Strictly speaking, due to the geological variations of each deposit, the results are site-specific. Therefore, the extrapolation of the findings of this work to the same commodities but from different locations requires a re-calibration of the methodology to the geological context of the deposit. In a similar way, the results are also product-specific and process-specific. As pointed out along this work, the processes are tailored to meet the particular needs of the markets, which in turn are very dynamic depending upon many factors such as the development of new applications, economics and even politics. For this reason, it is plausible that the parameters of analysis and the processes described here are subject to change in the future. Nevertheless, that scenario does not diminish the importance of this work, since its most important value relies on the methodological approach, which can be adapted to different commodities, processes and emerging applications. The versatility of the methodological approach is favourable in the industrial minerals sector since, commonly, one mineral serves several applications, or a specific application can take advantage of various minerals.

Regarding the economic aspect, industrial minerals are valued regarding the volume and tonnage of the production. Figure 11.1 shows the average price of natural and calcined kaolin, crude and expanded perlite, and natural DE and filter-grade diatomite for the period 2006-2015. In this period, the beneficiation process brought in average an added value of 533 % for calcined kaolin over the unprocessed product, 681 % for expanded perlite over crude perlite and 35 % for filter-grade perlite over the average unprocessed product. Following the prices of the commodities, these numbers suggest that the identification of factors that determine the quality of the final products would have a more significant impact in the production of calcined kaolin and expanded perlite than in the production of diatomaceous earth.

The commodity price of calcined kaolin has seen a decrease in the last years due to difficult conditions on the paper market –i.e., substitution for other products–. This situation has fostered the expansion of speciality applications to increase the revenue of the calcined products (IMERYS, 2018*a*). The soluble Al_2O_3 parameter is particularly important to ensure the added value of some speciality products. Consequently, the method for the infrared measurement of soluble Al_2O_3 developed in Chapters 6 and 7 has a big scope to support the expansion of the speciality applications. The Devon calciner, which was the subject of this study, produces more than 50 000 t of calcined kaolin per year (Imerys Minerals Ltd., personal communication January 12, 2017). The implementation of a

system currently priced at ±€60000 (Agilent Technologies, personal communication June 2016) could result in sufficient enhanced quality of the calcined product and optimisation of the production, resulting in a positive outcome regarding cost-utility. Nevertheless, a techno-economic assessment should be carried out to indicate more precisely the actual cost-benefit of such implementation.

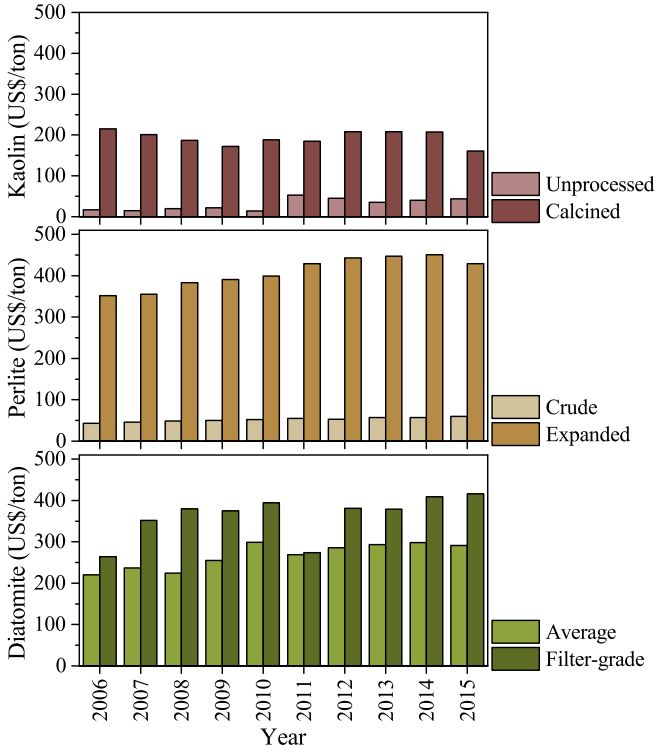

Figure 11.1: Commodity prices of natural and calcined kaolin, crude and expanded perlite, and natural DE and filter-grade diatomite for the period 2006-2015. Sources: **Kaolin:** 2006: Virta (2008), 2007: Virta (2010*a*), 2008: Virta (2010*b*), 2009: Virta (2011), 2010: Virta (2012), 2011: Virta (2013), 2012: Virta (2016), 2013: Virta (2015), 2014: Flanagan (2017), 2015: Flanagan (2018). **Perlite:** 2006: Bolen (2010*a*), 2007: Bolen (2010*a*), 2008: Bolen (2010*b*), 2009: Bolen (2011), 2010: Bolen (2012), 2011: Bolen (2013), 2012: Bolen (2016), 2013: Bennett (2015), 2014: Bennet (2016), 2015: Bennett (2017). **Diatomite:** 2006: Founie (2007), 2007: Crangle (2010*a*), 2008: Crangle (2010*b*), 2009: Crangle (2011), 2010: Crangle (2012), 2011: Crangle (2013), 2012: Crangle (2016*a*), 2013: Crangle (2015), 2014: Crangle (2016*b*), 2015: Crangle (2016*c*).

As for the possibility of using an infrared-based in-pit material characterisation of the kaolin ore, first, it is necessary to evaluate whether the observations performed on drill-cores and rock samples using hyperspectral imagers can be extended to face mapping. Based on this, the suitability of acquiring the respective instruments can be considered. In addition, even though this work focused on in-pit characterisation targeting specific products, at this stage of the mining value chain the in-pit analysis can also serve multiple end-products and markets, for example, the production of natural kaolin for ceramics. In this way, the broader scope of the in-pit characterisation should also be considered in a

cost-benefit assessment.

The performance additives business, in particular the applications for filtration, have seen continuous growth in the recent years (Figure 11.1), mainly due to the development of new products for applications like cosmetics and agriculture (IMERYS, 2018*a*). Regarding perlite production, the Zeytindağ deposit feeds a processing plant for the production of crude perlite that has an annual capacity of 100 000 t (Barker and Santini, 2006; IMERYS, 2018*b*). The relatively low prices of the commodities at first glance would discourage the implementation of a costly technique. However, the volume of the production and the market perspectives suggest that optimisation of the process following the results presented in Chapter 9 might lead to a significant increment of the revenue. As for the diatomite production, the Elche de la Sierra deposit feeds a processing plant located in Alicante (Spain) which has an annual capacity of 30 000 t (IGME, 2017; IMERYS, 2018*b*). The plant is also fed with material from other diatomite deposits, indicating that the volume of the production in Elche de la Sierra is rather small. In this case, the possibilities of implementing an infrared in-pit characterisation system might be constrained by the size of the operation. Likewise on the kaolin case, the implementation of the results of this work in the production of perlite and diatomite should follow a thorough techno-economic assessment.

REFERENCES

Barker, J. M. and Santini, K. (2006), Perlite, *in* J. E. Kogel, N. C. Trivedi, J. M. Barker and S. T. Krukowski, eds, 'Industrial Minerals and Rocks', 7th edn, Society for Mining, Metallurgy, and Exploration, pp. 685–702.

Bennet, S. M. (2016), Perlite, *in* '2014 Minerals yearbook', USGS, pp. 55.1–55.4.
URL: *https://minerals.usgs.gov/minerals/pubs/commodity/perlite/myb1-2014-perli.pdf [Accessed January 2019]*

Bennett, S. M. (2015), Perlite, *in* '2013 Minerals yearbook', USGS, pp. 55.1–55.5.
URL: *https://minerals.usgs.gov/minerals/pubs/commodity/perlite/myb1-2013-perli.pdf [Accessed January 2019]*

Bennett, S. M. (2017), Perlite, *in* '2015 Minerals yearbook', USGS, pp. 55.1–55.4.
URL: *https://minerals.usgs.gov/minerals/pubs/commodity/perlite/myb1-2015-perli.pdf [Accessed January 2019]*

Bolen, W. P. (2010*a*), Perlite, *in* '2007 Minerals yearbook', USGS, pp. 55.1–55.4.
URL: *https://minerals.usgs.gov/minerals/pubs/commodity/perlite/myb1-2007-perli.pdf [Accessed January 2019]*

Bolen, W. P. (2010*b*), Perlite, *in* '2008 Minerals yearbook', USGS, pp. 55.1–55.4.
URL: *https://minerals.usgs.gov/minerals/pubs/commodity/perlite/myb1-2008-perli.pdf [Accessed January 2019]*

Bolen, W. P. (2011), Perlite, *in* '2009 Minerals yearbook', USGS, pp. 55.1–55.4.
URL: *https://minerals.usgs.gov/minerals/pubs/commodity/perlite/myb1-2009-perli.pdf [Accessed January 2019]*

Bolen, W. P. (2012), Perlite, *in* '2010 Minerals yearbook', USGS, pp. 55.1–55.4.
URL: *https://minerals.usgs.gov/minerals/pubs/commodity/perlite/myb1-2010-perli.pdf [Accessed January 2019]*

Bolen, W. P. (2013), Perlite, *in* '2011 Minerals yearbook', USGS, pp. 55.1–55.4.
URL: *https://minerals.usgs.gov/minerals/pubs/commodity/perlite/myb1-2011-perli.pdf [Accessed January 2019]*

Bolen, W. P. (2016), Perlite, *in* '2012 Minerals yearbook', USGS, pp. 55.1–55.4.
URL: *https://minerals.usgs.gov/minerals/pubs/commodity/perlite/myb1-2012-perli.pdf [Accessed January 2019]*

Crangle, R. D. (2010*a*), Diatomite, *in* '2007 Minerals yearbook', USGS, pp. 22.1–22.6.
URL: *https://minerals.usgs.gov/minerals/pubs/commodity/diatomite/myb1-2007-diato.pdf [Accessed January 2019]*

Crangle, R. D. (2010*b*), Diatomite, *in* '2008 Minerals yearbook', USGS, pp. 22.1–22.6.
URL: *https://minerals.usgs.gov/minerals/pubs/commodity/diatomite/myb1-2008-diato.pdf [Accessed January 2019]*

Crangle, R. D. (2011), Diatomite, *in* '2009 Minerals yearbook', USGS, pp. 22.1–22.6.
URL: *https://minerals.usgs.gov/minerals/pubs/commodity/diatomite/myb1-2009-diato.pdf [Accessed January 2019]*

Crangle, R. D. (2012), Diatomite, *in* '2010 Minerals yearbook', USGS, pp. 22.1–22.6.
URL: *https://minerals.usgs.gov/minerals/pubs/commodity/diatomite/myb1-2010-diato.pdf [Accessed January 2019]*

Crangle, R. D. (2013), Diatomite, *in* '2011 Minerals yearbook', USGS, pp. 22.1–22.5.
URL: *https://minerals.usgs.gov/minerals/pubs/commodity/diatomite/myb1-2011-diato.pdf [Accessed January 2019]*

Crangle, R. D. (2015), Diatomite, *in* '2013 Minerals yearbook', USGS, pp. 22.1–22.5.
URL: *https://minerals.usgs.gov/minerals/pubs/commodity/diatomite/myb1-2013-diato.pdf [Accessed January 2019]*

Crangle, R. D. (2016*a*), Diatomite, *in* '2012 Minerals yearbook', USGS, pp. 22.1–22.6.
URL: *https://minerals.usgs.gov/minerals/pubs/commodity/diatomite/myb1-2012-diato.pdf [Accessed January 2019]*

Crangle, R. D. (2016*b*), Diatomite, *in* '2014 Minerals yearbook', USGS, pp. 22.1–22.5.
URL: *https://minerals.usgs.gov/minerals/pubs/commodity/diatomite/myb1-2014-diato.pdf [Accessed January 2019]*

Crangle, R. D. (2016*c*), Diatomite, *in* '2015 Minerals yearbook', USGS, pp. 22.1–22.5.
URL: *https://minerals.usgs.gov/minerals/pubs/commodity/diatomite/myb1-2015-diato.pdf [Accessed January 2019]*

Dalm, M. (2018), Raw material beneficiation in mining – sensor-based sorting opportunities for hydrothermal ore deposits, PhD thesis, Delft University of Technology.
URL: *https://repository.tudelft.nl/islandora/object/uuid[Accessed November 2018]*

Desta, F. S. and Buxton, M. W. N. (2018), Automation in sensing and raw material characterization - a conceptual framework, *in* '2018 IEEE/RSJ International Conference on Intelligent Robots and Systems (IROS)', pp. 1501–1506. DOI: 10.1109/IROS.2018.8593774

Ellis, R. J. and Scott, P. W. (2004), 'Evaluation of hyperspectral remote sensing as a means of environmental monitoring in the St. Austell China clay (kaolin) region, Cornwall, UK', *Remote Sensing of Environment* **93**, pp. 118–130.

Eyer, S. L. (1999), Estimating bauxite quality using FITR spectroscopy and multivariate calibration, *in* 'Proceedings of the Fifth International Alumina Quality Workshop', Vol. 1, pp. 86–95.

Flanagan, D. M. (2017), Clay and shale, *in* '2014 Minerals yearbook', USGS, pp. 18.1–18.23.
URL: *https://minerals.usgs.gov/minerals/pubs/commodity/clays/myb1-2014-clays.pdf [Accessed January 2019]*

Flanagan, D. M. (2018), Clay and shale, *in* '2015 Minerals yearbook', USGS, pp. 18.1–18.27.
URL: *https://minerals.usgs.gov/minerals/pubs/commodity/clays/myb1-2015-clays.pdf [Accessed January 2019]*

Founie, A. (2007), Diatomite, *in* '2006 Minerals yearbook', USGS, pp. 22.1–22.6.
URL: *https://minerals.usgs.gov/minerals/pubs/commodity/diatomite/myb1-2006-diato.pdf [Accessed January 2019]*

Fulton, R. B. (2006), Chemicals, *in* J. E. Kogel, N. C. Trivedi, J. M. Barker and S. T. Krukowski, eds, 'Industrial Minerals and Rocks', 7th edn, Society for Mining, Metallurgy, and Exploration, pp. 295–308.

Guatame-García, A. and Buxton, M. (2015), Visible and infrared reflectance spectroscopy for characterization of iron impurities in calcined kaolin clays, *in* J. Beyerer, F. Puente-Leon and T. Laengle, eds, 'OCM 2015 – Optical characterization of materials', Vol. 2, KIT Scientific Publishing, pp. 215–226.

Harvey, C. C., Headrick, W. L. and Hemrick, J. G. (2006), Refractory clays, *in* J. E. Kogel, N. C. Trivedi, J. M. Barker and S. T. Krukowski, eds, 'Industrial Minerals and Rocks', 7th edn, Society for Mining, Metallurgy, and Exploration, pp. 407–413.

Hill, V. G. and Sehnke, E. D. (2006), Bauxite, *in* J. E. Kogel, N. C. Trivedi, J. M. Barker and S. T. Krukowski, eds, 'Industrial Minerals and Rocks', 7th edn, Society for Mining, Metallurgy, and Exploration, pp. 227–261.

IGME (2017), 'Panorama minero - Diatomita y Trípoli 2016', Online. Instituto Geológico y Minero de Espaã.
URL: *http://www.igme.es/PanoramaMinero/PMLin.htm [Accessed March 2019]*

IMERYS (2018*a*), 2018 Half-year financial report, Technical report, Imerys Minerals, Ltd. Online.
URL: *https://www.imerys.com/ [Accessed March 2019]*

IMERYS (2018*b*), 'IMERYS Filtration division', Online.
URL: *https://imerys-filtration.com/europe-middle-east-and-africa/about-us/filtration-operations/ [Accessed March 2019]*

Kauppinen, T., Khajehzadeh, N. and Haavisto, O. (2014), 'Laser-induced fluorescence images and Raman spectroscopy studies on rapid scanning of rock drill-core samples', *International Journal of Mineral Processing* **132**, pp. 26–33. DOI: 10.1016/j.minpro.2014.09.003

Khajehzadeh, N., Haavisto, O. and Koresaar, L. (2017), 'On-stream mineral identification of tailing slurries of an iron ore concentrator using data fusion of LIBS, reflectance spectroscopy and XRF measurement techniques', *Minerals Engineering* **113**, pp. 83–94. DOI: 10.1016/j.mineng.2017.08.007

Kuhn, K., Meima, J. A. , Rammlmair, D. and Ohlendorf, C. (2016), 'Chemical mapping of mine waste drill cores with laser-induced breakdown spectroscopy (LIBS) and energy dispersive X-ray fluorescence (EDXRF) for mineral resource exploration', *Journal of Geochemical Exploration* **161**, pp. 72–84. DOI: 10.1016/j.gexplo.2015.11.005

Meyer-Jacob, C., Vogel, H. , Boxberg, F. , Rosén, P. , Weber, M. E. and Bindler, R. (2014), 'Independent measurement of biogenic silica in sediments by FTIR spectroscopy and PLS regression', *Journal of Paleolimnology* **52**(3), pp. 245–255. DOI: 10.1007/s10933-014-9791-5

PANalytical (2009), 'Pulsed Fast Thermal Neutron Activation (PFTNA)', Online.
URL: *https://www.malvernpanalytical.com/en/products/technology/ [Accessed March 2019]*

Pickering, S. M. and Heivilin, F. G. (2006), Clays - Fuller's Earth, *in* J. E. Kogel, N. C. Trivedi, J. M. Barker and S. T. Krukowski, eds, 'Industrial Minerals and Rocks', 7th edn, Society for Mining, Metallurgy, and Exploration, pp. 373–381.

Rifai, K., Doucet, F. , Özcan, L. and Vidal, F. (2018), 'LIBS core imaging at kHz speed: Paving the way for real-time geochemical applications', *Spectrochimica Acta Part B: Atomic Spectroscopy* **150**, pp. 43–48. DOI: 10.1016/j.sab.2018.10.007

SciAps (2013), 'Instant in-field chemical and mineral ID', Online.
URL: *https://www.sciaps.com/ [Accessed March 2019]*

Sharpe, R. and Cork, G. (2006), Gypsum and anhydrite, *in* J. E. Kogel, N. C. Trivedi, J. M. Barker and S. T. Krukowski, eds, 'Industrial Minerals and Rocks', 7th edn, Society for Mining, Metallurgy, and Exploration, pp. 519–540.

Sjöqvist, A. S. L., Arthursson, M. , Lundström, A. , Estrada, E. Calderón , Inerfeldt, A. and Lorenz, H. (2015), 'An innovative optical and chemical drill core scanner', *Scientific Drilling* **19**, pp. 13–16. DOI: 10.5194/sd-19-13-2015

Virta, R. L. (2008), Clay and shale, *in* '2006 Minerals yearbook', USGS, pp. 18.1–18.24.
URL: *https://minerals.usgs.gov/minerals/pubs/commodity/clays/myb1-2006-clays.pdf [Accessed January 2019]*

Virta, R. L. (2010*a*), Clay and shale, *in* '2007 Minerals yearbook', USGS, pp. 18.1–18.23.
URL: *https://minerals.usgs.gov/minerals/pubs/commodity/clays/myb1-2007-clays.pdf [Accessed January 2019]*

Virta, R. L. (2010*b*), Clay and shale, *in* '2008 Minerals yearbook', USGS, pp. 18.1–18.26.
URL: *https://minerals.usgs.gov/minerals/pubs/commodity/clays/myb1-2008-clays.pdf [Accessed January 2019]*

Virta, R. L. (2011), Clay and shale, *in* '2009 Minerals yearbook', USGS, pp. 18.1–18.23.
URL: *https://minerals.usgs.gov/minerals/pubs/commodity/clays/myb1-2009-clays.pdf [Accessed January 2019]*

Virta, R. L. (2012), Clay and shale, *in* '2010 Minerals yearbook', USGS, pp. 18.1–18.24.
URL: *https://minerals.usgs.gov/minerals/pubs/commodity/clays/myb1-2010-clays.pdf [Accessed January 2019]*

Virta, R. L. (2013), Clay and shale, *in* '2011 Minerals yearbook', USGS, pp. 18.1–18.20.
URL: *https://minerals.usgs.gov/minerals/pubs/commodity/clays/myb1-2011-clays.pdf [Accessed January 2019]*

Virta, R. L. (2015), Clay and shale, *in* '2013 Minerals yearbook', USGS, pp. 18.1–18.22.
URL: *https://minerals.usgs.gov/minerals/pubs/commodity/clays/myb1-2013-clays.pdf [Accessed January 2019]*

Virta, R. L. (2016), Clay and shale, *in* '2012 Minerals yearbook', USGS, pp. 18.1–18.23.
URL: *https://minerals.usgs.gov/minerals/pubs/commodity/clays/myb1-2012-clays.pdf [Accessed January 2019]*

XPLOREX (2017), 'The planet. Portable high-resolution X-ray powder diffraction', Online.
URL: *https://aspectus-gmbh.com/portable-xrd.html [Accessed March 2019]*

12

CONCLUSIONS AND RECOMMENDATIONS

The last chapter of this Thesis presents the general conclusions about the use of infrared spectroscopy for the characterisation of industrial minerals, and the particular applications in the mining and processing of kaolin, perlite and diatomite. The chapter also presents recommendations for further research as well for the implementation of the results of this work.

12.1. CONCLUSIONS

USE OF INFRARED SPECTROSCOPY IN INDUSTRIAL MINERALS

The properties of ores, feed and calcined products can be satisfactorily measured with the use of infrared spectroscopic techniques. Direct measurement of the relevant parameters can be performed when they are related to mineral composition or mineral structure. They are identified by the extraction of features that are particular for the minerals, or via the calculation of spectral indices. Other properties that are not detected straight from the spectra are inferred by establishing correlations between the spectra and data from other sources. For doing this, it is necessary to make use of chemometric methods that enable the development of new measurements or prediction models.

The ability to use data derived from infrared sensors to influence operational decision making in mining and processing depends upon the capability of collecting infrared measurements of good quality, with instruments that can work in in-the-field or in-the-plant conditions and that can generate data in real-time.

MINING AND PROCESSING OF KAOLIN

The factors that determine the ore quality of kaolin are iron-bearing mineralogy, clay minerals content and kaolinite crystallinity. All these factors are captured in the infrared spectra in the visible-near infrared and short-wavelength infrared ranges. Taking advantage of existing methods of feature extraction and spectral indices it is possible to retrieve the presence and distribution of the quality factors from hyperspectral images. Implementation of such a technique could assist with mine planning activities, having a positive impact in the water consumption and generation of waste.

For the feed for calcination, the factors that determine quality are the same ones as in the ore. However, the mineral content is predominantly kaolinite, and the occurrence of the other impurities is too low to be detected in the spectra. An existing spectral index in the short-wavelength infrared range measures the quality of the kaolinite, which is an essential parameter for the feed. The extraction of the index could assist with a proactive calcination control to enhance the performance of the furnace. The approach followed for the feed characterisation could be used to develop a sensor-based assisted blending program should ores from different deposits or different processing plants are combined.

Among the various parameters that determine the quality of the calcined kaolin product, the soluble Al_2O_3 content is of particular importance for some niche markets. The soluble Al_2O_3 content can be successfully estimated from the infrared spectra by making an indirect correlation between the soluble Al_2O_3 content and the presence of water in the calcined kaolin, as detected in the mid-wavelength infrared range. The prediction of the soluble Al_2O_3 content is made via Support Vector Regression methods. The measurement can be implemented to detect trends in the variation of the production of calcined kaolin. Its integration into the quality control strategy could give timely operational feedback to optimise the performance of the calciner. Such an optimisation could lead to a reduction in the energy consumption of the calciner, with an impact on the amount of CO_2 emissions.

MINING AND PROCESSING OF PERLITE AND DIATOMITE

Perlite and diatomite serve the same markets since the properties of their calcined products are similar, with opaline silica as the main constituent. However, their origin is entirely different as the parameters that define the quality of perlite and diatomite ores.

The quality of the perlite ore in the studied case is defined by the presence of heavy metals and by the possibility of generating fine particles during processing. These two parameters are estimated from the infrared spectra by determining the dominant mineralogy in the ore –opal or montmorillonite– with the aid of a spectral index developed in the short-wavelength infrared range. The implementation of this method in the mine site could be reflected in the amount of emission of fine particles and mine waste, at the time that it could advise the further beneficiation steps.

For the studied diatomite case, the presence of carbonate minerals defines the quality of the ore. The carbonates can be differentiated from the opal in the mid-wavelength infrared range. By integrating the spectral information with other types of data, it is possible to classify the ore based on the carbonate content by using Principal Component Analysis. The use of this classification in the mine site could assist with the development of a stock-pile and blending programme that optimises the beneficiation stages. Particularly, at the calcination stage, it could contribute to the reduction of CO_2 emissions by avoiding the unnecessary calcination or carbonate.

GENERAL CONCLUSION

The use of infrared spectroscopy has enabled the development of methods that detect some of the factors that determine or degrade the quality of calcined products of kaolin, perlite and diatomite. Such factors are most importantly detected at the pit, by characterising the ore, or at the calciner, by characterising the feed for calcination and the calcined products. It is at these two stages where the timely detection of factors has more influence in the process and where there is the most significant potential for process optimisation.

The factors that are subject of study in this Thesis, although specific for the presented commodities, represent the kind of challenges that can be found in other industrial minerals. Therefore, even though the results are specific for either kaolin, perlite or diatomite, the methodology used for the development of measurements and models can be adapted to other commodities. Their implementation in the different mining and processing operations could significantly contribute to the sustainable development in the minerals industry.

12.2. RECOMMENDATIONS

Some further studies would be required to take the results presented in this Thesis to a more mature level. The results of this research also raised some questions and challenges that could be addressed in future investigations.

- In the diatomite case, the results of the identification of carbonate suggested that by using chemometrics Partial Least Squares regression methods it would be possible to quantify the amount of carbonate for a more accurate quality grade classification. Due to the limited amount of samples available for this research, such quantification was not pursued. It would be therefore be recommended to attempt such

classification, including not only the parts of the deposit regarded as ore –as was the approach of this study– but also the layers that have higher carbonate content. The samples must also represent not only the vertical variations within the deposit but also lateral variations.

- In the discussion about the characterisation of the kaolin ore, attention was drawn to another study that used airborne hyperspectral images in the same deposit, but it did not identify iron-bearing minerals, unlike the hyperspectral images obtained from the drill cores and rock samples of this study. Should upscaling of the observations be desired to applications as, for example, face mapping, it is necessary to explore whether a change in the spatial resolution of the images –and to what extent– would hinder the identification of iron-bearing mineralogy.

- The discussion about the monitoring for the feed for calcination suggested that, instead of an infrared tool for monitoring, it would be more convenient to develop an infrared sensor-based assisted blending programme. For doing this, it is necessary to conduct experiments with the ores that could be potentially blended and, based on the parameters used in this work (spectral indices, specific features), determine a "formula" that will provide an optimum feed to the calciner.

- In the development of the proxy to the quality control standard in the production of calcined kaolin, it was pointed out that the production samples did not adequately represent the critical window where the soluble Al_2O_3 content goes above the accepted threshold. For a more accurate model and more reliable solution for the production, it is necessary to incorporate samples that include the undesired values and update the model once again.

- Notwithstanding that the model developed for the measurement of soluble Al_2O_3 seems to reduce the influence of environmental moisture, this work did not carry out controlled experiments to investigate this particular aspect. Therefore, in order to improve the confidence and reliability of the proposed measurement, and to maximise the benefits of the measuring system in the in-plant decision making, it is highly recommended to design and perform experiments that simulate the environmental conditions of the operations and use the results to optimise the soluble Al_2O_3 model.

- Even though the infrared instruments used for conducting this research are portable, a full on-site implementation of the methods proposed in this work requires adapting the spectrometers to the mine operations. The most promising application is the analysis of the calcined kaolin product. Adapting the spectrometer for this set-up would require a system to collect and present the samples to the instrument, protection of the spectrometer head to avoid the need for constant cleaning, protection against dust –which is abundant at the operations–, and protection against humidity or moisture, to minimise the influence from the environment. The full automation of the system would require major design modifications of the instrument to make it more robust and autonomous.

- After implementing the optimisation of the model for the measurement of soluble Al_2O_3 and the adaptation of the infrared system, according to the previous recommendations, the next step would be the development of protocols to embed the infrared measurement of soluble Al_2O_3 as an alternative technique to the standard operational procedure, which could be formally used for quality reporting.
- The results of this work serve as an example of the methodologies that are applicable to other industrial minerals. Some of them were identified in Section 11.1. It would be worth to explore the applicability of the methods proposed in this work.
- The general discussion pointed out that a challenge for the implementation of infrared sensors in the mining and processing operations would be related to the costs that it entails. Therefore, a techno-economic assessment of the feasibility for the implementation of the technique and the methods presented in this Thesis is highly recommended. Such a techno-economic assessment should take into account, for example, the prices and market trends of the commodities, the volume of the production, the costs related to the acquisition and modification/installation and maintenance of the technology, the calibration costs and the impact in other parts of the processing activities.

ACKNOWLEDGEMENTS

The days I spent working on my MSc thesis were so rewarding that I thought it would be a good idea to take that experience one step further... so I decided to start a PhD. I definitely had no idea what I was getting into. The last years have been a strongly emotional journey, where I have learned not only about minerals and sensors but also about myself. There were good and bad days, exciting, confusing and even boring moments, lots of experiences. The most important thing, however, is the people I was fortunate to share them with.

I am particularly grateful for the advice and guidance of my first promotor, **Dr Mike Buxton**. Mike, it has been a great pleasure to work with you, thanks for trusting me responsibilities that helped me to build confidence, and for supporting me whenever things became difficult for me or for the project. I appreciate the way you have shaped the Resource Engineering group, taking it beyond a bunch of colleagues to a true group of friends. I can say that I am not only among the few PhDs who barely have any reason to complain about their promotor, but also among those whose relationship candidate-promotor is built on trust and friendship.

I would like to offer my special thanks to my second promotor, **Prof. Jan Dirk Jansen**. You always had useful and constructive recommendations on this project. Thanks also for having interest in my career plans and expectations and providing me with advice on my next steps.

I wish to acknowledge the financial support by the FP7 programme and the EIT raw materials Kava funding through the **STOICISM** and **MONICALC** projects. I would like to extend my thanks to the people who participated in them and that provided input and assistance on the progress of my research, especially to **Imerys Minerals, Ltd.**, for organising the sampling campaigns and granting the access to the data. I am particularly grateful to **Jonathan Hearle**, for his bright insight about the key challenges in the processing of calcined kaolin; **David Mosely**, for his support and assistance throughout the project; **Maretva Baricot** for her warm welcome every time at the Par Moor office; **Saeid Moradi**, for all the interesting discussions and the reminders on the true purpose of a PhD; and to **Alex Coe** and **Tom Skuse** for attending all my sample requests. Appreciation is also due to the staff in the Geoscience & Engineering Laboratory (TU Delft), the Stevinlaboratory (TU Delft), and the GeoScience Laboratory (ITC- University of Twente) who assisted me with the preparation of samples and collection of data.

I would like to express my sincere gratitude to **Frank van Ruitenbeek** without whose trust and recommendation I probably would not have known about the opportunity for starting a PhD in Delft. My thanks are also extended to **Luke Palmer**, for his input on the kaolinite and the perlite characterisation; **Stefan Groeneheide**, for the fantastic work with the kaolin drill cores; **Volker Orterholt**, for his advice on the statistical methods, and to **Fiorenza Deon**, who assisted me on the interpretation of the XRD data and was always eager to discuss the perks of the amorphous mineral phases. I am very grateful to **Mafe Buitrago** and **Islam Fadel** who reviewed the manuscript and gave me valuable comments

for improving it. The most special thanks to **Floris Bonenkamp** for reading the almost 200 pages of the draft finding typos and many other mistakes.

To my colleagues and friends, the cool guys of the Resource Engineering section, I am so glad and so grateful I shared all these years with you. **Marinus**, you helped me from my very first day finding my way around in the campus, gave me a hand moving many kilograms of samples, and even translated the summary of the thesis; I cannot be more thankful with you. **Tom**, your critical thinking earned my respect and admiration, you became, in a way, a role-model for me. **Masoud**, literally the closest person to me in the office, my personal photographer, and even my occasional 'date'; thanks for all the tips you gave me particularly on the last stages of the PhD, you have been very kind and helpful at many moments, you are such a good man. **Cansin**, you always had so much energy and so many ideas to do fun things together, thanks for the awesome time. **Feven**, it has been very comforting to talk with you not only about spectroscopy and tedious project management but also about family and life; you make everyone feel good around you. **Jeroen**, you brought such a fresh vibe to our group, not only because you take us to PSOR but also because you are an open person, you are never afraid to ask questions, and you are eager to listen and help, it is lovely to have you around.

I feel very fortunate for having a big and beautiful family that is always supporting and loving me. My 'bonus family', **Ron, Ina, Matthijs, Unna, Jeroen, Annelies** and **Lucas**. You embraced me as one of your own and made me feel at home. You have taken so much interest in me and my research, even when all of that sounds like a strange world. You celebrated my achievements and cheered me up whenever I needed it. Ik hou van jullie! **Camilo**, thanks for the backstage family support, I know you are a friend I can count and rely on. Guatames García, despite the distance, you are always present, we are always together. **Carolina**, you are my greatest inspiration, you have opened the path I am walking on. Thank you for cultivating the love that I have for knowledge and for giving me the strength and the confidence for pursuing my own goals. **Carlos Julio**, hermano pez, thanks for reminding me that it is always possible to do better work, for letting me show you the wonderful things we are capable of, and thanks for compensating for my lack of artistic skills and helping me with the design of the cover of this thesis. I am very proud of the man you have become. **Pa y ma**, ustedes me han motivado siempre a ir un paso más allá, me han dado todas las herramientas y el amor que he necesitado para llegar hasta este punto; ustedes me han apoyado en todas las decisiones que he tomado, incluso cuando no es fácil para ustedes. Me hace inmensamente feliz llenarlos de orgullo, ¡este logro tan grande es mi regalo para ustedes!

The last lines are, of course, for the person who has been my best companion in this fantastic journey. **Thymen**, thanks for your never-ending love and patience, for holding my hand through all the ups and downs of the past years. Thanks for giving me clever ideas to get me out of the writers-block and for listening to endless hours of nerdy talk. Now you probably know more about clay minerals and calcination than some of my colleagues! Thanks for bringing Luna to our lives, she is certainly the best writing buddy I could have wished for. Thanks for joining me in this ride and for willing to stay by my side for the many adventures to come.

Adriana Guatame-García
Delft, August 2019

CURRICULUM VITÆ

Adriana Guatame-García was born on the 2nd of September 1986, in Chía, Colombia. After completing studies in Geology at the Universidad Nacional de Colombia in 2009, she worked at the Colombian Geological Survey (INGEOMINAS) in the Remote Sensing Division, and as a consultant for the Colombian-based NGO EQUITAS. In 2011, Adriana was granted a scholarship from the Netherlands Fellowship Program (NFP) to follow MSc. studies in Geo-information Science and Earth Observation at the ITC Faculty of the University of Twente. She obtained her MSc. Degree *Cum Laude* in 2013. The same year, Adriana started her doctoral research at the Department of Geoscience and Engineering at TU Delft, within the Resource Engineering section. The promotors of her doctorate were Dr M.W.N. Buxton and Prof. dr. ir. J.D. Jansen.

After defending her PhD thesis, Adriana will continue working with the TU Delft' s Resource Engineering section as a postdoctoral researcher.

PUBLICATIONS

JOURNAL PAPERS

4. **Guatame-García, A.** and Buxton, M. (2018). Prediction of soluble Al_2O_3 in calcined kaolin using infrared spectroscopy and multivariate calibration. *Minerals 8(4),* 136. doi: 10.3390/min8040136.

3. **Guatame-García, A.** and Buxton, M. (2018). The use of infrared spectroscopy to determine the quality of carbonate-rich diatomite ores. *Minerals 8(3),* 120. doi: 10.3390/min8030120.

2. **Guatame-García, A.**, Buxton, M., Deon, F., Lievens, C. and Hecker, C. (2018). Toward an online characterization of kaolin calcination process using short-wave infrared spectroscopy. *Mineral Processing and Extractive Metallurgy Review 39(6),* 420-431. doi: 10.1080/08827508.2018.1459617

1. **Guatame-García, A.** and Buxton, M. (2017). Infrared detection of ore variability that influences the environmental risks during perlite mining and processing. *Environmental Earth Sciences 76(21),* 741.doi: 10.1007/s12665-017-7074-y.

CONFERENCE PROCEEDINGS AND PRESENTATIONS

11. **Guatame-García, A.** and Buxton, M.(2018). Use of infrared spectroscopy for the estimation of soluble Al_2O_3 in calcined kaolin. 22nd General Meeting of the International Mineralogical Association (IMA 2018), August 2018, Melbourne, Australia.

10. **Guatame-García, A.** and Buxton, M.(2018). Infrared-based monitoring of the mining and processing of calcined kaolin. 22nd General Meeting of the International Mineralogical Association (IMA 2018), August 2018, Melbourne, Australia.

9. **Guatame-García, A.**, Buxton, M. and Tang, L. (2017). Prediction of soluble alumina in the kaolin calcination reaction from diffuse reflectance infrared spectra, 2nd International Conference on Applied Mineralogy and Advanced Materials – 13th International Conference on Applied Mineralogy (AMAM-ICAM), June 2017, Castellaneta Marina, Italy.

8. **Guatame-García, A.** and Buxton, M. (2017). Detection of mineral impurities in diatomite ores, In *Fiore, S. (Ed.) Proceedings of the 2nd International Conference on Applied Mineralogy and Advanced Materials – AMAM2017, ProScience 4*, 19-24. doi: 10.14644/amamicam.2017.004. June 2017, Castellaneta Marina, Italy.

7. Groenheide, S., **Guatame-García, A.**, Buxton, M. and van der Werff, H. (2017). Infrared detection of the mineralogical aspects that influence the processing of calcined kaolin, European Geosciences Union General Assembly, April 2017, Vienna, Austria.

6. **Guatame-García, A.** and Buxton, M. (2016). Integrating LIBS and NIR for detection of heavy metals in perlite ores, In *Thomas, P. and Wotruba, H. (Eds.) Proceedings of the 7th Sensor Based Sorting and Control Conference*, February 2016, Aachen, Germany.

5. **Guatame-García, A.** and Buxton, M. (2015). Determination of the origin of fine particles generated during the processing of perlite ore. Minerals and Metals Production from Mine to Market – IOM3 conference, December 2015, Cambridge, United Kingdom.

4. **Guatame-García, A.** and Buxton, M. (2015). Visible and infrared reflectance spectroscopy for characterization of iron impurities in calcined kaolin clays. In *Beyerer, J., Puente Leon, F., Langle, T. (Eds.) Proceedings of the 2nd International Conference on Optical Characterization of Materials* 215-226, March 2015. Karlsruhe, Germany.

3. **Guatame-García, A.** and Buxton, M. (2015). Determining iron impurities in calcined kaolin clays. An approach using short and long wavelength infrared spectroscopy.21st General Meeting of the International Mineralogical Association (IMA 2014), September 2014, Johannesburg, South Africa.

2. **Guatame-García, A.** and Buxton, M. (2014). Determination of CO_3 content in diatomite ores. Geometallurgy – IOM3 conference, June 2014, London, United Kingdom

1. **Guatame-García, A.**, van Ruitenbeek, F., de Smeth, B. and Hecker, C. (2013). Crystallinity variations of hydrothermal smectite-illite and kaolinite minerals by using reflectance spectra in the Rodalquilar Au deposit, Spain. 2013 Geological Remote Sensing Group Annual General Meeting – Status and Developments in Geological Remote Sensing, December 2013, Berlin, Germany.

OTHER PUBLICATIONS

1. Dalm, M., Buxton, M., **Guatame-García, A.**, Desta, F. S. and van Ruitenbeek, F. (2019). A review of sensors applicable to real-time raw material characterisation in mining. Manuscript in preparation.

MSc. and BSc. theses related to this research

MSc. theses

2. Groenheide, S. (2016). Mapping the kaolin mineralization of the St. Austell Granite (SW England) using VNIR and SWIR hyperspectral imaging. MSc. thesis, Delft University of Technology.

1. Klifman, E. (2015). Sensor technologies in diatomite mining and processing. MSc. thesis, Delft University of Technology.

BSc. theses

1. Kox, M. (2015). Characterization of heavy metals content in perlite ores from the Kiziltepe quarry (Turkey). BSc. thesis. Delft University of Technology.